Development of poly(2-oxazoline) based hemostatic materials

Proefschrift

ter verkrijging van de graad van doctor
aan de Radboud Universiteit Nijmegen
op gezag van de rector magnificus prof. dr. J.H.J.M. van Krieken,
volgens besluit van het college van decanen
in het openbaar te verdedigen op donderdag 2 november 2017
om 14.30 uur precies

door

Marcel Alexander Boerman
geboren op 17 januari 1988
te Woerden

Promotoren:
Prof. dr. ir. J.C.M. van Hest
Prof. dr. J.A. Jansen

Copromotor:
Dr. ir. S.C.G. Leeuwenburgh

Manuscriptcommissie:
Prof. dr. R.J.M. Nolte
Prof. dr. P.J. Dijkstra (Universiteit Twente)
Dr. J.P.A. Heuts (Technische Universiteit Eindhoven)

ISBN: 978-94-92801-08-1

The research presented in this thesis was financially supported by The Netherlands Institute for Regenerative Medicine (NIRM, Grant No. FES0908), NWO (KIEM 731.013.107), Europees Fonds voor Regionale Ontwikkeling (EFRO 2011-014237) and GATT Technologies bv.

Table of contents

List of abbreviations

%ID/g	percentage of injected dose per gram tissue
µPET/CT	micro-positron emission transmission computed tomography
µW	microwave
^{1}H-NMR	proton nuclear magenetic resonance
ASTM	American Society for Testing and Materials
Boc	1-(*tert*-butoxycarbonyl)
BSA	bovine serum albumin
C3-MestOx	2-methyl-carboxy-propyl-2-oxazoline
$CDCl_3$	deuterated chloroform
$CHCl_3$	chloroform
CO_2	carbon dioxide
COOH	carboxylic acid
CP	cloud point
*c*PropOx	2-*cyclo*-propyl-2-oxazoline
CROP	cationic ring opening polymerization
D_2O	deuterium oxide
DBU	1,8-diazabicyclo[5.4.0]undec-7-ene
DCM	dichloromethane
DIC	di-isopropylcarbodiimide
DMA	dimethylacetamide
DMAP	dimethylaminopyridine
DMF	dimethylformamide
DMSO	dimethylsulfoxide
DMSO-*d*6	deuterated dimethylsulfoxide
DP	degree of polymerization
DTPA	diethylene-triamine-pentaacetic acid
eq	equivalents
Et_3N	tri-ethylamine
EtOx	2-ethyl-2-oxazoline
FDA	Food and Drug Administation
FT	fourier transform
G′	storage modulus
G″	loss modulus
HCl	hydrochloric acid
iPropOx	2-*iso*-propyl-2-oxazoline
IR	infrared
ITLC	instant thin layer chromatography
kDa	kilo Dalton
KOH	potassium hydroxide
LCST	lower critical solution temperature
LiCl	lithium chloride
LiOH	lithium hydroxide
l-PEI	linear poly(ethylene imine)
MBq	mega Becquerel
MeCN	acetonitrile
MeOD	deuterated methanol
MeOH	methanol
MeOx	2-methyl-2-oxazoline
MES	(*N*-morpholino)ethanesulphonic acid
MestOx	2-methyl-carboxy-ethyl-2-oxazoline
M_n	number average molecular weight
MQ	milliQ water
MS	mass spectrometry
M_w	weight average molecular weight
Na_2CO_3	sodium carbonate
NaCl	sodium chloride
NaOH	sodium hydroxide
nButOx	2-*n*-butyl-2-oxazoline
NHS	*N*-hydroxysuccinimide
*n*PropOx	2-*n*-propyl-2-oxazoline
ORC	oxidized regenerated cellulose
P(EtOx)	poly(2-ethyl-2-oxazoline)
P(NIPAm)	poly(*N*-isopropylacrylamide)
p.i.	post injection
PBS	phosphate buffered saline
PEG	poly (ethylene glycol)
NHS-PEG	NHS-ester functionalized poly(ethylene glycol)
pH	measure for the acidity of an aqueous solution (pH = - log [H^+])
pKa	acid dissociation constant (pKa = pH - log ([A^-]/[HA]))
PMMA	poly(methyl methacrylate)
POx	poly(2-oxazoline)
NHS-POx	NHS-ester functionalized poly(2-oxazoline)
ppm	parts per million
rpm	revolutions per minute
SEC	size exclusion chromatography
SEM	scanning electron microscopy

SPECT/CT	single photon emission computed tomography
tan delta	loss tangent (ratio of loss modulus and storage modulus)
TFA	tri-fluoro acetic acid
THF	tetrahydrofuran
TTH	time to hemostasis
UV	ultraviolet
Vis	visible
WFE	wiped film evaporator
$Zn(OAc)_2$	zinc acetate

Chapter 1:

General introduction

1. Hemostatic biomaterials

Insufficient control over bleeding remains one of the biggest challenges in trauma surgery of soft tissues. This limited control is especially problematic during surgical procedures on highly venous organs (kidney, liver and spleen), particularly during removal of part of an organ (e.g. due to the presence of tumorous tissue), which compromises the veins close to the tissue surface. These bleedings cannot be treated by invasive methods like suturing or stitching, since this would create additional bleeding. Due to the severity of these bleedings, other methods like electrocautery[1] and ultrasonic sealing[2] often do not suffice during surgical treatment of these organs. Consequently, an alternative approach to control bleeding is required. As a result, a wide range of topical hemostatic agents has been developed[3-5], which are defined as materials which facilitate localized wound closure without compromising underlying tissues during their mechanism of action.

Two major surgeries which often require the use of topical hemostatic agents are partial nephrectomy[6] and liver resection[7], since both procedures are accompanied with severe blood loss[8, 9]. According to a survey among Japanese surgeons, 60% of the respondents indicated that topical hemostatic agents are standard treatment in case of a liver resection[10]. Another survey among Dutch surgeons indicated that 87% of the surgeons used topical hemostatic agents after liver resection. Moreover, 45% of the respondents were convinced that topical hemostats could aid in reducing complications during liver resection[11]. Nevertheless, liver resection remains a complex surgical procedure which often proceeds with the development of postoperative complications such as bile leakage[12], abscess formation[13, 14] and post-operative bleedings[15]. As a result, successful control over bleedings and postoperative management both remain a challenge in liver resection.

Although the quality of topical hemostatic agents has improved considerably over the past decades, the success rates of hemostatic agents are often not only determined by the efficacy of the agent, but also by external factors such as the type of surgical procedure, the severity of the procedure, the experience of the surgeon and the medical condition of the patient. Therefore, it is hard to predict *a priori* whether a specific topical hemostatic agent is effective for a specific procedure. Despite a large amount of studies on topical hemostatic agents[3], comparative studies are often performed for a limited number of products per study and often only few outcome parameters are considered. As a result, many studies on hemostatic agents are either inconclusive or offer contradictory results[16]. Evidently, extensive research is needed to improve the current generation of topical hemostatic agents and avoid the above-mentioned clinical complications.

In the next section, an overview of current clinically available topical hemostatic agents is provided in which the main advantages and shortcomings of these products are discussed in more detail.

1.2 Natural hemostats

The main class of hemostatic products is composed of polymeric materials of biological origin such as starch[17], chitosan[18], oxidized regenerated cellulose (ORC)[19, 20], collagen and gelatin[21, 22]. These biocompatible and biodegradable products accelerate the natural coagulation cascade by providing a sealing matrix where blood platelets can aggregate, thereby facilitating the formation of a blood clot. The products are available in various forms (powder, sponges, dressings) and are widely used in the clinic. In **Figure 1**, scanning electron microscopy (SEM) images of selected natural hemostats are displayed, revealing the fibrous structure of ORC-fibers (**Figure 1A and 1B**) and the porous nature of both collagen (**Figure 1C and 1D**) and gelatin sponges (**Figure 1E and 1F**). These products have the capacity to absorb blood due to their large surface area and permeabilility, and subsequently induce blood coagulation by providing a physical matrix for blood clot formation. The hemostatic efficacy of these materials is, however, limited for i) large areas of profuse bleedings, ii) patients suffering from bleeding disorders or iii) patients receiving anticoagulants (such as heparin) during surgery.

A promising class of natural hemostats involves biologically derived carriers which are coated with fibrinogen and thrombin. These proteins facilitate the final stage of the coagulation cascade, i.e., the formation of a fibrin clot[23]. As a result, the addition of these proteins to a collagen sponge results in reduced time to hemostasis (TTH) compared to collagen without these proteins, which has been reported by Chapman et al[24]. Tachosil® is such a collagen-based carrier coated with human-derived fibrinogen and thrombin which is considered a 'gold standard' due to its widespread use in many fields including liver resection[25-28]. Tachosil is covered with thrombin and fibrinogen (**Figure 2A, 2B and 2D**) on the active side, which is yellow colored due to the presence of riboflavin (E101) as a coloring agent (**Figure 2C**). The uncoated side displays a porous structure (**Figure 2E and 2F**). Tachosil has been tested in a wide range of surgical procedures. For liver resection procedures, Tachosil performed significantly better than electocautery[29, 30] regarding TTH, but not better than ORC[31]. In addition, this study also demonstrated that postoperative complications (e.g. bile leakage) were still observed - although at a lesser extent - in patients treated with Tachosil. Despite the favorable efficacy, Tachosil is still associated with several drawbacks. Recently, it was reported that Tachosil can cause undesired adhesion between organs[32]. Other drawbacks include a high cost price and the use of human- as well as animal-derived materials, which have a known risk of disease transmission

via viral or prion agents. Moreover, biologically derived hemostatic materials are only effective to a limited extent for patients receiving anticoagulants (such as heparin) during surgery. Since these factors are intrinsically connected to biologically derived hemostatic agents, many research groups have focused on the development of alternative hemostatic products based on synthetic polymers.

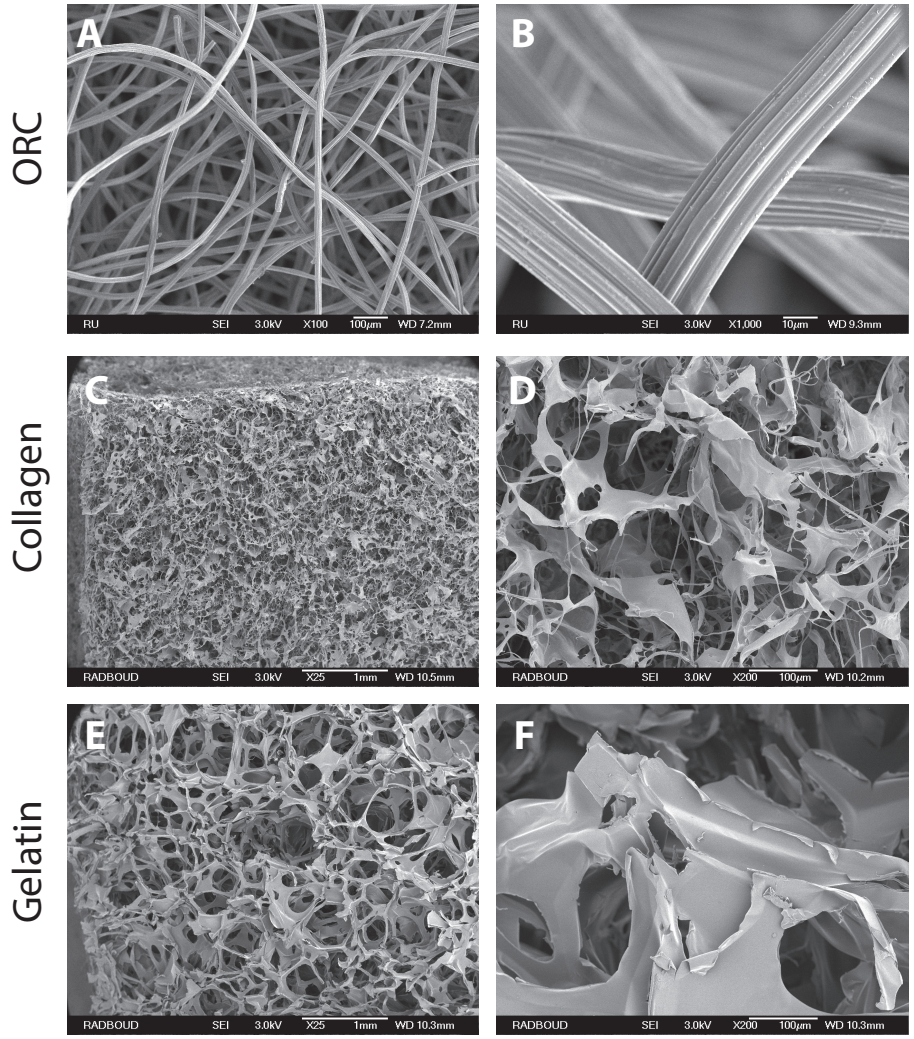

Figure 1 SEM images of hemostats composed of oxidized regenerated cellulose (ORC) (Snow®) (A&B), collagen (Hemotese®) (C&D) and porcine gelatin (E&F). Scale bars correspond to 1 mm (C&E), 100 µm (A, D&F) and 10 µm (B)

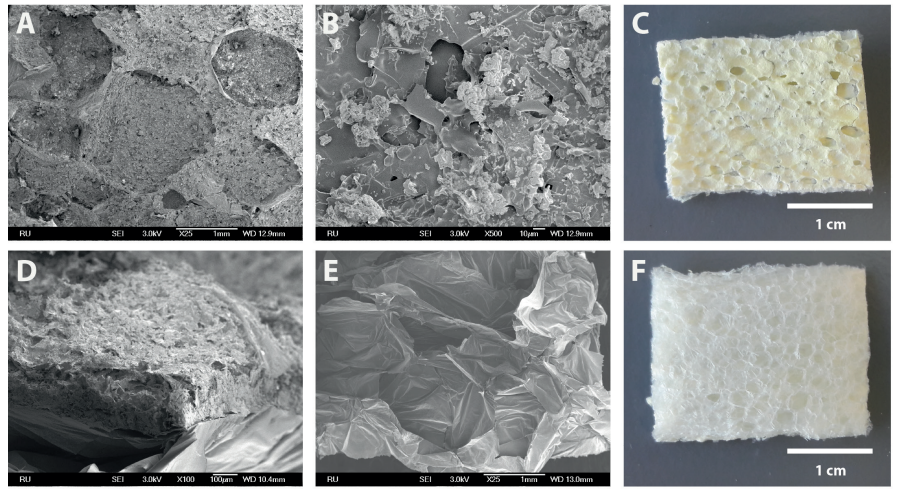

Figure 2 Overview of Tachosil. Images were recorded using SEM of the biologically active top side (A+B), cross section (D) and back side (E). Scale bars correspond to 1 mm (A&E), 100 µm (D) and 10 µm (B). Images were taken with a digital camera from top (C) and bottom (F).

1.3 Synthetic hemostats

Recently, synthetic polymer sealants[33] have been developed which act independently of the natural coagulation cascade due to their ability to seal the wound surface, thereby stopping the blood flow. Although the efficacy of these products is reported to be superior over naturally derived hemostats, the unknown biodegradability or excretability of some of these polymers as well as their toxicity (e.g. for cyanoacrylates)[34] are specific drawbacks of this class of materials.

A recently emerging approach entails the development of hybrid products, which combine the beneficial properties of both synthetic and natural polymers. A particularly interesting example of such a hybrid product is Veriset[35], which is an oxidized regenerated cellulose sheet impregnated with tri-lysine and *N*-hydroxysuccinimide ester-functional 4-arm poly(ethylene glycol) (**NHS-PEG**) (**Figure 3**). As can be observed from the SEM images, this product is composed of a coated side (**Figure 3A&B**), which is the tissue-reactive side due to application of **NHS-PEG**, and an uncoated side (**Figure 3D**), which shows the woven character of the ORC. The product has to be applied in dry state with the coated side facing the bleeding surface, whereafter blood penetrates through the product to allow fixation to the tissue. This fixation is achieved since **NHS-PEG** is reactive towards amines present in tissue, thereby sealing the wound site. Veriset has been tested in various model systems, for example in liver resection[36]. It was observed that Veriset performed better than Tachosil in terms of TTH, while both products had a similar

occurrence of adverse effects[35]. In another study, in a cardiovascular model, Veriset outperformed ORC without **NHS-PEG** (Surgicel®) in terms of TTH, demonstrating the benefit of the sealing effect of the tissue-reactive coating[37].

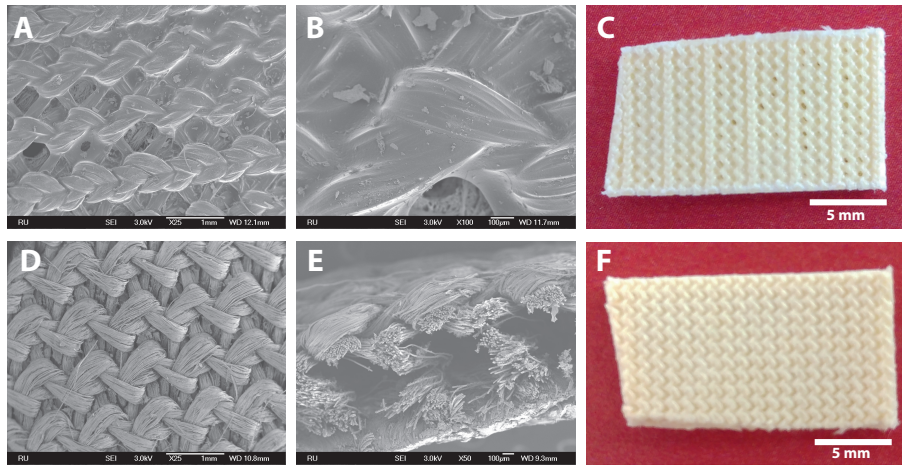

Figure 3 Overview of Veriset. Images were recorded using SEM of the protein-reactive top side (A&B), back side (D) and cross section (E). Scale bars correspond to 1 mm (A) and 100 µm (B, D&E). Images were taken with a digital camera from top (C) and bottom (F).

Another product in this class is Hemopatch[38-40], a flexible porous collagen carrier coated with **NHS-PEG** (**Figure 4**). Similar to Veriset, Hemopatch contains a tissue-reactive coated side (**Figure 4A-C**), which is partially coated with **NHS-PEG**, and a non-coated side (**Figure 4E and 4F**) which shows the porous nature of the collagen carrier. The mechanism of action of Hemopatch is based on instantaneous covalent crosslinking between **NHS-PEG** and amines present in tissue, blood proteins and the collagen carrier. This reaction seals the wound site and allows firm fixation of the patch to the tissue. Hemopatch has been thoroughly tested in the field[40], for example in liver resection where Hemopatch performed better than Tachosil[41] in terms of TTH. In this work, the authors claim that this phenomenon is related to the faster crosslinking reaction of **NHS-PEG** compared to the enzymatic conversion of fibrinogen to fibrin (forming a fibrin clot) in case of Tachosil. Moreover, a lower incidence of hematoma formation was observed for Hemopatch compared to Tachosil. However, a recent study reported that Tachosil and Hemopatch performed equally effective regarding TTH[42]. In another study, Hemopatch demonstrated shorter TTH compared to a product based on pure ORC[39], which also confirmed the beneficial effect of the **NHS-PEG**-coating.

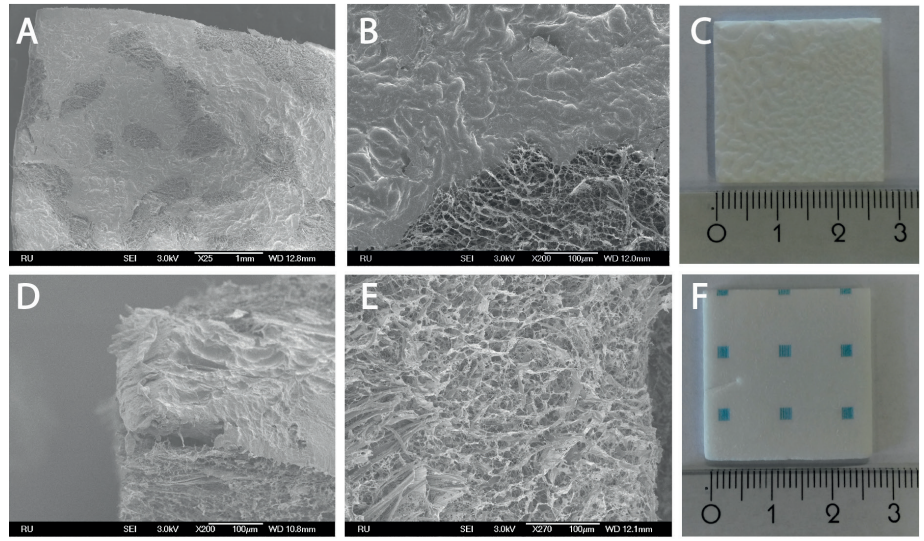

Figure 4 Overview of Hemopatch. Images were recorded using SEM of the protein-reactive side (A+B), cross section (D) and back side (E). Scale bars correspond to 1 mm (A) and 100 µm (B, D & E). Images were taken with a digital camera from protein-reactive top side (C) and back side (F).

1.4 Advantages and disadvantages of current hemostats

Traditionally, hemostatic products have been developed which rely on the natural coagulation cascade as mechanism of action and these products are generally used in view of their biocompatibility and biodegradability. However, the limited efficacy for complex surgical scenarios (e.g. in case of profuse bleedings) and drawbacks related to the use of biologically derived materials (e.g. transmission of animal-diseases) have led to an increased interest for synthetic alternatives.

These synthetic alternatives (in particular PEG-based systems) have specific benefits over their biological counterparts due to their highly tunable structure and mechanism, which has led to faster hemostasis compared to methods purely based on the natural coagulation cascade. Although favorable efficacy has been reported for the **NHS-PEG** based products Veriset and Hemopatch, the intrinsically fast crosslinking of **NHS-PEG** (in case of Hemopatch) might lead to irregular sealing of the wound site (by inhomogeneous crosslinking with tissue) or poor fixation to tissue (in case limited crosslinking with the collagen carrier is achieved), thereby rendering these hemostats less effective for some surgical bleedings. Moreover, PEG based materials are known to swell which can cause e.g. compression of neighbouring blood vessels or nerves. These potential drawbacks might be solved by modifying and fine-tuning the polymer architecture and properties. However, PEG has limited options for tailoring the degree of functionalization (only via the end groups) and polarity, which prompts further research on alternative polymers with hemostatic activity.

In summary, it remains a major challenge to develop a hemostatic device which is capable of both i) treating large areas of profuse bleedings in a non-invasive way and ii) reducing postoperative complications which improves surgical outcome and reduce hospitalization.
To this end, the ideal topical hemostatic agent should:

- seal large areas of profuse bleedings (including the wound site)
- attach to tissue in a non-invasive way
- be effective without adverse reactions
- prevent undesired adhesion between organs
- in dry state to be suitable for laparoscopic procedures
- be flexible in terms of folding
- be able to absorb sufficient amounts of blood
- be fully resorbable
- display favorable excretability

To achieve these requirements, novel polymeric materials with improved hemostatic efficacy should be developed that can be functionalized in a more versatile manner than currently available hemostatic products. A highly interesting class in this respect are the poly(2-alkyl-2-oxazolines).

2. Poly(2-oxazoline)s

2.1 Introduction

Poly(2-alkyl-2-oxazoline)s or POx are polymers, which were independently discovered in the 1960s by various research groups[43-46]. Due to their structural resemblance to peptides, versatile synthesis and excellent functionalization possibilities these polymers have gained increasing interest in many fields[47] including the development of responsive materials[48, 49], drug delivery[50, 51] and polymer therapeutics[52]. In the following section, the mechanism of cationic ring opening polymerization (CROP), the most common way of synthesizing POx, will be discussed. Moreover, various possibilities how POx functionalities can be introduced, the basic physicochemical properties of POx, as well as a current overview of the use of POx in biomedical applications will be described.

2.2 Mechanism

CROP is the most common method in the field for synthesizing POx. This polymerization method involves three consecutive steps: i) initiation, ii) propagation and iii) termination (**Figure 5**). The three steps will be discussed individually including

common reagents which are used for the respective steps. For a more detailed discussion on the mechanism, the reader is referred to an excellent review on this topic[53].

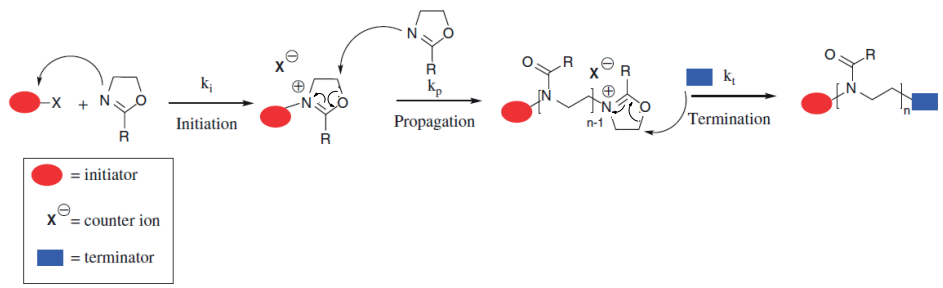

Figure 5 Simplified mechanism of CROP of 2-oxazolines. Reprinted with permission[53]

2.2.1 Initiation

During initiation, an electrophilic initiator forms a complex with the nucleophilic oxazoline (with initiation rate constant k_i) leading to the formation of an oxazolinium salt (**Figure 6A**). This cation is the reactive species, which is susceptible to nucleophilic attack of the oxazoline monomers, resulting in chain extension (propagation). However, this oxazolinium salt is in equilibrium with the covalently bound counter-ion, which limits successful propagation[54]. Experimentally, the occurrence of the reactive cationic species (determined by the equilibrium $k_{covalent}/k_{cation}$) is strongly determined by the type of initiator[55], counter-ion[56] and the experimental conditions (e.g. concentration[57], solvent[58], reaction temperature[59]). Common initiators employed for CROP include alkylating agents (triflates[60, 61], tosylates[55]), acid halides[62] and Lewis acids[43], but also multivalent initiator species (such as tetravalent triflates) have been employed for the design of star-shaped POx-architectures[63, 64].

2.2.2 Propagation

After the reactive cationic species is formed, nucleophilic attack of the oxazolines on this reactive species will result into chain extension, which is entropically driven by the formation a more stable tertiary amide from the cyclic oxazoline species [53]. Similar to the initiation process, chain extension (determined by propagation rate constant k_p) is dependent on the equilibrium between the cationic and covalent species[54] (**Figure 6B**). Additional factors which influence the propagation rate constant are the type of counter-ion[65], type of solvent[66, 67], concentration[57] and nucleophilicity of the incoming monomer[68-70].

Various kinetic studies[55, 61, 71] have shown (by measuring the monomer concentration in time by size exclusion chromatography (SEC) and ^{1}H-NMR spectroscopy) that the propagation of POx follows pseudo first-order kinetics, thereby being solely dependent on the propagating cationic species. The polymerization can be considered a 'living' polymerization[72, 73], if e.g. i) linear increase in molecular weight with conversion is observed, ii) complete and immediate initiation is achieved and iii) side reactions during polymerizations are circumvented[72, 73]. However, in practice, meeting these criteria is not trivial, since especially at higher conversions and when synthesizing high molecular weight polymers, chain transfer[74] and β-elimination[75] are commonly observed side reactions leading to chain branching.

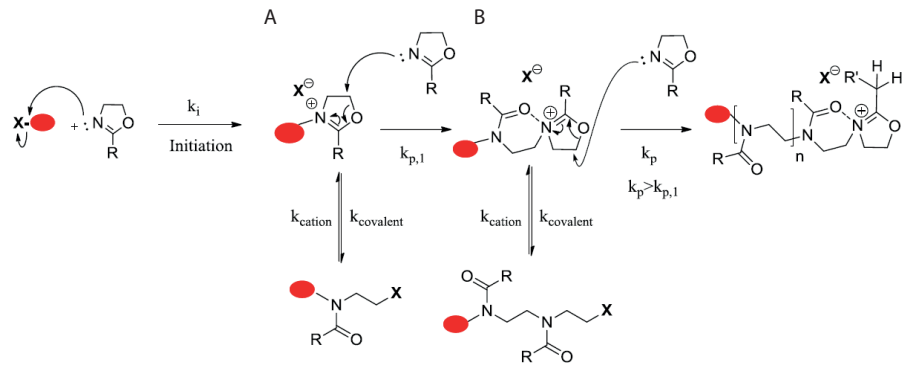

Figure 6 Detailed view of the initiation (**A**) and propagation steps (**B**) of CROP of 2-oxazolines: formation of the oxazolinium salt and the equilibrium between cationic and covalent species. Reprinted with permission[53]

2.2.3 Termination

After monomer consumption has been achieved, termination can be performed by end capping the polymer chains via addition of a nucleophile which will form a covalently bound end capped polymer and disables further propagation.

Termination can be achieved at the 2-position of the oxazoline ring (yielding a terminal ester)[76] or on the 5-position (yielding the terminating moiety next to the ethylene group) (**Figure 7**). The termination position (2 or 5) is dependent on the type of nucleophile used (hard or soft), the type of counter-ion and the identity of the reactive charged polymer end[77]. Termination at the 5-position is often preferred due to the higher selectivity, especially if a specific functional end group is desired. It is also evident that the reaction mixture should be free from nucleophilic impurities during CROP as this would lead to termination of the polymer chains during propagation resulting into ill-defined polymers. A wide range of termination agents has been studied, of which piperidine[77], water[77] and KOH/methanol[78] are most commonly used.

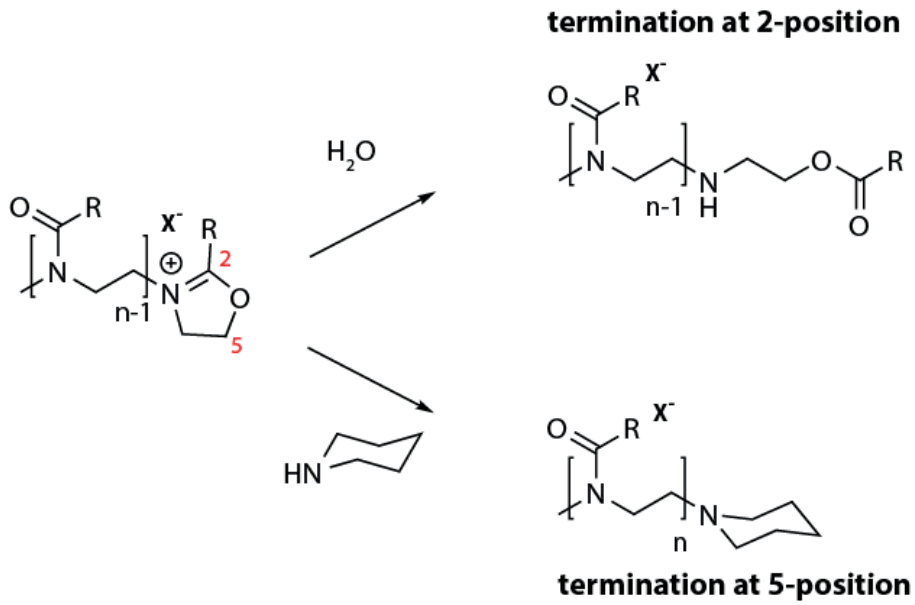

Figure 7 Detailed overview of the termination at either the 2-position (illustrated by water) or at the 5-position (illustrated by piperidine).

2.3 Functionalization possibilities

One of the most attractive features of POx-based polymers relates to the ease of their functionalization at either the polymer chain ends and/or the side chains[79-81], which is not possible for e.g. PEG where only functional end groups can be introduced.

2.3.1 Chain end functionalization

Functionalities can be introduced onto POx via initiation agents containing functional moieties which can be modified afterwards. Examples of initiators which have been reported include alkyne[82-84] and alkene (allyl[85], vinyl[83]) functional moieties. Initiators bearing amine[86], hydroxyl[87] and carboxylic acid groups[85, 88] have been used as well. However, because of their incompatibility with CROP, they require suitable protecting groups during CROP, which can be deprotected after synthesis.

Another possibility to introduce functional end groups onto POx is by using functional terminating agents. In principle, any nucleophilic species can be introduced, but the functionalization efficacy varies depending on the site of termination (2 or 5 position) and the compatibility with functional side chains. A selection of functional groups, which have been reported using functional terminating agents include primary amines (e.g. by ethylene diamine[89]), secondary amines (piperazine derivatives[90]), carboxylic acids[91] and azides[92, 93].

2.3.2 Side chain functionalization

Functionalization of POx side chains is particularly interesting since the number of functional groups can be precisely tuned by mixing oxazoline monomers with the desired functional group in the reaction mixture. To avoid compromised polymerization using CROP, nucleophilic species (amines, hydroxyl groups) and some electrophilic species (e.g. aldehydes) should be introduced in a protected manner, while other functional groups are compatible with CROP (alkynes, alkenes and azides). The protected groups can be deprotected after the polymer has been formed, revealing the masked functional group. In **Table 1**, an overview of selected functional oxazoline monomers is listed including most common functionalities and their deprotection strategies. For a complete overview, the reader is referred to extensive reviews on this topic[80, 81]. Alternative strategies to modify side chains of POx after polymerization are discussed in more detail in **Chapter 2**.

Table 1 Selection of functional oxazoline monomers

#	Oxazoline	Deprotection conditions after polymerization	Masked functionality	Reference
1	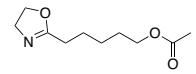	0.1M NaOH in methanol	hydroxyl	[94]
2	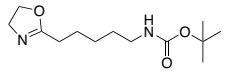	TFA/DCM (v/v, 1:1)	primary amine	[95]
3	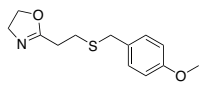	Anisole/TFA (v/v, 7:93)	thiol	[96]
4	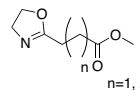	1M NaOH in water	carboxylic acid	[68, 71, 97-99]
5	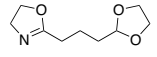	TFA/water (v/v, 5:95)	aldehyde	[100]
6	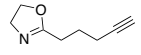	-	-	[101]
7	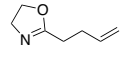	-	-	[102, 103]
8	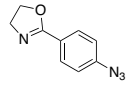	-	-	[104]
9	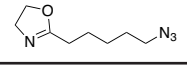	-	-	[105]

2.4 Solubility in aqueous solutions

The facile functionalization of POx has led to POx-based materials with a wide range of different physico-chemical properties[97, 106]. As an example, POx exhibits intriguing solubility behavior in aqueous solutions, which is mainly determined by the side chains of the polymer (**Figure 8**). While incorporation of 2-methyl-2-oxazoline (MeOx) groups renders these polymers polar and water-soluble, 2-*n*-butyl-2-oxazoline (nButOx) or longer alkyl side chains yield apolar and water-insoluble POx. Interestingly, the incorporation of specific monomers such as 2-ethyl-2-oxazoline (EtOx), 2-*n*-propyl-2-oxazoline (*n*PropOx), 2-*cyclo*-propyl-2-oxazoline (*c*PropOx), 2-*iso*-propyl-2-oxazoline (*i*PropOx), 2-methoxycarbonylethyl-2-oxazoline (MestOx) or 2-methoxycarbonylpropyl-2-oxazoline (C_3-MestOx) in the polymer structure results in polymers with so-called lower critical solution temperature (or LCST)[49, 97, 107-109]. These thermosensitive polymers are water-soluble below their so-called cloud point (CP), but insoluble above this critical temperature. This LCST-behavior is reported for other polymer systems as well, such as poly(*N*-isopropylacrylamide) (PNIPAm)[110]. This LCST behavior has been proven an interesting material characteristic for applications such as drug delivery[111] and a useful tool for the purification of e.g. pharmaceutical proteins in case of polymer-protein conjugates[112].

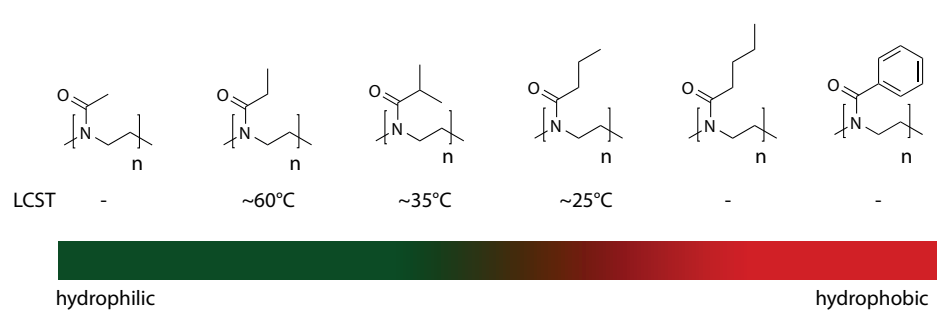

Figure 8 Schematic overview of the influence of side chain architecture on LCST behavior of POx-based polymers[108, 113].

2.5 POx in biomedical applications

In view of their structural resemblance to peptides and their excellent functionalization possibilities, POx has gained increasing interest for biomedical applications[52, 114-116]. Its use has been explored in areas such as gene delivery[117], drug delivery[118] and the development of antimicrobial polymers[86, 89, 119]. Various studies have been performed to test the biocompatibility of POx. In these studies, POx-based polymers were shown to be cyto- and hemocompatible[50, 89, 120-123]. Furthermore, it was observed that the polymers did not provoke an undesired immune response[118,

[123, 124]. Moreover, several biodistribution studies[50, 51, 88, 90, 91, 125-127] have demonstrated that POx-based materials can be excreted from animals after intravenous administration. Biodistribution studies on polymers consisting entirely of POx revealed that the excretion process was strongly controlled by the hydrodynamic volume and molecular weight distribution of the polymer[128].

Nevertheless, POx remains a relatively new candidate material in the field of polymer therapeutics. Although several companies have filed patents for the development of POx-based drug therapeutics[129, 130] and biomedical devices[131-134], the use of POx has only been approved by the FDA for indirect food-contacting agents (e.g. materials used for food packaging)[135] and drug delivery systems (Phase 1 clinical trial)[118]. Therefore, new formulations have to be thoroughly investigated and comply with regulatory requirements for clinical usage. Nevertheless, the possibilities for technology transfer and clinical translation seem numerous for POx as both the academic world and industry are looking into the possibilities of developing POx-based therapeutics.

3. Objectives of this thesis

Despite the fact that considerable progress has been made regarding the development of topical hemostatic agents, blood loss during surgery on soft tissue (e.g. liver resection) remains challenging, as these procedures are still associated with a high risk of hemorrhage and postoperative complications. As discussed in **section 1.3**, a promising class of hemostatic products is comprised of NHS-ester functionalized PEG. However, the limited possibilities of end-group functionalization as well as the limited opportunities in changing the polarity of the polymer restrict major improvements based on the polymer structure (**Figure 9**).

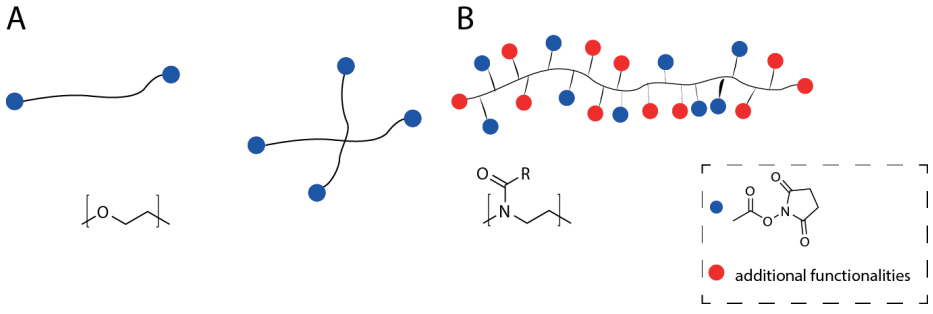

Figure 9 Overview of the differences in architecture between PEG (A) and POx (B).

POx is a promising class of biomaterials which can be functionalized both at the end groups and side chains. In addition, various POx have been shown to be e.g. cyto- and hemocompatible, which paves the way for its use in biomedical applications. As a result, we envision that NHS-ester functionalized POx (**NHS-POx**) is a strong candidate material for hemostatic applications, since the hemostatic efficacy of this polymer could be tuned by controlling the amount of amine-reactive NHS-ester groups. Moreover, in comparison to PEG, POx does not only allow the introduction of more functional groups than PEG, but also enables the introduction of various additional polar functionalities. These additional functionalities could be used to tune the water solubility of the polymers, which could also contribute to a higher reactivity towards amines and, as a result, an improved hemostatic efficacy.

In this work, we aim to develop a topical hemostatic agent based on NHS-ester functionalized POx for the non-invasive treatment of profuse bleedings in soft tissues. To this end, the most relevant steps of this development are discussed in separate chapters:

In **Chapter 2**, we will discuss various synthetic routes towards **NHS-POx** by CROP and post-modification polymerization strategies. Herein, we will investigate the most suitable and scalable strategy towards synthesis of **NHS-POx** both regarding the synthesis method and the properties of the final polymers.

In **Chapter 3**, the pH and thermoresponsive behavior of *n*PropOx based copolymers will be studied by turbidimetry. By introduction of various molar percentages of amine and carboxylic acid functionalities on these polymers, we aim to gain deeper insight into the thermoresponsive behavior of these materials.

In **Chapter 4**, we will study the hemostatic performance of various **NHS-POx** polymers (synthesized in **Chapter 2**) both *in vitro* as well as *in vivo* in comparison to commercially available controls.

In order to gain insight in the mechanism of action of **NHS-POx** as a synthetic hemostatic material, we will investigate the crosslinking of both **NHS-POx** and **NHS-PEG** with bovine serum albumin (BSA) using rheometry in **Chapter 5**.

In **Chapter 6**, we will study the degradation of **NHS-POx** in physiologically relevant media and study the excretion pathway of the degradation products after intravenous injection in a rat model. We will analyse the excretion of these polymers after radiolabeling using Single Photon Emission Computed Tomography (SPECT/CT) and by testing the radioactivity of dissected organs using an automated γ counter.

Finally, in **Chapter 7**, a summary of this thesis is provided as well as a perspective view on the future of POx-based hemostatic products.

4. References

1. P. F. Janssen, H. A. M. Brölmann and J. A. F. Huirne, *Surg. Endosc.*, 2012, **26**, 2892-2901.
2. R. J. Siegal, S. Vaezy, R. Martin and L. Crum, *Echocardiogr.*, 2001, **18**, 309-315.
3. Y. Tomizawa, *J. Artif. Organs*, 2005, **8**, 137-142.
4. P. J. M. Bouten, M. Zonjee, J. Bender, S. T. K. Yauw, H. van Goor, J. C. M. van Hest and R. Hoogenboom, *Prog. Polym. Sci.*, 2014, **39**, 1375-1405.
5. M. Emilia, S. Luca, B. Francesca, B. Luca, S. Paolo, F. Giuseppe, B. Gianbattista, M. Carmela, M. Luigi and L. Mauro, *Transfus. Apher. Sci.*, 2011, **45**, 305-311.
6. F. J. Kim, K. H. Rha, F. Hernandez, T. W. Jarrett, P. A. Pinto and L. R. Kavoussi, *J. Urol.*, 2003, **170**, 408-411.
7. R. Brustia, B. Granger and O. Scatton, *J. Hepatobiliary. Pancreat. Sci.*, 2016, **23**, 609-621.
8. J. D. Cunningham, Y. Fong, C. Shriver, J. Melendez, W. L. Marx and L. H. Blumgart, *Arch. Surg.*, 1994, **129**, 1050-1056.
9. R. J. Aragon and N. L. Solomon, *J. Gastrointest. Oncol.*, 2012, **3**, 28-40.
10. Y. Nakajima, T. Shimamura, T. Kamiyama, M. Matsushita, N. Sato and S. Todo, *Surg. Today*, 2002, **32**, 48-52.
11. E. A. Boonstra, I. Q. Molenaar, R. J. Porte and M. T. de Boer, *HPB*, 2009, **11**, 306-310.
12. J. W. Ostroff, *Gastroenterol. Hepatol.*, 2010, **6**, 264-272.
13. R. Andersson, A. Saarela, K. G. Tranberg and S. Bengmark, *Acta Chir. Scand.*, 1990, **156**, 707-710.
14. T. de Baère, A. Roche, J. M. Amenabar, C. Lagrange, M. Ducreux, P. Rougier, D. Elias, P. Lasser and C. Patriarche, *Hepatology*, 1996, **23**, 1436-1440.
15. W. R. Jarnagin, M. Gonen, Y. Fong, R. P. DeMatteo, L. Ben-Porat, S. Little, C. Corvera, S. Weber and L. H. Blumgart, *Ann. Surg.*, 2002, **236**, 397-407.
16. S. Samudrala, *AORN Journal*, 2008, **88**, S2-S11.
17. B. A. Bruckner, L. N. Blau, L. Rodriguez, E. E. Suarez, U. Q. Ngo, M. J. Reardon and M. Loebe, *J. Cardiothorac. Surg.*, 2014, **9**, 1-7.
18. A. E. Pusateri, S. J. McCarthy, K. W. Gregory, R. A. Harris, L. Cardenas, A. T. McManus and C. W. Goodwin, Jr., *J. Trauma*, 2003, **54**, 177-182.
19. Y. Wu, J. He, W. Cheng, H. Gu, Z. Guo, S. Gao and Y. Huang, *Carbohydr. Polym.*, 2012, **88**, 1023-1032.
20. K. M. Lewis, D. Spazierer, M. D. Urban, L. Lin, H. Redl and A. Goppelt, *Eur. Surg.*, 2013, **45**, 213-220.
21. R. Hajosch, M. Suckfuell, S. Oesser, M. Ahlers, K. Flechsenhar and B. Schlosshauer, *J. Biomed. Mater. Res. Part B Appl. Biomater.*, 2010, **94**, 372-379.
22. M. Kabiri, S. H. Emami, M. Rafinia and M. Tahriri, *Curr. Appl. Phys.*, 2011, **11**, 457-461.
23. S. Palta, R. Saroa and A. Palta, *Indian J. Anaesth.*, 2014, **58**, 515-523.
24. W. C. Chapman, P. Clavien, J. Fung, A. Khanna and A. Bonham, *Arch. Surg.*, 2000, **135**, 1200-1204.
25. G. L. Colombo, D. Bettoni, S. Di Matteo, C. Grumi, C. Molon, D. Spinelli, G. Mauro, A. Tarozzo and G. M. Bruno, *Vasc. Health Risk Manag.*, 2014, **10**, 569-576.
26. K. A. Simo, E. M. Hanna, D. K. Imagawa and D. A. Iannitti, *ISRN Surgery*, 2012, **2012**, 12.
27. C. Moench, W. O. Bechstein, V. Hermanutz, G. Hoexter and H. P. Knaebel, *Trials*, 2010, **11**, 109.
28. A. Rickenbacher, S. Breitenstein, M. Lesurtel and A. Frilling, *Expert Opin. Biol. Ther.*, 2009, **9**, 897-907.
29. L. Fischer, C. M. Seiler, C. E. Broelsch, B. de Hemptinne, J. Klempnauer, H.-J. Mischinger, H.-J. Gassel, M. Rokkjaer, R. Schauer, P. N. Larsen, V. Tetens and M. W. Büchler, *Surgery*, 2011, **149**, 48-55.
30. A. Frilling, G. A. Stavrou, H.-J. Mischinger, B. de Hemptinne, M. Rokkjaer, J. Klempnauer, A. Thörne, B. Gloor, S. Beckebaum, M. F. A. Ghaffar and C. E. Broelsch, *Langenbecks Arch. Surg.*, 2005, **390**, 114-120.

31. F. Kakaei, M. S. Seyyed Sadeghi, B. Sanei, S. Hashemzadeh and A. Habibzadeh, *HPB*, 2013, **2013**, 587608.
32. CBG-MEB, Risico op darmafsluiting bij gebruik TachoSil, https://www.cbg-meb.nl/actueel/nieuws/2016/02/03/risico-op-darmafsluiting-bij-gebruik-tachosil, (accessed 21-01-2017, 2017).
33. C. Ghobril and M. W. Grinstaff, *Chem. Soc. Rev.*, 2015, **44**, 1820-1835.
34. P. A. Leggat, D. R. Smith and U. Kedjarune, *ANZ J. Surg.*, 2007, **77**, 209-213.
35. R. Öllinger, A. L. Mihaljevic, C. Schuhmacher, H. Bektas, F. Vondran, M. Kleine, M. Sainz-Barriga, S. Weiss, P. Knebel, J. Pratschke and R. I. Troisi, *HPB*, 2013, **15**, 548-558.
36. C. Schuhmacher, J. Pratschke, S. Weiss, S. Schneeberger, A. L. Mihaljevic, R. Schirren, M. Winkler and N. Emmanouilidis, *Med. Devices. (Auckland, N.Z.)*, 2015, **8**, 167-174.
37. K. Howk, J. Fortier and R. Poston, *Ann. Vasc. Surg.*, 2016, **31**, 186-195.
38. K. M. Lewis, D. Spazierer, P. Slezak, B. Baumgartner, J. Regenbogen and H. Gulle, *J. Biomater. Appl.*, 2014, **29**, 780-788.
39. K. M. Lewis, A. Schiviz, H. C. Hedrich, J. Regenbogen and A. Goppelt, *Int. J. Surg.*, 2014, **12**, 940-944.
40. K. M. Lewis, C. E. Kuntze and H. Gulle, *Med. Devices (Auckl.)*, 2016, **9**, 1-10.
41. K. M. Lewis, J. McKee, A. Schiviz, A. Bauer, M. Wolfsegger and A. Goppelt, *ISRN Surgery*, 2014, **2014**, 7.
42. S. Scheurer, N. Schultz, J. Storkholm, C. Ingerslev, M. Haugaard and P. N. Larsen, *HPB*, **18**, e268.
43. D. A. Tomalia and D. P. Sheetz, *J. Polym. Sci., Part A-1: Polym. Chem.*, 1966, **4**, 2253-2265.
44. W. Seeliger, E. Aufderhaar, W. Diepers, R. Feinauer, R. Nehring, W. Thier and H. Hellmann, *Angew. Chem. Int. Ed.* , 1966, **5**, 875-888.
45. T. Kagiya, S. Narisawa, T. Maeda and K. Fukui, *J. Polym. Sci. B Polym. Lett.*, 1966, **4**, 441-445.
46. T. G. Bassiri, A. Levy and M. Litt, *J. Polym. Sci., Part B-1: Polym. Lett.*, 1967, **5**, 871-879.
47. R. Hoogenboom, *Angew. Chem. Int. Ed.* , 2009, **48**, 7978-7994.
48. H. Schlaad, C. Diehl, A. Gress, M. Meyer, A. L. Demirel, Y. Nur and A. Bertin, *Macromol. Rapid Commun.*, 2010, **31**, 511-525.
49. R. Hoogenboom and H. Schlaad, *Polym. Chem.*, 2017, **8**, 24-40.
50. T. X. Viegas, M. D. Bentley, J. M. Harris, Z. Fang, K. Yoon, B. Dizman, R. Weimer, A. Mero, G. Pasut and F. M. Veronese, *Bioconjug. Chem.*, 2011, **22**, 976-986.
51. K. L. Eskow Jaunarajs, D. G. Standaert, T. X. Viegas, M. D. Bentley, Z. Fang, B. Dizman, K. Yoon, R. Weimer, P. Ravenscroft, T. H. Johnston, M. P. Hill, J. M. Brotchie and R. W. Moreadith, *Mov. Disord.*, 2013, **28**, 1675-1682.
52. R. Luxenhofer, Y. Han, A. Schulz, J. Tong, Z. He, A. V. Kabanov and R. Jordan, *Macromol. Rapid Commun.*, 2012, **33**, 1613-1631.
53. B. Verbraeken, B. D. Monnery, K. Lava and R. Hoogenboom, *Eur. Polym. J.*, 2016, **88**, 451-469
54. A. Dworak, *Macromol. Chem. Phys.*, 1998, **199**, 1843-1849.
55. M. Glassner, D. R. D'hooge, J. Young Park, P. H. M. Van Steenberge, B. D. Monnery, M.-F. Reyniers and R. Hoogenboom, *Eur. Polym. J.*, 2015, **65**, 298-304.
56. M. W. M. Fijten, R. Hoogenboom and U. S. Schubert, *J. Polym. Sci. A Polym. Chem.*, 2008, **46**, 4804-4816.
57. R. Hoogenboom, R. M. Paulus, M. W. M. Fijten and U. S. Schubert, *J. Polym. Sci. A Polym. Chem.*, 2005, **43**, 1487-1497.
58. M. Vergaelen, B. Verbraeken, B. D. Monnery and R. Hoogenboom, *ACS Macro Letters*, 2015, **4**, 825-828.
59. R. Hoogenboom, M. W. M. Fijten and U. S. Schubert, *Macromol. Rapid Commun.*, 2004, **25**, 339-343.
60. F. Hu, S. Xie, L. Jiang and Z. Shen, *RSC Adv.*, 2014, **4**, 59917-59926.

61. R. Luxenhofer, M. Bezen and R. Jordan, *Macromol. Rapid Commun.*, 2008, **29**, 1509-1513.
62. R. M. Paulus, C. R. Becer, R. Hoogenboom and U. S. Schubert, *Macromol. Chem. Phys.*, 2008, **209**, 794-800.
63. A. Kowalczuk, J. Kronek, K. Bosowska, B. Trzebicka and A. Dworak, *Polymer International*, 2011, **60**, 1001-1009.
64. K.-M. Kim, Y. Ouchi and Y. Chujo, *Polym. Bull.*, 2003, **49**, 341-348.
65. T. Saegusa, S. Kobayashi and A. Yamada, *Makromol. Chem.*, 1976, **177**, 2271-2283.
66. B. D. Monnery, S. Shaunak, M. Thanou and J. H. G. Steinke, *Macromolecules*, 2015, **48**, 3197-3206.
67. Q. Liu, M. Konas and J. S. Riffle, *Macromolecules*, 1993, **26**, 5572-5576.
68. P. J. M. Bouten, D. Hertsen, M. Vergaelen, B. D. Monnery, M. A. Boerman, H. Goossens, S. Catak, J. C. M. van Hest, V. Van Speybroeck and R. Hoogenboom, *Polym. Chem.*, 2015, **6**, 514-518.
69. H. Goossens, S. Catak, M. Glassner, V. R. de la Rosa, B. D. Monnery, F. De Proft, V. Van Speybroeck and R. Hoogenboom, *ACS Macro Letters*, 2013, **2**, 651-654.
70. R. Hoogenboom, M. W. M. Fijten, H. M. L. Thijs, B. M. van Lankvelt and U. S. Schubert, *Des. Monomers. Polym.*, 2005, **8**, 659-671.
71. P. J. M. Bouten, D. Hertsen, M. Vergaelen, B. D. Monnery, S. Catak, J. C. M. van Hest, V. Van Speybroeck and R. Hoogenboom, *J. Polym. Sci., Part A-1: Polym. Chem.*, 2015, **53**, 2649-2661.
72. T. R. Darling, T. P. Davis, M. Fryd, A. A. Gridnev, D. M. Haddleton, S. D. Ittel, R. R. Matheson, G. Moad and E. Rizzardo, *J. Polym. Sci. A Polym. Chem.*, 2000, **38**, 1706-1708.
73. R. P. Quirk and B. Lee, *Polym. Int.*, 1992, **27**, 359-367.
74. M. Litt, A. Levy and J. Herz, *J. Macromol. Sci. A Chem.*, 1975, **9**, 703-727.
75. J. M. Warakomski and B. P. Thill, *J. Polym. Sci. A Polym. Chem.*, 1990, **28**, 3551-3563.
76. D. A. Tomalia and J. N. Paige, *J. Org. Chem.*, 1973, **38**, 422-430.
77. O. Nuyken, G. Maier, A. Groß and H. Fischer, *Macromol. Chem. Phys.*, 1996, **197**, 83-95.
78. G. H. Hsiue, A. X. Swamikannu and M. H. Litt, *J. Polym. Sci. A Polym. Chem.*, 1988, **26**, 3043-3069.
79. K. Lava, B. Verbraeken and R. Hoogenboom, *Eur. Polym. J.*, 2015, **65**, 98-111.
80. B. Guillerm, S. Monge, V. Lapinte and J. J. Robin, *Macromol. Rapid Commun.*, 2012, **33**, 1600-1612.
81. E. Rossegger, V. Schenk and F. Wiesbrock, *Polymers*, 2013, **5**, 956-1011.
82. B. Guillerm, V. Darcos, V. Lapinte, S. Monge, J. Coudane and J.-J. Robin, *Chem. Commun.*, 2012, **48**, 2879-2881.
83. K. Shiro, U. Hiroshi, M. Toshild and N. Yutaka, *Chem. Lett.*, 1991, **20**, 1771-1774.
84. M. W. M. Fijten, C. Haensch, B. M. van Lankvelt, R. Hoogenboom and U. S. Schubert, *Macromol. Chem. Phys.*, 2008, **209**, 1887-1895.
85. C. Giardi, V. Lapinte, C. Charnay and J. J. Robin, *React. Funct. Polym.*, 2009, **69**, 643-649.
86. C. J. Waschinski, V. Herdes, F. Schueler and J. C. Tiller, *Macromol. Biosci.*, 2005, **5**, 149-156.
87. M. Reif and R. Jordan, *Macromol. Chem. Phys.*, 2011, **212**, 1815-1824.
88. S. Zalipsky, C. B. Hansen, J. M. Oaks and T. M. Allen, *J. Pharm. Sci.*, 1996, **85**, 133-137.
89. C. P. Fik, C. Krumm, C. Muennig, T. I. Baur, U. Salz, T. Bock and J. C. Tiller, *Biomacromolecules*, 2012, **13**, 165-172.
90. F. C. Gaertner, R. Luxenhofer, B. Blechert, R. Jordan and M. Essler, *J. Control. Release*, 2007, **119**, 291-300.
91. A. Mero, Z. Fang, G. Pasut, F. M. Veronese and T. X. Viegas, *J. Control. Release*, 2012, **159**, 353-361.
92. G. Volet, T.-X. Lav, J. Babinot and C. Amiel, *Macromol. Chem. Phys.*, 2011, **212**, 118-124.
93. C. Guis and H. Cheradame, *Eur. Polym. J.*, 2000, **36**, 2581-2590.
94. G. Riess, *Prog. Polym. Sci.*, 2003, **28**, 1107-1170.
95. S. Cesana, J. Auernheimer, R. Jordan, H. Kessler and O. Nuyken, *Macromol. Chem. Phys.*, 2006, **207**, 183-192.
96. S. Cesana, A. Kurek, M. A. Baur, J. Auernheimer and O. Nuyken, *Macromol. Rapid Commun.*, 2007, **28**, 608-615.
97. P. Bouten, K. Lava, J. van Hest and R. Hoogenboom, *Polymers*, 2015, **7**, 1998-2008.

98. M. A. Boerman, H. L. Van der Laan, J. C. M. E. Bender, R. Hoogenboom, J. A. Jansen, S. C. Leeuwenburgh and J. C. M. Van Hest, *J. Polym. Sci., Part A-1: Polym. Chem.*, 2016, **54**, 1573-1582.
99. J. C. Rueda, E. Campos, H. Komber, S. Zschoche, L. Häussler and B. Voit, *Des. Monomers. Polym.*, 2013, **17**, 208-216.
100. C. Taubmann, R. Luxenhofer, S. Cesana and R. Jordan, *Macromol. Biosci.*, 2005, **5**, 603-612.
101. R. Luxenhofer and R. Jordan, *Macromolecules*, 2006, **39**, 3509-3516.
102. A. Gress, A. Völkel and H. Schlaad, *Macromolecules*, 2007, **40**, 7928-7933.
103. M. Schmitz, M. Kuhlmann, O. Reimann, C. P. R. Hackenberger and J. Groll, *Biomacromolecules*, 2015, **16**, 1088-1094.
104. W. H. Binder and H. Gruber, *Macromol. Chem. Phys.*, 2000, **201**, 949-957.
105. T.-X. Lav, P. Lemechko, E. Renard, C. Amiel, V. Langlois and G. Volet, *React. Funct. Polym.*, 2013, **73**, 1001-1008.
106. R. Hoogenboom, M. W. M. Fijten, H. M. L. Thijs, B. M. van Lankvelt and U. S. Schubert, *Des. Monomers Polym.*, 2005, **8**, 659-671.
107. P. I. Freeman and J. S. Rowlinson, *Polymer*, 1960, **1**, 20-26.
108. R. Hoogenboom, H. M. L. Thijs, M. J. H. C. Jochems, B. M. van Lankvelt, M. W. M. Fijten and U. S. Schubert, *Chem. Commun.*, 2008, **44**, 5758-5760.
109. M. M. Bloksma, C. Weber, I. Y. Perevyazko, A. Kuse, A. Baumgärtel, A. Vollrath, R. Hoogenboom and U. S. Schubert, *Macromolecules*, 2011, **44**, 4057-4064.
110. A. Halperin, M. Kröger and F. M. Winnik, *Angew. Chem. Int. Ed.*, 2015, **54**, 15342-15367.
111. D. Schmaljohann, *Adv. Drug Deliv. Rev.*, 2006, **58**, 1655-1670.
112. W. Hassouneh, S. R. MacEwan and A. Chilkoti, *Methods Enzymol.*, 2012, **502**, 215-237.
113. U. Hiroshi and K. Shiro, *Chem. Lett.*, 1992, **21**, 1643-1646.
114. N. Adams and U. S. Schubert, *Adv. Drug Deliv. Rev.*, 2007, **59**, 1504-1520.
115. V. R. de la Rosa, *J. Mater. Sci. Mater. Med.*, 2014, **25**, 1211-1225.
116. O. Sedlacek, B. D. Monnery, S. K. Filippov, R. Hoogenboom and M. Hruby, *Macromol. Rapid Commun.*, 2012, **33**, 1648-1662.
117. M. Mees, E. Haladjova, D. Momekova, G. Momekov, P. S. Shestakova, C. B. Tsvetanov, R. Hoogenboom and S. Rangelov, *Biomacromolecules*, 2016, **17**, 3580-3590.
118. R. W. Moreadith, T. X. Viegas, M. D. Bentley, J. M. Harris, Z. Fang, K. Yoon, B. Dizman, R. Weimer, B. P. Rae, X. Li, C. Rader, D. Standaert and W. Olanow, *Eur. Polym. J.*, 2016, **88**, 524-552
119. C. Krumm, S. Harmuth, M. Hijazi, B. Neugebauer, A.-L. Kampmann, H. Geltenpoth, A. Sickmann and J. C. Tiller, *Angew. Chem. Int. Ed.*, 2014, **53**, 3830-3834.
120. M. Bauer, C. Lautenschlaeger, K. Kempe, L. Tauhardt, U. S. Schubert and D. Fischer, *Macromol. Biosci.*, 2012, **12**, 986-998.
121. R. Luxenhofer, G. Sahay, A. Schulz, D. Alakhova, T. K. Bronich, R. Jordan and A. V. Kabanov, *J. Control. Release*, 2011, **153**, 73-82.
122. X. Wang, X. Li, Y. Li, Y. Zhou, C. Fan, W. Li, S. Ma, Y. Fan, Y. Huang, N. Li and Y. Liu, *Acta Biomater.*, 2011, **7**, 4149-4159.
123. R. Shah, Z. Kronekova, A. Zahoranova, L. Roller, N. Saha, P. Saha and J. Kronek, *J. Mater. Sci. Mater. Med.*, 2015, **26**, 157.
124. J. Kronek, E. Paulovičová, L. Paulovičová, Z. Kroneková and J. Lustoň, *J. Mater. Sci. Mater. Med.*, 2012, **23**, 1457-1464.
125. P. Goddard, L. E. Hutchinson, J. Brown and L. J. Brookman, *J. Control. Release*, 1989, **10**, 5-16.
126. Z. He, A. Schulz, X. Wan, J. Seitz, H. Bludau, D. Y. Alakhova, D. B. Darr, C. M. Perou, R. Jordan, I. Ojima, A. V. Kabanov and R. Luxenhofer, *J. Control. Release*, 2015, **208**, 67-75.
127. P. H. Kierstead, H. Okochi, V. J. Venditto, T. C. Chuong, S. Kivimae, J. M. J. Fréchet and F. C. Szoka, *J. Control. Release*, 2015, **213**, 1-9.
128. L. Wyffels, T. Verbrugghen, B. D. Monnery, M. Glassner, S. Stroobants, R. Hoogenboom and S. Staelens, *J. Control. Release*, 2016, **235**, 63-71.

129. J.M Harris, M.D. Bentley, K. Yoon and Z. Fang, US Patent 8088884, 2012.
130. K.Yoon, M.D. Bentley, J.M. Harris, Z. Fang and T. Viegas, US Patent 8501899, 2013.
131. J.C.M.E. Bender and M.A. Boerman, WO Patent 2016056901, 2016.
132. R. Hoogenboom, J.C.M.E. Bender and J.C.M. van Hest, WO Patent 2012057628, 2013.
133. J.C.M.E. Bender, R. Hoogenboom, J.C.M. van Hest and H. van Goor, WO2013137736, 2013.
134. R. Hoogenboom, WO Patent 2013103297, 2013.
135. FDA, CFR - Code of Federal Regulations Title 21, http://www.accessdata.fda.gov/scripts/cdrh/cfdocs/cfCFR/CFRSearch.cfm?fr=175.105, (accessed 24-01-2017, 2017).

Chapter 2:

Synthesis of NHS-ester functionalized poly(2-oxazoline)s (NHS-POx)

Abstract

In this chapter, we aim to develop a robust method for the preparation of NHS-ester functional poly(2-oxazoline)s (**NHS-POx**). Particular attention was paid to the application potential in hemostatic devices, solubility and scalability of the procedures. We discuss three different synthetic routes (**A**-**C**). In route **A**, we first hydrolyzed commercially available POx and then used post-polymerization modification strategies to introduce NHS-esters onto the polymers. In routes **B** and **C**, cationic ring opening polymerization (CROP) was employed to create copolymers with methyl ester side chains, which were further modified via post-polymerization strategies based on either hydrolysis, (route **B**) or amidation (route **C**) to develop **NHS-POx** polymers with different polarities. Synthesis of **NHS-POx** appeared to be most feasible via routes **B** and **C** since these routes proved robust, reproducible and scalable. Moreover, the polymers were obtained with good control over the number of functional groups and polymer dispersity. Finally, these polymers showed favorable solubility in both aqueous and organic media.

1. Introduction

Poly(2-oxazoline)s or POx[1-4] are a promising class of polymers which are interesting for biomedical applications due to their biocompatibility[5-7] as well as easy and versatile functionalization possibilities[8-10]. In this thesis, we aim to functionalize POx with activated esters for application in hemostatic devices[11]. One of the most commonly used activated esters to date is the N-hydroxy succinimide (NHS) ester[12, 13], which forms a stable amide bond upon reaction with primary amines. Since primary amines are widely present in soft tissue and blood, polymers equipped with NHS-esters are intrinsically able to form crosslinks with these tissues and induce the formation of artificial blood clots. As a result, polymers equipped with NHS-esters are excellent candidates for hemostatic applications. However, these polymers should meet a number of requirements for application in hemostatic devices.

First of all, the polymer should have sufficient reactive moieties for covalent crosslinking (e.g. with blood proteins). Secondly, the polymer composition should be soluble in both water (beneficial for their biological activity) and volatile organic solvents (beneficial for processing of the polymer). Moreover, the reactive moieties should be available for crosslinking, which requires reactive side chains of sufficient flexibility and length as well as an overall polymer polarity which allows for effective wetting under physiological conditions. To achieve this, the synthetic procedures towards these polymers should be robust, scalable and high yielding to guarantee constant quality. To meet these demands for both the polymer structure and the corresponding synthetic procedures, design criteria can be formulated in order to achieve optimal hemostatic performance (**Table 1**).

Table 1 Design criteria for **NHS-POx** and corresponding synthetic procedures

NHS-POx	Synthetic procedures
• Solubility in water • Solubility in volatile organic solvents • Degree of polymerization (DP=100) • Functional group ratio • Dispersity values ($Đ < 1.3$) • Purity (>95%)	• Scalable synthetic steps • Common and affordable reagents • Robustness of procedures • Scalable purification steps • Environmentally benign • High yield

As discussed in **Chapter 1**, the most common way to introduce functionalities in POx involves introduction of i) functional end groups (via initiation or termination agents) or ii) functional side chains by using monomers bearing functional moieties in cationic ring opening polymerization (CROP). However, in certain conditions the use of functional reagents for CROP is impractical or undesired. As an example, the

use of functional monomers is less preferred if the desired monomer is difficult to synthesize[14] or to purify, which is the case if the side chain consists of a labile moiety. Also, the kinetic profile and the incorporation rate can strongly differ between oxazolines bearing different side chains (e.g. due to electronic effects[15]), which has to be taken into account if a specific distribution of monomers within the polymer is desired[16]. Therefore, several alternative strategies have been developed for the introduction of functionalities into POx.

A first approach utilizes hydrolysis of the tertiary amide groups in POx, yielding linear poly(ethylene imine) (l-PEI) moieties. These nucleophilic l-PEI moieties are reactive towards electrophilic species like acyl chlorides[17, 18] and anhydrides, which allows reintroduction of the tertiary amide groups. If electrophilic reagents containing functional groups are used, these are introduced onto the polymer. Hydrolysis of the POx-amides can be achieved using a wide range of reagents, including HCl[19], NaOH[20], and HCl under microwave irradiation[21, 22]. Moreover, the kinetics of the hydrolysis of poly(2-ethyl-2-oxazoline) P(EtOx) at various elevated temperatures has been described[23], which allows for precise tuning of the number of secondary amines created, and thus the number of functional groups.

Another way to introduce functionalities into POx is by making use of post-polymerization modification strategies on copolymers containing modifiable side chains[24]. Using this method, a polymer is synthesized containing a specific number of functional groups, which can be chemically modified after the polymer structure has been synthesized. This strategy can be advantageous if the desired functional group is incompatible with the polymerization method, as can be the case for CROP. This concept was pioneered by the work of Hermann Staudinger in the 1930s[25, 26], and is nowadays a widely-applied approach in the field of polymer science[27]. To date, several groups have reported the use of post-polymerization modification strategies for the design of POx, e.g. by thiol-ene[28-30] or click chemistry[31-34].

Since NHS-esters are not compatible with CROP, these functional groups need to be introduced by post-modification functionalization strategies. A particularly interesting functional group in this respect is the methyl ester. This moiety can be effectively modified by hydrolysis or amidation which offers opportunities for the introduction of a wide range of functionalities[17, 35-38]. It has been demonstrated that the methyl ester group can be introduced into POx by reaction of l-PEI with methyl succinyl chloride or via copolymerization of 2-methoxycarbonyl-ethyl-2-oxazoline (MestOx) as functional monomer in CROP[17, 39]. The latter route has already been investigated with various monomers including 2-methyl-2-oxazoline (MeOx)[40], 2-ethyl-2-oxazoline (EtOx)[40] and 2-n-propyl-2-oxazoline (*n*PropOx)[41], which allows for the design of a great variety of MestOx-containing polymers with different polarities[42].

In this chapter, we investigate three different synthetic strategies towards NHS-ester functionalized POx (**NHS-POx**) (Route **A**-**C**) in order to select the most robust synthetic procedure towards these polymers (**Figure 1**). Subsequently, the advantages and disadvantages of these three routes as well as the physico-chemical properties (e.g. aqueous solubility) of the synthesized polymers are discussed.

In route **A**, we use selective hydrolysis of commercially available P(EtOx) (Aquazol 50®)[43], whereafter we first introduce the methyl ester moiety via the appropriate acyl chloride, and subsequently the NHS-ester group via a post-polymerization modification strategy. In route **B** and **C**, we synthesize copolymers based on MestOx with *n*PropOx and EtOx and use a similar approach to introduce the NHS-ester onto the polymers from the methyl ester side chains. A difference between routes **B** and **C** is the way the hydrophilic part of the polymer is introduced. In route **B** the hydrophilic groups (EtOx) are incorporated via copolymerization, whereas the hydrophilic groups are introduced by post-modification polymerization strategies in route **C**. Additionally, polymers prepared using route **C** bear a biodegradable ester linker in the side chain to facilitate hydrolytic degradation of crosslinked POx-based networks.

2. Results and discussion

2.1 Route A: Hydrolysis of P(EtOx) followed by NHS-ester modification

In this route, we used selective hydrolysis of the POx-backbone to yield linear l-PEI moieties. These secondary amines in the polymer backbone were post-modified towards NHS-esters yielding **NHS-POx**. Aquazol 50[43], a commercially available P(EtOx) (M_n 50 kDa, Đ 3-4), was applied. Using this approach, three types of NHS-ester functionalized polymers were prepared (**A1**-**A3**) (**Scheme 1**).

In route **A1** the preparation of polymer **P4** started with the partial hydrolysis of the alkyl side chains of POx to obtain polymer **P1**. By means of time-dependent heating in 6M HCl at 73°C, the desired degree of hydrolysis (11% l-PEI) was obtained as confirmed by ^{1}H-NMR spectroscopy. Subsequently, methyl succinyl chloride was coupled, resulting in the formation of a methyl ester functional polymer **P2**. These methyl ester groups were subsequently hydrolyzed using LiOH, yielding polymers containing carboxylic acid moieties (**P3**). In a final step, these carboxylic acid groups were converted to the desired NHS-esters (**P4**) as was characterized by ^{1}H NMR spectroscopy. It was observed that this polymer was soluble in both water and organic solvents (20 mg/mL). However, route **A1** proved to have certain limitations. First of all, coloration of the polymer occurred during the coupling of methyl

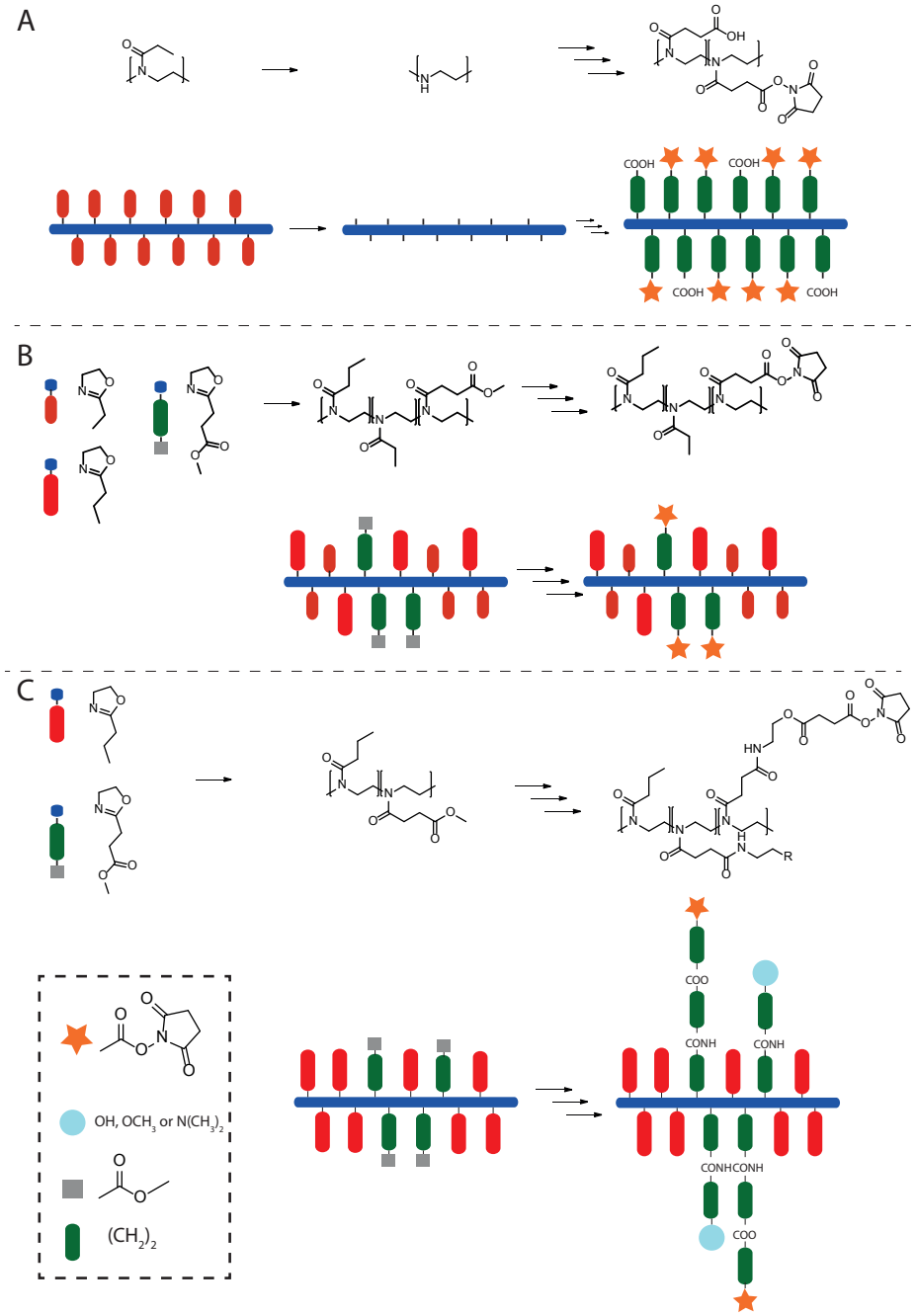

Figure 1 Synthetic routes (**A-C**) towards NHS-ester functionalized POx (**NHS-POx**). A) Hydrolysis approach and introduction of NHS-ester groups, B) CROP followed by introduction of NHS-ester groups, C) CROP followed by introduction of hydrophilic groups and NHS-ester groups.

succinyl chloride and residual salts (probably related to the use of Et_3N) could not be removed by precipitation. Furthermore, attempts to synthesize polymers with a higher number of functional NHS-esters (>20%) was not possible due to limited solubility of the intermediate products in organic solvents.

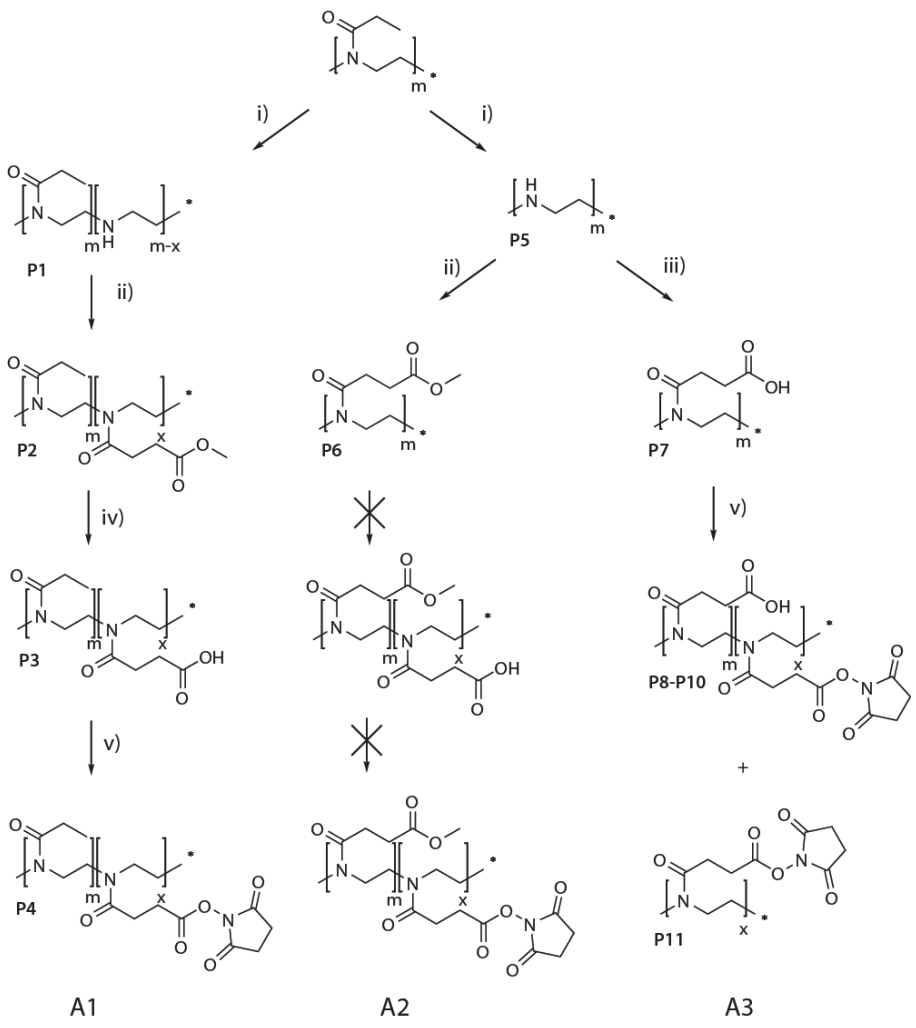

Scheme 1 Overview of synthetic routes **A1-A3** starting from Aquazol 50®. Reagents: i) HCl 6M, reflux, ii) methyl succinyl chloride, Et_3N, DCM, 0°C, iii) succinic anhydride, Et_3N, rt, iv) LiOH, MeOH, rt, v) NHS/DIC, DMF, rt.

In route **A2,** Aquazol 50 was fully hydrolyzed to create linear 100% l-PEI (**P5**). This was achieved in quantitative yield and high purity (>99%). Similar to the procedure described for **A1, P5** was reacted with an excess of methyl succinyl chloride in order to

obtain polymers which were fully functionalized with methyl esters (**P6**). Subsequently, it was attempted to partially hydrolyze these methyl esters into carboxylic acid groups using sub-stoichiometric amounts of LiOH (0.25 eq. compared to methyl ester groups), which could be activated into NHS-esters afterwards. However, the partial hydrolysis was not reproducible and therefore this route (**A2**) was considered not feasible.

In a third l-PEI-based synthesis route (**A3**), succinic anhydride was employed in the presence of tri-ethylamine (Et_3N) to fully convert **P5** into a carboxylic acid-functional polymer (**P7**). After overnight reaction, the characteristic ^{1}H-NMR signal of the ethylene units next to the secondary amine (2.8 ppm) disappeared, indicating full conversion of the l-PEI moieties into tertiary amide groups of POx. After multiple precipitation steps to remove the excess of reagents, the polymer was obtained as a white powder in a good yield (80 %). In contrast to the hydrolysis-based routes **A1** and **A2**, no color change was observed during this procedure, which was caused most likely due to the use of anhydrides instead of acyl chlorides in this route.

Polymer **P7** was partially functionalized with NHS-ester by reaction with 0.25-1 equivalents of N-hydroxysuccinimide in the presence of di-isopropylcarbodiimide (DIC) (**P8-P11**). The polymers were obtained with good control over the NHS-ester content, as demonstrated by ^{1}H-NMR spectroscopy. However, these polymers proved hygroscopic upon storage and were not soluble in volatile organic solvents, which renders processing of the material difficult. The analytical data of the synthesized polymers via routes **A1-A3** are listed in **Table 2**.

Table 2 Analytical data of **NHS-POx** polymers synthesized via route A

Route	#	Chemical structure	% funct.	% NHS	Yield[a]		Solubility	(Dis)advantages
			x	^{1}H-NMR	g	%		
A1	P4	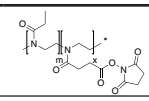	10	11	1.9	7	• DMF • DMSO • $CHCl_3$	-Insoluble polymers were obtained when x >20
A2	-	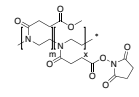	25	16 (COOH)	-	-	-	-Ester hydrolysis was not reproducible -No NHS-ester functionalized polymers were obtained
A3	P8	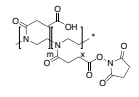	25	29	1.3	58	• DMF • DMSO • Water	+ Degree of functionalization - Polymers are not soluble in volatile organic solvents
	P9		50	44	0.9	50		
	P10		75	80	1.9	43		
	P11	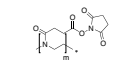	100	98	0.9	36	• DMF • DMSO	+ Degree of functionalization - Only soluble in non-volatile organic solvents

[a] Overall yield

2.2 Route B: CROP followed by NHS-ester modification

In route **B**, cationic ring opening polymerization (CROP) and post-polymerization modification strategies were used to synthesize **NHS-POx**. A great advantage of this approach as compared to route **A** is the precise control over polymerization parameters (e.g. monomer ratios, degree of polymerization (DP) and sequence of monomer addition), thereby facilitating excellent control over the polymer architecture[10, 44]. Additionally, the combination of functionalizable (MestOx) and non-functionalizable monomers (EtOx and *n*PropOx), allowed good control over the amount of incorporated functional groups in the side chains and overall polarity of the polymers. Using this route, we synthesized both copolymers containing *n*PropOx and NHS-ester groups (P(*n*PropOx-NHS), **P12-P20**) and copolymers containing *n*PropOx, EtOx and NHS-ester groups (P(*n*PropOx-EtOx-NHS), **P21-P24**). Similar reaction conditions were applied to convert methyl esters to NHS-esters, as reported for route **A1**.

2.2.1 Monomer synthesis

Since both *n*PropOx and MestOx are not commercially available, both monomers had to be synthesized, via procedures described in literature[45, 46]. In short, *n*PropOx (**1**) was obtained by refluxing butyronitrile and ethanolamine with zinc acetate ($Zn(OAc)_2$) as a catalyst (**Scheme 2**). For MestOx, a two-step approach was followed, because of the labile character of the methyl ester side chain. First, a monomer precursor (**2**) was formed, after which ring closure was facilitated by reaction with Na_2CO_3, which resulted in the formation of MestOx (**3**). This reaction was performed on the rotary evaporator to drive the reaction to completion by removal of the formed water and CO_2. After workup via washing steps, both crude monomers were obtained.

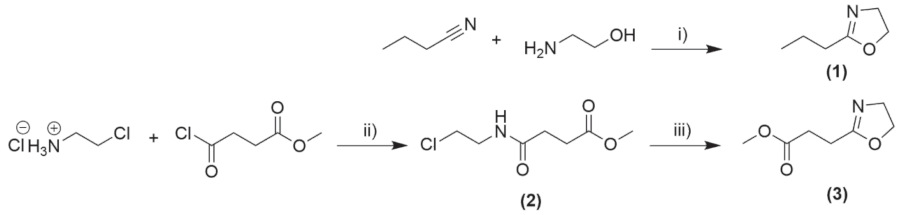

Scheme 2 Overview of monomer synthesis *n*PropOx (**1**) and MestOx (**3**). Conditions: i) $Zn(OAc)_2$ (cat.), 120°C, overnight, ii) Et_3N, DCM, 0°C, iii) Na_2CO_3 (0.9 eq.), 60°C, 20 mbar, overnight.

Monomer purity is crucial for successful cationic ring opening polymerization (CROP), since traces of residuals (solvent or other impurities) can terminate this reaction, resulting in ill-defined polymers. On smaller scale this can be achieved

by vacuum distillation using conventional laboratory equipment. In addition, for some substituted 2-oxazolines like MestOx, short path distillations (Kugelrohr) were advocated as a preferred distillation procedure. However, the scale of this equipment is mainly limited to small volumes (<100 mL). Therefore, we utilized wiped film evaporation (WFE), a purification approach which has proven its value in many applications, for example the purification of essential oils[47] and the removal of volatile components from polymer melts[48]. For our purpose, we used WFE for selective distillation of *n*PropOx and MestOx from the higher boiling impurities, which were still present after the washing workup steps. An additional benefit of WFE over other purification methods is that it allows for constant supply of crude amounts of monomer during distillation, thereby making it a continuous process.

Using this approach, the crude products (**1-3**) were distilled. An overview of the process, which involved several steps, is shown schematically in **Figure 2**. In the first step, the crude mixture was added dropwise (**Figure 2A**) from the feed onto the heated mantle equipped with a rotating blade (**Figure 2B**). Here, an agitated thin film was spread over the heated mantle, thereby creating a homogeneous surface for distillation. After optimizing the conditions for distillation (pressure, oil and condenser temperature), only the desired lower boiling products condensed on the internal condenser unit (based on cooling water), thereby separating them from the higher boiling contaminants (**Figure 2C**). As a result, the higher boiling contaminants were collected in the residual fraction (**Figure 2D**), while the product of interest (monomer) was collected separately (**Figure 2E**). It proved important to remove traces of volatile solvents from the crude mixture prior to distillation, since these were otherwise co-distilled together with the desired monomer. The experimental conditions of the distillation are listed in **Table 3**.

Both monomers **1** and **3** were purified twice by wiped film evaporation and were kept under argon atmosphere to ensure dry conditions for polymerization. Both monomers were obtained in large amounts, 168 g (26% yield) and 86 g (80% yield) for **1** and **3** respectively, demonstrating the scalability of both the synthesis route and the used distillation method.

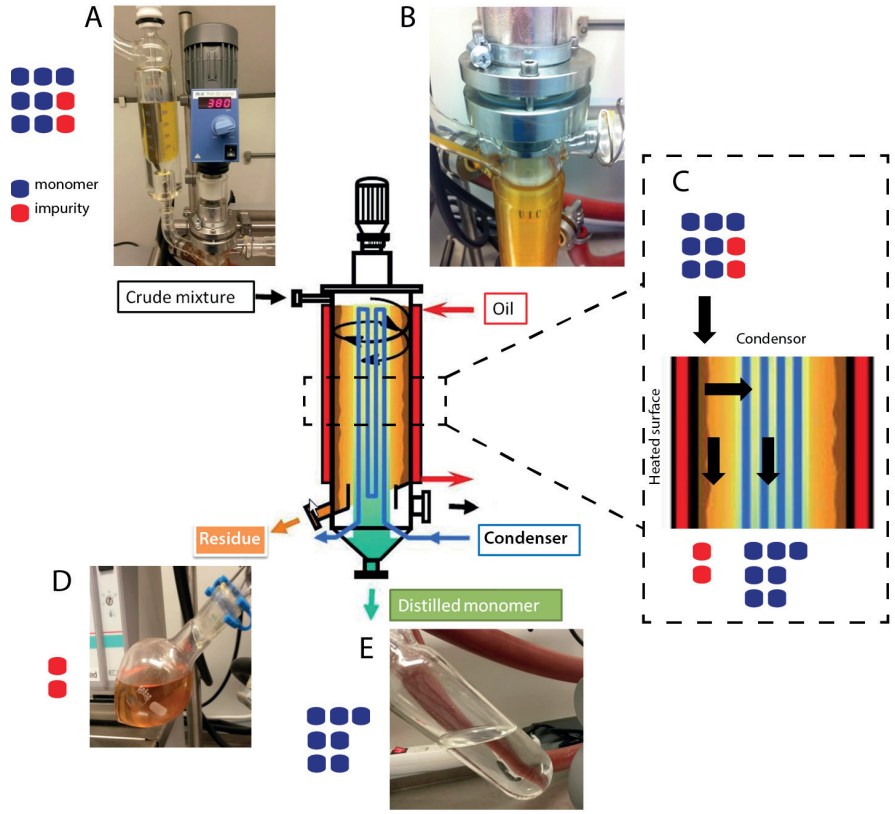

Figure 2 Overview of various stages of WFE purification. A) Addition of the crude mixture from the feed, B) Creation of a homogeneous film over the heated mantle, C) Schematic of the distillation process, D) Residue after distillation, E) Monomer obtained after distillation

Table 3 Experimental conditions during WFE-purification

#		T_{feed}	$T_{condenser}$	T_{oil}	pressure	Yield	
		(°C)	(°C)	(°C)	(mbar)	(g)	(%)
1	*n*PropOx	30	20	44	$1.5*10^{-1}$	167.7	26
2	MestOx-precursor	40	45	87	$4.4*10^{-2}$	186.5	53
3	MestOx	40	27	60	$2.3*10^{-1}$	86.3	80

2.2.2 Polymer synthesis

After successfully synthesizing the monomers, the polymers were prepared by cationic ring opening polymerization (CROP) using microwave reaction conditions[49] (**Scheme 4**). For the copolymerization, the monomers (EtOx, *n*PropOx and MestOx) were mixed in the desired ratios to form statistical copolymers with close to random monomer distribution as previously reported[40]. In these experiments, methyl tosylate was used as an initiator and piperidine as a terminating agent which prevents saponification of the methyl ester side chains of MestOx. After threefold precipitation in ether, **P12a-P24a** were obtained in multigram scale at high yields (>70%). Subsequently, these polymers were post-functionalized by hydrolysis of the methyl ester side chains to carboxylic acid moieties using 1M NaOH yielding **P12b-P24b** (**Scheme 3, ii**).

For the workup of these polymers (**P12b-P24b**), we exploited the lower critical solution temperature (or LCST-behavior) of *n*PropOx-containing polymers[50]. Since these polymers contained both *n*PropOx and carboxylic acid groups, these polymers were both temperature- and pH-responsive. The workup of these polymers was performed by decreasing the pH of the solution from 12 to 4 in order to protonate the carboxylate side chains, and subsequent heating, which caused the polymers to precipitate. After multiple cycles of i) dissolving the polymers in water, ii) precipitating the polymers by heating the polymer solution and iii) redissolving the polymer in water, the water-soluble impurities were separated from the polymers. Subsequently, polymers **P12b-P24b** were obtained as pure white powders in multigram quantities. It must be noted that syntheses of **P19b** and **P20b** (with 20 and 10 molar percent of *n*Propox groups, respectively) proceeded at low yield due to the low amount of thermoresponsive *n*PropOx groups. Nevertheless, the above-mentioned procedure confirms that the thermoresponsive behavior of these copolymers can be exploited for the purification of a wide range of *n*PropOx-containing polymers. A systematic study of the LCST-behavior of *n*PropOx-containing polymers is described in **Chapter 3**.

The purified polymers were further modified using DIC and NHS towards NHS-ester functional polymers. After workup by precipitation, they were obtained with good control over the number of functional groups, based on analysis by ^{1}H-NMR-spectroscopy. All polymers (except for **P19** and **P20**) were synthesized in multigram quantities using this route at overall yields (over three steps) ranging from 18-60% and with control over the dispersity values (Đ 1.1-1.3, **Table 4**). ^{1}H-NMR spectra of the assigned resonances of **P21** and the intermediate products can be found in Figure 3.

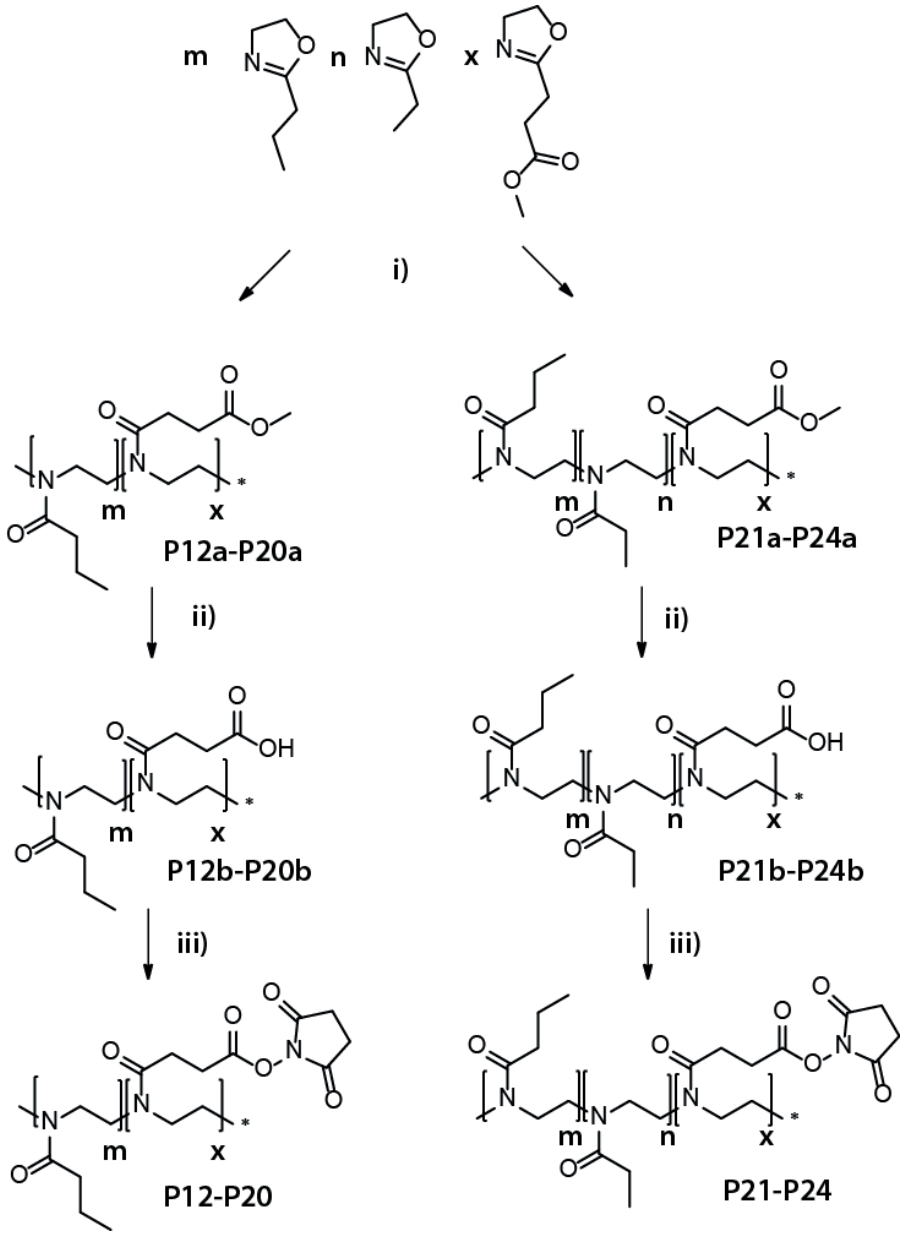

Scheme 3 Synthesis scheme of **P12**-**P24**. Conditions: i) methyl tosylate, 140°C, MeCN, ii) 0.1 M NaOH, rt, iii) NHS-OH, DIC, DMF/DCM (v/v, 1:9)), rt

Table 4 Analytical data of the synthesized polymers (**P12**-**P24**)

#	Chemical structure	%func. (theor.)	% funct. (^{1}H-NMR)			SEC (PMMA)[a]		Yield[b]	
	P(*n*PropOx-NHS)	x	MestOx	COOH	NHS	M_n (kDa)	*Đ*	g	%
P12	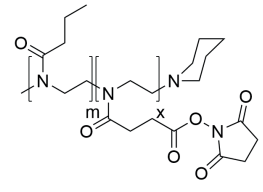	10	10	8	10	29.6	1.16	6.1	52
P13		20	21	20	21	[c]	[c]	6.4	54
P14		30	30	30	27	29.6	1.19	1.8	15
P15		40	42	39	42	34.5	1.23	1.3	23
P16		50	49	49	50	27.7	1.13	4.9	30
P17		60	60	60	54	30.8	1.29	1.4	62
P18		70	72	65	65	31.8	1.32	1.0	42
P19		80	79	75	[d]	21.0	1.24	[c]	[c]
P20		90	89	85	[d]	24.1	1.40	[c]	[c]
	P(*n*PropOx-EtOx-NHS)	m-n-x							
P21	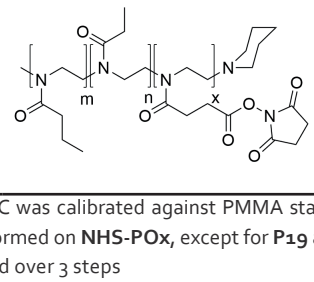	40-50-10	9	10	11	12.5	1.18	2.9	22
P22		50-40-10	11	11	12	12.3	1.16	5.6	42
P23		40-35-25	24	24	28	16.8	1.22	4.7	18
P24		50-25-25	23	20	24	14.6	1.18	4.5	35

[a] SEC was calibrated against PMMA standards, eluent: 0.1 % LiCl in DMA. SEC measurements were performed on **NHS-POx,** except for **P19** and **P20,** which were performed on COOH-functionalized POx
[b] Yield over 3 steps
[c] not determined
[d] not synthesized

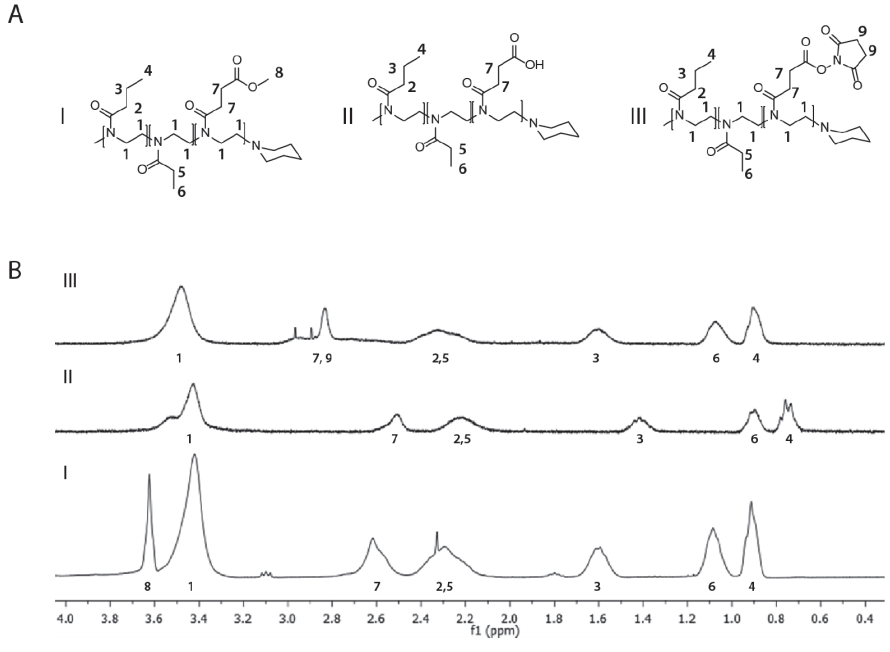

Figure 3 Representative ^{1}H-NMR spectra of P(*n*PropOx-c-EtOx-c-NHS) (**P21**) and intermediate products. A) Structural formulas of I (**P21a**), II (**P21b**) and III (**P21**), B) Assigned ^{1}H-NMR signals of **P21** and intermediate products.

2.3 Route C: CROP followed by post-polymerization modification and NHS-ester modification

Via route **C**, we synthesized a series of **NHS-POx** containing groups of different polarity, but in contrast to route **B**, post-polymerization modification strategies were used to introduce the hydrophilic moieties. To this end, we prepared copolymers consisting of *n*PropOx and MestOx, as described in route **B**. Since the methyl ester groups can be modified by direct amidation[17] using a wide range of functional amines, we utilized this to introduce a wide range of hydrophilic groups (hydroxyl, methyl ether and dimethylamine) on the polymer (**Scheme 4**). Subsequently, via the hydroxyl groups, we introduced carboxylic acid groups by reaction with succinic anhydride. In a final step, we activated the carboxylic acid groups to NHS-esters using the reaction conditions as used for routes **A** and **B**. This route offered several advantages over previously described routes. Firstly, we created polymers equipped with hydrolytically sensitive ester groups in the side chains, which should allow faster degradation than the polymers prepared in routes **A** and **B**. Moreover, the polymers prepared via this route (**A26**-**A28**) are equipped with an extended spacer length between the polymer backbone and the crosslinking group, compared to the

polymers prepared via routes **A** and **B**. This gives this class of polymers more mobile crosslinking groups, which can be beneficial in terms of crosslinking efficacy.

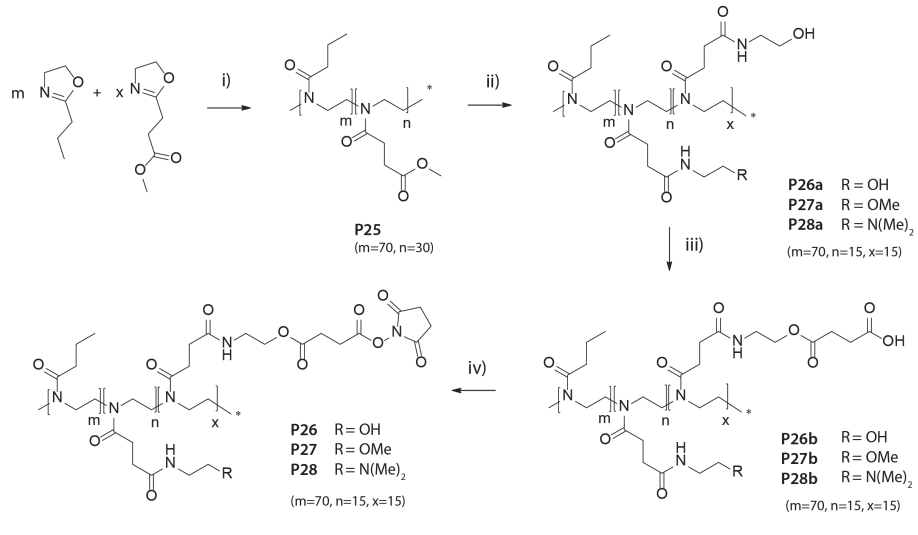

Scheme 4 Synthesis of **P26**-**P28**. Reaction conditions: i) methyl tosylate, 140°C, MeCN, ii) ratio of functional amines, 60°C, 300 mbar, rt (**P26a**, amine used: 2-amino-ethanol , 7 eq.; **P27a**, amines used: 2-amino-ethanol /2-methoxy-ethylamine (1:1), 7 eq. ; **P28a**, amines used: 2-amino-ethanol/N^1,N^1-dimethyl-1,2-ethylene diamine (1:3), 14 eq.), iii) succinic anhydride, DMAP, DMF/DCM (v/v, 1:9, rt), iv) acetic acid, NHS-OH, DIC, DCM, rt.

First, P(*n*PropOx-c-MestOx) (**P25**) was synthesized similar to route **B**. Subsequently, the methyl ester groups on the polymer were amidated by heating the polymer (60°C) in 2-amino-ethanol under reduced pressure (300 mbar), thereby driving the reaction to completion by favoring the release of methanol. As a consequence, a hydroxyl-functional polymer was obtained (**P26a**).

For **P27a** and **P28a**, we converted half of the ester groups to the hydroxyl moiety for further modification towards NHS-ester moieties, and half of the ester groups to a hydrophilic component (OMe for **P27** and $N(CH_3)_2$ for **P28**). To this end, we screened various ratios of functional amines to obtain the desired incorporation onto the polymer. An equimolar ratio of 2-amino-ethanol and 2-methoxyethylamine was needed for incorporation of a 1:1 molar ratio of functional groups into **P27a**. For **P28a**, a 3:1 molar ratio of N^1,N^1-dimethyl-1,2-ethylene diamine and 2-amino-ethanol was needed to achieve this. Subsequently, the hydroxyl-functionalized side chains of these polymers (**P26a**-**P28a**) were converted to carboxylic acid moieties, yielding **P26b**-**P28b.**

For **P26b**, we aimed to partially convert the hydroxyl groups into carboxylic acid moieties, thereby retaining half of the hydroxyl groups as hydrophilic component in the final polymer. Several conditions were screened for optimization of this reaction. Different equivalents of succinic anhydride (with respect to hydroxyl groups) were investigated and different catalysts were used, namely (I) tri-ethylamine (Et_3N), (II) 1,8-diazabicyclo[5.4.0]undec-7-ene (DBU) and (III) 4-dimethylaminopyridine (DMAP). The reactions were monitored by ^{1}H-NMR spectroscopy (**Figure 4**), since the protons next to the hydroxyl group at 3.3 ppm (**a**) shift downfield to 4.2 ppm (**b**) upon esterification of the side chains, thereby making a clear distinction between unreacted and reacted side chains, which allowed easy determination of the conversion. The reaction conditions and the results of these screening reactions are listed in **Table 5**.

As can be observed from **Table 5**, the reactions in which no base was utilized (Entries 1-5) resulted in poor control over the incorporation of functional groups since physical gels were formed during these reactions. In the screening reaction where DBU was used (Entry 6), the reaction mixture turned deep red and no conversion was observed by ^{1}H-NMR spectroscopy. Although conversion was observed using Et_3N (Entry 7), the reaction mixture turned pink and it was difficult to remove Et_3N using the consecutive precipitation steps in acetone and Et_2O. The reactions using DMAP proved most effective since precise incorporation of carboxylic acid groups could be achieved by adding a slight excess of succinic anhydride over the desired ratio of functional groups. Although most of the DMAP could be removed by precipitation steps, removal of the remaining traces required an additional filtration step over propylsulfonic acid bonded silica particles (SCX-2). This procedure resulted into the synthesis of P(*n*PropOx-c-OH-c-COOH) copolymer in good purity and therefore we selected the conditions used in Entry 9 for synthesis of **P26b**.

For **P26b**, the addition of DMAP as a catalyst resulted into a desired (1:1 molar) incorporation of functional groups (18 mol% COOH). For both **P27b** and **P28b**, all hydroxyl moieties needed to be converted to carboxylic acids. Therefore, an excess of succinic anhydride was used to drive the reaction to completion, which yielded polymers with the desired incorporation of carboxylic acid groups. Subsequently, these carboxylic acid moieties were fully converted to NHS-ester functional polymers thereby yielding **P26**-**P28** with the desired incorporation of functional groups as determined using ^{1}H-NMR spectroscopy (**Figure 5**). The analytical data of the synthesized polymers (**P26**-**P28**) and intermediate products are listed in **Table 6**.

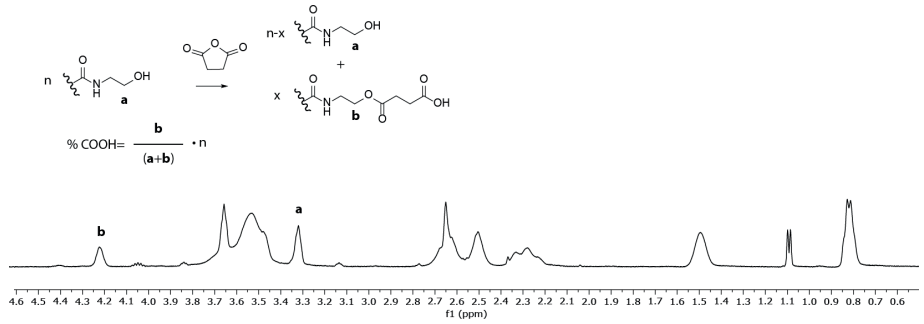

Figure 4 ^{1}H-NMR spectrum indicating the partial conversion of the hydroxy-terminal side chains into carboxylic acid-functionalized side chains by a shift of protons **a** (3.3 ppm) into **b** (4.2 ppm). (n = molar percentage of OH functionalized side chains)

Table 5 Reactions conditions optimization for **P26b**

	Succinic anhydride			T	%mol COOH[a]	
#	eq. towards OH	catalyst (eq.)	Solvent	(°C)	Theor.	^{1}H-NMR[b]
1	0.32	-	MeCN	100	10	4
2	0.45	-	MeCN	100	14	8
3	0.7	-	MeCN	100	21	10
4	0.85	-	MeCN	100	26	12
5	0.5	-	MeCN	100[c]	15	5
6	0.5	DBU (1)	MeCN (20 v% DMF)	rt	15	[d]
7	0.5	Et_3N (1)	MeCN (20 v% DMF)	rt	15	17
8	0.5	DMAP (0.7)	DCM (10v% DMF)	rt	15	12
9	0.67	DMAP (0.7)	DCM (10v% DMF)	rt	20	18

Conditions: All screening reactions (#1-#9) were performed on **P26a** using the reaction conditions described above using a reaction molarity of 1M. Theoretical amount % COOH= molar percentage of carboxylic acid groups on polymer at full conversion of succinic anhydride.

[a] Based on **P26a** (P(*n*PropOx-c-OH) 70-30 (n=30 hydroxyl groups))

[b] Samples were measured in D_2O.

[c] Sample was heated for 30 minutes under microwave irradiation

[d] No conversion was observed by ^{1}H-NMR spectroscopy.

Table 6 Analytical data of synthesized polymers (**P26-P28**) and intermediate products

#	Polymer	^{1}H-NMR (mol%)					M_n (kg/mol)		
	R=OH	MestOx	OH	R	COOH	NHS	Theor.	SEC[a]	Đ[a]
P25	P(*n*PropOx-c-MestOx)	31	-	-	-	-	12.7	11.3	1.12
P26a	P(*n*PropOx-c-OH)	-	31	-	-	-	13.6	13.9	1.11
P26b	P(*n*PropOx-c-OH-c-COOH)	-	13	-	18	-	15.1	-	-
P26	P(*n*PropOx-c-OH-c-NHS)	-	14	-	-	17	16.5	18.8	1.25
				OMe					
P27a	P(*n*PropOx-c-OMe-c-OH)	-	15	16	-	-	13.6	12.4	1.16
P27b	P(*n*PropOx-c-OMe-c-COOH)	-	-	17	14	-	15.1	-	-
P27	P(*n*PropOx-c-OMe-c-NHS)	-	-	17	-	14	16.5	21.1	1.35
				$N(CH_3)_2$					
P28a	P(*n*PropOx-c- $N(Me)_2$-c-OH))	-	14	17	-	-	13.6	11.0	1.15
P28b	P(*n*PropOx-c- $N(Me)_2$-c-COOH)	-	-	16	15	-	15.1	-	-
P28	P(*n*PropOx-c- $N(Me)_2$-c-NHS)	-	-	16	-	15	16.5	22.1	1.33

[a] SEC was calibrated against PMMA standards, eluent: 0.1 % LiCl in DMA

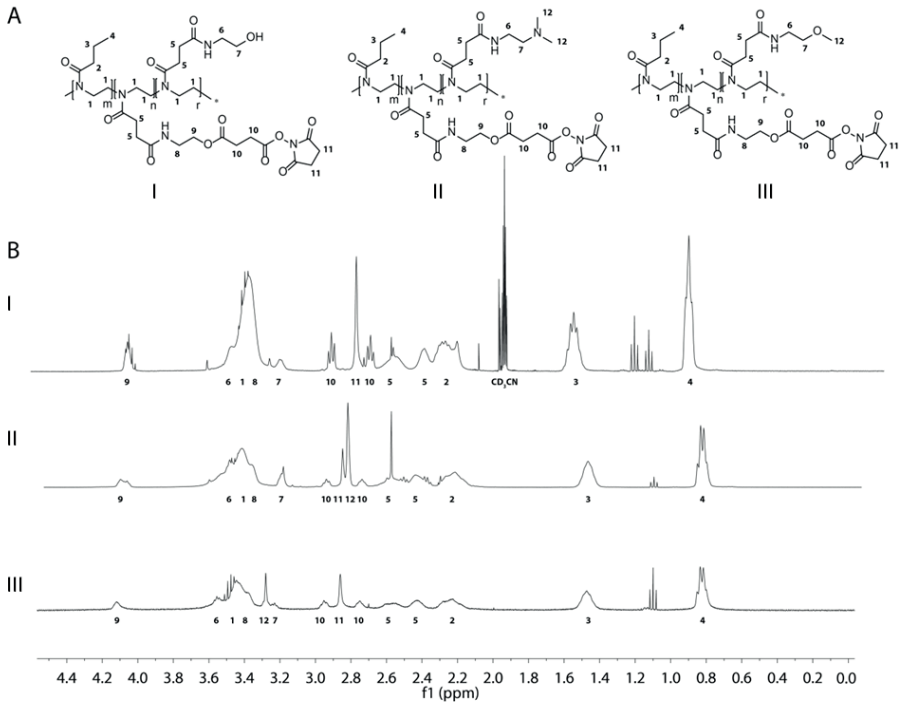

Figure 5 Overview of ^{1}H-NMR spectra of **P26-P28**. A) Structural formulas of **P26** (I), **P28** (II), **P27** III, B) Assigned signals of **P26** (I)(recorded in CD_3CN), **P28** (II) (recorded in D_2O), **P27** (III) (recorded in D_2O).

3. Discussion

After synthesis of the polymers, the three different routes (**A**-**C**) can be compared with respect to the various design criteria which have been set for both the polymer structure and synthetic procedures (see **Table 1**).

In route **A**, we prepared several polymers by both partial and complete hydrolysis of Aquazol 50, yielding l-PEI units, which were subsequently converted into NHS-esters, resulting in **NHS-POx** polymers **P1**-**P4**. Using this route, **P4** (P(EtOx-c-NHS) 90-10) was the only polymer which was obtained with sufficient control over the number of functional groups. Additionally, this polymer was soluble in both aqueous and organic solvents. However, attempts to increase the number of NHS-groups on this polymer resulted in insoluble polymers. Moreover, the total yield for **P4** was low (7%). Although polymers were obtained with the desired number of functional groups using route **A3**, none of these polymers displayed desired solubility characteristics (in both water and volatile organic solvents). In general, all reaction steps in this route proved scalable. However, the use of acyl chlorides resulted in undesired coloration of the polymers, which could not be resolved during workup. In summary, it was concluded that route **A** offered limited freedom to functionalize the polymers. Moreover, the majority of the polymers were poorly soluble in water and/or organic media. As a result, this route was not considered feasible for our purposes.

Using route **B**, different series of **NHS-POx** (P(*n*PropOx-c-NHS) (**P12**-**P18**) and P(*n*PropOx-c-EtOx-c-NHS) (**P21**-**P24**) based copolymers were prepared by CROP and post-polymerization modification strategies. It was demonstrated that both P(*n*PropOx-c-COOH) and P(*n*PropOx-c-EtOx-c-COOH) could be purified in a scalable way by exploiting the intrinsic LCST behavior of these polymers through consecutive heating and cooling cycles in water, thereby omitting the use of organic solvents. The polymers were obtained with good control over the ratio of functional groups. All synthesized **NHS-POx** polymers (**P12**-**P24**) were soluble in volatile organic solvents. The water solubility of **P12** was equal to 10 mg/mL at room temperature, while **P21**-**P24** were soluble up to 40 mg/mL at room temperature, indicating that incorporation of ethyl groups in the polymer structure renders the polymers more water soluble. In conclusion, this route offered the possibility to synthesize a series of different *n*PropOx-containing polymers by employing scalable workup procedures. No notable drawbacks were encountered using this synthetic route. Consequently, route **B** was considered feasible for synthesis of **NHS-POx** polymers.

In route **C**, three different polymers (**P26**-**P28**) were synthesized by CROP and post-polymerization modification strategies (amidation of the methyl esters side chains). The polymers were obtained with good control over the number of functional

groups according to ^{1}H-NMR spectroscopy. During the consecutive reaction steps only a minor increase in polymer dispersity was observed by SEC, which indicates that cross coupling between polymer chains is neglegible. The polymers prepared via route **C** were soluble in both organic and aqueous solvents (10 mg/mL). An additional benefit of these functionalized polymers is the presence of a hydrolytically cleavable linker which facilitates degradation *in vivo*. On the other hand, the synthesis of route **C** involves an additional reaction step compared to route **B**, which can be considered a minor drawback of this procedure. Nevertheless, this route offers the possibility to introduce a wide range of hydrophilic functionalities in addition to NHS-esters, thereby offering superior control over the reactivity of medical devices based on **NHS-POx**.

4. Conclusion

In this chapter, various synthetic routes (**A**-**C**) towards NHS-ester functionalized POx have been described. The main objective of this study was the development of a robust procedure, which would give much freedom in the choice and amounts of functional side chains on the polymers. The route based on hydrolysis of POx into l-PEI units and further postmodification into **NHS-POx** (route **A**) was not considered feasible since the synthetic procedures did not allow for easy functionalization. Moreover, most polymers prepared via this route lacked solubility in e.g. volatile organic solvents. Using route **B**, we prepared a series of P(*n*PropOx-c-NHS) and P(*n*PropOx-c-EtOx-c-NHS) polymers by CROP and post polymerization modification strategies. Using this route, polymers were prepared with good control over the number of functional groups. Moreover, the prepared polymers were soluble in volatile organic solvents and aqueous media. The synthesis procedures were scalable and applicable for the majority of polymers. Using route **C**, polymers were prepared by CROP and post-polymerization modification strategies with good control over the ratio of incorporated functional groups. The post modification was not only used to introduce the NHS esters, but also side chains with different polarities, which makes this route probably the most versatile of the three approaches reported.

Taken all factors into account, from a synthesis perspective, only route **B** and route **C** have proven to be viable routes for the development of **NHS-POx**. This provides us with a robust platform to prepare functional POx systems for application in hemostatic devices.

5. Acknowledgements

Petra Bouten, Bram Keereweer, Joost Opsteen, Elena Gago Benidí, Maria José Sanchez Fernandez, Harry van der Laan, Elvy de Hoog, Tim Janssen, Pieter Gilissen, Kerry McGowen and Jon Donkers are kindly acknowledged for their contributions to the work described in this chapter

6. Experimental procedures

6.1 Materials

All reagents (synthesis grade) for the synthesis of the monomers were purchased at Sigma Aldrich and used without further purification, unless stated otherwise. All reagents for the synthesis of the polymers were distilled twice before use in the polymerizations. Acetonitrile (obtained from Actu-all Chemicals) was dried and dispensed under nitrogen atmosphere by using an MBraun MB SPS-800 solvent dispersing system.

6.2 Characterization

^{1}H-NMR and ^{13}C-NMR spectra were recorded on a Bruker Avance III 500MHz spectrometer using the solvents D_2O, MeOD, $CDCl_3$ or DMSO-*d*6. FT-IR measurements were performed on a Bruker Tensor 27 IR ATR spectrometer. Microwave-assisted polymerizations were performed in a Biotage Initiator+, equipped with an autosampler. Size exclusion chromatography (SEC) was performed on an Agilent 1260 - series HPLC system equipped with a 1260 online degasser, a 1260 ISO-pump, a 1260 automatic liquid sampler, a thermostatted column compartment, a 1260 diode array detector (DAD) and a 1260 refractive index detector (RID). Analyses were performed on two Mixed-D and a guard column in series at 50 °C. As an eluent, *N,N*-dimethyl acetamide (DMA), containing LiCl (concentration 50 mM), was used at a flow rate of 0.593 ml min^{-1}. The SEC traces were analyzed using the Agilent Chemstation software with the GPC add on. Number average molecular weights (M_n), weight average molecular weights (M_w), and dispersity (Đ) values were calculated against poly(methyl methacrylate) (PMMA) standards. Monomers were distilled using a KDL-1 Wiped film evaporation setup (UIC GmbH) containing both an oil pump and an oil diffusion pump.

6.3 Synthesis route A

Synthesis of these polymers was based on a procedure described in literature[39].
Note: since highly polydisperse Aquazol 50® was used in this study as a starting

polymer (Đ 3-4), SEC measurements were not performed. End group functionality was furthermore not defined.

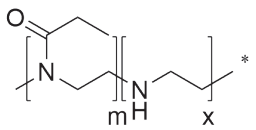

P1 P(EtOx-c-l-PEI) 90-10 - P(EtOx) (25 g, 0.50 mmol) was dissolved in a 6M-HCl-solution (525 ml) and heated in a pre-heated oil bath (73°C) for 2 hours and 20 minutes. Afterwards, the reaction mixture was evaporated to dryness. A 4M-NaOH-solution (600 mL) was added. The pH of the solution turned 10. The polymer was extracted from the aqueous layer twice with DCM (500 mL). The combined organic fractions were dried over anhydrous Na_2SO_4 and subsequently filtered. The solvent was evaporated under reduced pressure. **P1** was obtained as a white foam (21.4 g, 92% yield). **^{1}H NMR** (500 MHz, MeOD) δ 3.70-3.50 (b,m•4H, NCO-C$\underline{H}_2$C$\underline{H}_2$N), δ 2.73 (s,x•4H, NH-C$\underline{H}_2$-C$\underline{H}_2$-NH), 2.40-2.20 (b, m•2H, CO-C$\underline{H}_2$-CH$_3$), 1.10-1.00 (b, m•3H, CO-CH$_2$-C$\underline{H}_3$). Experimentally determined monomer ratio (m/x): 89/11

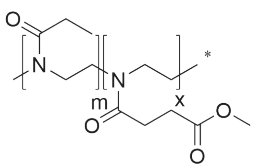

P2 P(EtOx-c-MestOx) 90-10 - P1 (21.4 g, 0.53 mmol, 26.3 mmol functional groups, 1 eq.) was added to a flame dried Schlenk-flask and subsequently dissolved in DCM (135 mL) under a flow of argon. Next, the solution was cooled using an ice bath (0°C) and methyl succinyl chloride (5.95 mL, 0.10 mol, 4 eq.) and Et$_3$N (9.1 mL, 0.13 mol, 5 eq.) were added dropwise. Next, the reaction mixture was stirred overnight and turned brown. Afterwards, the organic layer was washed twice with a 5% Na_2CO_3-solution (50 mL). The combined organic fractions were dried over anhydrous Na_2SO_4 and subsequently filtered. The solvent was evaporated under reduced pressure. Since residual Et$_3$N was present (observed by ^{1}H-NMR spectroscopy), the polymer was dissolved in toluene, and Et$_3$N was co-evaporated with this organic solvent (100 mL). Subsequently, the polymer was dissolved in DCM (100 mL) and precipitated in Et$_2$O (2 L). The precipitate was redissolved in DCM (100 mL) and finally the solvent was evaporated under reduced pressure. **P2** was obtained as a brown foam (19.2. g, 79% yield). **^{1}H NMR** (500 MHz, MeOD) δ 3.70 (br,x•3H, OC$\underline{H}_3$), δ 3.70-3.50 (b,(m+x)•4H, NCO-C$\underline{H}_2$C$\underline{H}_2$N), δ 2.80-2.60 (b,x•4H, CO-C$\underline{H}_2$-C$\underline{H}_2$-CO), 2.40-2.20 (b, m•2H, CO-C$\underline{H}_2$-CH$_3$), 1.10-1.00 (b, m•3H, CO-CH$_2$-C$\underline{H}_3$). Experimentally determined monomer ratio (m/x): 89/11

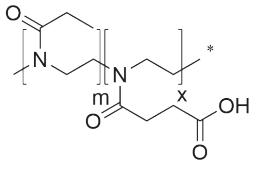

P3 P(EtOx-c-COOH) 90-10 - P2 (19.1 g, 0,36 mmol, 18.1 mmol functional groups, 1 eq.) was dissolved in MeOH (505 mL). Subsequently, water (505 mL) and LiOH (17.8 g, 0.43 mol, 24 eq) were added and the reaction mixture was stirred for 3 hrs. Next, the reaction mixture was concentrated under reduced pressure. Subsequently, the polymer was dissolved in MeOH (300 mL) and precipitated in cold acetone (2 L). The precipitate was redissolved

in MeOH (300 mL), dried over anhydrous Na_2SO_4 and subsequently filtered. The solvent was evaporated under reduced pressure. **P3** was obtained as a brown powder (11.3. g, 60% yield). **^{1}H NMR** (500 MHz, D$_2$O) δ 3.70-3.40 (b,(m+x)•4H, NCO-C$\underline{H}_2$C$\underline{H}_2$N), δ 2.80-2.60 (b,x•4H, CO-C$\underline{H}_2$-C$\underline{H}_2$-CO), 2.50-2.25 (b, m•2H, CO-C$\underline{H}_2$-CH$_3$), 1.15-1.00 (b, m•3H, CO-CH$_2$-C$\underline{H}_3$). Experimentally determined monomer ratio (m/x): 89/11

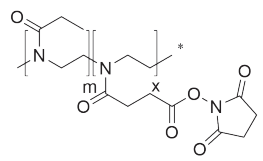

P4 P(EtOx-c-NHS) 90-10 - P3 (11.3 g, 0.36 mmol, 10.9 mmol functional groups, 1 eq.), EDC·HCl (4.7 g, 24.5 mmol, 2.2 eq.) and NHS-OH (2.82 g, 24.5 mmol, 2.2 eq.) were dissolved in DMA (141 mL) and the reaction mixture was stirred overnight. Next, the reaction mixture was concentrated under reduced pressure. Subsequently, the polymer was dissolved in DCM (300 mL) and the organic phase was washed with water (100 mL, 2x) and brine (100 mL, 2x), dried over anhydrous Na_2SO_4 and filtered. The solvent was evaporated under reduced pressure, yielding a sticky brown foam. Subsequently, the polymer was dissolved in DCM (100 mL) and precipitated in cold ether (1 L). This was performed 4 times. **P4** was obtained as a brown powder (1.9. g, 15% yield). **^{1}H NMR** (500 MHz, D$_2$O) δ 3.70-3.40 (b,(m+x)•4H, NCO-C$\underline{H}_2$C$\underline{H}_2$N), δ 3.00-2.45 (b,x•4H, CO-C$\underline{H}_2$-C$\underline{H}_2$-CO+ (b,x•4H, CO-C$\underline{H}_2$-C$\underline{H}_2$-CO (NHS)), 2.50-2.25 (b, m•2H, CO-C$\underline{H}_2$-CH$_3$), 1.15-1.00 (b, m•3H, CO-CH$_2$-C$\underline{H}_3$). Experimentally determined monomer ratio (m/x): 88/12

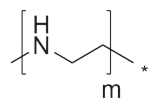

P5 l-PEI - P5 was synthesized similar as **P1** using identical amounts of reagents but different hydrolysis conditions (16 hrs at 110°C). **P5** was obtained as a white powder (9.2 g, 85% yield). **^{1}H NMR** (500 MHz, MeOD) δ 2.73 (s,x•4H, NH-C$\underline{H}_2$-C$\underline{H}_2$- NH).Experimentally determined monomer ratio (m/x): 0/100

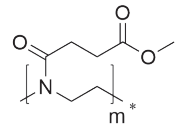

P6 P(MestOx) - The reaction was performed similar to **P3** using **P5** (3.0 g, 0.14 mmol, 70 mmol functional groups, 1 eq.), methyl succinyl chloride (23.8 mL, 29.8 g, 195 mmol, 2.8 eq.) and Et$_3$N (24.2 mL, 17.7 g, 174 mmol, 2.5 eq.) in DMA (200 mL). **P6** was obtained as a dark brown foam (7.3 g, 67% yield). **^{1}H NMR** (500 MHz, MeOD) δ 3.70 (br,m•3H, OC$\underline{H}_3$), δ 3.70-3.50 (b,m•4H, NCO-C$\underline{H}_2$C$\underline{H}_2$N), δ 2.80-2.60 (b,m•4H, CO-C$\underline{H}_2$-C$\underline{H}_2$-CO). Experimentally determined monomer ratio (m/x): 100/0

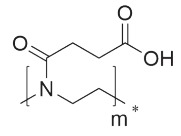

P7 P(COOH) - P5 (5.0 g, 0,23 mmol, 116.2 mmol functional groups, 1 eq.), succinic anhydride (23.2 g, 232.4 mmol, 2 eq) and Et$_3$N (40.3 mL, 29.4 g, 290.5 mmol, 2.5 eq.) were dissolved in DMSO (140 mL). The reaction mixture was stirred overnight. Next, the reaction mixture was

precipitated in cold acetone (2 L) and subsequently triturated for 2 hrs. Next, the precipitate was filtered off and subsequently washed on a glass filter with acetone (100 mL, 3x) and with Et_2O (100 mL, 3x). In a final step, the polymer was dried under reduced pressure. **P7** was obtained as a white powder (13.2 g, 80% yield).**^{1}H NMR** (500 MHz, D_2O) δ 3.70-3.30 (b, m•4H, NCO-C$\underline{H}_2$C$\underline{H}_2$N), δ 2.60-2.45 (b,m•4H, CO-C$\underline{H}_2$-C$\underline{H}_2$-CO). Experimentally determined monomer ratio (m/x): 100/0

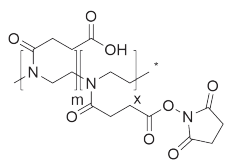

P8- P11

P8 P(COOH-c-NHS) 75-25 - P7 (1.3 g, 0.018 mmol, 9 mmol functional groups, 1 eq.), NHS-OH (0.26 g, 2.2 mmol, 0.25 eq.), DIC (2.81 mL, 2.27 g, 18 mmol, 2 eq.) and DMAP (112 mg, 0.9 mmol, 0.1 eq) were dissolved in DMSO (15 mL). The reaction mixture was stirred overnight. Next, the reaction mixture was precipitated in cold THF (500 mL). Subsequently, the precipitate was dissolved in DMF (30 mL) and precipitated in cold Et_2O (500 mL). The precipitate was filtered off and subsequently washed on a glass filter with DCM (100 mL, 3x), acetone (100 mL, 3x) and Et_2O (100 mL, 3x). In a final step, the polymer was dried under reduced pressure. **P8** was obtained as a grey powder (1.32 g, 86% yield). **^{1}H NMR** (500 MHz, D_2O) δ 3.70-3.30 (b, (m+x)•4H, NCO-C$\underline{H}_2$C$\underline{H}_2$N), δ 3.00-2.45 (b,(m+x)•4H, CO-C$\underline{H}_2$-C$\underline{H}_2$-CO+ (b,x•4H, CO-C$\underline{H}_2$-C$\underline{H}_2$-CO (NHS)). Experimentally determined monomer ratio (m/x): 71/29

P9 P(COOH-c-NHS) 50-50 - The reaction was performed similar to **P8** using **P7** (1.0 g, 0.02 mmol, 6.9 mmol functional groups, 1 eq.), NHS-OH (0.40 g, 3.5 mmol, 0.50 eq.), DIC (2.15 mL, 1.74 g, 13.8 mmol, 2 eq.) and DMAP (84.3 mg, 0.69 mmol, 0.1 eq). **P9** was obtained as a white powder (0.9 g, 74% yield)**. ^{1}H NMR** (500 MHz, D_2O) δ 3.70-3.30 (b, (m+x)•4H, NCO-C$\underline{H}_2$C$\underline{H}_2$N), δ 3.00-2.45 (b,(m+x)•4H, CO-C$\underline{H}_2$-C$\underline{H}_2$-CO+ (b,x•4H, CO-C$\underline{H}_2$-C$\underline{H}_2$-CO (NHS)). Experimentally determined monomer ratio (m/x): 56/44

P10 P(COOH-c-NHS) 25-75 - The reaction was performed similar to **P8** using **P7** (2.0 g, 0.028 mmol, 13 mmol functional groups, 1 eq.), NHS-OH (1.12 g, 9.75 mmol, 0.75 eq.), DIC (4.30 mL, 3.48 g, 27.6 mmol, 2 eq.) and DMAP (168.6 mg, 1.3 mmol, 0.1 eq). **P10** was obtained as a white powder (1.9 g, 63% yield). **^{1}H NMR** (500 MHz, D_2O) δ 3.70-3.30 (b, (m+x)•4H, NCO-C$\underline{H}_2$C$\underline{H}_2$N), δ 3.00-2.45 (b,(m+x)•4H, CO-C$\underline{H}_2$-C$\underline{H}_2$-CO+ (b,x•4H, CO-C$\underline{H}_2$-C$\underline{H}_2$-CO (NHS)). Experimentally determined monomer ratio (m/x): 20/80

P11 P(COOH-c-NHS) 0-100 - The reaction was performed similar to **P8** using **P7** (1.0 g, 0.014 mmol, 6.9 mmol functional groups, 1 eq.), NHS-OH (1.59 g, 13.8 mmol, 2 eq.), DIC (2.15 mL, 1.74 g, 13.8 mmol, 2 eq.) and DMAP (84.3 mg, 0.69 mmol, 0.1 eq). **P11** was obtained as a white powder (0.9 g, 53% yield). **^{1}H NMR** (500 MHz, D_2O) δ 3.70-3.30 (b, (m+x)•4H, NCO-C$\underline{H}_2$C$\underline{H}_2$N), δ 3.00-2.45 (b,(m+x)•4H, CO-C$\underline{H}_2$-C$\underline{H}_2$-CO+ (b,x•4H, CO-C$\underline{H}_2$-C$\underline{H}_2$-CO (NHS)). Experimentally determined monomer ratio (m/x): 2/98

6.4 Route B

6.4.1 Monomer synthesis

***n*PropOx (1)** was synthesized using a modified literature procedure[51]. Butyronitrile (500 mL, 5.75 mol, 1 eq.), 2-amino ethanol (520 mL, 8.61 mol, 1.5 eq.) and $Zn(OAc)_2 \cdot 2H_2O$ (24.7 g; 0.11 mol, 0.02 eq.) as a catalyst were mixed and heated to reflux (~130°C) overnight. The resulting yellow-orange reaction mixture was cooled down to room temperature. Afterwards DCM (1000 mL) was added and the organic layer was washed with water (2x 500 mL) and brine (500 mL). The organic phase was dried over anhydrous Na_2SO_4 and subsequently filtered. The solvent was evaporated under reduced pressure, yielding a yellow oil (256.8 g). This oil was distilled twice ($1.5 \cdot 10^{-2}$ mbar) using the KDL-1. *n*PropOx **(1)** was obtained as a colorless liquid (167.74 g, 26% yield). **^{1}H NMR** (500 MHz, $CDCl_3$) δ 4.13 (t, *J* = 9.5 Hz, 2H, C$\underline{H}_2$-O), 3.74 (t, *J* = 10 Hz, 2H, C$\underline{H}_2$N), 2.16 (m, 2H, C$\underline{H}_2$-CH_2-CH_3), 1.58 (m, 2H, CH_2-C$\underline{H}_2$-CH_3), 0.89 (t, *J* = 7.4 Hz, 3H, CH_2-CH_2-C$\underline{H}_3$) **^{13}C NMR** (500 MHz, $CDCl_3$) δ 167.96, δ 66.66, δ 53.94, δ 29.43, δ 18.98, δ 13.30 **TLC** R_f = 0.82, (MeOH/DCM, v/v, 9:1)

MestOx-precursor (2) was synthesized following a modified literature procedure[40] **-** Methyl succinyl chloride (271.8 g, 1.805 mol, 1 eq.) was dissolved in DCM (2.00 L) and 2-chloroethylamine·HCl (209.2 g, 1.804 mol, 1 eq.) was added. The reaction mixture was cooled to 0°C and Et_3N (535 mL, 3.84 mol, 2.13 eq.) was added drop wise over 2 hours. The reaction mixture was stirred for 4 days. The reaction mixture turned orange and a precipitate (Et_3N-HCl) was formed. Subsequently, the reaction mixture was filtered and divided into three equal parts. Each part was washed twice with water (2 x 80 mL) and brine (1 x 80 mL). The organic layers were combined and dried over anhydrous Na_2SO_4 and subsequently filtered. The mixture was evaporated under reduced pressure yielding a brown oil (323.7 g). The oil was distilled twice ($4.4 \cdot 10^{-3}$ mbar) using the KDL-1. MestOx-precursor **(2)** was obtained as a colorless oil which solidified in time (186.5 g, 53% yield). **^{1}H NMR** (500 MHz, $CDCl_3$) δ 6.32 (s, 1H, N$\underline{H}$CO), 3.70 (s, 1H, C$\underline{H}_3$-O-CO), 3.66 (t, *J* = 7.4 Hz, 2H, C$\underline{H}_2$-Cl), 3.54 (t, *J* = 7.4 Hz, 2H, C$\underline{H}_2$-NH-CO), 2.69 (t, *J* = 7.4 Hz, 2H, NH-CO-C$\underline{H}_2$), 2.59 (t, *J* = 7.4 Hz, 2H, C$\underline{H}_2$-CO-O)

MestOx (3) was synthesized following a modified literature procedure[40]**.** MestOx-precursor **2** (132.3 g, 0.68 mol, 1 eq.) was heated to 45°C to melt the solid. Subsequently, sodium carbonate (70.62 g, 0.67 mol, 1 eq.) was added gently, which caused the formation of CO_2. The reaction mixture was heated and stirred overnight (60°C, 20 mbar) using a rotary evaporator. After overnight reaction, the absence of CO_2 formation indicated full conversion. The reaction mixture was diluted with Et_2O (500 mL) and the resulting viscous suspension was filtered. The solvent was removed under reduced pressure yielding a yellow oil (104.7 g). This oil was distilled twice ($2.3 \cdot 10^{-2}$ mbar) using the KDL-1. MestOx **(3)** was obtained as a colorless oil which solidified over time. (86.3 g, 80% yield). **^{1}H NMR** (500 MHz, $CDCl_3$) δ 4.20 (t, J = 9.5

Hz, 1H, C<u>H</u>$_2$O), 3.78 (t, J = 9.4 Hz, 1H, C<u>H</u>$_2$N), 3.66 (s, 3H, C<u>H</u>$_3$-OCO), 2.64 (t, J = 9.5 Hz, 2H, CH$_2$C<u>H</u>$_2$COO), 2.55 (t, J = 7.5 Hz, 2H, C<u>H</u>$_2$CH$_2$COO). **^{13}C NMR** (500 MHz, $CDCl_3$) δ 172.67, δ 166.97, δ 67.45, δ 54.35, δ 51.73, δ 30.01, δ 23.04. **LCQ MS**: m/z 158.1 $[M+H]^+$ (calc. 158.1)

6.4.2 Route B: Polymer synthesis

Protocol 1: General procedure polymerization (P12a-P24a)

Methyl tosylate (1 eq.), *n*PropOx (m eq.), EtOx (n eq.), MestOx (x eq.) and acetonitrile were mixed in the desired ratios in a dry microwave vial (concentration 4M) under inert atmosphere (argon). The polymerization was heated for 30 min under microwave irradiation (140°C) after which dry piperidine (5 eq.) was added to the reaction mixture, which was stirred for three hours. The polymer was dissolved in DCM and precipitated in diethylether (DCM/Et_2O, v/v, 1:20). This procedure was performed two times. The resulting suspension was filtered and the residue dissolved in DCM (100 mL). The solvent was evaporated under reduced pressure yielding the MestOx-functionalized polymers (**P12a-24a)** as white powders.

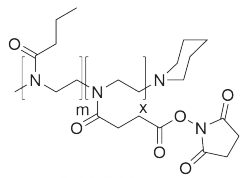

P12a P(*n*PropOx-c-MestOx) 90-10 - **P12a** was synthesized according to protocol **1** with a monomer ratio of m/x of 90/10. **P12a** was obtained as a white foam (1.9 g, 76% yield). **^{1}H NMR** (500 MHz, D_2O) δ 3.60 (b, x•3H, OC<u>H</u>$_3$), 3.60-3.40 (b,(m+x)•4H, NC<u>H</u>$_2$C<u>H</u>$_2$N), 2.70-2.50 (b, x•4H, CO-C<u>H</u>$_2$-C<u>H</u>$_2$-CO), 2.40-2.10 (b, m•2H, CO-C<u>H</u>$_2$-CH$_2$-CH$_3$), 1.60-1.40 (b, m•2H, CO-CH$_2$-C<u>H</u>$_2$-CH$_3$), 0.90-0.80 (b, m•3H, CO-CH$_2$-CH$_2$-C<u>H</u>$_3$). Experimentally determined monomer ratio (m/x): 90/10. **SEC** (PMMA) M_n 19.1 kg/mol, Đ 1.23

P13a P(*n*PropOx-c-MestOx) 80-20 - **P13a** was synthesized according to protocol **1** with a monomer ratio of m/x of 80/20. **P13a** was obtained as a white foam (9.1 g, 87% yield). **^{1}H NMR** (500 MHz, D_2O) δ 3.60 (b, x•3H, OC<u>H</u>$_3$), 3.60-3.40 (b,(m+x)•4H, NC<u>H</u>$_2$C<u>H</u>$_2$N), 2.70-2.50 (b, x•4H, CO-C<u>H</u>$_2$-C<u>H</u>$_2$-CO), 2.40-2.10 (b, m•2H, CO-C<u>H</u>$_2$-CH$_2$-CH$_3$), 1.60-1.40 (b, m•2H, CO-CH$_2$-C<u>H</u>$_2$-CH$_3$), 0.90-0.80 (b, m•3H, CO-CH$_2$-CH$_2$-C<u>H</u>$_3$). Experimentally determined monomer ratio (m/x): 79/21.

P14a P(*n*PropOx-c-MestOx) 70-30 - **P14a** was synthesized according to protocol **1** with a monomer ratio of m/x of 70/30. **P14a** was obtained as a white foam (4.5 g, 90% yield). **^{1}H NMR** (500 MHz, D_2O) δ 3.60 (b, x•3H, OC<u>H</u>$_3$), 3.60-3.40 (b,(m+x)•4H, NC<u>H</u>$_2$C<u>H</u>$_2$N), 2.70-2.50 (b, x•4H, CO-C<u>H</u>$_2$-C<u>H</u>$_2$-CO), 2.40-2.10 (b, m•2H, CO-C<u>H</u>$_2$-CH$_2$-CH$_3$), 1.60-1.40 (b, m•2H, CO-CH$_2$-C<u>H</u>$_2$-CH$_3$), 0.90-0.80 (b,m•3H, CO-CH$_2$-CH$_2$-C<u>H</u>$_3$). Experimentally determined monomer ratio (m/x): 70/30. **SEC** (PMMA) M_n 21.0 kg/mol, Đ 1.24

P15a P(*n*PropOx-c-MestOx) 60-40 - **P15a** was synthesized according to protocol **1** with a monomer ratio of m/x of 60/40. **P15a** was obtained as a white foam (1.9 g, 76% yield). **^{1}H NMR** (500 MHz, D_2O) δ 3.60 (b, x•3H, OC<u>H</u>$_3$), 3.60-3.40 (b,(m+x)•4H, NC<u>H</u>$_2$C<u>H</u>$_2$N), 2.70-2.50 (b, x•4H, CO-C<u>H</u>$_2$-C<u>H</u>$_2$-CO), 2.40-2.10 (b, m•2H, CO-C<u>H</u>$_2$-CH$_2$-CH$_3$), 1.60-1.40 (b, m•2H, CO-CH$_2$-C<u>H</u>$_2$-CH$_3$), 0.90-0.80 (b,m•3H, CO-CH$_2$-CH$_2$-C<u>H</u>$_3$). Experimentally determined monomer ratio (m/x): 58/42. **SEC** (PMMA) M_n 21.6kg/mol, Đ 1.31

P16a P(*n*PropOx-c-MestOx) 50-50 - **P16a** was synthesized according to protocol **1** with a monomer ratio of m/x of 50/50. **P16a** was obtained as a white foam (2.4 g, 96% yield). **^{1}H NMR** (500 MHz, D_2O) δ 3.60 (b, x•3H, OC<u>H</u>$_3$), 3.60-3.40 (b,(m+x)•4H, NC<u>H</u>$_2$C<u>H</u>$_2$N), 2.70-2.50 (b, x•4H, CO-C<u>H</u>$_2$-C<u>H</u>$_2$-CO), 2.40-2.10 (b, m•2H, CO-C<u>H</u>$_2$-CH$_2$-CH$_3$), 1.60-1.40 (b, m•2H, CO-CH$_2$-C<u>H</u>$_2$-CH$_3$), 0.90-0.80 (b, m•3H, CO-CH$_2$-CH$_2$-C<u>H</u>$_3$). Experimentally determined monomer ratio (m/x): 51/49. **SEC** (PMMA) M_n 23.5 kg/mol, Đ 1.29

P17a P(*n*PropOx-c-MestOx) 40-60 - **P17a** was synthesized according to protocol **1** with a monomer ratio of m/x of 40/60. **P17a** was obtained as a white foam (2.4 g, 96% yield). **^{1}H NMR** (500 MHz, D_2O) δ 3.60 (b, x•3H, OC<u>H</u>$_3$), 3.60-3.40 (b,(m+x)•4H, NC<u>H</u>$_2$C<u>H</u>$_2$N), 2.70-2.50 (b, x•4H, CO-C<u>H</u>$_2$-C<u>H</u>$_2$-CO), 2.40-2.10 (b, m•2H, CO-C<u>H</u>$_2$-CH$_2$-CH$_3$), 1.60-1.40 (b, m•2H, CO-CH$_2$-C<u>H</u>$_2$-CH$_3$), 0.90-0.80 (b, m•3H, CO-CH$_2$-CH$_2$-C<u>H</u>$_3$). Experimentally determined monomer ratio (m/x): 40/60. **SEC** (PMMA) M_n 24.8 kg/mol, Đ 1.25

P18a P(*n*PropOx-c-MestOx) 30-70 - **P18a** was synthesized according to protocol **1** with a monomer ratio of m/x of 30/70. **P18a** was obtained as a white foam (2.7 g, quant. yield). **^{1}H NMR** (500 MHz, D_2O) δ 3.60 (b, x•3H, OC<u>H</u>$_3$), 3.60-3.40 (b,(m+x)•4H, NC<u>H</u>$_2$C<u>H</u>$_2$N), 2.70-2.50 (b, x•4H, CO-C<u>H</u>$_2$-C<u>H</u>$_2$-CO), 2.40-2.10 (b, m•2H, CO-C<u>H</u>$_2$-CH$_2$-CH$_3$), 1.60-1.40 (b, m•2H, CO-CH$_2$-C<u>H</u>$_2$-CH$_3$), 0.90-0.80 (b, m•3H, CO-CH$_2$-CH$_2$-C<u>H</u>$_3$). Experimentally determined monomer ratio (m/x): 28/72. **SEC** (PMMA) M_n 24.1 kg/mol, Đ 1.32

P19a P(*n*PropOx-c-MestOx) 20-80 - **P19a** was synthesized according to protocol **1** with a monomer ratio of m/x of 20/80. **P19a** was obtained as a white foam (2.5 g, quant. yield). **^{1}H NMR** (500 MHz, D_2O) δ 3.60 (b, x•3H, OC<u>H</u>$_3$), 3.60-3.40 (b,(m+x)•4H, NC<u>H</u>$_2$C<u>H</u>$_2$N), 2.70-2.50 (b, x•4H, CO-C<u>H</u>$_2$-C<u>H</u>$_2$-CO), 2.40-2.10 (b, m•2H, CO-C<u>H</u>$_2$-CH$_2$-CH$_3$), 1.60-1.40 (b,m•2H, CO-CH$_2$-C<u>H</u>$_2$-CH$_3$), 0.90-0.80 (b, m•3H, CO-CH$_2$-CH$_2$-C<u>H</u>$_3$). Experimentally determined monomer ratio (m/x): 21/79. **SEC** (PMMA) M_n 23.1 kg/mol, Đ 1.36

P20a P(*n*PropOx-c-MestOx) 10-90 - **P20a** was synthesized according to protocol **1** with a monomer ratio of m/x of 10/90. **P20a** was obtained as a white foam (2.5 g, quant. yield). **^{1}H NMR** (500 MHz, D_2O) δ 3.60 (b, x•3H, OC<u>H</u>$_3$), 3.60-3.40 (b,(m+x)•4H, NC<u>H</u>$_2$C<u>H</u>$_2$N), 2.70-2.50 (b, x•4H, CO-C<u>H</u>$_2$-C<u>H</u>$_2$-CO), 2.40-2.10 (b, m•2H, CO-C<u>H</u>$_2$-CH$_2$-

CH_3), 1.60-1.40 (b, m•2H, CO-CH_2-$C\underline{H}_2$-CH_3), 0.90-0.80 (b, m•3H, CO-CH_2-CH_2-$C\underline{H}_3$). Experimentally determined monomer ratio (m/x): 11/89. **SEC** (PMMA) no signal could be obtained

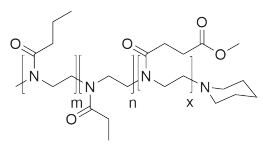
P21a-P24a

P21a P(*n*PropOx-c-EtOx-c-MestOx) 40-50-10 - **P21a** was synthesized according to protocol **1** with a monomer ratio of m/n/x of 40/50/10. **P21a** was obtained as a white foam (7.5 g, 78% yield). **^{1}H NMR** (500 MHz, D_2O) δ 3.60 (b, x•3H, OC$\underline{H}_3$), 3.60-3.40 (b,(m+n+x)•4H, NC$\underline{H}_2$C$\underline{H}_2$N), 2.70-2.50 (b, x•4H, CO-C$\underline{H}_2$-C$\underline{H}_2$-CO), 2.40-2.10 (b, (m+n)•2H, CO-C$\underline{H}_2$-CH_2-CH_3+ CO-C$\underline{H}_2$-CH_3), 1.60-1.40 (b, m•2H, CO-CH_2-C$\underline{H}_2$-CH_3), 1.15-1.05 (b, n•3H, CO-CH_2-C$\underline{H}_3$), 0.90-0.80 (b, m•3H, CO-CH_2-CH_2-C$\underline{H}_3$). Experimentally determined monomer ratio (m/n/x): 40/51/9.

P22a P(*n*PropOx-c-EtOx-c-MestOx) 50-40-10 - **P22a** was synthesized according to protocol **1** with a monomer ratio of m/n/x of 50/40/10. **P22a** was obtained as a white foam (7.8 g, 79% yield). **^{1}H NMR** (500 MHz, D_2O) δ 3.60 (b, x•3H, OC$\underline{H}_3$), 3.60-3.40 (b,(m+n+x)•4H, NC$\underline{H}_2$C$\underline{H}_2$N), 2.70-2.50 (b, x•4H, CO-C$\underline{H}_2$-C$\underline{H}_2$-CO), 2.40-2.10 (b, (m+n)•2H, CO-C$\underline{H}_2$-CH_2-CH_3+ CO-C$\underline{H}_2$-CH_3), 1.60-1.40 (b, m•2H, CO-CH_2-C$\underline{H}_2$-CH_3), 1.15-1.05 (b, n•3H, CO-CH_2-C$\underline{H}_3$), 0.90-0.80 (b, m•3H, CO-CH_2-CH_2-C$\underline{H}_3$). Experimentally determined monomer ratio (m/n/x): 40/51/9.

P23a P(*n*PropOx-c-EtOx-c-MestOx) 40-35-25 - **P23a** was synthesized according to protocol **1** with a monomer ratio of m/n/x of 40/35/25. **P23a** was obtained as a white foam (18.9 g, 93% yield). **^{1}H NMR** (500 MHz, D_2O) δ 3.60 (b, x•3H, OC$\underline{H}_3$), 3.60-3.40 (b,(m+n+x)•4H, NC$\underline{H}_2$C$\underline{H}_2$N), 2.70-2.50 (b, x•4H, CO-C$\underline{H}_2$-C$\underline{H}_2$-CO), 2.40-2.10 (b, (m+n)•2H, CO-C$\underline{H}_2$-CH_2-CH_3+ CO-C$\underline{H}_2$-CH_3), 1.60-1.40 (b, m•2H, CO-CH_2-C$\underline{H}_2$-CH_3), 1.15-1.05 (b, n•3H, CO-CH_2-C$\underline{H}_3$), 0.90-0.80 (b, m•3H, CO-CH_2-CH_2-C$\underline{H}_3$). Experimentally determined monomer ratio (m/n/x): 41/35/24. **SEC** (PMMA) M_n 11.1 kg/mol, Đ 1.19

P24a P(*n*PropOx-c-EtOx-c-MestOx) 50-25-25 - **P24a** was synthesized according to protocol **1** with a monomer ratio of m/n/x of 50/25/25. **P24a** was obtained as a white foam (8.2 g, 78% yield). **^{1}H NMR** (500 MHz, D_2O) δ 3.60 (b, x•3H, OC$\underline{H}_3$), 3.60-3.40 (b,(m+n+x)•4H, NC$\underline{H}_2$C$\underline{H}_2$N), 2.70-2.50 (b, x•4H, CO-C$\underline{H}_2$-C$\underline{H}_2$-CO), 2.40-2.10 (b, (m+n)•2H, CO-C$\underline{H}_2$-CH_2-CH_3+ CO-C$\underline{H}_2$-CH_3), 1.60-1.40 (b, m•2H, CO-CH_2-C$\underline{H}_2$-CH_3), 1.15-1.05 (b, n•3H, CO-CH_2-C$\underline{H}_3$), 0.90-0.80 (b, m•3H, CO-CH_2-CH_2-C$\underline{H}_3$). Experimentally determined monomer ratio (m/n/x): 51/26/23.

Protocol 2: General procedure methyl ester hydrolysis (P12b-P24b)

Polymers **P12a-P24a** were dissolved in a NaOH solution (0.1 M) to a polymer concentration of 1 M and this reaction mixture was stirred overnight. Afterwards, the reaction mixture was acidified to pH 4 by dropwise addition of an HCl solution

(0.1 M). The reaction mixture was stirred in a heated water bath (45°C) which caused precipitation of the polymer as a sticky white precipitate. This precipitate was dissolved in cold water (100 mL) and the reaction mixture was stirred again in the heated water bath, which caused the polymer to precipitate again. The pH of the resulting solution was 4. The sticky white precipitate was either (1) dissolved again in DCM (100 mL) and concentrated under reduced pressure or (2) precipitated from DMF (20 mL) into diethyl ether (2000 mL) and subsequently filtered and dried under high vacuum, yielding the COOH-functionalized polymers (**P12b-P24b**) as white fluffy powders.

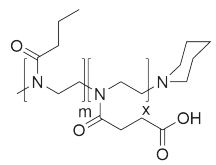
P12b-P20b

P12b P(*n*PropOx-c-COOH) 90-10 - **P12b** was synthesized according to protocol **2** starting from **P12a** (10.2 g). **P12b** was obtained as a white foam (6.8 g, 69% yield). **^{1}H NMR** (500 MHz, D_2O) δ 3.70-3.40 (b,(m+x)•4H, NC$\underline{H}_2$C$\underline{H}_2$N), 2.60-2.50 (b, x•4H, CO-C$\underline{H}_2$-C$\underline{H}_2$-CO), 2.40-2.20 (b, m•2H, CO-C$\underline{H}_2$-CH_2-CH_3), 1.60-1.40 (b, m•2H, CO-CH_2-C$\underline{H}_2$-CH_3), 0.90-0.80 (b, m•3H, CO-CH_2-CH_2-C$\underline{H}_3$). Experimentally determined monomer ratio (m/x): 92/8. **SEC** (PMMA) M_n 20.5 kg/mol, Đ 1.16

P13b P(*n*PropOx-c-COOH) 80-20 - **P13b** was synthesized according to protocol **2** starting from **P13a** (9.05 g). **P13b** was obtained as a white foam (7.0 g, 79% yield). **^{1}H NMR** (500 MHz, D_2O) δ 3.70-3.40 (b,(m+x)•4H, NC$\underline{H}_2$C$\underline{H}_2$N), 2.60-2.50 (b, x•4H, CO-C$\underline{H}_2$-C$\underline{H}_2$-CO), 2.40-2.20 (b, m•2H, CO-C$\underline{H}_2$-CH_2-CH_3), 1.60-1.40 (b, m•2H, CO-CH_2-C$\underline{H}_2$-CH_3), 0.90-0.80 (b, m•3H, CO-CH_2-CH_2-C$\underline{H}_3$). Experimentally determined monomer ratio (m/x): 80/20.

P14b P(*n*PropOx-c-COOH) 70-30 - **P14b** was synthesized according to protocol **2** starting from **P14a** (10 g). **P14b** was obtained as a white foam (2.4 g, 25% yield). **^{1}H NMR** (500 MHz, D_2O) δ 3.70-3.40 (b,(m+x)•4H, NC$\underline{H}_2$C$\underline{H}_2$N), 2.60-2.50 (b, x•4H, CO-C$\underline{H}_2$-C$\underline{H}_2$-CO), 2.40-2.20 (b, m•2H, CO-C$\underline{H}_2$-CH_2-CH_3), 1.60-1.40 (b, m•2H, CO-CH_2-C$\underline{H}_2$-CH_3), 0.90-0.80 (b, m•3H, CO-CH_2-CH_2-C$\underline{H}_3$). Experimentally determined monomer ratio (m/x): 70/30. **SEC** (PMMA) M_n 24.8 kg/mol, Đ 1.16

P15b P(*n*PropOx-c-COOH) 60-40 - **P15b** was synthesized according to protocol **2** starting from **P15a** (1.60 g). **P15b** was obtained as a white foam (0.5 g, 33% yield). **^{1}H NMR** (500 MHz, D_2O) δ 3.70-3.40 (b,(m+x)•4H, NC$\underline{H}_2$C$\underline{H}_2$N), 2.60-2.50 (b, x•4H, CO-C$\underline{H}_2$-C$\underline{H}_2$-CO), 2.40-2.20 (b, m•2H, CO-C$\underline{H}_2$-CH_2-CH_3), 1.60-1.40 (b, m•2H, CO-CH_2-C$\underline{H}_2$-CH_3), 0.90-0.80 (b, m•3H, CO-CH_2-CH_2-C$\underline{H}_3$). Experimentally determined monomer ratio (m/x): 61/39. **SEC** (PMMA) M_n 23.5 kg/mol, Đ 1.17

P16b P(*n*PropOx-c-COOH) 50-50 - **P16b** was synthesized according to protocol **2** starting from **P16a** (2.2 g). **P16b** was obtained as a white foam (0.3 g, 14% yield). **^{1}H NMR** (500 MHz, D_2O) δ 3.70-3.40 (b,(m+x)•4H, NC$\underline{H}_2$C$\underline{H}_2$N), 2.60-2.50 (b, x•4H, CO-C$\underline{H}_2$-C$\underline{H}_2$-CO), 2.40-2.20 (b, m•2H, CO-C$\underline{H}_2$-CH_2-CH_3), 1.60-1.40 (b, m•2H, CO-

CH_2-C$\underline{H}_2$-CH_3), 0.90-0.80 (b, m•3H, CO-CH_2-CH_2-C$\underline{H}_3$). Experimentally determined monomer ratio (m/x): 51/49. **SEC** (PMMA) M_n 18.4 kg/mol, Đ 1.20

P17b P(*n*PropOx-c-COOH) 40-60 - **P17b** was synthesized according to protocol **2** starting from **P17a** (2.1 g). **P17b** was obtained as a white foam (1.9, 80% yield). **^{1}H NMR** (500 MHz, D_2O) δ 3.70-3.40 (b,(m+x)•4H, NC$\underline{H}_2$C$\underline{H}_2$N), 2.60-2.50 (b, x•4H, CO-C$\underline{H}_2$-C$\underline{H}_2$-CO), 2.40-2.20 (b, m•2H, CO-C$\underline{H}_2$-CH_2-CH_3), 1.60-1.40 (b, m•2H, CO-CH_2-C$\underline{H}_2$-CH_3), 0.90-0.80 (b, m•3H, CO-CH_2-CH_2-C$\underline{H}_3$). Experimentally determined monomer ratio (m/x): 40/60. **SEC** (PMMA) M_n 18.7 kg/mol, Đ 1.21

P18b P(*n*PropOx-c-COOH) 30-70 - **P18b** was synthesized according to protocol **2** starting from **P18a** (2.2 g). **P18b** was obtained as a white foam (1.4 g, 66% yield). **^{1}H NMR** (500 MHz, D_2O) δ 3.70-3.40 (b,(m+x)•4H, NC$\underline{H}_2$C$\underline{H}_2$N), 2.60-2.50 (b, x•4H, CO-C$\underline{H}_2$-C$\underline{H}_2$-CO), 2.40-2.20 (b, m•2H, CO-C$\underline{H}_2$-CH_2-CH_3), 1.60-1.40 (b, m•2H, CO-CH_2-C$\underline{H}_2$-CH_3), 0.90-0.80 (b, m•3H, CO-CH_2-CH_2-C$\underline{H}_3$). Experimentally determined monomer ratio (m/x): 35/65. **SEC** (PMMA) M_n 19.2 kg/mol, Đ 1.25

P19b P(*n*PropOx-c-COOH) 20-80 - **P19b** was synthesized according to protocol **2** starting from **P19a** (2.1 g). **P19b** was obtained as a white foam (0.2 g, 10% yield). **^{1}H NMR** (500 MHz, D_2O) δ 3.70-3.40 (b,(m+x)•4H, NC$\underline{H}_2$C$\underline{H}_2$N), 2.60-2.50 (b, x•4H, CO-C$\underline{H}_2$-C$\underline{H}_2$-CO), 2.40-2.20 (b, m•2H, CO-C$\underline{H}_2$-CH_2-CH_3), 1.60-1.40 (b, m•2H, CO-CH_2-C$\underline{H}_2$-CH_3), 0.90-0.80 (b, m•3H, CO-CH_2-CH_2-C$\underline{H}_3$). Experimentally determined monomer ratio (m/x): 25/75. **SEC** (PMMA) M_n 21.1 kg/mol, Đ 1.24

P20b P(*n*PropOx-c-COOH) 10-90 - **P20b** was synthesized according to protocol **2** starting from **P20a** (2.1 g). **P20b** was obtained as a white foam (0.3 g, 10% yield). **^{1}H NMR** (500 MHz, D_2O) δ 3.70-3.40 (b,(m+x)•4H, NC$\underline{H}_2$C$\underline{H}_2$N), 2.60-2.50 (b, x•4H, CO-C$\underline{H}_2$-C$\underline{H}_2$-CO), 2.40-2.20 (b, m•2H, CO-C$\underline{H}_2$-CH_2-CH_3), 1.60-1.40 (b, m•2H, CO-CH_2-C$\underline{H}_2$-CH_3), 0.90-0.80 (b, m•3H, CO-CH_2-CH_2-C$\underline{H}_3$). Experimentally determined monomer ratio (m/x): 15/85. **SEC** (PMMA) M_n 23.7 kg/mol, Đ 1.40

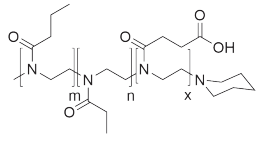

P21b-P24b

P21b P(*n*PropOx-c-EtOx-c-COOH) 50-40-10 - **P21b** was synthesized according to protocol **2** starting from **P21a** (7.5 g). **P21b** was obtained as a white foam (4.0 g, 52% yield). **^{1}H NMR** (500 MHz, D_2O) δ 3.70-3.40 (b,(m+n+x)•4H, NC$\underline{H}_2$C$\underline{H}_2$N), 2.60-2.50 (b, x•4H, CO-C$\underline{H}_2$-C$\underline{H}_2$-CO), 2.40-2.20 (b, (m+n)•2H, CO-C$\underline{H}_2$-CH_2-CH_3 + CO-C$\underline{H}_2$-CH_3), 1.60-1.40 (b, m•2H, CO-CH_2-C$\underline{H}_2$-CH_3), 1.15-1.05 (b, n•3H, CO-CH_2-C$\underline{H}_3$) 0.90-0.80 (b, m•3H, CO-CH_2-CH_2-C$\underline{H}_3$). Experimentally determined monomer ratio (m/n/x): 50/40/10

P22b P(*n*PropOx-c-EtOx-c-COOH) 40-50-10 - **P22b** was synthesized according to protocol **2** starting from **P22a** (7.8 g). **P22b** was obtained as a white foam (6.5 g, 83% yield). **^{1}H NMR** (500 MHz, D_2O) δ 3.70-3.40 (b,(m+n+x)•4H, NC$\underline{H}_2$C$\underline{H}_2$N), 2.60-2.50 (b, x•4H, CO-C$\underline{H}_2$-C$\underline{H}_2$-CO), 2.40-2.20 (b, (m+n)•2H, CO-C$\underline{H}_2$-CH_2-CH_3 + CO-

C$\underline{H}_2$-CH_3), 1.60-1.40 (b, m•2H, CO-CH_2-C$\underline{H}_2$-CH_3), 1.15-1.05 (b, n•3H, CO-CH_2-C$\underline{H}_3$) 0.90-0.80 (b, m•3H, CO-CH_2-CH_2-C$\underline{H}_3$). Experimentally determined monomer ratio (m/n/x): 40/49/11

P23b P(*n*PropOx-c-EtOx-c-COOH) 40-35-25 - **P23b** was synthesized according to protocol **2** starting from **P23a** (18.4 g). **P23b** was obtained as a white foam (10.0 g, 54% yield). **^{1}H NMR** (500 MHz, D_2O) δ 3.70-3.40 (b,(m+n+x)•4H, NC$\underline{H}_2$C$\underline{H}_2$N), 2.60-2.50 (b, x•4H, CO-C$\underline{H}_2$-C$\underline{H}_2$-CO), 2.40-2.20 (b, (m+n)•2H, CO-C$\underline{H}_2$-CH_2-CH_3 + CO-C$\underline{H}_2$-CH_3), 1.60-1.40 (b, m•2H, CO-CH_2-C$\underline{H}_2$-CH_3), 1.15-1.05 (b, n•3H, CO-CH_2-C$\underline{H}_3$) 0.90-0.80 (b, m•3H, CO-CH_2-CH_2-C$\underline{H}_3$). Experimentally determined monomer ratio (m/n/x): 40/36/24

P24b P(*n*PropOx-c-EtOx-c-COOH) 50-25-25 - **P24b** was synthesized according to protocol **2** starting from **P24a** (8.2 g). **P24b** was obtained as a white foam (4.3 g, 54% yield). **^{1}H NMR** (500 MHz, D_2O) δ 3.70-3.40 (b,(m+n+x)•4H, NC$\underline{H}_2$C$\underline{H}_2$N), 2.60-2.50 (b, x•4H, CO-C$\underline{H}_2$-C$\underline{H}_2$-CO), 2.40-2.20 (b, (m+n)•2H, CO-C$\underline{H}_2$-CH_2-CH_3 + CO-C$\underline{H}_2$-CH_3), 1.60-1.40 (b, m•2H, CO-CH_2-C$\underline{H}_2$-CH_3), 1.15-1.05 (b, n•3H, CO-CH_2-C$\underline{H}_3$) 0.90-0.80 (b, m•3H, CO-CH_2-CH_2-C$\underline{H}_3$). Experimentally determined monomer ratio (m/n/x): 50/30/20

Protocol 3: General procedure NHS activation (P12-P24)

Polymers **P12b-P24b**, *N,N'*-Diisopropylcarbodiimide (DIC) (1.1 eq. compared to COOH) and N-hydroxysuccinimide (NHS) (1.1 eq. compared to COOH) were dissolved in a mixture of solvents (DMF/DCM, v:v, 1:9) yielding a 0.1 M solution. This mixture was stirred overnight. A white precipitate (urea byproduct of DIC) was formed which was removed by filtration of the reaction mixture over celite. Afterwards, the reaction mixture was concentrated to dryness under reduced pressure. Subsequently, the polymers were dissolved in DCM (100 mL) and precipitated in Et_2O (250 mL). This procedure was performed three times. After the final precipitation step, the polymers were collected by filtration and dried under high vacuum yielding the NHS-ester functionalized polymers (**P12-P24**) as white fluffy powders.

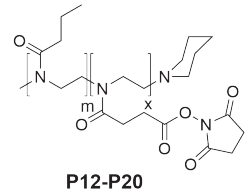

P12-P20

P12 P(*n*PropOx-c-NHS) 90-10 - **P12** was synthesized according to protocol **3** starting from **P12b** (6.5 g). **P12** was obtained as a white foam (6.2 g, 87% yield). **^{1}H NMR** (500 MHz, D_2O) δ 3.70-3.40 (b,(m+x)•4H, NC$\underline{H}_2$C$\underline{H}_2$N), 3.00-2.60 (b, (m+x)•4H, CO-C$\underline{H}_2$-C$\underline{H}_2$-CO + (b, x•4H, CO-C$\underline{H}_2$-C$\underline{H}_2$-CO (NHS)), 2.40-2.20 (b, m•2H, CO-C$\underline{H}_2$-CH_2-CH_3), 1.60-1.40 (b, m•2H, CO-CH_2-C$\underline{H}_2$-CH_3), 0.90-0.80 (b, m•3H, CO-CH_2-CH_2-C$\underline{H}_3$). Experimentally determined monomer ratio (m/x): 90/10. **SEC** (PMMA) M_n 29.6 kg/mol, Đ 1.16

P13 P(*n*PropOx-c-NHS) 80-20 - **P13** was synthesized according to protocol **3** starting from **P13b** (7.0 g). **P13** was obtained as a white foam (6.4 g, 79% yield). **^{1}H**

NMR (500 MHz, D_2O) δ 3.70-3.40 (b,(m+x)•4H, NCH_2CH_2N), 3.00-2.60 (b, (m+x)•4H, $CO\text{-}CH_2\text{-}CH_2\text{-}CO$ + (b, x•4H, $CO\text{-}CH_2\text{-}CH_2\text{-}CO$ (NHS)), 2.40-2.20 (b, m•2H, $CO\text{-}CH_2\text{-}CH_2\text{-}CH_3$), 1.60-1.40 (b, m•2H, $CO\text{-}CH_2\text{-}CH_2\text{-}CH_3$), 0.90-0.80 (b, m•3H, $CO\text{-}CH_2\text{-}CH_2\text{-}CH_3$). Experimentally determined monomer ratio (m/x): 79/21.

P14 P(*n*PropOx-c-NHS) 70-30 - **P14** was synthesized according to protocol **3** starting from **P14b** (2.1 g). **P14** was obtained as a white foam (1.8 g, 69% yield). **^{1}H NMR** (500 MHz, D_2O) δ 3.70-3.40 (b,(m+x)•4H, NCH_2CH_2N), 3.00-2.60 (b, (m+x)•4H, $CO\text{-}CH_2\text{-}CH_2\text{-}CO$ + (b, x•4H, $CO\text{-}CH_2\text{-}CH_2\text{-}CO$ (NHS)), 2.40-2.20 (b, m•2H, $CO\text{-}CH_2\text{-}CH_2\text{-}CH_3$), 1.60-1.40 (b, m•2H, $CO\text{-}CH_2\text{-}CH_2\text{-}CH_3$), 0.90-0.80 (b, m•3H, $CO\text{-}CH_2\text{-}CH_2\text{-}CH_3$). Experimentally determined monomer ratio (m/x): 73/27. **SEC** (PMMA) M_n 29.6 kg/mol, Đ 1.19

P15 P(*n*PropOx-c-NHS) 60-40 - **P15** was synthesized according to protocol **3** starting from **P15b** (0.5 g). **P15** was obtained as a white foam (0.3 g, 46% yield). **^{1}H NMR** (500 MHz, D_2O) δ 3.70-3.40 (b,(m+x)•4H, NCH_2CH_2N), 3.00-2.60 (b, (m+x)•4H, $CO\text{-}CH_2\text{-}CH_2\text{-}CO$ + (b, x•4H, $CO\text{-}CH_2\text{-}CH_2\text{-}CO$ (NHS)), 2.40-2.20 (b, m•2H, $CO\text{-}CH_2\text{-}CH_2\text{-}CH_3$), 1.60-1.40 (b, m•2H, $CO\text{-}CH_2\text{-}CH_2\text{-}CH_3$), 0.90-0.80 (b, m•3H, $CO\text{-}CH_2\text{-}CH_2\text{-}CH_3$). Experimentally determined monomer ratio (m/x): 58/42. **SEC** (PMMA) M_n 34.5 kg/mol, Đ 1.23

P16 P(*n*PropOx-c-NHS) 50-50 - **P16** was synthesized according to protocol **3** starting from **P16b** (0.3 g). **P16** was obtained as a white foam (0.2 g, 46% yield). **^{1}H NMR** (500 MHz, D_2O) δ 3.70-3.40 (b,(m+x)•4H, NCH_2CH_2N), 3.00-2.60 (b, (m+x)•4H, $CO\text{-}CH_2\text{-}CH_2\text{-}CO$ + (b, x•4H, $CO\text{-}CH_2\text{-}CH_2\text{-}CO$ (NHS)), 2.40-2.20 (b, m•2H, $CO\text{-}CH_2\text{-}CH_2\text{-}CH_3$), 1.60-1.40 (b, m•2H, $CO\text{-}CH_2\text{-}CH_2\text{-}CH_3$), 0.90-0.80 (b, m•3H, $CO\text{-}CH_2\text{-}CH_2\text{-}CH_3$). Experimentally determined monomer ratio (m/x): 50/50. **SEC** (PMMA) M_n 27.7 kg/mol, Đ 1.13

P17 P(*n*PropOx-c-NHS) 40-60 - **P17** was synthesized according to protocol **3** starting from **P17b** (1.4 g). **P17** was obtained as a white foam (1.3 g, 81% yield). **^{1}H NMR** (500 MHz, D_2O) δ 3.70-3.40 (b,(m+x)•4H, NCH_2CH_2N), 3.00-2.60 (b, (m+x)•4H, $CO\text{-}CH_2\text{-}CH_2\text{-}CO$ + (b, x•4H, $CO\text{-}CH_2\text{-}CH_2\text{-}CO$ (NHS)), 2.40-2.20 (b, m•2H, $CO\text{-}CH_2\text{-}CH_2\text{-}CH_3$), 1.60-1.40 (b, m•2H, $CO\text{-}CH_2\text{-}CH_2\text{-}CH_3$), 0.90-0.80 (b, m•3H, $CO\text{-}CH_2\text{-}CH_2\text{-}CH_3$). Experimentally determined monomer ratio (m/x): 36/64. **SEC** (PMMA) M_n 30.8 kg/mol, Đ 1.29

P18 P(*n*PropOx-c-NHS) 30-70 - **P18** was synthesized according to protocol **3** starting from **P18b** (1.0 g). **P18** was obtained as a white foam (1.0 g, quant yield). **^{1}H NMR** (500 MHz, D_2O) δ 3.70-3.40 (b,(m+x)•4H, NCH_2CH_2N), 3.00-2.60 (b, (m+x)•4H, $CO\text{-}CH_2\text{-}CH_2\text{-}CO$ + (b, x•4H, $CO\text{-}CH_2\text{-}CH_2\text{-}CO$ (NHS)), 2.40-2.20 (b, m•2H, $CO\text{-}CH_2\text{-}CH_2\text{-}CH_3$), 1.60-1.40 (b, m•2H, $CO\text{-}CH_2\text{-}CH_2\text{-}CH_3$), 0.90-0.80 (b, m•3H, $CO\text{-}CH_2\text{-}CH_2\text{-}CH_3$). Experimentally determined monomer ratio (m/x): 35/65. **SEC** (PMMA) M_n 31.8 kg/mol, Đ 1.32

P19 + **P20** could not be synthesized because of limited solubility

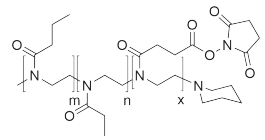

P21-P24

P21 P(*n*PropOx-c-EtOx-c-NHS) 40-50-10 - **P21** was synthesized according to protocol **3** starting from **P21b** (4.0 g). **P21** was obtained as a white foam (2.9 g, 53% yield). **^{1}H NMR** (500 MHz, D_2O) δ 3.70-3.40 (b,(m+n+x)•4H, NCH_2CH_2N), 3.00-2.60 (b, (m+n+x)•4H, $CO\text{-}CH_2\text{-}CH_2\text{-}CO$ + (b, x•4H, $CO\text{-}CH_2\text{-}CH_2\text{-}CO$ (NHS)), 2.40-2.20 (b, (m+n)•2H, $CO\text{-}CH_2\text{-}CH_2\text{-}CH_3$ + $CO\text{-}CH_2\text{-}CH_3$), 1.60-1.40 (b, m•2H, $CO\text{-}CH_2\text{-}CH_2\text{-}CH_3$), 0.90-0.80 (b, n•3H, $CO\text{-}CH_2\text{-}CH_3$), 0.90-0.80 (b, m•3H, $CO\text{-}CH_2\text{-}CH_2\text{-}CH_3$). Experimentally determined monomer ratio (m/n/x): 40/49/11. **SEC** (PMMA) M_n 12.5 kg/mol, Đ 1.18 **FT-IR (cm^{-1})** 1626 (C=O amide), 1738 + 1785 + 1815 (NHS-ester).

P22 P(*n*PropOx-c-EtOx-c-NHS) 50-40-10 - **P22** was synthesized according to protocol **3** starting from **P22b** (6.5 g). **P22** was obtained as a white foam (5.6 g, 65% yield). **^{1}H NMR** (500 MHz, D_2O) δ 3.70-3.40 (b,(m+n+x)•4H, NCH_2CH_2N), 3.00-2.60 (b, (m+n+x)•4H, $CO\text{-}CH_2\text{-}CH_2\text{-}CO$ + (b, x•4H, $CO\text{-}CH_2\text{-}CH_2\text{-}CO$ (NHS)), 2.40-2.20 (b, (m+n)•2H, $CO\text{-}CH_2\text{-}CH_2\text{-}CH_3$ + $CO\text{-}CH_2\text{-}CH_3$), 1.60-1.40 (b, m•2H, $CO\text{-}CH_2\text{-}CH_2\text{-}CH_3$), 0.90-0.80 (b, n•3H, $CO\text{-}CH_2\text{-}CH_3$), 0.90-0.80 (b, m•3H, $CO\text{-}CH_2\text{-}CH_2\text{-}CH_3$). Experimentally determined monomer ratio (m/n/x): 49/39/12. **SEC** (PMMA) M_n 12.3 kg/mol, Đ 1.16 **FT-IR (cm^{-1})** 1626 (C=O amide), 1738 + 1785 + 1815 (NHS-ester).

P23 P(*n*PropOx-c-EtOx-c-NHS) 40-35-25 - **P23** was synthesized according to protocol **3** starting from **P23b** (10 g). **P23** was obtained as a white foam (4.7 g, 35% yield). **^{1}H NMR** (500 MHz, D_2O) δ 3.70-3.40 (b,(m+n+x)•4H, NCH_2CH_2N), 3.00-2.60 (b, (m+n+x)•4H, $CO\text{-}CH_2\text{-}CH_2\text{-}CO$ + (b, x•4H, $CO\text{-}CH_2\text{-}CH_2\text{-}CO$ (NHS)), 2.40-2.20 (b, (m+n)•2H, $CO\text{-}CH_2\text{-}CH_2\text{-}CH_3$ + $CO\text{-}CH_2\text{-}CH_3$), 1.60-1.40 (b, m•2H, $CO\text{-}CH_2\text{-}CH_2\text{-}CH_3$), 0.90-0.80 (b, n•3H, $CO\text{-}CH_2\text{-}CH_3$), 0.90-0.80 (b, m•3H, $CO\text{-}CH_2\text{-}CH_2\text{-}CH_3$). Experimentally determined monomer ratio (m/n/x): 39/33/28. **SEC** (PMMA) M_n 16.8 kg/mol, Đ 1.22 **FT-IR (cm^{-1})** 1626 (C=O amide), 1738 + 1785 + 1815 (NHS-ester).

P24 P(*n*PropOx-c-EtOx-c-NHS) 50-25-25 - **P24** was synthesized according to protocol **3** starting from **P24b** (5.4 g). **P24** was obtained as a white foam (4.5 g, 83% yield). **^{1}H NMR** (500 MHz, D_2O) δ 3.70-3.40 (b,(m+n+x)•4H, NCH_2CH_2N), 3.00-2.60 (b, (m+n+x)•4H, $CO\text{-}CH_2\text{-}CH_2\text{-}CO$ + (b, x•4H, $CO\text{-}CH_2\text{-}CH_2\text{-}CO$ (NHS)), 2.40-2.20 (b, (m+n)•2H, $CO\text{-}CH_2\text{-}CH_2\text{-}CH_3$ + $CO\text{-}CH_2\text{-}CH_3$), 1.60-1.40 (b, m•2H, $CO\text{-}CH_2\text{-}CH_2\text{-}CH_3$), 0.90-0.80 (b, n•3H, $CO\text{-}CH_2\text{-}CH_3$), 0.90-0.80 (b, m•3H, $CO\text{-}CH_2\text{-}CH_2\text{-}CH_3$). Experimentally determined monomer ratio (m/n/x): 50/26/24. **SEC** (PMMA) M_n 14.6 kg/mol, Đ 1.18 **FT-IR (cm^{-1})** 1626 (C=O amide), 1738 + 1785 + 1815 (NHS-ester).

6.5 Route C

P25 P(*n*PropOx-c-MestOx) 70-30 - **P25** was synthesized according to protocol **1** with a monomer ratio of m/x of 70/30 and by using 2-amino-ethanol (5 eq.) as a

terminating agent. **P25** was obtained as a white foam (27.0 g, 71% yield). **^{1}H NMR** (500 MHz, D_2O) δ 3.60 (b, n•3H, OC$\underline{H}_3$), 3.60-3.40 (b,(m+n)•4H, NC$\underline{H}_2$C$\underline{H}_2$N), 2.75-2.50 (b, x•4H, CO-C$\underline{H}_2$-C$\underline{H}_2$-CO), 2.40-2.15 (b, m•2H, CO-C$\underline{H}_2$-CH$_2$-CH$_3$), 1.70-1.50 (b, m•2H, CO-CH$_2$-C$\underline{H}_2$-CH$_3$), 1.00-0.85 (b,m•3H, CO-CH$_2$-CH$_2$-C$\underline{H}_3$). Experimentally determined monomer ratio (m/x): 69/31. **SEC** (PMMA) M_n 11.3 kg/mol, Đ 1.12

P26a P(*n*PropOx-c-OH) 70-30 - **P25** (8 g, 0.63 mmol polymer, 20 mmol ester, 1 eq.) was dissolved in 2-amino-ethanol (8.35 mL, 8.4 g, 138 mmol, 7 eq.) and the reaction mixture was allowed to reflux overnight at 60°C under reduced pressure (300 mbar). After this, 2-amino-ethanol was removed under reduced pressure and the polymer was precipitated twice from isopropanol (100 mL) into Et_2O (2 L). Subsequently, the precipitate was dissolved in isopropanol (100 mL) and the solvent was evaporated under reduced pressure. Since residual 2-amino-ethanol and isopropanol were present (^{1}H-NMR), the polymer was precipitated from methanol (100 mL) into Et_2O (2 L) and subsequently filtered off and dried overnight under vacuum. **P26a** was obtained as a white foam (5.09 g, 59% yield). **^{1}H NMR** (500 MHz, D_2O): δ 3.60 (b, n•2H, NHC$\underline{H}_2$CH$_2$OH), δ 3.60-3.40 (b, (m+n)•4H, NC$\underline{H}_2$C$\underline{H}_2$N), 3.35-3.28 (b, n•2H, NHCH$_2$C$\underline{H}_2$OH), 2.76-2.48 (b, n•4H, O=CC$\underline{H}_2$C$\underline{H}_2$C=ONH), 2.43-2.20 (b, m•2H, C$\underline{H}_2$CH$_2$CH$_3$), 1.65-1.50 (b, m•2H, CH$_2$C$\underline{H}_2$CH$_3$), 0.98-0.85 (b, m•3H, CH$_2$CH$_2$C$\underline{H}_3$). Experimentally determined monomer ratio (m/n): 69/31 . **SEC** (PMMA) M_n 13.9 kg/mol, Đ 1.11

P26b P(*n*PropOx-c-OH-c-COOH) 70-15-15 - **P26a** (3.43 g, 0.21 mmol polymer, 6.5 mmol OH, 1 eq.) and succinic anhydride (0.53 g, 5.08 mmol, 0.78 eq) and DMAP (0.48 g, 3.93 mmol, 0.6 eq) were dissolved in DCM (30 mL) and the reaction mixture was stirred at room temperature overnight under inert atmosphere. Next, the reaction mixture was evaporated under reduced pressure to dryness. Subsequently, the polymer was precipitated twice from DCM (20 mL) into acetone (200 mL). Hereafter, the resulting white solid was dissolved in methanol (50 mL) and charged on an SCX-2 column (1.4 g, 0.69 mmol/g) and the loaded column was flushed twice with methanol (50 mL). After this, the combined fractions of methanol were concentrated to dryness under reduced pressure. **P26b** was obtained as a white solid (0.52 g, 13% yield). **^{1}H NMR (400 MHz, D_2O)**: δ 4.23-4.14 (b, x•2H, O=CNHCH$_2$C$\underline{H}_2$OC=O), δ 3.60 (b, n•2H, NHC$\underline{H}_2$CH$_2$OH), δ 3.60-3.40 (b, (m+n+x)•4H, NC$\underline{H}_2$C$\underline{H}_2$N), δ 3.40 (b, x•2H, O=CNHC$\underline{H}_2$CH$_2$OC=O), 3.35-3.28 (b, n•2H, NHCH$_2$C$\underline{H}_2$OH), 2.76-2.48 (b, (n+x)•4H, O=CC$\underline{H}_2$C$\underline{H}_2$C=ONH + x•4H, O=CC$\underline{H}_2$C$\underline{H}_2$C=O), 2.43-2.20 (b, m•2H, C$\underline{H}_2$CH$_2$CH$_3$), 1.65-1.50 (b, m•2H, CH$_2$C$\underline{H}_2$CH$_3$), 0.98-0.85 (b, m•3H, CH$_2$CH$_2$C$\underline{H}_3$). Experimentally determined monomer ratio (m/n): 69/13/18. **SEC** (PMMA) no signal could be obtained

P26 P(*n*PropOx-c-OH-c-NHS) 70-15-15 - **P26b** (0.5 g, 32 µmol polymer, 0.5 mmol COOH, 1 eq.)), DIC (0.3 mL, 2.0 mmol; 3.5 eq), acetic acid (33 µL, 0.5 mmol, 1 eq) and N-hydroxysuccinimide (0.2 g; 2.0 mmol; 3.5 eq) were dissolved in DCM (10

mL). The solution was stirred overnight at room temperature under argon. After overnight reaction, a white precipitate (urea of DIC) was formed. Subsequently, the precipitate was filtered off over cotton wool. Next, the solvent was concentrated under reduced pressure. Subsequently, the polymer was precipitated twice from DCM (2.5 mL) into acetone (25 mL) and once from DCM (2.5 mL) into Et_2O (25 mL). The white fluffy precipitate was filtered off, dried under high vacuum. **P26** was obtained as a white powder (0.2 g, 42% yield). **^{1}H NMR** (400 MHz, D_2O): δ 4.23-4.14 (b, x•2H, O=CNHCH$_2$C$\underline{H}_2$OC=O), δ 3.60 (b, n•2H, NHC$\underline{H}_2$CH$_2$OH), δ 3.60-3.40 (b, (m+n+x)•4H, NC$\underline{H}_2$C$\underline{H}_2$N), δ 3.40 (b, x•2H, O=CNHC$\underline{H}_2$CH$_2$OC=O), 3.35-3.28 (b, n•2H, NHCH$_2$C$\underline{H}_2$OH), 3.08-2.99 (b, x•2H, O=CC$\underline{H}_2$C$\underline{H}_2$COON), 3.01-2.90 (b, x•4H, ONO=CC$\underline{H}_2$C$\underline{H}_2$C=ONO), 2.88-2.80 (b, x•2H, O=CC$\underline{H}_2$C$\underline{H}_2$COON), 2.76-2.48 (b, (n+x)•4H, O=CC$\underline{H}_2$C$\underline{H}_2$C=ONH + x•4H, O=CC$\underline{H}_2$C$\underline{H}_2$C=O), 2.43-2.20 (b, m•2H, C$\underline{H}_2$CH$_2$CH$_3$), 1.65-1.50 (b, m•2H, CH$_2$C$\underline{H}_2$CH$_3$), 0.98-0.85 (b, m•3H, CH$_2$CH$_2$C$\underline{H}_3$). Experimentally determined monomer ratio (m/n): 69/15/16. **SEC** (PMMA) M_n 18.8 kg/mol, Đ 1.25

P27a P(*n*PropOx-c-OMe-c-OH) 70-15-15 - **P27a** was synthesized similar to **P26a** starting from **P25** (8 g, 0.63 mmol polymer, 20 mmol OH) using a mixture of 2-amino-ethanol (4.2 mL, 4.2 g, 69 mmol, 3.5 eq.) and 2-methoxyethylamine (6.0 mL, 5.1 g, 69 mmol, 3.5 eq.). **P27a** was obtained as a white foam (8.5 g, 97% yield). **^{1}H NMR** (500 MHz, D_2O): δ 3.60 (b, x•2H, NHC$\underline{H}_2$CH$_2$OH), δ 3.70-3.40 (b, (m+n+x)•4H, NC$\underline{H}_2$C$\underline{H}_2$N), 3.40 (b, n•3H, NHCH$_2$CH$_2$OC$\underline{H}_3$), 3.35-3.28 (b, x•2H, NHCH$_2$C$\underline{H}_2$OH + n•2H, NHCH$_2$C$\underline{H}_2$OCH$_3$), 2.76-2.48 (b, n•4H, O=CC$\underline{H}_2$C$\underline{H}_2$C=ONH), 2.43-2.20 (b, m•2H, C$\underline{H}_2$CH$_2$CH$_3$), 1.65-1.50 (b, m•2H, CH$_2$C$\underline{H}_2$CH$_3$), 0.98-0.85 (b, m•3H, CH$_2$CH$_2$C$\underline{H}_3$). Experimentally determined monomer ratio (m/n/x): 69/16/15. **SEC** (PMMA) M_n 12.4 kg/mol, Đ 1.16

P27b P(*n*PropOx-c-OMe-c-COOH) 70-15-15 - **P27b** was synthesized similar to **P26a** starting from **P27a** (6.4 g, 0.46 mmol polymer, 6.9 mmol ester, 1 eq.). **P27b** was obtained as a white solid (2.2 g, 30% yield). **^{1}H NMR** (400 MHz, D_2O): δ 4.23-4.14 (b, x•2H, O=CNHCH$_2$C$\underline{H}_2$OC=O), δ 3.60 (b, n•2H, NHC$\underline{H}_2$CH$_2$OCH$_3$), δ 3.60-3.40 (b, (m+n+x)•4H, NC$\underline{H}_2$C$\underline{H}_2$N), 3,45 (b, n•3H, NHCH$_2$CH$_2$OC$\underline{H}_3$), δ 3.40 (b, x•2H, O=CNHC$\underline{H}_2$CH$_2$OC=O), 3.35-3.28 (b, n•2H, NHCH$_2$C$\underline{H}_2$OCH$_3$), 2.76-2.48 (b, (n+x)•4H, O=CC$\underline{H}_2$C$\underline{H}_2$C=ONH + x•4H, O=CC$\underline{H}_2$C$\underline{H}_2$C=O), 2.43-2.20 (b, m•2H, C$\underline{H}_2$CH$_2$CH$_3$), 1.65-1.50 (b, m•2H, CH$_2$C$\underline{H}_2$CH$_3$), 0.98-0.85 (b, m•3H, CH$_2$CH$_2$C$\underline{H}_3$). Experimentally determined monomer ratio (m/n/x): 69/17/14. **SEC** (PMMA) no signal could be obtained

P27 P(*n*PropOx-c-OMe-c-NHS) 70-15-15 - **P27** was synthesized similar to **P26** starting from **P27b** (2.1 g, 2.0 mmol polymer, 29 mmol COOH). **P27** was obtained as a white foam (0.3 g, 15% yield).). **^{1}H NMR** (400 MHz, D_2O): δ 4.23-4.14 (b, x•2H, O=CNHCH$_2$C$\underline{H}_2$OC=O), δ 3.60 (b, n•2H, NHC$\underline{H}_2$CH$_2$OCH$_3$), δ 3.60-

3.40 (b, (m+n+x)•4H, NC$\underline{H}_2$C$\underline{H}_2$N), δ 3.40 (b, x•2H, O=CNHC$\underline{H}_2$CH$_2$OC=O), 3.35-3.28 (b, n•2H, NHCH$_2$C$\underline{H}_2$OCH$_3$), 3.08-2.99 (b, x•2H, O=CC$\underline{H}_2$C$\underline{H}_2$COON), 3.01-2.90 (b, x•4H, ONO=CC$\underline{H}_2$C$\underline{H}_2$C=ONO), 2.88-2.80 (b, x•2H, O=CC$\underline{H}_2$C$\underline{H}_2$COON), 2.76-2.48 (b, (n+x)•4H, O=CC$\underline{H}_2$C$\underline{H}_2$C=ONH + x•4H, O=CC$\underline{H}_2$C$\underline{H}_2$C=O), 2.43-2.20 (b, m•2H, C$\underline{H}_2$CH$_2$CH$_3$), 1.65-1.50 (b, m•2H, CH$_2$C$\underline{H}_2$CH$_3$), 0.98-0.85 (b, m•3H, CH$_2$CH$_2$C$\underline{H}_3$). Experimentally determined monomer ratio (m/n): 69/17/14. **SEC** (PMMA) M_n 21.1 kg/mol, Đ 1.35

P28a P(*n*PropOx-c-N(Me)$_2$-c-OH) 70-15-15 - **P28a** was synthesized similar to **P26a** starting from **P25** (7 g, 0.54 mmol polymer, 17 mmol ester, 1 eq.) using a mixture of 2-amino-ethanol (3.5 mL, 3.5 g, 59 mmol, 3.5 eq.) and *N*^{1},*N*^{1}-dimethyl ethylene-1,2-diamine (18.9 mL, 12.9 g, 179 mmol, 10.5 eq.). **P28a** was obtained as a white foam (7.4 g, 96% yield). **^{1}H NMR** (500 MHz, D$_2$O + 1v% HCl): δ 3.60 (b, x•2H, NHC$\underline{H}_2$CH$_2$OH), δ 3.70-3.40 (b, (m+n+x)•4H, NC$\underline{H}_2$C$\underline{H}_2$N), 3.35-3.28 (b, x•2H, NHCH$_2$C$\underline{H}_2$OH + n•2H, NHCH$_2$C$\underline{H}_2$ N(CH$_3$)$_2$), 2,85 (b, n•6H, NHCH$_2$CH$_2$N(C$\underline{H}_3$)$_2$), 2.76-2.48 (b, n•4H, O=CC$\underline{H}_2$C$\underline{H}_2$C=ONH), 2.43-2.20 (b, m•2H, C$\underline{H}_2$CH$_2$CH$_3$), 1.65-1.50 (b, m•2H, CH$_2$C$\underline{H}_2$CH$_3$), 0.98-0.85 (b, m•3H, CH$_2$CH$_2$C$\underline{H}_3$) Experimentally determined monomer ratio (m/n/x): 69/17/14 . **SEC** (PMMA) M_n 11.0 kg/mol, Đ 1.15

P28b P(*n*PropOx-c-N(Me)$_2$-c-COOH) 70-15-15 - **P28b** was synthesized similar to **P26b** starting from **P28a** (5.9 g, 0.42 mmol polymer, 6.3 mmol OH, 1 eq.). **P28b** was obtained as a white solid (4.2 g, 68% yield). **^{1}H NMR** (400 MHz, D$_2$O): δ 4.23-4.14 (b, x•2H, O=CNHCH$_2$C$\underline{H}_2$OC=O), δ 3.60-3.40 (b, (m+n+x)•4H, NC$\underline{H}_2$C$\underline{H}_2$N), 3.45 (b, n•3H, NHCH$_2$CH$_2$OC$\underline{H}_3$), δ 3.40 (b, x•2H, O=CNHC$\underline{H}_2$CH$_2$OC=O), 3.35-3.28 (b, n•2H, NHCH$_2$C$\underline{H}_2$N(CH$_3$)$_2$), 2.85 (b, n•6H, NHCH$_2$CH$_2$N(C$\underline{H}_3$)$_2$), 2.76-2.48 (b, (n+x)•4H, O=CC$\underline{H}_2$C$\underline{H}_2$C=ONH + x•4H, O=CC$\underline{H}_2$C$\underline{H}_2$C=O), 2.43-2.20 (b, m•2H, C$\underline{H}_2$CH$_2$CH$_3$), 1.65-1.50 (b, m•2H, CH$_2$C$\underline{H}_2$CH$_3$), 0.98-0.85 (b, m•3H, CH$_2$CH$_2$C$\underline{H}_3$). Experimentally determined monomer ratio (m/n/x): 69/15/16. **SEC** (PMMA) no signal could be obtained.

P28 P(*n*PropOx-c-OMe-c-NHS) 70-15-15 - **P28** was synthesized similar to **P26** starting from **P28b** (4.2 g, 0.27 mmol polymer, 4.2 mmol COOH, 1 eq.). **P28** was obtained as a white foam (4.2 g, 68% yield).). **^{1}H NMR** (400 MHz, D$_2$O): δ 4.23-4.14 (b, x•2H, O=CNHCH$_2$C$\underline{H}_2$OC=O), δ 3.60 (b, n•2H, NHC$\underline{H}_2$CH$_2$N(CH$_3$)$_2$), δ 3.60-3.40 (b, (m+n+x)•4H, NC$\underline{H}_2$C$\underline{H}_2$N), δ 3.40 (b, x•2H, O=CNHC$\underline{H}_2$CH$_2$OC=O), 3.35-3.28 (b, n•2H, NHCH$_2$C$\underline{H}_2$OCH$_3$), 3.08-2.99 (b, x•2H, O=CC$\underline{H}_2$C$\underline{H}_2$COON), 3.01-2.90 (b, x•4H, ONO=CC$\underline{H}_2$C$\underline{H}_2$C=ONO), 2.88-2.80 (b, x•2H, O=CC$\underline{H}_2$C$\underline{H}_2$COON), 2.85 (b, n•6H, NHCH$_2$CH$_2$N(C$\underline{H}_3$)$_2$), 2.76-2.48 (b, (n+x)•4H, O=CC$\underline{H}_2$C$\underline{H}_2$C=ONH + x•4H, O=CC$\underline{H}_2$C$\underline{H}_2$C=O), 2.43-2.20 (b, m•2H, C$\underline{H}_2$CH$_2$CH$_3$), 1.65-1.50 (b, m•2H, CH$_2$C$\underline{H}_2$CH$_3$), 0.98-0.85 (b, m•3H, CH$_2$CH$_2$C$\underline{H}_3$). Experimentally determined monomer ratio (m/n/x): 69/15/16. **SEC** (PMMA) M_n 22.1 kg/mol, Đ 1.33

7. References

1. D. A. Tomalia and D. P. Sheetz, *J. Polym. Sci. A Polym. Chem.*, 1966, **4**, 2253-2265.
2. W. Seeliger, E. Aufderhaar, W. Diepers, R. Feinauer, R. Nehring, W. Thier and H. Hellmann, *Angew. Chem. Int. Ed.*, 1966, **5**, 875-888.
3. T. G. Bassiri, A. Levy and M. Litt, *J. Polym. Sci. B Polym. Lett.*, 1967, **5**, 871-879.
4. T. Kagiya, S. Narisawa, T. Maeda and K. Fukui, *J. Polym. Sci. B Polym. Lett.*, 1966, **4**, 441-445.
5. R. Luxenhofer, Y. Han, A. Schulz, J. Tong, Z. He, A. V. Kabanov and R. Jordan, *Macromol. Rapid Commun.*, 2012, **33**, 1613-1631.
6. N. Adams and U. S. Schubert, *Adv. Drug Deliv. Rev.*, 2007, **59**, 1504-1520.
7. V. R. De La Rosa, *J. Mater. Sci. Mater. Med.*, 2014, **25**, 1211-1225.
8. B. Guillerm, S. Monge, V. Lapinte and J. J. Robin, *Macromol. Rapid Commun.*, 2012, **33**, 1600-1612.
9. R. Hoogenboom, *Angew. Chem. Int. Ed.*, 2009, **48**, 7978-7994.
10. E. Rossegger, V. Schenk and F. Wiesbrock, *Polymers*, 2013, **5**, 956-1011.
11. J.C.M.E. Bender and M.A. Boerman, WO Patent 2016056901, 2016.
12. H.-G. Batz, G. Franzmann and H. Ringsdorf, *Angew. Chem. Int. Ed.*, 1972, **11**, 1103-1104.
13. P. Ferruti, A. Bettelli and A. Feré, *Polymer*, 1972, **13**, 462-464.
14. K. Kempe, M. Lobert, R. Hoogenboom and U. S. Schubert, *J. Comb. Chem.*, 2009, **11**, 274-280.
15. H. Goossens, S. Catak, M. Glassner, V. R. de la Rosa, B. D. Monnery, F. De Proft, V. Van Speybroeck and R. Hoogenboom, *ACS Macro Letters*, 2013, **2**, 651-654.
16. B. Verbraeken, B. D. Monnery, K. Lava and R. Hoogenboom, *Eur. Polym. J.*, 2016, **88**, 451-469
17. M. A. Mees and R. Hoogenboom, *Macromolecules*, 2015, **48**, 3531-3538.
18. M. Jager, S. Schubert, S. Ochrimenko, D. Fischer and U. S. Schubert, *Chem. Soc. Rev.*, 2012, **41**, 4755-4767.
19. R. Tanaka, I. Ueoka, Y. Takaki, K. Kataoka and S. Saito, *Macromolecules*, 1983, **16**, 849-853.
20. T. Saegusa, H. Ikeda and H. Fujii, *Polym. J.*, 1972, **3**, 35-39.
21. H. M. L. Lambermont-Thijs, F. S. van der Woerdt, A. Baumgaertel, L. Bonami, F. E. Du Prez, U. S. Schubert and R. Hoogenboom, *Macromolecules*, 2010, **43**, 927-933.
22. L. Tauhardt, K. Kempe, K. Knop, E. Altuntaş, M. Jäger, S. Schubert, D. Fischer and U. S. Schubert, *Macromol. Chem. Phys.*, 2011, **212**, 1918-1924.
23. H. P. C. Van Kuringen, J. Lenoir, E. Adriaens, J. Bender, B. G. De Geest and R. Hoogenboom, *Macromol. Biosci.*, 2012, **12**, 1114-1123.
24. M. A. Gauthier, M. I. Gibson and H.-A. Klok, *Angew. Chem. Int. Ed.*, 2009, **48**, 48-58.
25. H. Staudinger, E. Geiger and E. Huber, *Ber. Dtsch. Chem. Ges.*, 1929, **62**, 263-267.
26. H. Staudinger, *Rubber Chem. Technol.*, 1939, **12**, 117-118.
27. K. A. Günay, P. Theato and H.-A. Klok, *J. Polym. Sci. A Polym. Chem.*, 2013, **51**, 1-28.
28. A. Gress, A. Völkel and H. Schlaad, *Macromolecules*, 2007, **40**, 7928-7933.
29. L. Tauhardt, D. Pretzel, K. Kempe, M. Gottschaldt, D. Pohlers and U. S. Schubert, *Polym. Chem.*, 2014, **5**, 5751-5764.
30. M. Schmitz, M. Kuhlmann, O. Reimann, C. P. R. Hackenberger and J. Groll, *Biomacromolecules*, 2015, **16**, 1088-1094.
31. G. Volet, T.-X. Lav, J. Babinot and C. Amiel, *Macromol. Chem. Phys.*, 2011, **212**, 118-124.
32. R. Luxenhofer and R. Jordan, *Macromolecules*, 2006, **39**, 3509-3516.
33. M. W. M. Fijten, C. Haensch, B. M. van Lankvelt, R. Hoogenboom and U. S. Schubert, *Macromol. Chem. Phys.*, 2008, **209**, 1887-1895.
34. K. Lava, B. Verbraeken and R. Hoogenboom, *Eur. Polym. J.*, 2015, **65**, 98-111.
35. M. A. Boerman, H. L. Van der Laan, J. C. M. E. Bender, R. Hoogenboom, J. A. Jansen, S. C. Leeuwenburgh and J. C. M. Van Hest, *J. Polym. Sci. A Polym. Chem.*, 2016, **54**, 1573-1582.
36. M. M. Contreras, C. Mattea, J. C. Rueda, S. Stapf and F. Bajd, *Des. Monomers. Polym.*, 2014, **18**, 170-179.

37. J. C. Rueda, M. Asmad, V. Ruiz, H. Komber, S. Zschoche and B. Voit, *Des. Monomers. Polym.*, 2015, **18**, 761-769.
38. J. C. Rueda, E. Campos, H. Komber, S. Zschoche, L. Häussler and B. Voit, *Des. Monomers. Polym.*, 2013, **17**, 208-216.
39. P. J. M. Bouten, PhD-Thesis, Radboud University, Nijmegen, 2016.
40. P. J. M. Bouten, D. Hertsen, M. Vergaelen, B. D. Monnery, M. A. Boerman, H. Goossens, S. Catak, J. C. M. van Hest, V. Van Speybroeck and R. Hoogenboom, *Polym. Chem.*, 2015, **6**, 514-518.
41. P. J. M. Bouten, D. Hertsen, M. Vergaelen, B. D. Monnery, S. Catak, J. C. M. van Hest, V. Van Speybroeck and R. Hoogenboom, *J. Polym. Sci. A Polym. Chem.*, 2015, **53**, 2649-2661.
42. P. J. M. Bouten, K. Lava, J. C. M. van Hest and R. Hoogenboom, *Polymers*, 2015, **7**, 1998-2008.
43. B. Gordon, L. Stratton, R. Verma and T. W. Smith, *Abstr. Pap. Am. Chem. Soc.*, 2014, **248**, 1.
44. B. Guillerm, S. Monge, V. Lapinte and J. J. Robin, *Macromol Rapid Commun*, 2012, **33**, 1600-1612.
45. A. Levy and M. Litt, *J. Polym. Sci. A Polym. Chem.*, 1968, **6**, 1883-1894.
46. H. Witte and W. Seeliger, *Liebigs Ann.*, 1974, **1974**, 996-1009.
47. S. Zeboudj, N. Belhanèche-Bensemra and R. Belabbès, *J. Food Eng.*, 2005, **67**, 507-512.
48. T. F. McKenna, *Chem. Eng. Sci.*, 1995, **50**, 453-467.
49. F. Wiesbrock, R. Hoogenboom, C. H. Abeln and U. S. Schubert, *Macromol. Rapid Commun.*, 2004, **25**, 1895-1899.
50. R. Hoogenboom, H. M. L. Thijs, M. J. H. C. Jochems, B. M. van Lankvelt, M. W. M. Fijten and U. S. Schubert, *Chem. Commun.*, 2008, **44**, 5758-5760.
51. R. Hoogenboom, M. W. M. Fijten, H. M. L. Thijs, B. M. van Lankvelt and U. S. Schubert, *Des. Monomers. Polym.*, 2005, **8**, 659-671.

Chapter 3:

Synthesis of pH- and thermoresponsive poly(2-*n*-propyl-2-oxazoline) based copolymers

Abstract

Polymers which possess lower critical solution temperature (LCST) behavior such as poly(2-alkyl-2-oxazoline)s (POx) are interesting for their application as stimulus-responsive materials, for example in the biomedical field. In this chapter, we discuss the scalable and controlled synthesis of a library of pH- and temperature-sensitive 2-*n*-propyl-2-oxazoline P(*n*PropOx) based copolymers containing amine and carboxylic acid functionalized side chains by cationic ring opening polymerization and post-polymerization functionalization strategies. Using turbidimetry, we found that the cloud point temperature (CP) is strongly dependent on both the polymer concentration and the polymer charge (as a function of pH). Furthermore, we observed that the CP decreased with increasing salt concentration, whereas the CP increased linearly with increasing amount of carboxylic acid groups. Finally, turbidimetry studies in PBS-buffer indicate that CPs of these polymers are close to body temperature at biologically relevant polymer concentrations, which demonstrates the potential of P(*n*PropOx) as stimulus-responsive polymeric systems in e.g. drug delivery applications.

Part of this chapter has been published
M. A. Boerman, H. L. Van der Laan, J. C. M. E. Bender, R. Hoogenboom, J. A. Jansen, S. C. Leeuwenburgh and J.C.M. Van Hest, *J. Polym. Sci. Part A-1: Polym. Chem.*, 2016, **54**, 1573-1582

1. Introduction

Stimuli-responsive polymeric systems are of great interest due to their potential in a wide range of applications (for e.g. drug delivery[1-3] and coating applications[4]). Polymers which possess lower critical solution temperature (or LCST) behavior are particularly interesting in that respect, since these thermosensitive polymers are water soluble below their so-called cloud point (CP), but insoluble above this critical temperature. This behavior is driven by an unfavorable entropy of mixing above the CP, which causes precipitation of the polymer from aqueous solutions. This CP depends on a large number of parameters including monomer composition, polymer concentration, overall hydrophobic/hydrophilic nature, polymer length, as well as external factors like the type of solvent, pH, salt concentration and other additives[5-10]

Poly(*N*-isopropyl acrylamide) (P(NIPAm)) is one of the most frequently studied thermoresponsive polymers (LCST ~ 32°C). Its occasionally challenging synthesis procedure, the occurrence of hysteresis between heating and cooling, as well as poor tunability of the transition temperature have, however, stimulated the search for polymer alternatives[11]. New candidates have been identified recently, such as the poly(oligo ethylene glycol) methacrylate family[12-14]. Another very promising type of polymers are the poly(2-alkyl-2-oxazoline)s[15-18] or POx, which are a class of pseudo-polypeptides that have gained increasing research interest because of their ease of synthesis, structural versatility and potential for application as biomaterials[19-21]. The wide range of studies on the thermoresponsive properties of POx that have been performed to date include the LCST behavior of 2-ethyl-2-oxazoline (EtOx, CP ~ 65°C), 2-isopropyl-2-oxazoline (*i*PropOx, CP ~ 37°C) and 2-n-propyl-2-oxazoline (*n*PropOx, CP~ 24°C) homopolymers, as well as a great number of POx based copolymers[22-26]. For application in the human body, a transition temperature around body temperature is essential. As a consequence, *i*PropOx based copolymers have been studied most extensively. The lower transition temperature of *n*PropOx based copolymers appears to make them the less obvious choice for biomedical purposes. Nevertheless, these more hydrophobic *n*PropOx based polymers can be of interest because of their solubility in a wide range of organic solvents, which renders them particularly suitable in e.g. coating applications, but also can make them of interest for preparing polymer-drug conjugates. Moreover, in comparison to P(*i*PropOx), P(*n*PropOx) has the additional advantage to be amorphous and does not show irreversible crystallization upon annealing above the CP[27-29]. Finally, taken into account that cationic ring opening polymerization allows for the introduction of a wide range of hydrophilic co-monomers, carrying for example carboxylic acid or amine moieties, these polymers can be made both temperature and pH responsive around body temperature.

To date however, no polymeric systems have been designed that combine both the beneficial properties of *n*PropOx and the structural versatility of POx in forming both pH and thermoresponsive polymers. Moreover, the solution properties of both pH and temperature responsive polymeric systems consisting entirely of POx are only scarcely reported and have not systematically been investigated in the field[30].

Since the direct incorporation of both amine and carboxylic acid moieties would interfere with the cationic ring opening polymerization of 2-oxazolines, both functionalities have to be introduced in a protected manner. To this end, the methyl ester-functionalized MestOx **3** is highly suitable[18]. After polymerization, it allows the introduction of both functional groups via a one-step modification reaction. The polymerization kinetics of this monomer with various 2-alkyl-2-oxazoline comonomers has been reported by Bouten et al.[31] and this monomer has also been copolymerized with P(NIPAm) and postmodified forming temperature- and pH-responsive polymers[30, 32]. In this respect, MestOx seems to be an ideal monomer for the synthesis of more polar and stimuli-responsive *n*PropOx-based copolymers.

Herein, we present the preparation and stimulus-responsive properties of P(*n*PropOx)-based copolymers containing carboxylic acid and amine functional side chains. We demonstrate a versatile scalable synthesis strategy of these polymers based on the copolymerization of *n*PropOx and MestOx followed by a modification reaction, yielding both pH- and thermoresponsive copolymers. Finally, using turbidimetry, a detailed study in various aqueous solutions is performed to determine the behavior of these polymers at various biologically relevant conditions.

2. Results and discussion

2.1 Polymer synthesis

The polymers were synthesized by cationic ring opening polymerization (CROP), using microwave reaction conditions[35] (**Scheme 1**). For the copolymerization of MestOx and *n*PropOx, the monomers were mixed in the desired ratios to form statistical copolymers with close to random monomer distribution as recently reported[36]. In these experiments, methyl tosylate was used as an initiator and piperidine as a terminating agent which prevents saponification of the methyl ester side chains of MestOx. After threefold precipitation in ether, **P1-P5** were obtained in multigram scale in overall high yields (76%). The polymers containing MestOx-side chains **P2-P5** were post-functionalized after polymerization. This was achieved either by (1) hydrolysis of the methyl ester side chains to carboxylic acid moieties using 1M NaOH, (**Scheme 1, ii**) or by (2) an amidation reaction in bulk using ethylene diamine as a solvent, yielding the polymer with amine-functionalized side chains (**Scheme 1, iii**)

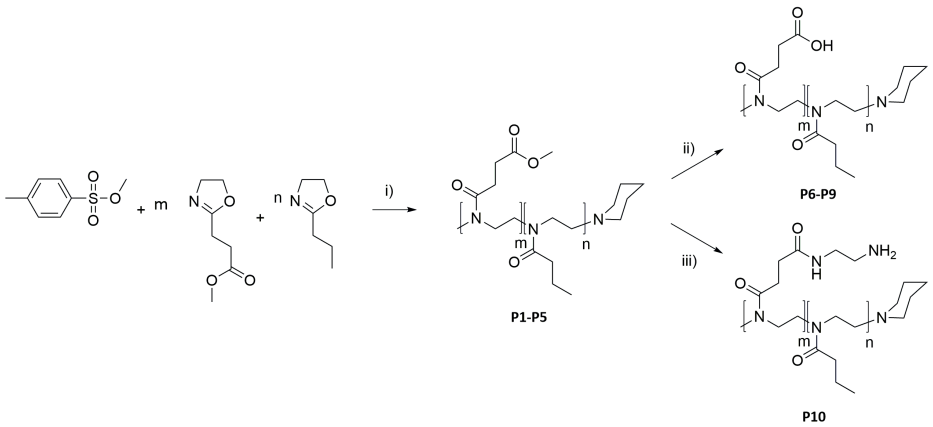

Scheme 1 Synthesis of polymers **P1-P10**; conditions: i) MeCN, 140°C, µW, 30 min, ii) NaOH (1M), rt, overnight, iii) ethylene diamine, rt, overnight.

The workup of **P6-P9** was performed by decreasing the pH of the solution to 4 in order to protonate the side chains, and subsequent heating, which caused the polymers to precipitate. After multiple cycles of dissolving the polymers and precipitation by heating, the polymers **P6-P9** were obtained as pure white powders in multigram quantities. This demonstrates that the thermoresponsive behavior of these copolymers can be utilized for the workup of these polymers.

For the amidation reaction, we aimed to synthesize polymers containing various molar percentages of amine functionalities. Unfortunately, we observed intermolecular crosslinking for polymers with higher degrees (>20%) of MestOx-functionalization. In future experiments, this could be circumvented by using e.g. mono-Boc-protected ethylene diamine, which can be coupled via the free amine group and subsequently be deprotected under acidic conditions. However, we chose to continue with the polymer that was successfully synthesized (**P10**). Since the work-up of this polymer (evaporation of solvent, followed by threefold precipitation in ether) proved insufficient to remove all ethylene diamine, a similar workup approach as for **P6-P9** was performed. The crude polymer was dissolved in water and brine was added, which caused precipitation of the polymer. After drying the polymer, **P10** was obtained in a pure state (30% yield).

The analytical data of the synthesized polymers are displayed in **Table 1** and the ^{1}H-NMR spectra of **P1**, **P2**, **P6** and **P10** are shown in **Figure 1**. The amount of MestOx that was incorporated into the polymers was well controlled as evidenced by ^{1}H-NMR spectroscopy and close to the theoretical value. This was also the case for the post-polymerization modifications (COOH and NH_2), indicating near-quantitative conversions. The deviations between theoretical and experimental M_n values as observed for all the synthesized polymers can be attributed to the

Table 1 Analytical data of synthesized polymers (**P1-P10**)

		Theor.	^{1}H-NMR			Yield		M_n (kg/mol)		
	Polymer	**mol% MestOx**	**mol% MestOx**	**mol% COOH**	**mol% NH_2**	**%**	**g**	**Theor.**	**SEC[a]**	**Đ**
P1	P(*n*PropOx)	-	-	-	-	76	1.9	11.4	20.2	1.20
P2	P(*n*PropOx-c-MestOx)	10	10	-	-	86	51.3	11.9	16.7	1.23
P3	P(*n*PropOx-c-MestOx)	30	30	-	-	87	23.4	12.7	20.1	1.17
P4	P(*n*PropOx-c-MestOx)	50	49	-	-	81	14.2	13.6	20.3	1.12
P5	P(*n*PropOx-c-MestOx)	70	72	-	-	q.	2.7	14.5	24.1	1.32
P6	P(*n*PropOx-c-COOH)	10	-	8	-	69	6.8	11.5	20.6	1.16
P7	P(*n*PropOx-c-COOH)	30	-	30	-	25	2.4	12.3	24.8	1.16
P8	P(*n*PropOx-c-COOH)	50	-	49	-	60	5.7	12.9	21.2	1.11
P9	P(*n*PropOx-c-COOH)	70	-	65	-	66	1.4	13.5	19.2	1.25
P10	P(*n*PropOx-c-NH_2)	10	-	-	9	30	1.4	12.1	21.4	1.20

[a] SEC was calibrated against PMMA standards, eluent: 0.1 % LiCl in DMA

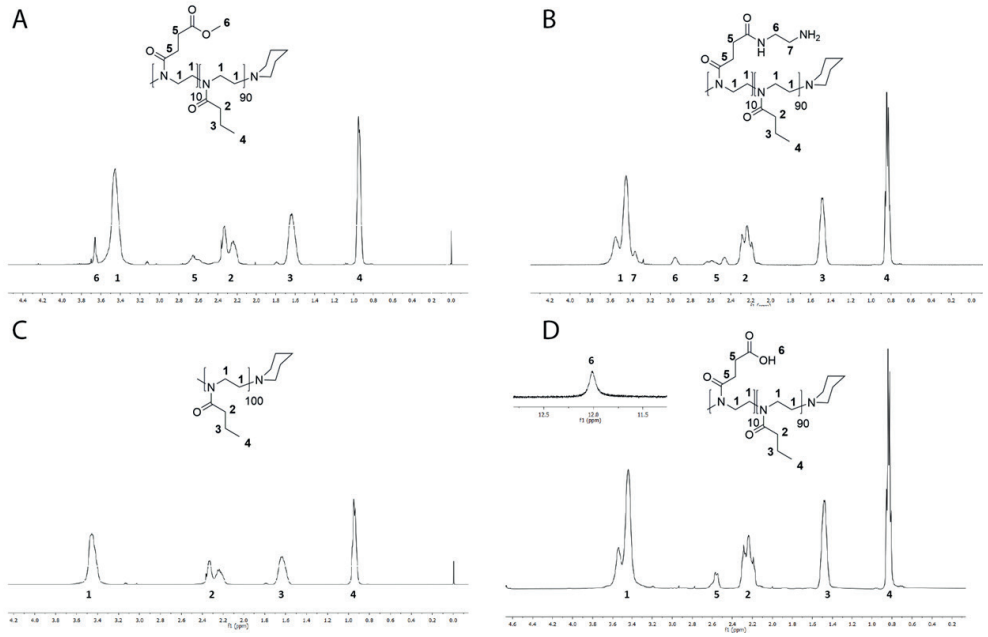

Figure 1 Overview of ^{1}H-NMR spectra of selected polymers. (**A**) **P2** recorded in $CDCl_3$, (**B**) **P10** recorded in D_2O, (**C**) **P1** recorded in $CDCl_3$, (**D**) **P6** recorded in D_2O + DMSO-*d*6 (COOH 12 ppm). The integrals of the end groups (Me (3 ppm) and piperidine) were observed only in case of **P1** and **P2**, but these were too small for accurate integration.

differences in hydrodynamic volume of the synthesized POx compared to the PMMA standards which were used for calibration. Integration of the end groups of the synthesized polymers proved to be too inaccurate for proper determination of the M_n by ^{1}H-NMR. The Đ of the polymers ranged from 1.1-1.3, indicating a precise control over the distribution of polymer chains.

2.2 Turbidimetry

2.2.1 Polymer concentration

Since polymer concentration is a key parameter in affecting the CP, this was investigated for **P1** and **P6-P8** (**Figure 2A**). It was expected that at lower polymer concentrations hydrogen bonds are more easily formed with surrounding water molecules, while at higher polymer concentrations competition with interchain aggregation of hydrophobic regions in the polymer chain would occur, which results in CP-induction. At higher polymer concentrations (20 mg/mL up to 5 mg/mL) the CPs of **P6-P8** were similar to the CPs of **P1** (~ 25°C), indicating that at these concentrations interchain aggregation causes these polymers to precipitate out of solution which results in cloud point formation, despite the hydrophilic side chains. At lower polymer concentrations (1 mg/mL) however, the ability of **P6-P8** to form hydrogen bonds with the surrounding water molecules was more predominant. This effect became more pronounced with increasing hydrophilicity of the side chains, as can be observed for polymers containing 10, 30 and 50% of carboxylic acid groups (from **P6** to **P8**), which showed CPs of 38, 47 and 55 °C, respectively. This is in contrast with **P1,** which was not easily hydrated due to the lack of hydrophilic side chains. As a result, the CPs recorded for this polymer were around 25 °C for all polymer concentrations.

2.2.2 Amount of COOH groups

Next, the influence of the molar percentage of carboxylic acid groups on the polymer's transition temperature was investigated (**Figure 2B**).

It was expected that incorporation of hydrophilic carboxylic acid groups would increase the water solubility, resulting into a higher CP. These studies were performed using polymers with 0 to 70 mol% of COOH. It was observed, as depicted in **Figure 2B**, that indeed a linear relationship existed between the amount of carboxylic acid groups on the polymer chain and the CP of the polymer solution in MQ (5 mg/mL). These results are in agreement with the findings of Hoogenboom et al.[27] and Park et al.[37] in which statistical copolymers of *n*PropOx with non-ionic hydrophilic co-monomers showed similar trends. Overall, increasing the amount of hydrophilic groups results in better polymer hydration and consequently a shift in CP from 24°C (0% COOH) to 39°C (70% COOH), as can be observed from **P1** to **P9**.

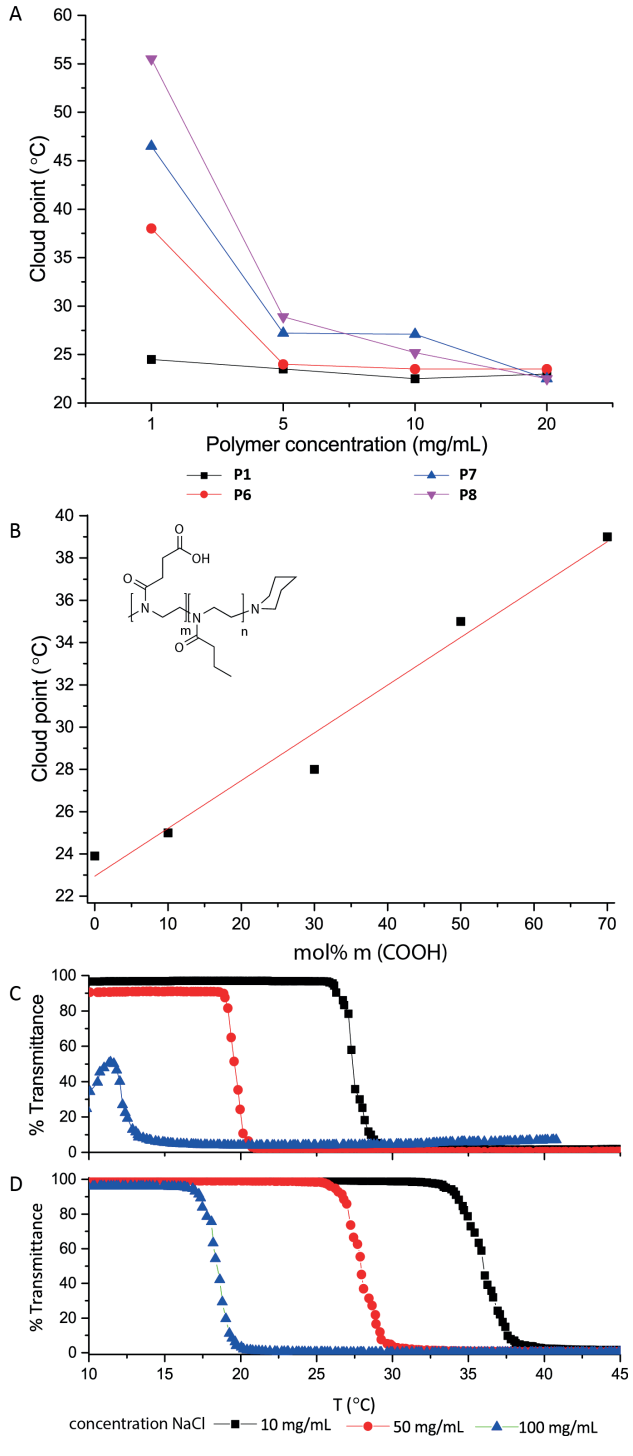

Figure 2 Turbidimetry study (**A**) Overview of cloud points of **P1, P6-P8** at various polymer concentrations in MQ water, (**B**) Overview of cloud points of **P1, P6-P9** in MQ-water (polymer concentration: 5 mg/mL), (**C**) **P6** at various concentrations of NaCl, (**D**) **P10** at various concentrations of NaCl. Polymer concentration: 5 mg/mL (**C** &**D**)

2.2.3 Influence of NaCl

To study the Hofmeister-related salting out effect[38] on the CP of the synthesized polymers, a turbidimetric study was performed for **P6** and **P10** at various salt concentrations, as depicted in **Figure 2C** and **2D**. As expected, at increasing salt concentrations, the CPs of the polymers dropped since the increased ionic strength of the solution as well as a salting out effect of NaCl facilitated precipitation of both polymers. This phenomenon was exploited in the synthesis of **P6** and **P10,** as was discussed before. This effect was more pronounced for the carboxylic acid-functionalized polymer as compared to the amine-functionalized polymer. It should be emphasized that **P6** (**Figure 2C**) seems to be at the limit of solubility for the measurement in a 100 mg/mL NaCl solution, since 100% transmittance was not reached in the consecutive heating and cooling cycles.

2.2.4 Effect of pH

The cloud points of polymers **P1,** acid-functional **P6** and amine-functional **P10** were also determined using turbidimetry measurements in buffers of different pH. This study was performed to investigate the influence of the ionization state/charge of the side chains of the polymers on their cloud points. In view of the consecutive pKa values of carboxylic acids (~4-5) and amines (~8-9), this experiment was conducted at pH 2 and pH 12 to ensure that the majority of the functional groups were in the protonated or deprotonated state. **P1** was measured as well to study the effect on the CP of a polymer without functional side chains in these solvent systems.

At pH 2 only **P1** and **P6** showed a CP (around 24 °C), while **P10** did not in the temperature range of 15-50 °C (**Figure 3A**). A CP was observed for **P6** since the carboxylic acid groups were protonated (**Figure 3B**), thereby reducing the charge and polarity of the side chains. The resulting polymers were less hydrophilic and as a consequence CP formation was observed. Another possible explanation for this phenomenon could be related to the formation of intramolecular hydrogen bonds with the amide groups present in the backbone of POx resulting from protonation of the carboxylic acid groups, thereby reducing the interaction with surrounding water molecules. This is in agreement with the findings of Weber et al. on copolymers based on P(EtOx) and methacrylic acid.[39] In contrast, **P10** was positively charged and consequently soluble over the entire temperature range.

At pH 12, a similar relationship between the charge of the side chains and the transition temperature was observed (**Figure 3C**). In this case, however, **P6** was fully deprotonated (**Figure 3D**) and did not show any transition temperature between 10 to 50 °C due to the hydrophilic side chains. Both **P1** and **P10** polymers, on the other hand, showed a transition temperature of 19 and 27 °C respectively, which can be explained by the absence of charge of the side chains, which plays a role

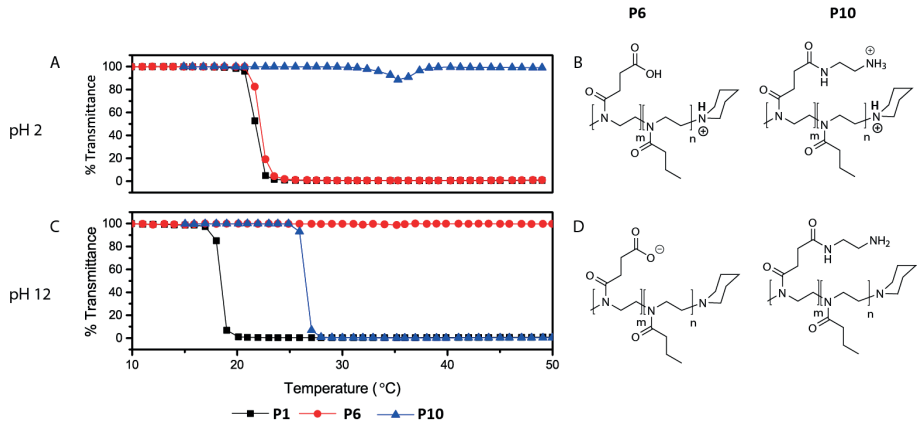

Figure 3 Turbidimetry plots of **P1, P6** and **P10** in phosphate buffers pH 2 (**A**) and pH 12 (**C**). The ionization states are given respectively in **B** (pH 2) and **D** (pH 12). Polymer concentration: 10 mg/mL.

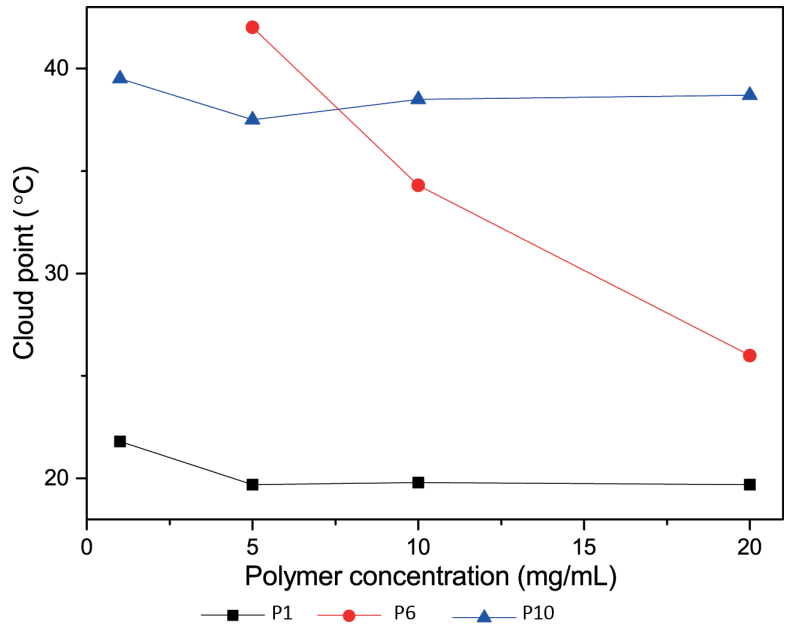

Figure 4 Overview of cloud points of **P1, P6** and **P10** at various polymer concentrations in PBS buffer (0.1 M)

in the hydration of the polymer chains. The lower CP of **P1** at pH 12 compared to pH 2 might be explained by the partial deprotonation of the piperidine end groups, thereby making the polymer less charged (less hydrophilic) which induced a small decrease in the CP compared to the measurement at pH 2. In addition, the minor change in ionic strength may also have a small influence on the CP.

2.2.5 PBS

To study the solution behavior of these polymers in biologically relevant conditions, turbidimetry measurements were performed in PBS buffer using **P1**, **P6** and **P10** at various polymer concentrations (**Figure 4**).

As expected, **P1** showed a cloud point at 20 °C, irrespective of the polymer concentration because of the lack of hydrophilic side chains; this value was slightly lower than in the measurements in MQ because of the salting out effect. By introduction of functional groups (**P6** and **P10**), however, the cloud points increased and these polymers became soluble around body temperature. **P6** showed a similar behavior as observed in water, since a CP was not observed by turbidimetry at a polymer concentration of 1 mg/mL, presumably because of the more hydrophilic nature of the deprotonated carboxylic acid groups. In contrast, **P10** did not show an effect on the polymer concentration. It seems that the amines are more easily hydrated/dehydrated independent of the polymer concentration, resulting in a constant CP around 38 °C for these polymers. It is evident that incorporation of carboxylic acid or amine groups renders the polymers more hydrophilic and soluble around body temperature.

3. Conclusions

Various P(*n*PropOx-c-MestOx) copolymers were successfully synthesized and functionalized with amine and carboxylic acid groups, thereby allowing for precise control over their chemical composition. Turbidimetry studies showed that the CP of these polymers was lowered by the addition of sodium chloride due to charge screening and/or salting out. The CP increased linearly with increasing amount of carboxylic acid groups on the polymer. Moreover, a sharp increase in CP was observed at lower polymer concentrations (1 mg/mL) compared to higher polymer concentrations. The pH of the solution was a key parameter since the charge of the polymer chains dominated the CP. As a consequence, the CP can be tuned by changing the pH of the polymer solution. As evidenced by measurements in PBS, these copolymers become soluble around body temperature upon incorporation of amine and carboxylic acid groups, which demonstrates the potential of these

P(*n*PropOx) based co-polymers as both temperature and pH- responsive systems at physiologically relevant conditions.

4. Acknowledgements

Harry van der Laan is kindly acknowledged for his contributions to the work described in this chapter.

5. Experimental

5.1 Materials

All reagents (synthesis grade) for the synthesis of the monomers were purchased at Sigma Aldrich and used without further purification, unless stated otherwise. All reagents for the synthesis of the polymers were distilled twice before use in the polymerizations. Acetonitrile was dried and dispensed under nitrogen atmosphere by using an MBraun MB SPS-800 solvent dispersing system. For turbidimetry measurements, ultrapure Milli-Q water (MQ) was obtained from a WaterPro PS polisher (Labconco, Kansas City, MO) set to 18.2 MΩ/cm.

5.2 Characterization

^{1}H-NMR and ^{13}C-NMR spectra were recorded on a Bruker Avance III 500MHz spectrometer using the solvents D_2O, MeOD, $CDCl_3$ or DMSO-d6. FT-IR measurements were performed on a Bruker Tensor 27 IR ATR spectrometer. Microwave-assisted polymerizations were performed in a Biotage Initiator+, equipped with an autosampler. Size exclusion chromatography (SEC) was performed on an Agilent 1260 - series HPLC system equipped with a 1260 online degasser, a 1260 ISO-pump, a 1260 automatic liquid sampler, a thermostatted column compartment, a 1260 diode array detector (DAD) and a 1260 refractive index detector (RID). Analyses were performed on two Mixed-D and a guard column in series at 50 °C. As an eluent, *N,N*-dimethylacetamide (DMA), containing LiCl (concentration 50 mM), was used at a flow rate of 0.593 ml min^{-1}. The SEC traces were analyzed using the Agilent Chemstation software with the GPC add on. Number average molecular weights (M_n), weight average molecular weights (M_w), and dispersity (Đ) values were calculated against poly(methyl methacrylate) (PMMA) standards. Monomers were distilled using a KDL-1 Wiped film evaporation setup (UIC GmbH) containing both an oil pump and an oil diffusion pump. Details can be found in **Chapter 2**.

5.3 Synthesis

The synthetic procedures of monomers can be found in the experimental section of **Chapter 2**.

Polymer synthesis

The polymers were prepared analogous to the polymers described in **Chapter 2**

P1- P(*n*PropOx) - Methyl tosylate (0.131 mL, 0.870 mmol), *n*PropOx (4.83 mL, 43.5 mmol) and acetonitrile (7.60 mL) were mixed in a dry microwave vial under inert atmosphere (Ar). The polymerization was heated for 30 min under microwave irradiation after which dry piperidine (0.430 mL, 4.35 mmol) was added to the reaction mixture, which was stirred for three hours. The polymer was dissolved in an appropriate amount of DCM and precipitated in diethylether (DCM/Et_2O, v/v, 1:20). This procedure was performed two times. The resulting suspension was filtered and the residue dissolved in DCM (100 mL). The solvent was evaporated under reduced pressure. P(*n*PropOx) (**P1**) was obtained as a white foam (1.9 g, 76% yield). **^{1}H NMR** (500 MHz, $CDCl_3$) δ 3.48 (b, n·4H, $NC\underline{H}_2C\underline{H}_2N$), 3.05 (b, 3H, $C\underline{H}_3$-NCHCH-), 2.35-2.20 (b, n·2H, CO-$C\underline{H}_2$-CH_2-CH_3), 1.60-1.40 (b, n·2H, CO-CH_2-$C\underline{H}_2$-CH_3), 0.92-1.01 (b, n·3H, CO-CH_2-CH_2-$C\underline{H}_3$) **FT-IR**: 1636 cm^{-1} (CO amide) **SEC** (PMMA) M_n 20.2 kg/mol, Đ 1.20

P2- P(*n*PropOx-c-MestOx) 90-10 - Methyl tosylate (0.131 mL, 0.870 mmol), *n*PropOx (4.83 mL, 43.5 mmol), MestOx (2.99 mL, 21.8 mmol) and acetonitrile (7.60 mL) were mixed in a Schlenk flask under inert atmosphere (Ar). After the addition, the flask was put in a preheated oil bath (80 °C) and stirred during 10 hrs. Next, dry piperidine (0.430 mL, 4.35 mmol) was added to the reaction mixture, which was stirred for three hours. The polymer was dissolved in an appropriate amount of DCM and precipitated in diethyl ether (DCM/Et_2O, v/v, 1:20). This procedure was performed two times. The resulting suspension was filtered and the residue dissolved in DCM (100 mL). The solvent was evaporated under reduced pressure. P(nPropOx)-c-MestOx) 90-10 (**P2**) was obtained as a white foam (53.1 g, 76% yield). **^{1}H NMR** (500 MHz, $CDCl_3$) δ 3.66 (b, m·3H, CO-O-$C\underline{H}_3$), δ 3.48 (b, (m+n)·4H, $NC\underline{H}_2C\underline{H}_2N$), 3.03 (b, 3H, $C\underline{H}_3$-NCHCH-), 2.70-2.60 (b, m·4H, $COC\underline{H}_2C\underline{H}_2CO$), 2.35-2.20 (b, n·2H, CO-$C\underline{H}_2$-CH_2-CH_3), 1.70-1.60 (b, n·2H, CO-CH_2-$C\underline{H}_2$-CH_3), 0.91-1.02 (b, n·3H, CO-CH_2-CH_2-$C\underline{H}_3$) **SEC** (PMMA) M_n 16.7 kg/mol, Đ 1.23

P3- P(*n*PropOx-c-MestOx) 70-30 - The reaction was performed similar to **P2** using methyl tosylate (0.131 mL, 0.870 mmol), *n*PropOx (4.83 mL, 43.5 mmol), MestOx (2.99 mL, 21.8 mmol) and acetonitrile (7.60 mL). P(*n*PropOx)-c-MestOx) 90-10 (**P3**) was obtained as a white foam (23.4 g, 86% yield). **^{1}H NMR** (500 MHz, $CDCl_3$) δ 3.66 (b, m·3H, CO-O-$C\underline{H}_3$), δ 3.48 (b, (m+n)·4H, $NC\underline{H}_2C\underline{H}_2N$), 3.03 (b, 3H, $C\underline{H}_3$-NCHCH-), 2.70-2.60 (b, m·4H, $COC\underline{H}_2C\underline{H}_2CO$), 2.35-2.20 (b, n·2H, CO-$C\underline{H}_2$-CH_2-CH_3), 1.70-1.60 (b, n·2H, CO-CH_2-$C\underline{H}_2$-CH_3), 0.93-1.01 (b, n·3H, CO-CH_2-CH_2-$C\underline{H}_3$) **SEC** (PMMA) M_n 20.1 kg/mol, Đ 1.17

P4- P(*n*PropOx-c-MestOx) 50-50 - The reaction was performed similar to **P2** using methyl tosylate (0.131 mL, 0.870 mmol), *n*PropOx (4.83 mL, 43.5 mmol), MestOx (2.99 mL, 21.8 mmol) and acetonitrile (7.60 mL). P(*n*PropOx)-c-MestOx) 50-50 (**P4**) was obtained as a white foam (14.2 g, 81% yield). **^{1}H NMR** (500 MHz, $CDCl_3$) δ 3.66 (b, n·3H, CO-O-$C\underline{H}_3$), δ 3.48 (b, (m+n)·4H, $NC\underline{H}_2C\underline{H}_2N$), 3.03 (b, 3H, $C\underline{H}_3$-NCHCH-), 2.70-2.60 (b, m·4H, $COC\underline{H}_2C\underline{H}_2CO$), 2.35-2.20 (b, n·2H, CO-$C\underline{H}_2$-CH_2-CH_3), 1.70-1.60 (b, n·2H, CO-CH_2-$C\underline{H}_2$-CH_3), 0.90-1.01 (b, n·3H, CO-CH_2-CH_2-$C\underline{H}_3$) **SEC** (PMMA) M_n 20.3 kg/mol, Đ 1.12

P5- P(*n*PropOx-c-MestOx) 30-70 - The reaction was performed similar to **P1** using methyl tosylate (0.032 mL, 0.214 mmol), *n*PropOx (0.713 mL, 6.4 mmol), MestOx (2.06 mL, 21.8 mmol) and acetonitrile (2.54 mL). P(*n*PropOx)-c-MestOx) 30-70 (**P5**) was obtained as a white foam (2.7 g, quant. yield). **^{1}H NMR** (500 MHz, $CDCl_3$) δ 3.60 (b, m·3H, CO-O-$C\underline{H}_3$), δ 3.45 (b, (m+n)·4H, $NC\underline{H}_2C\underline{H}_2N$), 2.70-2.50 (b, m·4H, $COC\underline{H}_2C\underline{H}_2CO$), 2.35-2.15 (b, n·2H, CO-$C\underline{H}_2$-CH_2-CH_3), 1.50 (b, n·2H, CO-CH_2-$C\underline{H}_2$-CH_3), 0.91-1.01 (b, n·3H, CO-CH_2-CH_2-$C\underline{H}_3$) **SEC** (PMMA) M_n 20.7 kg/mol, Đ 1.32

Protocol 1: General procedure ester hydrolysis (P6-P9)

P(*n*PropOx-c-MestOx) (**P2-P5**) was dissolved in a 0.1 M-solution of NaOH (100 mL) and stirred overnight. The reaction mixture was acidified to pH 4 by dropwise addition of a 0.1M-solution of HCl. The reaction mixture was stirred in a heated water bath (45°C) which caused precipitation of the polymer as a sticky white precipitate. The precipitate was dissolved in cold water (100 mL) and the reaction mixture was stirred again in the heated water bath, which caused the polymer to precipitate again. The pH of the solution was 4. The sticky white precipitate was either (1) dissolved again in DCM (100 mL) and concentrated under reduced pressure or (2) precipitated from DMF (20 mL) into diethyl ether (2000 mL) and subsequently filtered and dried under high vacuum, yielding the final polymer as a white fluffy powder.

P6- P(*n*PropOx-c-COOH) 90-10 was synthesized from **P2** (10.2 g, 9 mmol functional groups) according to protocol 1, yielding P(*n*PropOx-c-COOH) 90-10 (**P6**) as a white solid (6.8 g, 68% yield). **^{1}H NMR** (500 MHz, D_2O) δ 3.71-3.30 (b, (m+n)·4H, $NC\underline{H}_2C\underline{H}_2N$), 2.60-2.50 (b, m·4H, $COC\underline{H}_2C\underline{H}_2CO$), 2.35-2.20 (b, n·2H, CO-$C\underline{H}_2$-CH_2-CH_3), 1.50-1.40 (b, n·2H, CO-CH_2-$C\underline{H}_2$-CH_3), 0.90-1.00 (b, n·3H, CO-CH_2-CH_2-$C\underline{H}_3$) (500 MHz, DMSO-d6) δ 12.01 (b, m·1H, COOH) **FT-IR**: 1639 cm^{-1} (CO amide), 1729 cm^{-1} (CO carboxylic acid), 3503 cm^{-1} (OH carboxylic acid) **SEC** (PMMA) M_n 20.6 kg/mol, Đ 1.16

P7- P(*n*PropOx-c-COOH) 70-30 was synthesized from **P3** (10.0 g, 24 mmol functional groups) according to protocol 1, yielding P(*n*PropOx-c-COOH) 70-30 (**P7**) as a white solid (2.4 g, 25% yield). **^{1}H NMR** (500 MHz, D_2O) δ 3.72-3.32 (b, (m+n)·4H, $NC\underline{H}_2C\underline{H}_2N$), 2.60-2.50 (b, m·4H, $COC\underline{H}_2C\underline{H}_2CO$), 2.35-2.20 (b, n·2H, CO-$C\underline{H}_2$-CH_2-

CH_3), 1.50-1.40 (b, n·2H, CO-CH_2-$C\underline{H}_2$-CH_3), 0.90-1.00 (b, n·3H, CO-CH_2-CH_2-$C\underline{H}_3$) **SEC** (PMMA) M_n 24.8 kg/mol, Đ 1.16

P8- **P(nPropOx-c-COOH) 50-50** was synthesized from **P4** (10.0 g, 40 mmol functional groups) according to protocol 1, yielding P(*n*PropOx-COOH) 50-50 (**P8**) as a white solid (6.8 g, 68% yield). **^{1}H NMR** (500 MHz, D_2O) δ 3.70-3.30 (b, (m+n)·4H, NC$\underline{H}_2$C$\underline{H}_2$N), 2.60-2.50 (b, m·4H, COC$\underline{H}_2$C$\underline{H}_2$CO), 2.35-2.20 (b, n·2H, CO-C$\underline{H}_2$-CH_2-CH_3), 1.50-1.40 (b, n·2H, CO-CH_2-$C\underline{H}_2$-CH_3), 0.90-1.00 (b, n·3H, CO-CH_2-CH_2-$C\underline{H}_3$) (500 MHz, DMSO-d6) δ 11,68 (b, n·1H, COOH) **FT-IR**: 1619 cm^{-1} (CO amide), 1721 cm^{-1} (CO carboxylic acid), 3413 cm^{-1} (OH carboxylic acid) **SEC** (PMMA) M_n 21.2 kg/mol, Đ 1.11

P9- **P(*n*PropOx-c-COOH) 30-70** was synthesized from **P4** (2.21 g, 10 mmol functional groups) according to protocol 1, yielding P(*n*PropOx-COOH) 30-70 (**P9**) as a white solid (1.4 g, 66% yield). **^{1}H NMR** (500 MHz, D_2O) δ 3.71-3.42 (b, (m+n)·4H, NC$\underline{H}_2$C$\underline{H}_2$N), 2.71-2.51 (b, m·4H, COC$\underline{H}_2$C$\underline{H}_2$CO), 2.42-2.12 (b, n·2H, CO-C$\underline{H}_2$-CH_2-CH_3), 1.60-1.41 (b, n·2H, CO-CH_2-$C\underline{H}_2$-CH_3), 0.91-0.89 (b, n·3H, CO-CH_2-CH_2-$C\underline{H}_3$) **FT-IR**: 1627 cm^{-1} (CO amide), 1714 cm^{-1} (CO carboxylic acid), 3363 cm^{-1} (OH carboxylic acid) **SEC** (PMMA) M_n 19.2 kg/mol, Đ 1.25

Amidation

P10-P(*n*PropOx-c-NH_2) 90-10 was synthesized following a modified literature procedure[40] **- P2** (4.21 g, 4 mmol functional groups) was dissolved in ethylene diamine (25 mL, 22.5 g, 0.37 mol, 10 eq.) . The reaction mixture was allowed to stir overnight. Excess ethylene diamine was removed under reduced pressure. The polymer was dissolved in methanol (20 mL) and precipitated in diethyl ether (250 mL). A sticky precipitate was formed. This was repeated twice. In order to remove residual ethylene diamine, the polymer was subsequently dissolved in cold water (50 mL), after which brine (10 mL) was added and the mixture was stirred in a water bath (50 °C), causing the polymer to precipitate. After this, the polymer was dissolved in methanol (30 mL). After concentration of the solvent under reduced pressure, P(*n*PropOx-c-NH_2) (**P10**) was obtained as a white solid (1,4 g, 30% yield) **^{1}H NMR** (500 MHz, D_2O) δ 3.55-3.35 (b, n·4H, NC$\underline{H}_2$C$\underline{H}_2$N), 3.35-3.30 (b, m·2H, CONH-CH_2C$\underline{H}_2$-NH_2), 2.95-2.90 (b, m·2H, CONH-C$\underline{H}_2$$CH_2$-$NH_2$), 2.70-2.55 (b, m·2H, COC$\underline{H}_2$$CH_2$CO), 2.55-2.40 (b, m·2H, COCH_2C$\underline{H}_2$CO), 2.35-2.20 (b, n·2H, CO-C$\underline{H}_2$-CH_2-CH_3), 1.55-1.40 (b, n·2H, CO-CH_2-$C\underline{H}_2$-CH_3), 0.90-0.80 (b, 3H, n·CO-CH_2-CH_2-$C\underline{H}_3$) **FT-IR**: 1670 cm^{-1} (CO amide), 3470 cm^{-1} (NH stretch) **SEC** (PMMA) M_n 21.4 kg/mol, Đ 1.20

5.4 Turbidimetry

UV-VIS spectra were recorded on a Jasco V650 containing a temperature controller at a wavelength of 500 nm. Measurements were conducted at various polymer

concentrations using different aqueous solutions, both specified in the main text. For these measurements, two subsequent cycles of heating and cooling were conducted. The CPs were recorded as the temperature (°C) at which 50% transmittance was observed during the second heating cycle without stirring. The measurements at the different pH-values were performed using phosphate buffers of pH 2 and pH 12 as a solvent.

6. References

1. A. S. Hoffman, *Adv. Drug Deliv. Rev.*, 2013, **65**, 10-16.
2. S. Mura, J. Nicolas and P. Couvreur, *Nat. Mater.*, 2013, **12**, 991-1003.
3. R. Cheng, F. Meng, C. Deng, H. A. Klok and Z. Zhong, *Biomaterials*, 2013, **34**, 3647-3657.
4. C. Alexander and K. M. Shakesheff, *Adv. Mater.*, 2006, **18**, 3321-3328.
5. S. Huber and R. Jordan, *Colloid Polym. Sci*, 2008, **286**, 395-402.
6. S. Ahn, E. C. Monge and S.-C. Song, *Langmuir* 2009, **25**, 2407-2418.
7. M. M. Bloksma, D. J. Bakker, C. Weber, R. Hoogenboom and U. S. Schubert, *Macromol. Rapid Commun.*, 2010, **31**, 724-728.
8. H. Du, R. Wickramasinghe and X. Qian, *J. Phys. Chem. B*, 2010, **114**, 16594-16604.
9. S. B. Lee, S.-C. Song, J.-I. Jin and Y. S. Sohn, *Polym. Bull.*, 2000, **45**, 389-396.
10. K. Van Durme, H. Rahier and B. Van Mele, *Macromolecules*, 2005, **38**, 10155-10163.
11. J.-F. Lutz, Ö. Akdemir and A. Hoth, *J. Am. Chem. Soc.*, 2006, **128**, 13046-13047.
12. M. A. Ward and T. K. Georgiou, *Polymers*, 2011, **3**, 1215.
13. C. Weber, R. Hoogenboom and U. S. Schubert, *Prog. Polym. Sci.*, 2012, **37**, 686-714.
14. J.-F. Lutz, *J. Polym. Sci. Part A: Polym. Chem.*, 2008, **46**, 3459-3470.
15. W. Seeliger, E. Aufderhaar, W. Diepers, R. Feinauer, R. Nehring, W. Thier and H. Hellmann, *Angew. Chem. Int. Ed.*, 1966, **5**, 875-888.
16. D. A. Tomalia and D. P. Sheetz, *J. Polym. Sci. A Polym. Chem.*, 1966, **4**, 2253-2265.
17. T. Kagiya, S. Narisawa, T. Maeda and K. Fukui, *J. Polym. Sci. B Polym. Lett.*, 1966, **4**, 441-445.
18. T. G. Bassiri, A. Levy and M. Litt, *J. Polym. Sci. B Polym. Lett.*, 1967, **5**, 871-879.
19. N. Adams and U. S. Schubert, *Adv. Drug Deliv. Rev.*, 2007, **59**, 1504-1520.
20. R. Hoogenboom, *Angew. Chem. Int. Ed.*, 2009, **48**, 7978-7994.
21. R. Luxenhofer, Y. Han, A. Schulz, J. Tong, Z. He, A. V. Kabanov and R. Jordan, *Macromol. Rapid Commun.*, 2012, **33**, 1613-1631.
22. M. Meyer, M. Antonietti and H. Schlaad, *Soft Matter*, 2007, **3**, 430.
23. R. Obeid, F. Tanaka and F. M. Winnik, *Macromolecules*, 2009, **42**, 5818-5828.
24. C. Diehl, P. Cernoch, I. Zenke, H. Runge, R. Pitschke, J. Hartmann, B. Tiersch and H. Schlaad, *Soft Matter*, 2010, **6**, 3784-3788.
25. R. Hoogenboom and H. Schlaad, *Polym. Chem.*, 2017, **8**, 24-40.
26. P. J. M. Bouten, K. Lava, J. C. M. van Hest and R. Hoogenboom, *Polymers*, 2015, **7**, 1998-2008.
27. R. Hoogenboom, H. M. L. Thijs, M. J. H. C. Jochems, B. M. van Lankvelt, M. W. M. Fijten and U. S. Schubert, *Chem. Commun.*, 2008, **44**, 5758-5760.
28. C. Diehl and H. Schlaad, *Macromol. Biosci.*, 2009, **9**, 157-161.
29. K. Kempe, C. Weber, K. Babiuch, M. Gottschaldt, R. Hoogenboom and U. S. Schubert, *Biomacromolecules*, 2011, **12**, 2591-2600.
30. J. C. Rueda, M. Asmad, V. Ruiz, H. Komber, S. Zschoche and B. Voit, *Des. Monomers. Polym.*, 2015, **18**, 761-769.
31. P. J. M. Bouten, D. Hertsen, M. Vergaelen, B. D. Monnery, S. Catak, J. C. M. van Hest, V. Van Speybroeck and R. Hoogenboom, *J. Polym. Sci. A Polym. Chem.*, 2015, **53**, 2649-2661.
32. J. C. Rueda, E. Campos, H. Komber, S. Zschoche, L. Häussler and B. Voit, *Des. Monomers. Polym.*, 2013, **17**, 208-216.
33. A. Levy and M. Litt, *J. Polym. Sci. A Polym. Chem.*, 1968, **6**, 1883-1894.
34. H. Witte and W. Seeliger, *Liebigs Ann.*, 1974, **1974**, 996-1009.
35. F. Wiesbrock, R. Hoogenboom, C. H. Abeln and U. S. Schubert, *Macromol. Rapid Commun.*, 2004, **25**, 1895-1899.
36. P. J. M. Bouten, D. Hertsen, M. Vergaelen, B. D. Monnery, M. A. Boerman, H. Goossens, S. Catak, J. C. M. van Hest, V. Van Speybroeck and R. Hoogenboom, *Polym. Chem.*, 2015, **6**, 514-518.

37. J.-S. Park and K. Kataoka, *Macromolecules*, 2007, **40**, 3599-3609.
38. F. Hofmeister, *Arch. Exp. Pathol. Pharmakol*, 1888, **24**, 247-260.
39. C. Weber, C. Remzi Becer, W. Guenther, R. Hoogenboom and U. S. Schubert, *Macromolecules*, 2010, **43**, 160-167.
40. M. A. Mees and R. Hoogenboom, *Macromolecules*, 2015, **48**, 3531-3538

Chapter 4:

Next generation hemostatic materials based on NHS-ester functionalized poly(2-oxazoline)s

Abstract

In order to prevent hemorrhage during surgical procedures on soft tissue, a wide range of hemostatic agents have been developed in the field so far. However, their efficacy is variable and the majority of these agents are derived from animal or human material and/or use bioactive components to accelerate coagulation. In this chapter, we develop a synthetic, non-bioactive hemostatic product by coating N-hydroxysuccinimide ester (NHS)-functional poly(2-oxazoline)s (**NHS-POx**) onto gelatin patches, which act by formation of covalent crosslinks between polymer, host blood proteins, gelatin and tissue to seal the wound site and prevent hemorrhage during surgery. We study different process parameters (including polymer, carrier and coating technique) in direct comparison with clinical products (Hemopatch® and Tachosil®) to obtain deeper understanding of this class of hemostatic products. In this work, we successfully prove the hemostatic efficacy of **NHS-POx** as polymer powders and coated patches both *in vitro* and *in vivo* against Hemopatch® and Tachosil®, demonstrating that **NHS-POx** are excellent candidate polymers for the development of next generation hemostatic patches.

Part of this chapter has been published

M.A. Boerman, E.Roozen, M.J. Sánchez-Fernández, A.R. Keereweer, R.P. Félix Lanao, J.C.M.E. Bender, R. Hoogenboom, S.C. Leeuwenburgh, J.A. Jansen, H. Van Goor, J.C.M. Van Hest, *Biomacromolecules*, 2017, **18**, 2529-2538

1. Introduction

One of the main challenges during surgical procedures on parenchymatous tissue is to attain control over bleeding[1]. Suture control, electrocautery[2] and ultrasonic sealing[3] often do not suffice during operations on for example liver or kidneys. As a result, procedures like hepatic resections[4] or partial nephrectomy[5] require an alternative approach to control bleeding. For this purpose, a wide range of topical hemostatic products has been developed and are clinically available[6-8].

Nevertheless, as has been described in detail in **Chapter 1**, currently available products (both natural and synthetic) suffer from drawbacks which limits their use for treatment of profuse bleedings during surgery on soft tissue. Naturally derived hemostatic products [9-15] (e.g. gelatin sponges), which act by means of the natural blood coagulation cascade, have a limited capability to seal large wound areas. In addition, these products are only effective to a limited extent in patients receiving anticoagulants during surgery, while they also are associated with potential transmission of animal borne diseases. Synthetic hemostatic products[16,17] act independently of the natural coagulation cascade by sealing the bleeding surface of the wound. Although for this class superior hemostatic efficacy has been reported over their natural counterparts, these products have not found widespread acknowledgement in the field yet, since for some of these polymers toxicity has been reported during application[17]. In addition, some of these polymers have been considered biocompatible (e.g. non-toxic and cytocompatible) (such as poly(ethyleneglycol) (**PEG**)), where for other polymer classes this has yet to be eludicated.

A promising recent approach entails the development of hybrid products, which combine the beneficial properties of both synthetic and natural polymers, such as Veriset[18] (an oxidized regenerated cellulose sheet impregnated with tri-lysine and *N*-hydroxysuccinimide ester functional 4-arm poly(ethylene glycol) (**NHS-PEG**)) and Hemopatch[19-21] (a porous collagen carrier coated with **NHS-PEG**). These products have been demonstrated improved hemostatic efficacy compared to carriers without this coating[20, 22] and other commercially available products[18-20]. Nevertheless, the limited efficacy in sealing profuse bleedings might be related to the use of **NHS-PEG** in these devices, as the intrinsic fast crosslinking of **NHS-PEG** (in case of Hemopatch) might lead to poor fixation to tissue (by limited crosslinking with the collagen carrier) or irregular sealing of the wound site (by inhomogeneous crosslinking with tissue). Moreover, swelling of PEG based materials is a problematic issue which might lead to weakening of the seal or compression of blood vessels or nerves after application. These potential drawbacks might be solved by modifying and fine-tuning the polymer architecture and properties. However, since PEG has limited options for tailoring the degree of functionalization (only via the end groups)

and polarity, this has stimulated the search for alternative polymers which can be used as hemostatic materials.

Poly(2-oxazoline)s (or POx[23-26]) are promising polymers for biomedical applications due to their versatile synthesis[27-29], favorable cytocompatibility[30,31] and promising excretability[32-38]. In terms of polymer architecture and function, POx possesses important advantages over PEG-based systems when applied in hemostatic materials. Firstly, cationic ring opening polymerization (CROP) allows for the introduction of both functional side chains and end-groups, which is not easily achieved by anionic polymerization of PEG-based systems. Moreover, this polymerization technique allows for the synthesis of a range of copolymers, which makes it possible to accurately control the polarity and degree of side-chain functionalization of the resulting polymer.

In order to achieve optimal hemostatic performance, three main aspects of the hemostatic device should be optimized, namely (1) the carrier, (2) the polymer coating and (3) the coating application method onto the carrier material. As a carrier, we selected a porous gelatin sponge. Although this carrier is animal derived, it has advantages over other synthetic materials, since it is fully biodegradable (4-8 weeks), shows effective uptake of blood and is already CE-registered as a hemostatic product[13]. Moreover, primary amines are available in gelatin to allow for the formation of covalent crosslinks between the carrier, blood proteins and tissue in order to create a gel which seals the wound surface and stops the bleeding (**Figure 1**).

Regarding polymer design, for optimal hemostatic performance, the polymer should have sufficient reactive moieties (NHS-esters) for covalent crosslinking (e.g. with blood proteins). The polymer composition should furthermore be chosen in such a way that the polymers are soluble in water (beneficial for their biological activity) and in organic solvents (beneficial for polymer processing). Moreover, the reactive moieties should be available for crosslinking, which requires reactive side chains of sufficient flexibility and length as well as an overall polymer composition which is polar enough to allow effective wetting under physiological conditions. The crosslinking capacity should be optimized to ensure that the polymer has sufficient time to crosslink with the various components (blood, carrier and tissue).

Regarding the coating of the hemostatic patch, we hypothesized that various parameters are important to achieve the desired hemostatic properties. First, the reactive polymer should be equally distributed over the carrier in order to obtain homogeneous hemostatic properties over the whole area of the coated patch. Secondly, the polymer and carrier should be combined in such a way that undesired crosslinking during the coating process is prevented. Moreover, after coating, porosity should be partially conserved in order to obtain a hemostatic patch with a dual mechanism of action of both gelatin (natural coagulation cascade) and the

reactive polymer (sealing the wound site by covalent crosslinking). Moreover, the blood uptake of the coated patches should be satisfactory to allow for crosslinking with all patch components (gelatin, reaction polymer, blood and tissue), but also resistant enough to prevent excessive blood flow through the patch.

In this chapter, we demonstrate a versatile strategy for the preparation of a poly(2-oxazoline) based hemostatic device. First, a series of NHS-ester functionalized POx (**NHS-POx**) with different ratios of NHS esters and polar groups was synthesized. We studied the capacity for covalent crosslinking between these polymers and whole blood (hemostatic performance) in order to correlate the hemostatic performance with the polarity of the polymers (measured by contact angle measurements). With the preselected polymers, we utilized a spraying procedure to create a series of homogeneously coated patches. The coated patches were tested *in vitro*, for e.g. blood uptake and crosslinking ability. The best-performing patches in these tests were selected to demonstrate *in vivo* efficacy in a compromised liver and spleen injury model of profuse bleedings in heparinized pigs.

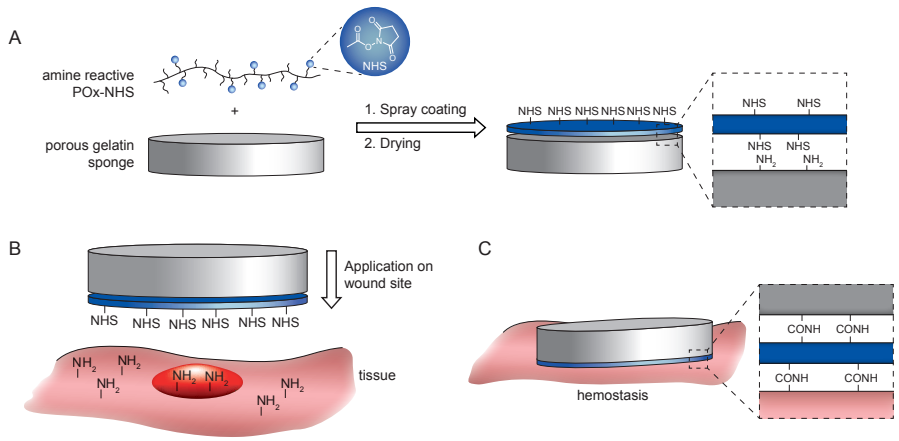

Figure 1 Schematic overview of application method and mechanism of action of poly(2-oxazoline) coated hemostatic patches. A) Preparation of a hemostatic patch by spray-coating **NHS-POx** onto a gelatin sponge, B) Application of the patch onto the wound site, C) Hemostasis is obtained by covalent crosslinking between the gelatin sponge, **NHS-POx**, blood proteins and tissue in order to create a gel which seals the wound surface and stops the bleeding.

2. Results and discussion

2.1. Synthesis

In order to create poly(2-oxazolines) with the desired characteristics for application as reactive coating in a hemostatic patch, both polarity and reactivity had to be optimized. We selected NHS-esters as the reactive moieties in view of their reactivity towards primary amines and their routine application in related medical devices[7]. Since direct incorporation of NHS-esters as functional group is not compatible with cationic ring opening polymerization (CROP), we used methyl ester functionalized 2-methoxycarbonylethyl-2-oxazoline (MestOx) instead. This group can be easily modified after the polymerization by direct amidation[39] or hydrolysis[40-42], as has been described in literature, and in **Chapters 2 and 3**. Furthermore, it has been efficiently copolymerized before with various co-monomers (including 2-ethyl-2-oxazoline (EtOx)[43] and 2-*n*-propyl-2-oxazoline (*n*PropOx)[44]). For the synthesis of the various **NHS-POx** (**P1-P7**) we used two different synthetic routes, as depicted in **Scheme 1**, and which were described in more detail in **Chapter 2**. In all cases, polymers were synthesized by CROP of different ratios of EtOx, *n*PropOx and MestOx under inert atmosphere using microwave conditions[45], yielding both *n*PropOx-MestOx and *n*PropOx-EtOx-MestOx-copolymers. In the first route, the MestOx groups were hydrolyzed (0.1M NaOH) resulting in a copolymer containing carboxylic acid moieties, which were subsequently activated with N-hydroxysuccinimide yielding **P1-P6**. In the second route, MestOx was post-modified by an amidation reaction with ethanol amine, yielding copolymers equipped with a hydroxyl moiety in the side chain. Subsequently, these hydroxyl groups were partially converted to carboxylic acid moieties using succinic anhydride, which were subsequently modified into reactive esters by coupling with N-hydroxysuccinimide (**P7**). Importantly, this second route installs a hydrolytically sensitive group in the side chain, favorable for degradation. As listed in **Table 1**, polymers **P1-P7** were synthesized with good control over the ratio of functional groups, number average molar mass and dispersity values. The various synthesized polymers (**P1-P7**) were analyzed with regard to the amount of NHS groups present using both ^{1}H NMR and UV-Vis spectroscopy, confirming a good agreement between the theoretical and experimental compositions.

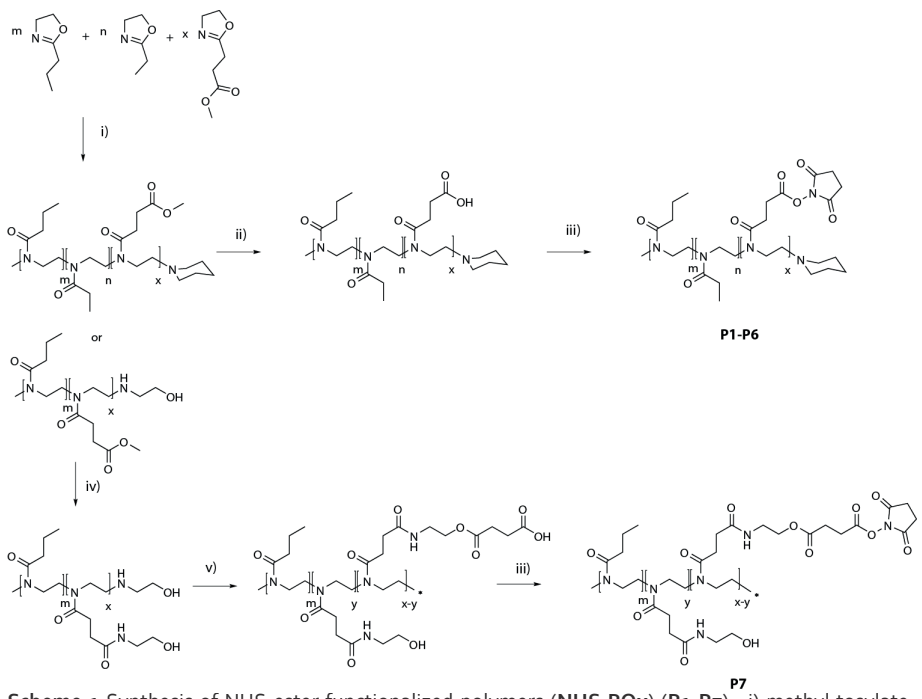

Scheme 1 Synthesis of NHS-ester functionalized polymers (**NHS-POx**) (**P1-P7**). i) methyl tosylate, 140°C, CH_3CN, ii) 0.1 M NaOH, rt, iii) NHS-OH, DIC, DCM, rt , iv) 2-amino-ethanol, 60°C, 300 mbar, v) succinic anhydride, DMAP, DMF/DCM (v/v, 1:9, rt)

Table 1 Analytical data of synthesized polymers (**P1-P7**)

			% funct. (^{1}H-NMR)						
#	**Polymer**		**m**	**n**	**y**	**x**	**UV**	**Mn (kg/mol)**	
		m/n/x	*n*PropOx	EtOx	OH	NHS	NHS	SEC[a)]	Đ[a)]
P1	P(*n*PropOx-*c*-NHS)	90-0-10	90	-	-	10	11	12.6	1.15
P2	P(*n*PropOx-*c*-NHS)	75-0-25	71	-	-	29	26	13.9	1.11
P3	P(*n*PropOx-*c*-EtOx-NHS)	40-50-10	40	49	-	11	9	12.4	1.18
P4	P(*n*PropOx-*c*-EtOx-NHS)	40-35-25	40	36	-	24	22	12.4	1.26
P5	P(*n*PropOx-*c*-EtOx-NHS)	50-40-10	49	40	-	11	11	12.3	1.16
P6	P(*n*PropOx-*c*-EtOx-NHS)	50-25-25	50	26	-	24	23	14.6	1.18
P7	P(*n*PropOx-*c*-OH-NHS)	70-10-20	70	-	15	15	15	18.8	1.25

[a)] SEC was calibrated against PMMA standards, eluent: 0.1 % LiCl in DMA

2.2 Hemostatic performance

As a first screening for hemostatic activity, the **NHS-POx** polymers were brought in contact with human whole blood and the formation of gels by mixing polymers with blood was analyzed using the inverted vial test. Besides the **NHS-POx** series, negative controls (polymers without NHS ester) were tested as well. In addition, a benchmark

polymer (**NHS-PEG** used in Hemopatch) was included as a positive control to compare functional group density (mmol NHS/g polymer) in relation to the usage of different polymers. The results of these tests are listed in **Table 2**. As expected, polymers with NHS-esters (**P1**-**P7**) gelated with blood due to the presence of the amine-reactive NHS-esters, unlike the negative controls (**P8**-**P12**), which did not. Gelation times of the **NHS-POx** series (**P1**-**P7**) varied between 1 minute (**P7**) to 6 minutes (**P1**-**P2**), which was slower than the **NHS-PEG** benchmark polymer, which formed a gel with blood instantaneously.

As polarity was anticipated to be an important feature of the hemostatic capacity of the polymers, POx films were spincoated on glass slides after which static contact angle measurements were performed[46]. Based on these contact angle measurements, it can be concluded that polymers functionalized with hydrophilic groups (PEG, OH or EtOX) (**P3**-**P8** + **P10**-**P11**) exhibit contact angles in a similar hydrophilic range (21°-26°), while polymers without hydrophilic groups (**P1**-**P2**+**P9**) have higher contact angles, thereby making a clear difference between hydrophilic and somewhat more hydrophobic copolymers. It was further calculated that the PEG-based control (**P11**) shows a much lower density of NHS-functional groups (0.36 mmol/g polymer) compared to **P1**-**P7** with values ranging from 0.76 mmol/g polymer for **P1** to 2.19 mmol/g polymer for **P2**, which is a direct result of the limited functionalization possibilities of PEG via the end-groups.

Table 2 Overview of hemostatic performance (**P1**-**P7**)

#	**Polymer**	**%NHS**	**Functional group content**	**Contact angle**	**Gelation time**
			(mmol NHS/g polymer)[a)]	**(°)[b)]**	**(min)[c)]**
P1	P(*n*PropOx-*c*-NHS)	10	0.76	36	6
P2	P(*n*PropOx-*c*-NHS)	29	2.19	57	6
P3	P(*n*PropOx-*c*-EtOx-NHS)	11	0.89	26	3
P4	P(*n*PropOx-*c*-EtOx-NHS)	24	1.59	24	3
P5	P(*n*PropOx-*c*-EtOx-NHS)	11	0.88	23	3
P6	P(*n*PropOx-*c*-EtOx-NHS)	24	1.57	21	3
P7	P(*n*PropOx-*c*-OH-NHS)	15	0.91	23	1
	Controls				
P8	P(EtOx)	-	-	26	no gel
P9	P(*n*PropOx)	-	-	57	no gel
P10	mPEG-OH	-	-	24	no gel
P11	NHS-PEG[d)]	-	0.36	21	instantaneous

[a)] Calculated using NHS-content which was determined by ^{1}H-NMR spectroscopy
[b)] The measurements were conducted in triplo, blank measurement glass slide (66°)
[c)] The gelation was determined by the inverted vial method
[d)] Obtained from commercial source

From both tests, it can be concluded that NHS-esters are essential for the formation

of chemical cross links with blood proteins. However, having a surplus of NHS-esters does not result in faster gelation. POx-prototypes which contain both NHS-esters and hydrophilic groups show faster gelation (**P3**-**P7**) compared to polymers without hydrophilic groups (**P1**-**P2**), but slower than **NHS-PEG** (**P11**), which crosslinked instantaneously. It was observed that the fast-gelating polymers also exhibited low contact angles. The difference in gelation speed between **NHS-PEG** and **NHS-POx** prototypes could, however, not be explained from the contact angle measurements. We assume that polarity and mobility of the polymer chains (limited by the spacer length between the polymer backbone and NHS-ester groups) are important parameters. **NHS-PEG** shows the fastest gelation, since the NHS-ester groups are highly mobile because of their attachment to the hydrophilic chain ends of the PEG-polymer. Within the **NHS-POx** series, **P7** shows the fastest gelation (1 min) because it has a longer spacer compared to **P1**-**P6**. Finally, the differences between **P1**-**P6**, with the same spacer length, can be explained because of polarity of the polymers; polymers containing hydrophilic EtOx groups (**P3**-**P6**) show gelation within 3 minutes, while polymers without these groups (**P1**-**P2**) show gelation times around 6 minutes. Due to its fast gelation, we selected P(*n*PropOx-OH-NHS) (**P7)** as the main candidate for further development of hemostatic patches.

2.3 Spray coating deposition

To cover the gelatin carrier with a polymer (**P7)** coating, a procedure was required that would result in a homogeneous polymer layer without compromising the beneficial properties of the gelatin carrier in terms of e.g. blood uptake capacity. Therefore, we used an ultrasonic spraying technique to deposit the polymer from volatile organic solvents of low toxicity onto the gelatin sponge and tune the amount of polymer by coating multiple layers (coating cycles) followed by drying the coated patches in a vacuum oven.

Using this approach, hemostatic patches (**G1-G4**) were prepared at various coating densities (0-9 mg/cm²) using a polymer solution of **P7** (90 mg/mL in 2-propanol/2-butanone (v/v, 1:1)). We observed a linear relationship between the coating density (mg/cm²) and the amount of coating cycles (**Table 3**). Additionally, the coated patches were analyzed by scanning electron microscopy (SEM) (**Figure 2**) which revealed that the pores of the carrier were not sealed by the polymer coating after applying up to six coating cycles. Furthermore, the coating was homogenously spread onto the carrier material, unlike Hemopatch (based on **NHS-PEG**), which showed a heterogeneous coverage revealing PEG-coated and uncoated domains. The analytical data of **G1**-**G4** are summarized in **Table 3**. Importantly, as POx is functionalized with a higher number of NHS-esters than PEG, a lower amount of polymer was required (5.7 mg/cm² for **G3**) in order to obtain a similar functional

group density as Hemopatch (~5.2 µmol NHS/cm²), which is beneficial if an open, porous structure is required for the carrier material.

Table 3 Coating and functional group densities of patches prepared with **P7** (**G1**-**G4**)

Samples	Coating density (mg/cm²)				Functional group density
#	Theoretical	Measured			
		mean	st dev	n	(µmol NHS/cm²)[a]
G1	0	-	-	-	-
G2	3	3.06[a]	0.01	3	2.80
G3	6	5.71[a]	0.13	9	5.18
G4	9	9.22[a]	0.01	3	8.36
Hemopatch (PEG)	-	16.8[b]	2.2	5	5.38

[a] Mass difference before (gelatin) and after coating (gelatin + **NHS-POx**)

[b] Determined by extraction of the polymer with DCM

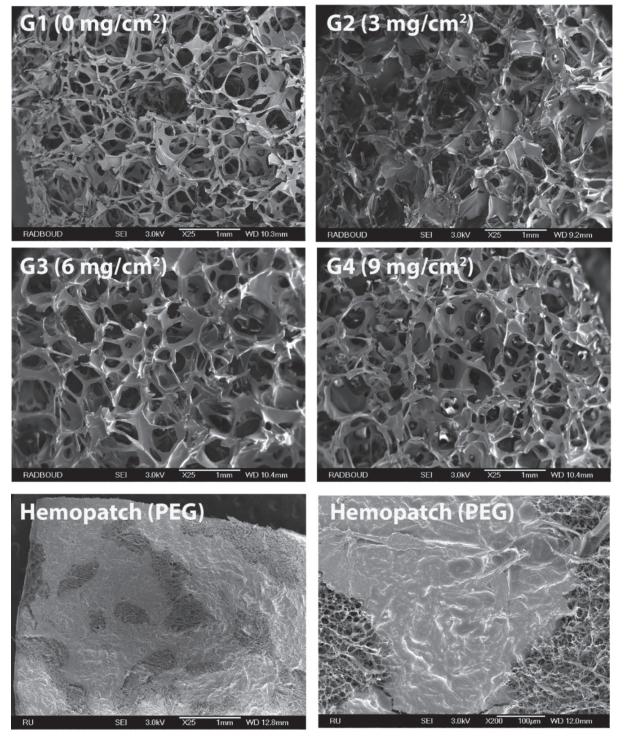

Figure 2 SEM images of **NHS-POx** coated patches (**G1-G4**) and Hemopatch (PEG). Scale bars correspond to 1 mm or 100 µm (bottom right picture).

2.4 *In vitro* tests

2.4.1 Blood uptake

The blood uptake of the different **NHS-POx** coated patches (**G1-G4**) and Hemopatch was evaluated by soaking the patches (with the coated side in contact with blood) in a mixture of blood/PBS for 30 seconds and determining the blood uptake by weighing the carriers before and after the soaking process (**Figure 3A**). It was observed that the uptake capacity of the patches was reduced with increasing coating density. Although the polymer coating did not seal the pores of the underlying gelatin carrier (**Figure 2**), the blood uptake was clearly compromised by the deposition of **NHS-POx** onto the patches. Hemopatch was included as well in these measurements, and showed significantly lower blood uptake values compared to **G1-G3.** Since blood uptake is necessary for satisfactory blood distribution throughout the patch and subsequent crosslinking, we conclude that **G3** was the best-performing prototype in this test, as it allowed for more effective blood uptake compared to **G4** and Hemopatch, but still prevented bleeding through the patches, which was observed for **G1** and **G2**.

2.4.2 Adhesion test

An *in vitro* adhesion test was performed (according to ASTM F2258-05 standards) to study the attachment between the coated patches upon contact with blood (**Figure 3B**). The different patches (**G1-G4**) were allowed to covalently crosslink onto each other for 1, 5 or 15 min, after which the adhesion force (N) was measured until the patches were separated. Both a negative control (**G1**, carrier without polymer) and a benchmark (Hemopatch) were included in this study. The data demonstrated that the NHS-ester free blank samples (**G1**) did not adhere to each other as reflected by adhesion forces of less than 0.5 N, which confirms that NHS-ester groups are necessary for the formation of covalent crosslinks. The coated samples (**G2-G4**) showed an entirely different behavior. At 1 and 5 minutes contacting time, low adhesion forces were measured which were comparable to **G1**, indicating a low degree of crosslinking. At 15 minutes, however, a threefold larger force (1.5 N) was needed to separate both patches. This indicates that more crosslinks are formed during the extended crosslinking time (15 min), resulting in larger adhesion forces. However, since these forces were in the same range for all three patches, it can be concluded that coating density did not affect the extent of adhesion in this experiment. When testing Hemopatch, adhesion forces after 1 and 5 minutes crosslinking were similar to the adhesion forces of **G2-G4** after 15 minutes. We conclude that this product generally crosslinks fast and forms strong gels with blood and carrier, which is in agreement with the blood gelation tests. While the differences regarding adhesion forces between the **NHS-POx** samples (**G2-G4**)

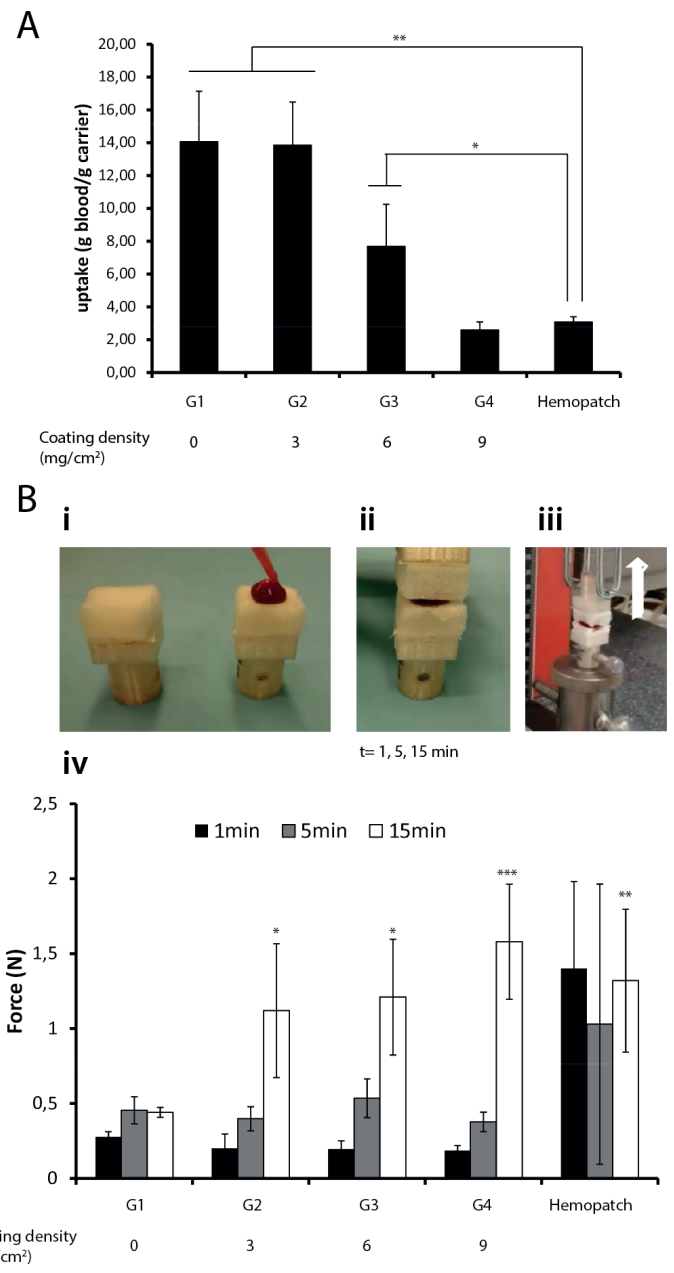

Figure 3A+B *In vitro* tests A) Blood uptake capacity as a function of coating density. (** P< 0,001, *P<0,01), B) *In vitro* adhesion test. i) blood was applied between the patches, ii) the patches were allowed to crosslink for defined time points (t1, t5, t15 min), iii) The samples were placed in a Zwick Roell tensile bench and a vertical force was applied until failure, iv) Results of the adhesion test. (* P <0.05, ** P< 0,01, ***P<0,001)

and Hemopatch (15 min) were statistically significant compared to NHS-ester free **G1** (15 min), adhesion forces after 15 min were not statistically different between Hemopatch and the **NHS-POx** samples (**G2**-**G4**). In summary, it can be concluded that Hemopatch crosslinked faster than the **NHS-POx** samples, whereas the final adhesion strength after 15 min was comparable for both samples.

2.5 *In vivo* efficacy test

NHS-POx functionalized patches were also evaluated in a clinically relevant setting by using an established *in vivo* pig model for profuse bleedings[47]. In brief, standardized bleedings (8 mm diameter, 3mm deep) were created in the liver and spleen of heparinized pigs (n = 4, 30 kg, 10 k heparin). The bleedings were imaged at selected time points (0, 1 and 5 min after creation of the bleeding) (**Figure 4A**) and the hemostatic efficacy of the different patches was assessed at 0, 1 and 5 min (bleeding/no bleeding). In addition, the bleeding score after 5 minutes was assessed using a visual scoring system ranging from 0 (no bleeding) to 4 (severe bleeding) **Figure 4B**. The efficacy of hemostasis of **NHS-POx** coatings was tested for **G3**, which had a similar functional group density as the benchmark Hemopatch (~5.2 mmol NHS/cm^2) (**Table 3**), but with a different polymer coating coverage. **G1** was used as negative control (no coating). In addition, Tachosil (a collagen carrier coated with human derived fibrinogen and thrombin) was selected because of its common use during liver resections[15]. The results of this study are depicted in **Figure 4A+B**. **G3** was the best-performing hemostatic patch in this pig model; in 7 out of 8 events, hemostasis was obtained, and bleedings after 5 minutes were scored (0, no bleeding) (**Figure 4B**). In the remaining event (1 out of 8), insufficient pressure during application resulted in poor hemostatic action and a bleeding score of 2 (slight bleeding) (**Figure 4B**). In all cases, no significant blood flow through the patch was observed using **G3,** as was expected from the blood uptake experiments. Evidently, **G1** was not effective at all in this bleeding model and significant blood flow through the patch was observed, in line with the *in vitro* blood uptake experiments (**Figure 3A**). Moreover, in none of the events hemostasis was obtained, which can be related to the absence of chemical crosslinkers. As a result, in all events, severe bleedings were scored after 5 minutes (**Figure 4B**). In the experiments using Tachosil, only in 2 out of 8 events hemostasis was observed, whereas moderate bleedings were scored for all other cases (**Figure 4**). This poor hemostatic efficacy might be due to the use of a high heparin dose (10 k units) in this pig model, which inhibits hemostasis solely based on the natural coagulation cascade. Using Hemopatch, effective hemostasis was obtained in 5 out of 8 events (**Figure 4A**) and bleeding scores after 5 minutes varied from no bleeding (0) to moderate bleedings (3) (**Figure 4B**). Generally, Hemopatch adhered well and quickly to the tissue which made repositioning challenging, a trend which was

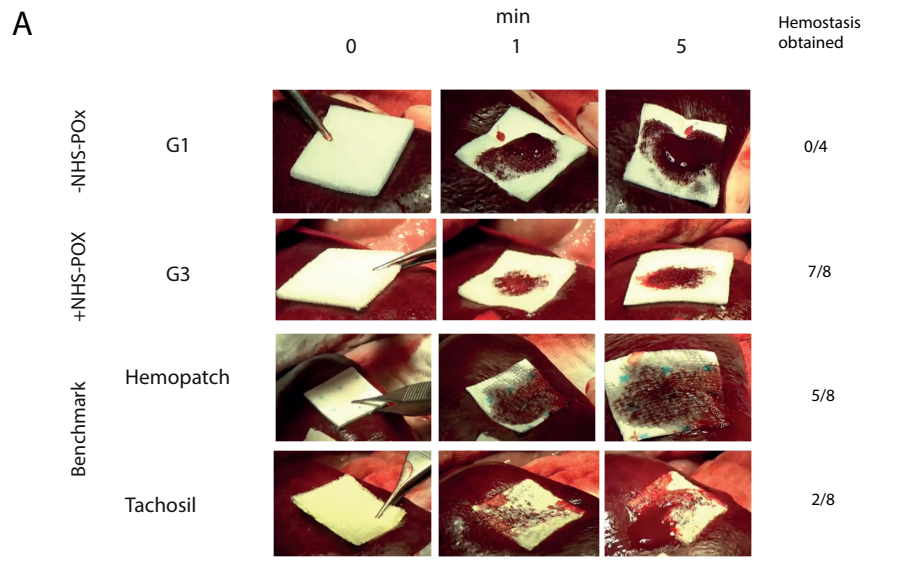

Figure 4 In vivo study on pig spleen. A) Images of the different prototypes at selected time points (0, 1, 5 min) including the success rate of hemostasis, B) Bleeding scores after 5 minutes according to the scoring system[47]

observed in the *in vitro* gelation tests as well. Unlike **G3**, slight bleeding at the edges of the patch was observed in cases where hemostasis was not obtained (**Figure 4A**), which is possibly related to the inhomogeneous deposition of the polymer coating compared to the **NHS-POx** coated patches (**Figure 2**). From this *in vivo* study, it can be concluded that sealants that rely on chemical crosslinking with surrounding soft tissues and blood proteins (**G3** and Hemopatch®) hold great promise for the treatment of profuse bleeding models, unlike patches which are solely dependent on the natural coagulation cascade (non-coated patch (**G1**) and Tachosil®) which were not effective in obtaining hemostasis in these models. Comparing **G3** and Hemopatch, **NHS-POx** samples have the additional benefit that they are coated more homogeneously than Hemopatch, which results in equal sealing of the wound site. In addition, **NHS-POx** samples are easier to handle due to their slower adhesion which allows repositioning of the patch if required.

3. Conclusions

In this chapter, we have successfully developed a hemostatic device based on NHS-ester functionalized POx coated on a gelatin patch. We observed that the polymer should contain both NHS-esters as well as hydrophilic groups to ensure optimal hemostatic performance. Furthermore, we found that coating homogeneity and density are crucial parameters in order achieve the desired hemostatic action *in vitro* (measured by adhesion tests) as well as the desired amount of blood uptake. *In vivo* efficacy tests in a compromised pig model using heparin demonstrated that **NHS-POx** coated patches displayed a similar hemostatic efficacy as compared to Hemopatch. **NHS-POx** coated patches were superior to products relying on activation of the natural coagulation cascade. In contrast to PEG, the structural versatility of POx allows further fine tuning of the hemostatic performance, thereby rendering **NHS-POx** polymers excellent candidates for further development of hemostatic patches.

4. Experimental Section

4.1 Synthesis

The experimental procedures for the synthesis of the monomers, intermediate products and final polymers (**P1**-**P7**) can be found in the experimental section of **Chapter 2.** The analytical details of the synthetic polymers (**P1**-**P7**) as well ^{1}H-NMR spectra of both **P3**-**P6** and **P7** (including intermediate products), can be found in the appendix of this chapter.

4.2 Gelation test

This experiment was performed using an inverted vial test adapted from literature.[48] Polymer powders (20 mg) were mixed with freshly obtained heparinized human whole blood (1 mL) in a glass vial and vortexed until a visible gel was formed (gelation time).

4.3 Contact angle measurements

Microscope cover slips (2 cm^2) were soaked in absolute ethanol, sonicated (30 seconds) and dried under reduced pressure for 15 min. Polymer films were prepared by spincoating the polymer solutions (15 mg/mL in DCM, 1 mL) onto the microscope cover slips (12000 rpm, 30 seconds) using a Spin 150 spincoater. Subsequently, the coated slides were dried overnight under reduced pressure. Static contact angles were measured on an OCA-20 goniometer. For each measurement, 1 µL of doubly distilled water was placed onto the spincoated films at room temperature. The spreading of the droplet was imaged using a high-speed video camera using 1 frame/second for 30 seconds. The contact angle was determined based upon the Laplace Young fitting using the imaging software provided by the supplier (SCA 20, version 2.1.5 build 16). To determine the contact angle, the first representative frame in which a drop shape was observed was selected for analysis. The measurements were conducted in triplo per sample (n = 3).

4.4 Coating deposition

Spray coating was performed using an Exactacoat spraying machine (Sono-Tek) equipped with an Accumist ultrasonically agitated nozzle. Coating was performed at a dispensing rate of 1 mL/min, a pressure of 40 mbar and a coating speed of 40 mm/s, by moving both in the xy-direction over a programmed area. The nozzle height was set 30 mm from the top of the substrate. The coating density was adjusted by spraying multiple layers of polymer (coating cycles (n)) onto the substrate. Polymer solutions were prepared in 2-butanone/2-propanol (v/v, 1:1) with a final polymer concentration of 90 mg/mL. After coating, the patches were dried in a vacuum oven (50 mbar, 50°C). The coating density (mg/cm^2) was determined by weighing the patches (before (carrier) and after coating (carrier + polymer) (mg)) divided by the coated area (cm^2).

4.5 Scanning electron microscopy

Samples were attached to an aluminum holder by conducting carbon tape. Afterwards, these samples were sputter coated using a gold/palladium coater (Cressington 208 HR) for 30 sec (80 mA). At different magnifications, images were acquired at an accelerating voltage of 3kV using a JEOL 6330 Field Emission Scanning Electron Microscope (SEM).

4.6 Blood uptake

This experiment was performed using a procedure adapted from literature[13]. Coated gelatin patches with different coating densities (0, 3, 6, 9 mg/cm2) were weighed ('dry weight' (mg)) and soaked into a mixture of heparinized blood/PBS (v/v, 1:1) with the coated side facing the blood mixture. The patches were allowed to absorb blood for 30 sec. After this, superficial blood was removed using a filter paper and the patches were weighed again ('weight after' (mg)) and the amount of absorbed blood ('blood' (mg)) was determined (weight after (mg) – weight before (mg)). The blood uptake was defined by calculating the amount of absorbed blood per g patch. The measurements were performed in sixfold for each sample (*n* =6). Significant differences between samples were analyzed using ANOVA followed by a post hoc Tukey-Kramer multi comparison test.

4.7 Adhesion test

This experiment was performed and designed according to modified ASTM F2258-05 standards[49]. The samples were attached with double sided tape to 3D-printed grip tabs of 2 cm^2 and these tabs were placed into a single column tensile tester (Z2.5, Zwick/Roell, Ulm, Germany, containing a 20 N load cell). Heparinized blood (200 µL) was put between the coated patches which were pressed down using a weight of 20 g. The patches were allowed to crosslink with blood for defined times (1, 5 and 15 min). Subsequently, the patches were pulled apart and the load at failure (F_{max}, N) was measured. The measurements were performed in sixfold for each sample (*n* = 6). Significant differences between samples were analyzed using ANOVA followed by a post hoc Tukey-Kramer multicomparison test.

4.8 In vivo efficacy test

Heparinized (10k units) pigs (*n* = 4, 30 kg) were used in this study. Permission for this experiment was granted by the responsible ethical comitees at the Ministry of Education of the Czech Republic (project # 56-2015/processing #MSMT-42725/2015-6). Surgery was performed using standard aseptic techniques. A midline laparotomy was performed to access liver and spleen. Using a biopsy punch, standardized lesions were created in liver and spleen (8 mm diameter, 3 mm deep). Hemostatic patches of 2.7 x 2.7 cm were used in this study (*n* = 8 per prototype randomized per organ using a balanced latin square). After the lesion was created, the blood flow was assessed according to a visual scoring system (0 = no bleeding, 0.5 = oozing, 1 = very slight, 2 = slight, 3 = moderate, 4 = severe) described in literature[47]. Afterwards, superficial blood was removed using a dry gauze. Subsequently, the patches were applied with the coated side facing the organ and digital pressure was applied for 1 min using a dry gauze. The efficacy of the patches was evaluated after 0, 1 and 5 minutes

by monitoring the bleeding (yes or no). Successful hemostasis was achieved if no bleeding was observed after 5 minutes without pressure (yes or no). Additionally, after 5 minutes, the bleeding was scored according to the scoring system and the adhesion of the patch to the organ was tested.

4.9 Statistics

Statistical analyses were conducted using GraphPad Instat software. All results were reported as mean ± standard deviation. Differences among groups were analyzed by ANOVA using a Tukey-Kramer Multi comparison test and p-values of 0.05 or lower were considered as significantly different.

5. Acknowledgements

Multiple persons are kindly acknowledged for their contributions to this work: Elvy de Hoog, Bram Keereweer and Maria Jose Sanchez Fernandez for help with the polymer synthesis. Paul Riedel (Rubroeder GmbH) for assisting with the spraying experiments. Edwin Roozen and Roger Lomme (both Department of Surgery (Radboud University Medical Center) and Rosa Felix Lanao for assisting with the adhesion experiments and *in vivo* study and Els van der Leyden (Ghent University) for the assisting with the contact angle measurements.

6. References

1. M. Marietta, L. Facchini, P. Pedrazzi, S. Busani and G. Torelli, *Transplant. Proc.*, 2006, **38**, 812-814.
2. P. F. Janssen, H. A. M. Brölmann and J. A. F. Huirne, *Surg. Endosc.*, 2012, **26**, 2892-2901.
3. R. J. Siegal, S. Vaezy, R. Martin and L. Crum, *Echocardiogr.*, 2001, **18**, 309-315.
4. R. Brustia, B. Granger and O. Scatton, *J. Hepatobiliary. Pancreat. Sci.*, 2016, **23**, 609-621.
5. F. J. Kim, K. H. Rha, F. Hernandez, T. W. Jarrett, P. A. Pinto and L. R. Kavoussi, *J. Urol.*, 2003, **170**, 408-411.
6. Y. Tomizawa, *J. Artif. Organs*, 2005, **8**, 137-142.
7. P. J. M. Bouten, M. Zonjee, J. Bender, S. T. K. Yauw, H. van Goor, J. C. M. van Hest and R. Hoogenboom, *Prog. Polym. Sci.*, 2014, **39**, 1375-1405.
8. M. Emilia, S. Luca, B. Francesca, B. Luca, S. Paolo, F. Giuseppe, B. Gianbattista, M. Carmela, M. Luigi and L. Mauro, *Transfus. Apher. Sci.*, 2011, **45**, 305-311.
9. B. A. Bruckner, L. N. Blau, L. Rodriguez, E. E. Suarez, U. Q. Ngo, M. J. Reardon and M. Loebe, *J. Cardiothorac. Surg.*, 2014, **9**, 1-7.
10. A. E. Pusateri, S. J. McCarthy, K. W. Gregory, R. A. Harris, L. Cardenas, A. T. McManus and C. W. Goodwin, Jr., *J. Trauma.*, 2003, **54**, 177-182.
11. Y. Wu, J. He, W. Cheng, H. Gu, Z. Guo, S. Gao and Y. Huang, *Carbohydr. Polym.*, 2012, **88**, 1023-1032.
12. K. M. Lewis, D. Spazierer, M. D. Urban, L. Lin, H. Redl and A. Goppelt, *Eur. Surg.*, 2013, **45**, 213-220.
13. R. Hajosch, M. Suckfuell, S. Oesser, M. Ahlers, K. Flechsenhar and B. Schlosshauer, *J. Biomed. Mater. Res. Part B Appl. Biomater.*, 2010, **94**, 372-379.
14. M. Kabiri, S. H. Emami, M. Rafinia and M. Tahriri, *Curr. Appl. Phys.*, 2011, **11**, 457-461.
15. C. Moench, W. O. Bechstein, V. Hermanutz, G. Hoexter and H. P. Knaebel, *Trials*, 2010, **11**, 109.
16. C. Ghobril and M. W. Grinstaff, *Chem. Soc. Rev.*, 2015, **44**, 1820-1835.
17. P. A. Leggat, D. R. Smith and U. Kedjarune, *ANZ J. Surg.*, 2007, **77**, 209-213.
18. R. Öllinger, A. L. Mihaljevic, C. Schuhmacher, H. Bektas, F. Vondran, M. Kleine, M. Sainz-Barriga, S. Weiss, P. Knebel, J. Pratschke and R. I. Troisi, *HPB*, 2013, **15**, 548-558.
19. K. M. Lewis, D. Spazierer, P. Slezak, B. Baumgartner, J. Regenbogen and H. Gulle, *J. Biomater. Appl.*, 2014, **29**, 780-788.
20. K. M. Lewis, A. Schiviz, H. C. Hedrich, J. Regenbogen and A. Goppelt, *Int. J. Surg.*, 2014, **12**, 940-944.
21. K. M. Lewis, C. E. Kuntze and H. Gulle, *Med. Devices (Auckl.)*, 2016, **9**, 1-10.
22. K. Howk, J. Fortier and R. Poston, *Ann. Vasc. Surg.*, 2016, **31**, 186-195.
23. D. A. Tomalia and D. P. Sheetz, *J. Polym. Sci., Part A-1: Polym. Chem.*, 1966, **4**, 2253-2265.
24. W. Seeliger, E. Aufderhaar, W. Diepers, R. Feinauer, R. Nehring, W. Thier and H. Hellmann, *Angew. Chem. Int. Ed.* , 1966, **5**, 875-888.
25. A. Levy and M. Litt, *J. Polym. Sci., Part A-1: Polym. Chem.*, 1968, **6**, 1883-1894.
26. T. Kagiya, S. Narisawa, T. Maeda and K. Fukui, *J. Polym. Sci. Part B Polym. Lett.*, 1966, **4**, 441-445.
27. R. Hoogenboom, *Angew. Chem. Int. Ed.* , 2009, **48**, 7978-7994.
28. E. Rossegger, V. Schenk and F. Wiesbrock, *Polymers*, 2013, **5**, 956-1011.
29. B. Guillerm, S. Monge, V. Lapinte and J. J. Robin, *Macromol. Rapid Commun.*, 2012, **33**, 1600-1612.
30. J. Kronek, E. Paulovičová, L. Paulovičová, Z. Kroneková and J. Lustoň, *J. Mater. Sci. Mater. Med.*, 2012, **23**, 1457-1464.
31. M. Bauer, C. Lautenschlaeger, K. Kempe, L. Tauhardt, U. S. Schubert and D. Fischer, *Macromol. Biosci.*, 2012, **12**, 986-998.
32. F. C. Gaertner, R. Luxenhofer, B. Blechert, R. Jordan and M. Essler, *J. Control. Release*, 2007, **119**, 291-300.
33. L. Wyffels, T. Verbrugghen, B. D. Monnery, M. Glassner, S. Stroobants, R. Hoogenboom and S. Staelens, *J. Control. Release*, 2016, **235**, 63-71.
34. V. R. de la Rosa, *J. Mater. Sci. Mater. Med.*, 2014, **25**, 1211-1225.
35. N. Adams and U. S. Schubert, *Adv. Drug. Deliv. Rev.*, 2007, **59**, 1504-1520.
36. K. L. Eskow Jaunarajs, D. G. Standaert, T. X. Viegas, M. D. Bentley, Z. Fang, B. Dizman, K. Yoon, R. Weimer, P. Ravenscroft, T. H. Johnston, M. P. Hill, J. M. Brotchie and R. W. Moreadith, *Mov. Disord.*, 2013, **28**, 1675-1682.
37. R. W. Moreadith, T. X. Viegas, M. D. Bentley, J. M. Harris, Z. Fang, K. Yoon, B. Dizman, R. Weimer, B. P. Rae, X. Li, C. Rader, D. Standaert and W. Olanow, *Eur. Polym. J.*, 2016, **88**, 524-552
38. S. Zalipsky, C. B. Hansen, J. M. Oaks and T. M. Allen, *J. Pharm. Sci.*, 1996, **85**, 133-137.
39. M. A. Mees and R. Hoogenboom, *Macromolecules*, 2015, **48**, 3531-3538.
40. J. C. Rueda, E. Campos, H. Komber, S. Zschoche, L. Häussler and B. Voit, *Des. Monomers Polym.*, 2013, **17**, 208-216.
41. M. A. Boerman, H. L. Van der Laan, J. C. M. E. Bender, R. Hoogenboom, J. A. Jansen, S. C. Leeuwenburgh and J. C. M. Van Hest, *J. Polym. Sci., Part A-1: Polym. Chem.*, 2016, **54**, 1573-1582.
42. J. C. Rueda, M. Asmad, V. Ruiz, H. Komber, S. Zschoche and B. Voit, *Des. Monomers Polym.*, 2015, **18**, 761-769.
43. P. J. M. Bouten, D. Hertsen, M. Vergaelen, B. D. Monnery, M. A. Boerman, H. Goossens, S. Catak, J. C. M. van Hest, V. Van Speybroeck and R. Hoogenboom, *Polym. Chem.*, 2015, **6**, 514-518.
44. P. J. M. Bouten, D. Hertsen, M. Vergaelen, B. D. Monnery, S. Catak, J. C. M. van Hest, V. Van Speybroeck and R. Hoogenboom, *J. Polym. Sci., Part A-1: Polym. Chem.*, 2015, **53**, 2649-2661.
45. F. Wiesbrock, R. Hoogenboom, M. A. M. Leenen, M. A. R. Meier and U. S. Schubert, *Macromolecules*, 2005, **38**, 5025-5034.
46. S. Wijnans, B.-J. de Gans, F. Wiesbrock, R. Hoogenboom and U. S. Schubert, *Macromol. Rapid Commun.*, 2004, **25**, 1958-1962.
47. G. L. Adams, R. J. Manson, V. Hasselblad, L. K. Shaw and J. H. Lawson, *J. Thromb. Thrombolysis*, 2009, **28**, 1-5.
48. E. Lih, J. S. Lee, K. M. Park and K. D. Park, *Acta Biomater.*, 2012, **8**, 3261-3269.
49. ASTM F2258-05(2015), Standard Test Method for Strength Properties of Tissue Adhesives in Tension, ASTM International, West Conshohocken, PA, 2015, www.astm.org.

Appendix

S1 Analytical details of the synthesized polymers (P1-P7)

P1 P(*n*PropOx-NHS) 90-10 - ^{1}H NMR (500 MHz, D_2O) δ 3.70-3.40 (b,(m+x)•4H, NC$\underline{H}_2$C$\underline{H}_2$N), 3.00-2.60 ((b, x•4H, CO-C$\underline{H}_2$-C$\underline{H}_2$-CO) + (b, x•4H, CO-C$\underline{H}_2$-C$\underline{H}_2$-CO (NHS))), 2.40-2.20 (b, m•2H, CO-C$\underline{H}_2$-CH_2-CH_3), 1.60-1.40 (b, m•2H, CO-CH_2-C$\underline{H}_2$-CH_3), 0.90-0.80 (b, m•3H, CO-CH_2-CH_2-C$\underline{H}_3$). Experimentally determined monomer ratio (m/x): 90/10. **UV (NH_4OH)** 11% NHS. **SEC** (PMMA) M_n 12.6 kg/mol, Đ 1.15

P2 P(*n*PropOx-NHS) 75-25 - ^{1}H NMR (500 MHz, D_2O) δ 3.70-3.40 (b,(m+x)•4H, NC$\underline{H}_2$C$\underline{H}_2$N), 3.00-2.60 ((b, x•4H, CO-C$\underline{H}_2$-C$\underline{H}_2$-CO + (b, x•4H, CO-C$\underline{H}_2$-C$\underline{H}_2$-CO (NHS))), 2.40-2.20 (b, m•2H, CO-C$\underline{H}_2$-CH_2-CH_3), 1.60-1.40 (b, m•2H, CO-CH_2-C$\underline{H}_2$-CH_3), 0.90-0.80 (b, m•3H, CO-CH_2-CH_2-C$\underline{H}_3$). Experimentally determined monomer ratio (m/x): 71/29. **UV (NH_4OH)** 26% NHS. **SEC** (PMMA) M_n 20.9 kg/mol, Đ 1.20

P3 P(*n*PropOx-EtOx-NHS) 40-50-10 - ^{1}H NMR (500 MHz, D_2O) δ 3.70-3.40 (b,(m+n+x)•4H, NC$\underline{H}_2$C$\underline{H}_2$N), 3.00-2.60 ((b, x•4H, CO-C$\underline{H}_2$-C$\underline{H}_2$-CO + (b, x•4H, CO-C$\underline{H}_2$-C$\underline{H}_2$-CO (NHS))), 2.40-2.20 (b, (m+n)•2H, CO-C$\underline{H}_2$-CH_2-CH_3 + CO-C$\underline{H}_2$-CH_3), 1.60-1.40 (b, m•2H, CO-CH_2-C$\underline{H}_2$-CH_3), 0.90-0.80 (b, n•3H, CO-CH_2-C$\underline{H}_3$), 0.90-0.80 (b, m•3H, CO-CH_2-CH_2-C$\underline{H}_3$). Experimentally determined monomer ratio (m/n/x): 40/49/11. **FT-IR (cm^{-1})** 1626 (C=O amide), 1738 + 1785 + 1815 (NHS-ester). **UV (NH_4OH)** 11% NHS. **SEC** (PMMA) M_n 12.5 kg/mol, Đ 1.18

P4 P(*n*PropOx-EtOx-NHS) 40-35-25 - ^{1}H NMR (500 MHz, D_2O) δ 3.70-3.40 (b,(m+n+x)•4H, NC$\underline{H}_2$C$\underline{H}_2$N), 3.00-2.60 ((b, x•4H, CO-C$\underline{H}_2$-C$\underline{H}_2$-CO + (b, x•4H, CO-C$\underline{H}_2$-C$\underline{H}_2$-CO (NHS))), 2.40-2.20 (b, (m+n)•2H, CO-C$\underline{H}_2$-CH_2-CH_3 + CO-C$\underline{H}_2$-CH_3), 1.60-1.40 (b, m•2H, CO-CH_2-C$\underline{H}_2$-CH_3), 0.90-0.80 (b, n•3H, CO-CH_2-C$\underline{H}_3$), 0.90-0.80 (b, m•3H, CO-CH_2-CH_2-C$\underline{H}_3$). Experimentally determined monomer ratio (m/n/x): 39/33/28. **FT-IR (cm^{-1})** 1626 (C=O amide), 1738 + 1785 + 1815 (NHS-ester). **UV (NH_4OH)** 32% NHS. **SEC** (PMMA) M_n 16.8 kg/mol, Đ 1.22

P5 P(*n*PropOx-EtOx-NHS) 50-40-10 - ^{1}H NMR (500 MHz, D_2O) δ 3.70-3.40 (b,(m+n+x)•4H, NC$\underline{H}_2$C$\underline{H}_2$N), 3.00-2.60 ((b, x•4H, CO-C$\underline{H}_2$-C$\underline{H}_2$-CO + (b, x•4H, CO-C$\underline{H}_2$-C$\underline{H}_2$-CO (NHS))), 2.40-2.20 (b, (m+n)•2H, CO-C$\underline{H}_2$-CH_2-CH_3 + CO-C$\underline{H}_2$-CH_3), 1.60-1.40 (b, m•2H, CO-CH_2-C$\underline{H}_2$-CH_3), 0.90-0.80 (b, n•3H, CO-CH_2-C$\underline{H}_3$), 0.90-0.80 (b, m•3H, CO-CH_2-CH_2-C$\underline{H}_3$). Experimentally determined monomer ratio (m/n/x): 49/39/12. **FT-IR (cm^{-1})** 1626 (C=O amide), 1738 + 1785 + 1815 (NHS-ester). **UV (NH_4OH)** 9% NHS. **SEC** (PMMA) M_n 12.3 kg/mol, Đ 1.16

P6 P(*n*PropOx-EtOx-NHS) 50-25-25 - ^{1}H NMR (500 MHz, D_2O) δ 3.70-3.40 (b,(m+n+x)•4H, NC$\underline{H}_2$C$\underline{H}_2$N), 3.00-2.60 ((b, x•4H, CO-C$\underline{H}_2$-C$\underline{H}_2$-CO + (b, x•4H, CO-C$\underline{H}_2$-C$\underline{H}_2$-CO (NHS))), 2.40-2.20 (b, (m+n)•2H, CO-C$\underline{H}_2$-CH_2-CH_3 + CO-C$\underline{H}_2$-CH_3), 1.60-1.40 (b, m•2H, CO-CH_2-C$\underline{H}_2$-CH_3), 0.90-0.80 (b, n•3H, CO-CH_2-C$\underline{H}_3$), 0.90-0.80 (b, m•3H, CO-CH_2-CH_2-C$\underline{H}_3$). Experimentally determined monomer ratio (m/n/x): 50/26/24. **FT-IR (cm^{-1})** 1626 (C=O amide), 1738 + 1785 + 1815 (NHS-ester). **UV (NH_4OH)** 22% NHS. **SEC** (PMMA) M_n 14.6 kg/mol, Đ 1.18

P7 P(*n*PropOx-OH-NHS) 70-15-15- ^{1}H NMR (400 MHz, D_2O) δ 4.23-4.14 (b, z•2H, O=CNHC$\underline{H}_2$$CH_2$OC=O), 3.70-3.40 (b, (m+y+z)•4H, NC$\underline{H}_2$C$\underline{H}_2$N), 3.69-3.60 (b, (y+z)•2H, C=ONHCH_2C$\underline{H}_2$OH & C=ONHCH_2C$\underline{H}_2$OC=O), 3.35-3.28 (b, y•2H, C=ONHC$\underline{H}_2$$CH_2$OH), 3.08-2.99 (b, z•2H, O=CC$\underline{H}_2$C$\underline{H}_2$COON), 3.01-2.90 (b, z•4H, ONO=CC$\underline{H}_2$C$\underline{H}_2$C=ONO), 2.88-2.80 (b, z•2H, O=CC$\underline{H}_2$C$\underline{H}_2$COON), 2.76-2.59 (b, (y+z)•2H, O=CC$\underline{H}_2$$CH_2$C=ONH), 2.60-2.48 (b, (y+z) •2H, O=CCH_2C$\underline{H}_2$C=ONH), 2.43-2.23 (b, m•2H, C$\underline{H}_2$$CH_2$$CH_3$), 1.65-1.50 (b, m•2H, CH_2C$\underline{H}_2$$CH_3$), 0.98-0.85 (b, m•3H, $CH_2$$CH_2C\underline{H}_3$). Experimentally determined monomer ratio (m/y/z): 69/16/15. **UV (Fe(III)chloride)** 15% NHS. **SEC** (PMMA) M_n 18.8, Đ 1.25

S2 ^{1}H-NMR spectra of P3-P6 and intermediate products

A

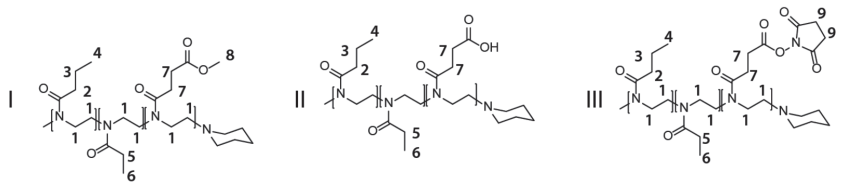

B

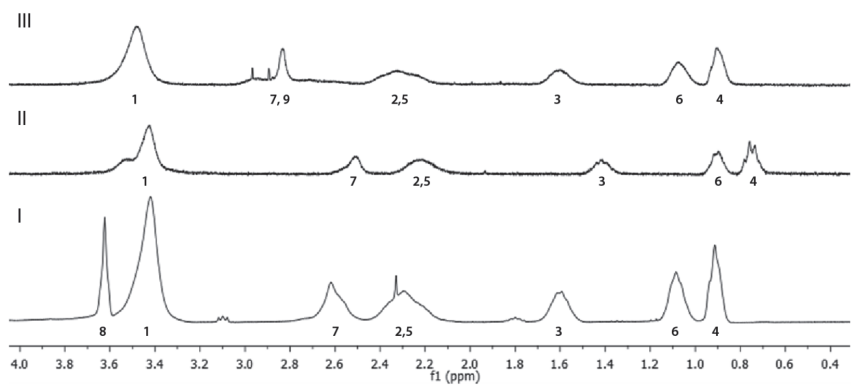

Figure S1 Representative ^{1}H-NMR spectra of P(*n*PropOx-EtOx-NHS) based polymers (**P3**-**P6**) and intermediate products. A) Structural formulas of I ((P(*n*PropOx-EtOx-MestOx), II P(*n*PropOx-EtOx-COOH), III P(*n*PropOx-EtOx-NHS)), B) ^{1}H-NMR signals of I, II and III.

S3 ^{1}H-NMR spectra of P7 and intermediate products

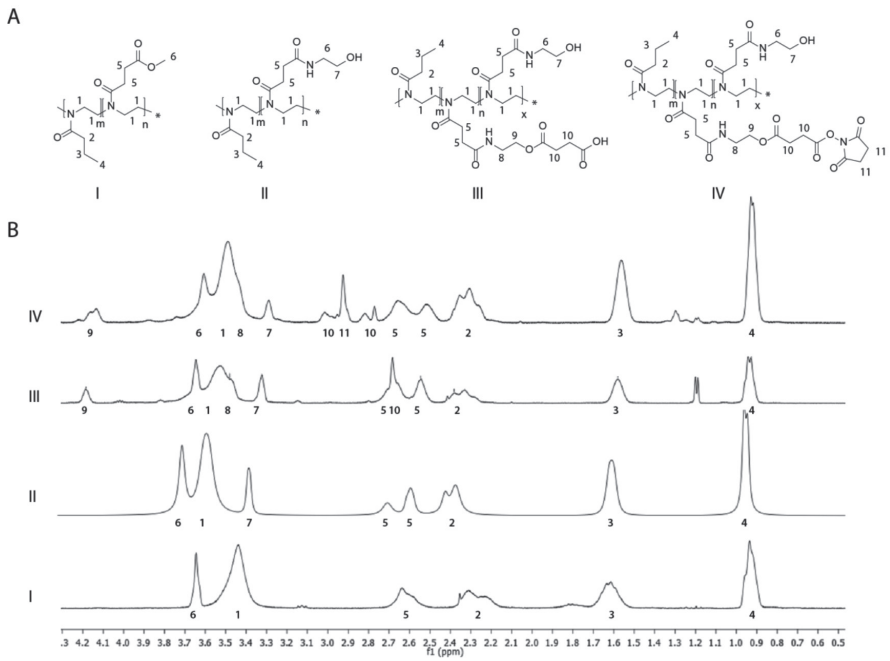

Figure S2 Representative ^{1}H-NMR spectra of P(*n*PropOx-OH-NHS) (**P7**) and intermediate products. A) Structural formulas of I (P(*n*PropOx-MestOx)), II (P(*n*PropOx-OH)), III (P(*n*PropOx-OH-COOH)), IV (P(*n*PropOx-OH-NHS)), B) ^{1}H-NMR signals of I-IV

Chapter 5:

Understanding hemostatic polymers: a rheological study on the gelation of NHS-ester functionalized poly(2-oxazoline)s and poly(ethylene glycol) with bovine serum albumin

Abstract

In this chapter, we performed a systematic rheological study on the reaction of NHS-ester functionalized poly(2-oxazoline)s (**NHS-POx**) or NHS-ester functional 4-arm poly(ethylene glycol) (**NHS-PEG**) with bovine serum albumin (BSA) as a mimic for blood proteins. The aim of this study was to obtain better insight into the network formation of **NHS-POx** and **NHS-PEG** as hemostatic polymers, as a function of i) the configuration of the crosslinking amine-reactive NHS-ester groups on the polymer and ii) the presence of hydrophilic side chains, i.e., hydroxyl (OH) or dimethylamine ($N(CH_3)_2$) (in case of **NHS-POx**). In these experiments, we have performed i) oscillatory time sweeps for 30 minutes to determine the gelation time, ii) oscillatory frequency sweeps to study the viscoelastic behavior of the formed networks over a broad angular frequency range (0.1-100 rad/s), and iii) strain sweeps to study the flexibility of the formed networks (0.1-1000% strain) and the yield strain of these networks. The oscillatory time sweeps revealed that both **NHS-POx** and **NHS-PEG** formed crosslinked networks with BSA instantaneously, while **NHS-PEG** formed more elastic networks with BSA than **NHS-POx**. Both **PEG-** and **POx-**based networks showed predominantly elastic behavior over a wide frequency range. Interestingly, in contrast to crosslinked **NHS-PEG** networks, crosslinked **NHS-POx** networks showed strain stiffening behavior as demonstrated by strain sweeps, which can be attributed to the presence of the crosslinking groups on the side chains. Furthermore, a pH of 8.5 or higher was needed to obtain the most elastic networks between **NHS-POx** and BSA. No clear effect of the type of hydrophilic moieties (OH or $N(CH_3)_2$) on network formation was observed. In summary, we conclude that **NHS-POx** and **NHS-PEG** can be successfully utilized for the development of hemostatic polymers as they both form crosslinked networks with BSA instantaneously. It was furthermore demonstrated that the configuration and corresponding mobility of the crosslinking NHS-ester groups have a clear effect on the network structure which is formed.

1. Introduction

Insufficient control over bleeding is one of the major threats during surgery on soft tissues. As an example, a hepatic resection involves partial removal of the liver, which is a complex surgical procedure associated with major blood loss. As a result, the success rates of these procedures strongly vary depending on the medical condition of the patient and the amount of blood loss[1]. Inefficient hemostasis[2] can severely complicate the recovery rate of the patient and even lead to mortality. Since the liver is a highly venous organ, traditional methods like suturing and stapling are often not sufficient to ensure successful hepatic resection, which has stimulated the development of tissue adhesive materials[3]. These are polymeric materials which form a sealing network in the presence of wounded tissue, thereby facilitating wound closure.

For the development of tissue adhesives, a wide range of polymeric materials (both natural and synthetic) is currently available on the market[3-5]. Natural polymers like fibrin glues[6,7] are biodegradable and achieve effective tissue adhesion, although the risk of the transmission of animal-borne diseases and the lack of mechanical properties are drawbacks of this class of materials. Synthetic materials, on the other hand, are reported to adhere tightly to soft tissue, although toxicity has been reported for materials such as e.g. cyanoacrylates[8].

Another particular interesting class of tissue adhesives are polymeric hydrogels, which are hydrophilic crosslinked three-dimensional polymer networks which are used in tissue adhesives and hemostats[3, 9, 10], but also in other biomedical fields[11] including drug delivery[12], tissue engineering[13, 14] and 3D-cell culture[15]. In these polymeric hydrogels, polymeric network structures are formed upon formation of crosslinks between polymer chains. These networks can be formed via a wide range of physical and chemical interactions such as ionic[16], hydrogen[17], covalent bonds, or combinations thereof[18]. The formation of covalent bonds is highly advantageous if semi-permanent or permanent crosslinked networks are required. This can be achieved via various chemistries including condensation reactions[19], enzymatic cross coupling[20] or UV-mediated polymerization[21]. The formation of crosslinked networks prevents direct dissolution of the polymers upon hydration, resulting into absorption of large amounts of water by the crosslinked polymer network. The mechanical properties of these hydrogels are largely determined by i) the physicochemical characteristics of the specific polymer, ii) the type of crosslinks which are formed (irreversible or reversible), and iii) the crosslinking density (number of crosslinks between polymer chains within a specific volume).

In order to develop polymeric hydrogels as tissue adhesive sealants, several properties are required[9]. For example, the polymer should be non-toxic, non-immunogenic, degradable and excretable after application. Moreover, the formed network should be sufficiently strong to withstand physiological loading. A wound sealant or hemostat should at least mimic the elasticity of a fibrin clot (storage modulus (G') of ~10-100 Pa) in order to withstand blood pressure after wound closure[22-25]. Moreover, the crosslinking strategy should be selected in such way that no toxic byproducts or heat are generated during the reaction with tissue. Finally, crosslinks should ideally be formed only with the desired tissue (blood or soft tissue), while undesired crosslinking with surrounding tissues should be prevented as this may cause undesired adhesion (between organs)[26].

For the development of tissue adhesives, poly(ethylene glycol) (abbreviated as PEG) is the most commonly investigated synthetic material because of its biocompatibility and excellent solubility in both aqueous and organic media[27]. Additionally, since the end groups of this material can be equipped with a wide variety of crosslinking groups[28, 29], various PEG-based biomedical devices have been developed[3, 30, 31]. An example of a PEG-based hemostatic product is Hemopatch[32,33], which consists of a porous collagen sponge coated with *N*-hydroxysuccinimide ester functional 4-arm poly(ethylene glycol) (**NHS-PEG**). Hemopatch acts by means of the instantaneous formation of covalent crosslinks between **NHS-PEG** and amines present in tissue, blood proteins and the collagen sponge. The formed crosslinked network seals the wound site and allows firm fixation of the patch to the tissue. This product is used as a hemostatic agent for non-invasive treatment of bleedings of soft tissue. Although clinical efficacy has been reported for PEG-based products, the limited crosslinking capacity (using end-groups only) and extensive swelling of the crosslinked networks (as reported for certain PEG-based medical devices[34]) has prompted research on alternative polymeric hydrogels.

Poly(2-oxazoline)s or POx[35-39] are emerging polymers within the biomedical field[40, 41] due to the extensive functionalization possibilities[42, 43], limited cytotoxicity[44-46] and excretability[47-49]. Since both side chains and end groups of POx can be functionalized, these polymers can be crosslinked in multiple ways. Consequently, these polymers are increasingly used for the development of crosslinked networks[50, 51]. Network formation has been reported using different chemistries including thiol-ene chemistry[52, 53], amine-isothiocyanate chemistry[54] and Diels-Alder chemistry[55].

In **Chapter 4**, we have successfully utilized the crosslinking capacity of N-hydroxysuccinimide (NHS) ester functionalized POx (**NHS-POx**) in hemostatic applications. To this end, we designed hemostatic **NHS-POx** equipped with three types of side chain modifications, i.e., i) NHS-ester groups to allow for crosslinking with amines, ii) hydrophobic (*n*PropOx) groups to allow for solubility in organic solvents (polymer processability), and iii) hydrophilic side chains to render the polymer hydrophilic enough for efficient crosslinking with human-derived whole

blood. By coating the polymers on gelatin scaffolds, these so called hemostatic patches showed promising hemostatic efficacy *in vitro* and *in vivo* in comparison with benchmark products based on **NHS-PEG** based materials. Although both POx and PEG-based samples were able to stop bleedings in these experiments, we observed strong differences regarding their mode of action (e.g. crosslinking speed), which indicates that the kinetics and/or type of network which is formed differs between **NHS-PEG** and **NHS-POx**.

A major structural difference between **NHS-PEG** and **NHS-POx** is the way the crosslinking moieties are positioned onto the polymer. In **NHS-PEG** the crosslinking groups are located at the polymer chains ends, whereas in **NHS-POx** these groups are present at the side chains of the polymer. Another structural difference between these types of polymers involves the hydrophilicity/polarity of the polymers. **NHS-PEG** are hydrophilic due to the abundance of ethylene glycol units in the polymer backbone, whereas in **NHS-POx** hydrophilic (hydroxyl) functional side chains render the polymer hydrophilic to allow for efficient crosslinking. In addition, the type and amount of hydrophilic side chains will have an effect on the polarity of the polymer and as a result on the network formation as well. Both factors will have an influence on the hemostatic action of **NHS-POx**.

In this chapter, we perform a systematic rheological study on the crosslinking behavior of two different hydrophilic side chain activated **NHS-POx** polymers (containing either OH and $N(CH_3)_2$) with bovine serum albumin (BSA) as a model protein (**Figure 1**). For reasons of comparison, we also studied chain-end functional tetravalent **NHS-PEG** because of its routine use in hemostatic devices. In order to gain a deeper insight and a better understanding into the mechanism of action of both **NHS-PEG** and **NHS-POx** as hemostatic polymers, we aimed to study the effect of i) the positioning of the crosslinking groups on the polymer (side chains vs. chain ends) and ii) the type of the hydrophilic co-substituents (OH and $N(CH_3)_2$) on the network formation. Furthermore, we investigated the effect of pH on the network formation.

2. Results and discussion

2.1 Synthesis

The synthesis of **P1** and **P2** has been described in detail in **Chapter 2**. The analytical data of the polymers which are used in this chapter are listed in **Table 1**.

2.2 Rheometry

In order to investigate the crosslinking behavior of the different side chain functional POx polymers (**P1** and **P2**) with BSA, oscillatory rheometry was used. To study the

effect of the spatial configuration of the crosslinking groups, we also studied included end chain functionalized tetravalent **NHS-PEG** as a control, a polymer which is routinely used in PEG-based biomedical devices[32, 33]. Using oscillatory time sweeps, we monitored the storage modulus (G') and loss modulus (G'') for 30 minutes to study the change of these viscoelastic properties resulting from network formation between the polymer and BSA. Subsequently, after formation of crosslinked networks, angular frequency sweeps (0.1-100 rad/s) and strain sweeps (0.1-1000% strain) were performed to study the viscoelastic parameters of the BSA-polymer network as a function of frequency and measure the yield strain of these networks, respectively.

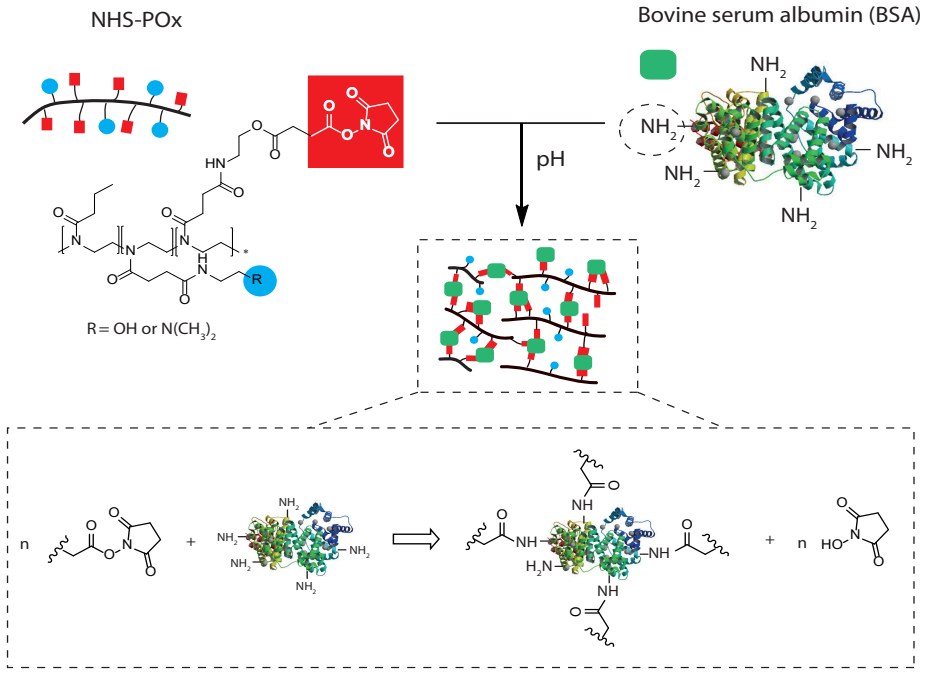

Figure 1 Schematic overview of the crosslinking reaction between **NHS-POx** and bovine serum albumin (BSA) thereby forming a **POx-BSA** network.

Table 1: Analytical data of the synthesized polymers

#	Polymer	^{1}H-NMR (mol%)				M_n (kg/mol)		
		nPropOx	OH	$N(CH_3)_2$	NHS	Theor.	SEC[a]	Đ[a]
P1	P(nPropOx-c-OH-c-NHS) (**P1**)	69	14	-	17	16.5	18.8	1.25
P2	P(nPropOx-c-$N(CH_3)_2$-c-NHS) (**P2**)	69	-	16	15	16.5	22.1	1.33

[a] SEC was calibrated against PMMA standards, eluent: 0.1 % LiCl in DMA

2.2.1 Time sweep experiments

In this experiment, polymer solutions (**P1**, **P2** and **NHS-PEG**) (100 mg/mL) and BSA solutions (70 mg/mL) were mixed together and pipetted onto the rheometer plate (t=0). All experiments were performed at a fixed BSA (35 mg/mL) and polymer concentration (50 mg/mL). Since the crosslinking of NHS-esters with amines is strongly influenced by pH, we performed this experiment at an elevated pH (~8.3) to ensure crosslinking. The results of these tests are displayed in **Figure 2** and **Table 2**.

In all these measurements, we observed that the crosslinking mixture reached the gelation point (G' = G'') before the measurement was started. Furthermore, we observed that the loss modulus (G'') was significantly lower than the storage modulus (G'). These data indicate that elastic gel networks were formed resulting from a crosslinking reaction between the synthetic polymers and BSA. We observed that both **P1** and **P2** formed a hydrogel network instantaneously (G'>G'') with a tan delta value <1 from the first data point and a comparable storage modulus (G') after 30 min of gelation of 351 ± 101 Pa (**P1**) and 400 ± 139 Pa **(P2)**. These values were lower than previously reported values (G' 1100 Pa) for a comparable side chain functionalized POx crosslinked system, as reported by Dargaville and coworkers[50]. This difference can be explained by the fact that crosslinkers of low molecular weight were used, whereas in our case a macromolecular crosslinker (BSA) was used, which strongly affects e.g. the mobility of the crosslinker. In the present experiment, differences in the final storage modulus between **P1** and **P2** were statisticaly insignificant. It was, however, observed that these final values were reached faster for **P1** than **P2**, which indicates that the dimethylamine groups influence protonation of the ammonium groups of the lysine residues, but not the amount of crosslinks which are eventually formed. When mixing BSA with **NHS-PEG**, a crosslinked network was also formed instantaneously with a storage modulus of 7667 ± 1973 Pa, consistent with literature values, which indicates that a stiffer network was formed using **NHS-PEG** [56,57]. The final storage modulus of the PEG-based network also was significantly higher than the gels prepared from **P1** and **P2**.

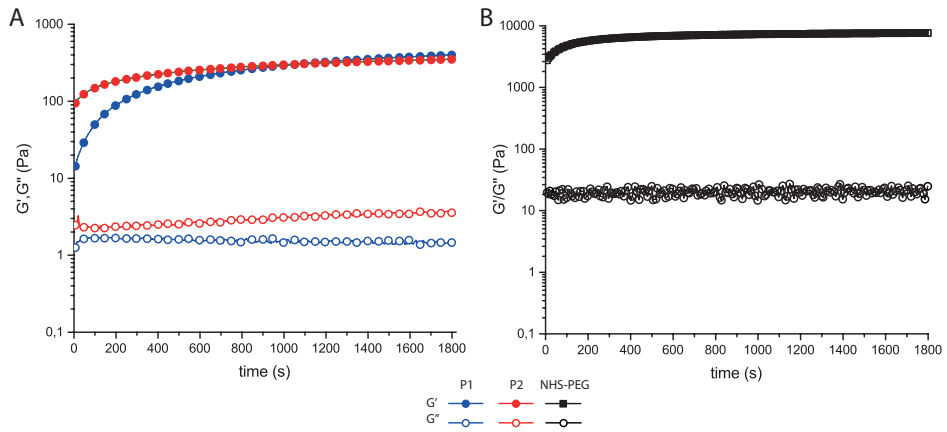

Figure 2 Oscillatory time sweep of mixtures of **P1**, **P2** (A) and **NHS-PEG** (B) with BSA (35 mg/mL).

Table 2 Experimental results oscillatory time sweep

	polymer[a]	ratio NHS/NH_2[b]	Tan delta (t=30 min) (n=6)		G' (Pa)[c] after 30 min		
#	µmol NHS		Mean	SD	Mean	SD	P-value
P1	45.5	2.4	$1.1 \cdot 10^{-2}$	$2.1 * 10^{-3}$	351	101	ns
P2	44.4	2.4	$3.7 * 10^{-3}$	$6.5 * 10^{-4}$	400	139	ns
NHS-PEG	16.7	0.9	$3.2 * 10^{-3}$	$4.1 * 10^{-3}$	7667	1973	<0.001[d]

[a] Calculated from the NHS-content which was determined by ^{1}H-NMR spectroscopy. The end group NHS content of **NHS-PEG** was determined to be 96% (^{1}H-NMR)

[b] Number of primary amines in BSA calculated from the information supplied by the manufacturer: M_w 66 kDa and 30-35 available lysines per protein, 18.6 µmol of amines in each measurement

[c] Measurements were performed in sixfold (n=6)

[d] Against both **P1** and **P2** (ns = not significant)

2.2.2 Frequency sweeps

After the oscillatory time sweeps, frequency sweeps were performed between an angular frequency range of 0.1-100 rad/s (**Figure 3**). Herein, we observed that **P1** and **P2** as well as **NHS-PEG** displayed a frequency-independent elastic behavior characterized by considerably higher storage moduli as compared to corresponding loss moduli; this highly elastic behavior was previously reported for tetravalent PEG-systems by multiple groups[56, 57]. In our experiments, a slight increase of the loss modulus at higher frequencies was observed in case of **P1** and **P2**, but not for **NHS-PEG**.

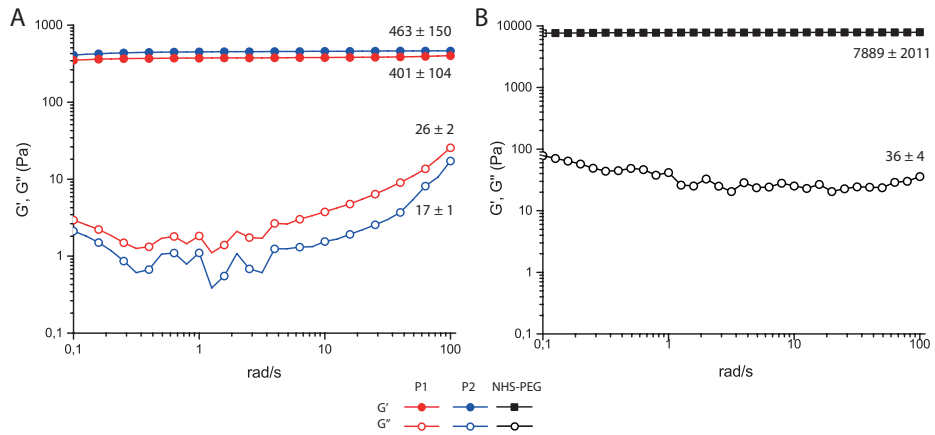

Figure 3 Oscillatory frequency sweeps (0.1-100 Hz) for **P1** + **P2** (A) and **NHS-PEG** (B). Experiments were performed (n=6)

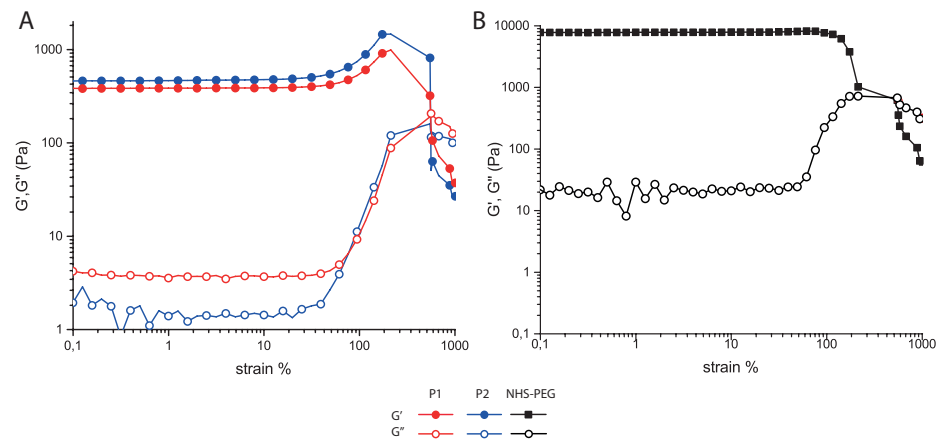

Figure 4 Strain sweep for **P1** + **P2** (A) and **NHS-PEG** (B) from 0.1 -1000% strain.

Table 3 Experimental results of the strain sweep

	Strain stiffening behavior		Yield strain (%)		
#	% strain	Ratio G′ (max strain)/G′ (0.05 % strain)[b]	Mean	SD	P-value
P1	between 30-210	2.6	542	118	ns
P2	between 30-210	3.1	649	94	<0.05[c]
NHS-PEG	-	1.05	473	54	ns

[a] The experiments were performed (n=6)
[b] G′ (max) = G′ maximum strain values
[c] Only against **NHS-PEG**, not against **P1**

2.2.3 Strain sweeps

Subsequently, we performed strain sweeps between 0.1 -1000% strain on the formed networks to quantify the yield strain (**Figure 4** and **Table 3**). Polymers **P1** and **P2** stiffened at increasing strain values (between 30% and 210%), which is indicative of strain stiffening behavior. This phenomenon was not observed for **NHS-PEG** (**Table 3**). At strain values higher than 200%, the storage modulus dropped to values below the loss modulus was seen, which corresponds to disruption of the network structure. The yield strains – defined as the strain at which the storage modulus was equal to the loss modulus (G'=G'') - were 542 ± 118 % and 649 ± 94 % for **P1** and **P2** respectively. In case of **NHS-PEG**, the network was destroyed at a yield strain of 473 ± 54 %. The differences in yield strain were only statistically significant between **P2** and **NHS-PEG**.

2.3 Structural differences between POx-BSA and PEG-BSA networks

By comparing the results of the time sweep, frequency sweep and strain sweep experiments respectively, both **NHS-POx** and **NHS-PEG** exhibit a different crosslinking behavior with BSA, which results in a different network structure. In the oscillatory time sweep measurements, we found that stiffer **PEG-BSA** networks were formed in comparison with **POx-BSA** networks. We suspect that the differences in stiffness can be explained from the difference in architecture of both polymer classes (**Figure 5**). Using **NHS-PEG** (**Figure 5A**), the NHS-ester groups are present at the end of the extended hydrophilic chains. As a result, crosslinks are formed instantaneously because of the accessibility of the end groups which results in a high G′. Regarding network formation, because of the limited amount of crosslinking possibilities (max. 4 crosslinks per polymer) and the extended spacer length, it is not expected that one PEG-molecule forms multiple covalent bonds with one BSA protein at the same time. It is rather expected that only intermolecular covalent bonds between polymer and protein (crosslinks) are formed in which one PEG binds multiple proteins at the same time, at a maximum of 4. This efficient crosslinking mechanism ensures the formation of a homogeneously crosslinked network.

In contrast, **NHS-POx** polymers (**P1** and **P2**) contain multiple reactive NHS-ester groups as polymer side chains (**Figure 5B**). Compared to **NHS-PEG**, these polymers present a larger number of reactive groups (theoretically 2.7 times more, **Table 2**) available for reaction with BSA. Additionally, the ratio between amines (BSA) and the crosslinking groups on the polymer is higher in case of **NHS-POx** (molar ratio NHS/amines: 2.4) compared to **NHS-PEG** (molar ratio NHS/amines: 0.9). Consequently, it was expected that a stiffer network would be formed. However, the lower G′ values which were observed experimentally for **NHS-POx** polymers indicate that less intermolecular crosslinks were formed between BSA and **NHS-POx**, which

contribute to the strength of the network. This phenomenon can be attributed to the specific architecture of the **NHS-POx** polymer. Because of the higher amount of reactive functional groups and the higher functional group density (at the side chains) compared to **NHS-PEG**, it is expected that **NHS-POx** forms multiple bonds with the same BSA molecule in addition to intermolecular crosslinks. However, these covalent bonds do not contribute to the stiffness/strength of the network, since no additional crosslinks between polymer chains are generated in this case. Overall, this results in a more heterogeneously crosslinked network as compared to **NHS-PEG** (**Figure 5B**).

An additional explanation for the lower storage modulus of gels containing **NHS-POx** could be related to the fact that this heterogeneous crosslinking prevents complete crosslinking. In order to test whether stiffer gels were formed upon prolonged crosslinking time, we performed an oscillatory time sweep experiment of 9 hrs (instead of 30 min) for **P1**, **P2** and **NHS-PEG**. It was found that for **P1** and **P2**, a continuous increase in G' and G'' was seen even after 9 hrs (G' of 800 Pa (**P1**) and 671 Pa (**P2**)), while the G' of **NHS-PEG** reached a plateau (G' 8500 after 2 hrs). This suggests that further crosslinking is not hampered by the structure of the network for **P1** and **P2**, but more research is needed to prove statistically significant differences.

In the oscillatory strain sweeps, strain stiffening was observed for **NHS-POx**, but not for **NHS-PEG**. This strain stiffening behavior is reported for natural polymers such as collagen[58] and actin[59] as well as for physically crosslinked synthetic hydrogels[60, 61], but not yet for POx-based networks. Several important parameters[61,62] have been reported to play a role in strain stiffening, such as the network microstructure[59] and the identity of the crosslinker[62]. Because of the apparent structural differences between **NHS-POx** and **NHS-PEG** but identical crosslinker (BSA), we suggest that the strain stiffening behavior can be explained from the different network structures which are formed (**PEG-BSA** vs. **POx-BSA** (**Figure 5**).

If strain is continuously increased for crosslinked networks, the polymer chains will be stretched until the network structure is disrupted. In case of **POx-BSA**, the network consists of covalent crosslinks between polymer chains and BSA (which govern the network structure), but also domains in which one POx chain binds a single BSA protein via multiple covalent crosslinks. We hypothesize that if increasing strain is applied to these crosslinked POx-networks (**P1** and **P2**), the complete stretching and disruption of the network is hampered by these densely crosslinked domains, which prevent full stretching of the network. Instead, the networks stiffen upon increasing strain until network disruption occurs. In case of **PEG-BSA**, the network predominantly consists of covalent crosslinks between polymer and BSA. Due to this more homogeneous network structure, the network can be fully stretched and disrupted with increasing strain without demonstrating strain stiffening behavior.

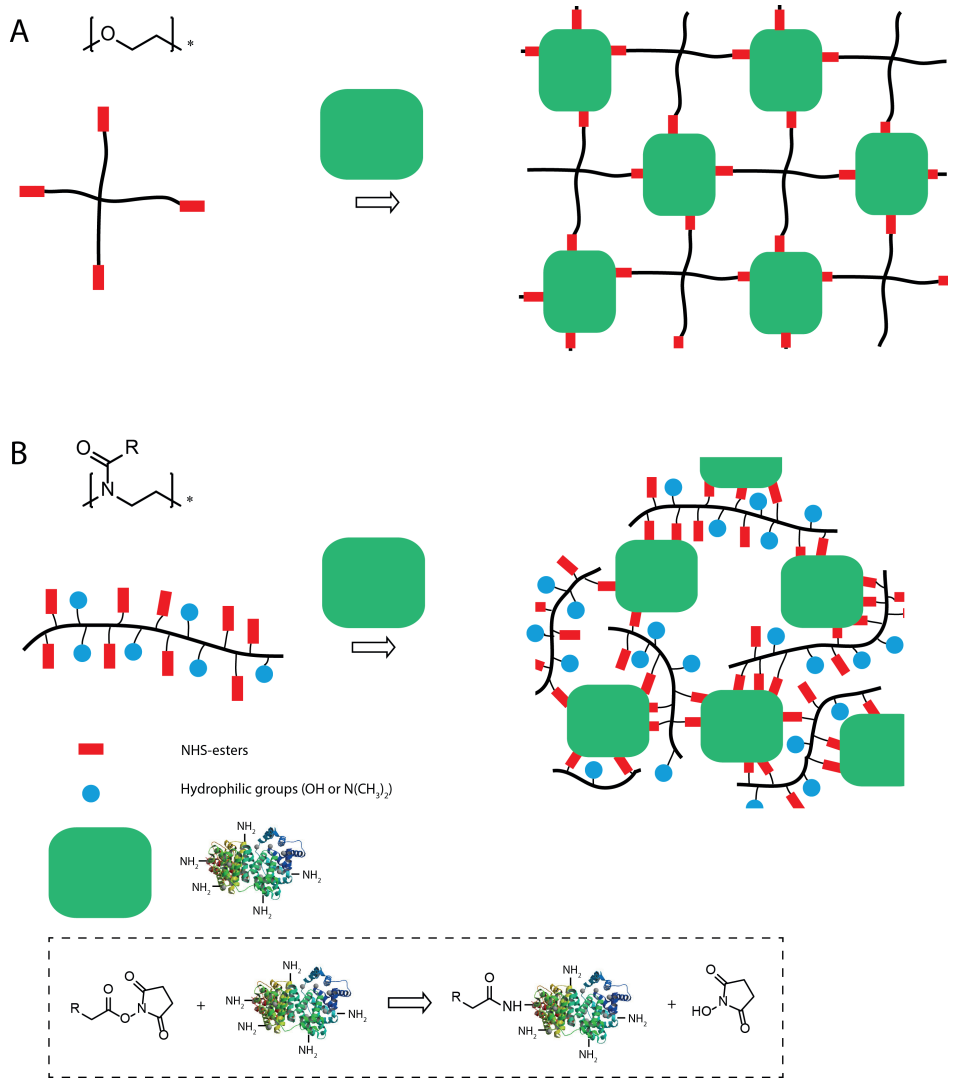

Figure 5 Differences in network formation with BSA for **NHS-PEG** (A) and **NHS-POx** (B).

These experiments have demonstrated that the configuration of the amine-reactive NHS ester groups is of great importance for the formation of crosslinked networks. No differences in network structure were observed between **P1** and **P2**, which indicates that nature of the hydrophilic moiety which is incorporated into the polymer influenced the obtained network structure.

In view of therapeutic application, it must be emphasized that both **NHS-PEG** and **NHS-POx** are suitable as hemostatic polymers since they both crosslink with BSA

instantaneously (tan delta <1). The mechanical properties of both **NHS-PEG** and **NHS-POx** based networks exceed the minimal stiffness of fibrin clots (~ G' 10-100 Pa)[22-23] and show highly elastic behavior over a wide frequency, which renders these polymer networks theoretically capable to withstand forces within the body (such as blood pressure) upon clinical application. A benefit of **NHS-POx** could be that the slower crosslinking via side chains – as opposed to faster crosslinking via flexible end groups for **NHS-PEG** - may allow for more controlled application of the hemostatic patch in clinical applications. We observed in **Chapter 4** that this was impossible for **NHS-PEG** based hemostatic agent Hemopatch which adhered directly to tissue, leading to inhomogeneous coverage of the bleeding site. It must, however, be taken into account that these studies were based on the use of BSA as a model protein and not on whole blood. Consequently, direct translation of these results towards clinical applications is not possible based on the current experimental design.

2.4 Effect of the pH on crosslinking behavior of NHS-POx

Since the reaction of NHS-esters with amines is highly sensitive to pH, we investigated the influence of the pH on both the formation speed and stiffness of the crosslinked networks containing **P1** and **P2**. To this end, we performed time sweeps at fixed polymer (50 mg/mL) and BSA concentrations (35 mg/mL), but at different pH values by adjusting the pH of the BSA solution. By mixing the polymer solution (pH ~5) with the basic BSA solution (pH 8-11), the pH of the crosslinking mixture can be precisely tuned in order to obtain the desired pH value (7-9.5). At basic pH, crosslinking with amines is in competition with hydrolysis of the NHS-esters. Consequently, we expected an optimum pH for the crosslinking reaction to be in place, resulting into the formation of the stiffest networks. Therefore, we studied network formation of **P1** and **P2** over a range of pH-values (7-9.5). The results of this experiment are displayed in **Figure 6A** (**P1**) + **6b** (**P2**).

It can be observed from **Figure 6A** that gels were formed by mixing BSA with **P1** at all pH values (tan delta <1). However, the stiffest gels were formed at an optimum pH of 8.5. For **P2** (**Figure 6B**), gels were formed after 30 min (tan delta <1). It must be noted, however, that the crosslinking reaction should occur at a pH of 8.5 or higher to obtain the stiffest gels within this series. In the experiments which were performed at a pH <8, softer gels were formed, which was attributed to the fact that the lysine residues in BSA were not sufficiently deprotonated to allow effective network formation. Since the stiffness of the gels (G') decreased again at pH values higher than 8.5 (for **P1**), we hypothesized that the hydrolysis of the NHS-ester was predominant at this pH over the network formation by means of amidation. In order to test this, a control experiment was performed by ^{1}H-NMR spectroscopy to study the hydrolysis rate of NHS-esters at pH 8 and pH 9. It was found that after

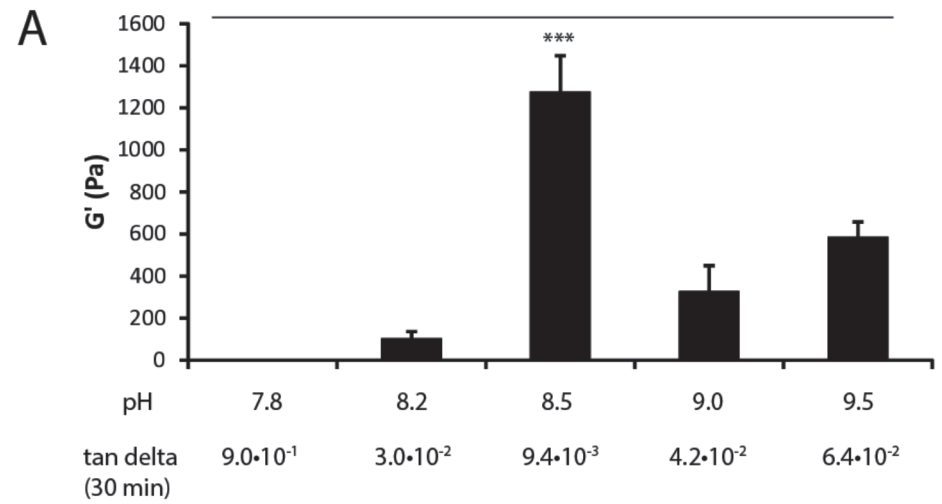

Figure 6 Effect of the pH on the network formation for **P1** (A) and **P2** (B). Experiments were performed in triplo (n=3). P(*** P< 0.001, ** P< 0.01, * P<0.05)

30 minutes, 60% of the NHS-ester groups were hydrolyzed at pH 8 and 90 % at pH 9, indicating that during 30 minutes the majority of the functional groups either reacted with amines or were hydrolyzed. No differences between **P1** and **P2** were observed in these hydrolysis experiments.

This study on the effect on pH on the formation of the network structure is particularly relevant from a clinical perspective. By tuning the pH of the device through the addition of a biocompatible basic component (e.g. sodium carbonate),

the pH of the area around the wound site will be locally elevated to the desired pH (~8.5) which speeds up crosslinking. After crosslinking has been achieved, the pH will be normalized by the buffering ability of the blood. This approach towards control of reaction pH has already been suitably employed in various commercially available tissue adhesives and hemostatic products in the biomedical field, such as Duraseal[63] and Coseal[31].

3. Conclusion

We have performed a systematic rheological study on the crosslinking of **NHS-POx** and **NHS-PEG** with BSA (as a mimic for blood proteins) in order to study the effect of i) the positioning of the crosslinking groups and ii) the identity of the hydrophilic side chains (OH (**P1**) and $N(CH_3)_2$ (**P2**)) on the network structure. It was found that both **NHS-POx** (**P1** and **P2)** and **NHS-PEG** were able to form crosslinked networks with BSA, however we observed that **NHS-PEG** and **NHS-POx** clearly formed different network structures with BSA. During oscillatory time sweeps, we have found that **NHS-PEG** formed stiffer homogeneous networks than **NHS-POx**, which formed inhomogeneous networks of lower stiffness, because of the different distribution of functional groups along the polymer chain. Both **PEG-BSA** and **POx-BSA** networks showed elastic behavior over the entire frequency range which was tested. During oscillatory strain sweeps, it was observed that in contrast to **PEG-BSA** networks, **POx-BSA** networks showed strain stiffening behavior upon increased strain (30-210% strain), which can be related to the different network structure which is formed. For **NHS-POx**, it was found that by performing the crosslinking reaction at a pH of 8.5, the stiffest crosslinked networks were obtained (G'=1200) for **P1** and (G'=800) for **P2**. In conclusion, these experiments demonstrate that the positioning of the crosslinking groups on the polymer chains and the pH at which the crosslinking is performed is of great influence on the characteristics of network structure. In contrast, the identity of the hydrophilic moiety (OH or $N(CH_3)_2$) is of little influence on the network struture which is formed.

4. Acknowledgements

Jon Donkers and Nathalie Pers are kindly acknowledged for their contributions to the work described in this chapter.

5. Materials and methods

5.1 Materials

N-hydroxysuccinimide ester functional 4-arm poly(ethylene glycol) (**NHS-PEG**) was obtained from NOF America corporation. BSA (66.3 kDa, >95% pure, protease free) was obtained from Sigma-Aldrich.

5.2 Synthesis

The synthetic procedures of **P1** and **P2** are described in the experimental section of **Chapter 2**. ^{1}H-NMR spectra of **P1** and **P2** are shown in the Appendix (**Figure S1**)

5.3 Rheology

Rheological measurements were conducted with a TA Instruments AR 2000 Rheometer equipped with a Peltier plate. For all measurements, a flat geometry with a diameter of 20mm was used. All gels were prepared as follows (**Figure 7**): solution A was prepared by dissolving bovine serum albumin (BSA) in a solution of sodium borate (0.1-0.4 M) or a solution of sodium carbonate (0.01-0.1 M) to a final BSA concentration of 70 mg/mL. Solution B was prepared by dissolving **P1**, **P2** or **NHS-PEG** in demineralized water to a final polymer concentration of 100 mg/mL. **P1** was shortly cooled on crushed ice to allow full solubilization. The formulations used for the rheology experiments were prepared by mixing both solution A and solution B (v/v, 1:1) to a final volume of 500 µL. This solution (A+B) was vortexed for 5 seconds and 200 µL was transferred to the rheometer plate. (**Figure 7**). Directlty thereafter, three consecutive rheological experiments were performed, starting with a time sweep experiment at an oscillation frequency of 10 rad/s and a constant strain of 5% during 30 minutes. Secondly, frequency sweep experiments were performed at an increasing oscillation frequency from 0.1 rad/s to 100 rad/s and a constant strain of 5%. Finally, strain sweep experiments were performed at a constant oscillation frequency of 10 rad/s and an increasing strain from 0% to 1000%, to measure the yield strain of the networks. In these experiments, the yield strain was defined as the strain at which the storage modulus was equal to the loss modulus (G'=G''). Unless stated otherwise, the experiments were carried out at 25°C in six-fold (n=6). The pH of the different formulations was assesed as follows: after preparation of the solution A+B, the pH of the solution was directly measured using a Mettler Toledo FE-280-Basic pH meter equipped with an in-Lab micro pH electrode (3 mm).

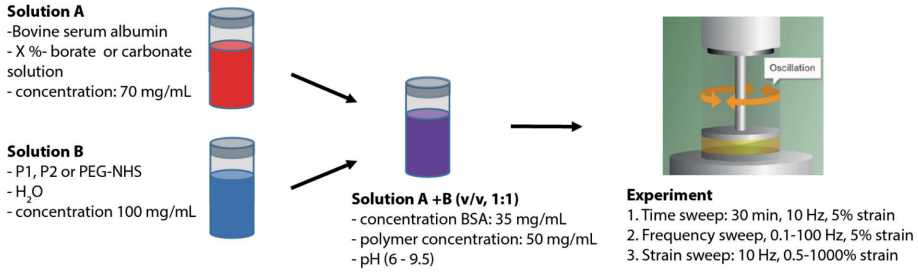

Figure 7 Overview of the experimental procedure for the rheological experiments

5.4 Hydrolysis experiments

The polymers (**P1** and **P2**) were dissolved in D_2O (15 mg/mL) and hydrolysis was determined at different pH values (7, 8 and 9) by performing ^{1}H-NMR measurements over the time course of 60 minutes. The percentage of hydrolysis was determined from the ratio of the integrals corresponding to the polymer-bound NHS (2.8 ppm) and free NHS (2.7 ppm) (**Figure S2**).

5.5 Statistics

Statistical analyses were conducted using GraphPad Instat software. All results were reported as mean ± standard deviation. Differences among groups were analyzed by ANOVA using a Tukey-Kramer Multi comparison test and p-values of 0.05 or lower were considered as significantly different.

6. References

1. R. G. Dan, O. M. Creau, O. Mazilu, L. V. Sima, D. Iliescu, A. Blidiæel, R. Tirziu, A. Istodor and E. F. Hua, *Chirurgia (Romania)*, 2012, **109**, 737-741.
2. L. J. Wrighton, K. R. O'Bosky, J. P. Namm and M. Senthil, *J. Gastrointest. Oncol.*, 2012, **3**, 41-47.
3. P. J. M. Bouten, M. Zonjee, J. Bender, S. T. K. Yauw, H. van Goor, J. C. M. van Hest and R. Hoogenboom, *Prog. Polym. Sci.*, 2014, **39**, 1375-1405.
4. M. Ryou and C. C. Thompson, *Tech. Gastrointest. Endosc.*, 2006, **8**, 33-37.
5. J. C. Dumville, P. Coulthard, H. V. Worthington, P. Riley, N. Patel, J. Darcey, M. Esposito, M. van der Elst and O. J. F. van Waes, *Cochrane Database Syst. Rev.*, 2014, 44.
6. M. R. Jackson, *Am. J. Surg.*, 2001, **182**, S1-S7.
7. W. D. Spotnitz, *Am. J. Surg.*, 2001, **182**, S8-S14.
8. G. Pascual, S. Sotomayor, M. Rodriguez, B. Perez-Kohler, A. Kuhnhardt, M. Fernandez-Gutierrez, J. San Roman and J. M. Bellon, *PLoS One*, 2016, **11**, e0157920.
9. C. Ghobril and M. W. Grinstaff, *Chem. Soc. Rev.*, 2015, **44**, 1820-1835.
10. M. Mehdizadeh and J. Yang, *Macromol. Biosci.*, 2013, **13**, 271-288.
11. A. S. Hoffman, *Adv. Drug Deliv. Rev.*, 2012, **64**, 18-23.
12. T. R. Hoare and D. S. Kohane, *Polymer*, 2008, **49**, 1993-2007.
13. J. L. Drury and D. J. Mooney, *Biomaterials*, 2003, **24**, 4337-4351.
14. J. Zhu and R. E. Marchant, *Expert Rev. Med. Devices*, 2011, **8**, 607-626.
15. M. W. Tibbitt and K. S. Anseth, *Biotechnol. Bioeng.*, 2009, **103**, 655-663.
16. M. M. Ozmen and O. Okay, *Polymer*, 2005, **46**, 8119-8127.
17. J. Zhang, N. Wang, W. Liu, X. Zhao and W. Lu, *Soft Matter*, 2013, **9**, 6331.
18. A. R. Fajardo, S. L. Fávaro, A. F. Rubira and E. C. Muniz, *React. Funct. Polym.*, 2013, **73**, 1662-1671.
19. E. F. d. Reis, F. S. Campos, A. P. Lage, R. C. Leite, L. G. Heneine, W. L. Vasconcelos, Z. I. P. Lobato and H. S. Mansur, *Mat. Res.*, 2006, **9**, 185-191.
20. F. Chen, S. Yu, B. Liu, Y. Ni, C. Yu, Y. Su, X. Zhu, X. Yu, Y. Zhou and D. Yan, *Sci. Rep.*, 2016, **6**, 20014.
21. G. J. M. Fechine, J. A. G. Barros and L. H. Catalani, *Polymer*, 2004, **45**, 4705-4709.
22. H. Schöchl and C. J. Schlimp, *Anesth. Analg.*, 2014, **119**, 1064-1073.
23. J. W. Weisel, *J. Thromb. Haemost.*, 2007, **5**, 116-124.
24. O. V. Kim, R. I. Litvinov, J. W. Weisel and M. S. Alber, *Biomaterials*, 2014, **35**, 6739-6749.
25. L. W. G. Chan, X. Wang, H. Wei, L. D. Pozzo, N. J. White and S. H. Pun, *Sci. Transl. Med.*, 2015, **7**, 277ra229-277ra229.
26. R. P. G. ten Broek, C. Strik, Y. Issa, R. P. Bleichrodt and H. van Goor, *Ann. Surg.*, 2013, **258**, 98-106.
27. J. M. Harris, in *Poly(Ethylene Glycol) Chemistry: Biotechnical and Biomedical Applications*, ed. J. M. Harris, Springer US, Boston, MA, 1992, 1-14.
28. M. Cencer, Y. Liu, A. Winter, M. Murley, H. Meng and B. P. Lee, *Biomacromolecules*, 2014, **15**, 2861-2869.
29. D. Mazunin, N. Broguiere, M. Zenobi-Wong and J. W. Bode, *ACS Biomater. Sci. Eng.*, 2015, **1**, 456-462.
30. G. Rees Cosgrove, Johnny B. Delashaw, J. Andre Grotenhuis, John M. Tew, Harry van Loveren, Robert F. Spetzler, Troy Payner, Gail Rosseau, Mark E. Shaffrey, L. Nelson Hopkins, Richard Byrne and Alex Norbash, *J. Neurosurg.*, 2007, **106**, 52-58.
31. C. Tan, M. Utley, C. Paschalides, J. Pilling, J. D. Robb, K. M. Harrison-Phipps, L. Lang-Lazdunski and T. Treasure, *Eur. J. Cardiothorac. Surg.*, 2011, **40**, 304-308.
32. K. M. Lewis, A. Schiviz, H.-C. Hedrich, J. Regenbogen and A. Goppelt, *Int. J. Surg.*, 2014, **12**, 940-944.
33. K. M. Lewis, D. Spazierer, P. Slezak, B. Baumgartner, J. Regenbogen and H. Gulle, *J. Biomater. Appl.*, 2014, **29**, 780-788.
34. S. L. B. Patrick K. Campbell, Art Driscoll, Amar S. Sawhney, Evaluation of Absorbable Surgical Sealants: In vitro Testing, http://www.covidien.com/imageServer.aspx/doc179399.pdf?contentID=14109&contenttype=application/pdf, (accessed 12/12/2016, 2016).

35. R. Hoogenboom, *Angew. Chem. Int. Ed.* , 2009, **48**, 7978-7994.
36. T. G. Bassiri, A. Levy and M. Litt, *J. Polym. Sci. B-1 Polym. Lett.*, 1967, **5**, 871-879.
37. A. Levy and M. Litt, *J. Polym. Sci. A-1 Polym.Chem.*, 1968, **6**, 1883-1894.
38. D. A. Tomalia and D. P. Sheetz, *J. Polym. Sci. A-1 Polym. Chem.*, 1966, **4**, 2253-2265.
39. W. Seeliger, E. Aufderhaar, W. Diepers, R. Feinauer, R. Nehring, W. Thier and H. Hellmann, *Angew. Chem. Int. Ed.* , 1966, **5**, 875-888.
40. N. Adams and U. S. Schubert, *Adv. Drug Deliv. Rev.*, 2007, **59**, 1504-1520.
41. V. R. De La Rosa, *J. Mater. Sci. Mater. Med.*, 2014, **25**, 1211-1225.
42. E. Rossegger, V. Schenk and F. Wiesbrock, *Polymers*, 2013, **5**, 956-1011.
43. B. Guillerm, S. Monge, V. Lapinte and J. J. Robin, *Macromol. Rapid Commun.*, 2012, **33**, 1600-1612.
44. J. Kronek, E. Paulovičová, L. Paulovičová, Z. Kroneková and J. Lustoň, *J. Mater. Sci. Mater. Med.*, 2012, **23**, 1457-1464.
45. J. Kronek, E. Paulovičová, L. Paulovičová, Z. Kroneková and J. Lustoň, *Biocompatibility and Immunocompatibility Assessment of Poly(2-Oxazolines)*, 2013, *DOI: 10.5772/51501*
46. M. Bauer, C. Lautenschlaeger, K. Kempe, L. Tauhardt, U. S. Schubert and D. Fischer, *Macromol. Biosci.*, 2012, **12**, 986-998.
47. F. C. Gaertner, R. Luxenhofer, B. Blechert, R. Jordan and M. Essler, *J. Control. Release*, 2007, **119**, 291-300.
48. L. Wyffels, T. Verbrugghen, B. D. Monnery, M. Glassner, S. Stroobants, R. Hoogenboom and S. Staelens, *J. Control. Release*, 2016, **235**, 63-71.
49. R. W. Moreadith, T. X. Viegas, M. D. Bentley, J. M. Harris, Z. Fang, K. Yoon, B. Dizman, R. Weimer, B. P. Rae, X. Li, C. Rader, D. Standaert and W. Olanow, *Eur. Polym. J.*, 2016, **88**, 524-552
50. T. R. Dargaville, R. Forster, B. L. Farrugia, K. Kempe, L. Voorhaar, U. S. Schubert and R. Hoogenboom, *Macromol. Rapid Commun.*, 2012, **33**, 1695-1700.
51. M. Hartlieb, K. Kempe and U. S. Schubert, *J. Mater. Chem. B*, 2015, **3**, 526-538.
52. B. L. Farrugia, K. Kempe, U. S. Schubert, R. Hoogenboom and T. R. Dargaville, *Biomacromolecules*, 2013, **14**, 2724-2732.
53. T. R. Dargaville, B. G. Hollier, A. Shokoohmand and R. Hoogenboom, *Cell. Adh. Migr.*, 2014, **8**, 88-93.
54. S. Cesana, J. Auernheimer, R. Jordan, H. Kessler and O. Nuyken, *Macromol. Chem. Phys.*, 2006, **207**, 183-192.
55. Y. Chujo, K. Sada and T. Saegusa, *Macromolecules*, 1990, **23**, 2636-2641.
56. A. M. Jonker, A. Borrmann, E. R. H. van Eck, F. L. van Delft, D. W. P. M. Löwik and J. C. M. van Hest, *Adv. Mater.*, 2015, **27**, 1235-1240.
57. A. M. Jonker, S. A. Bode, A. H. Kusters, J. C. M. van Hest and D. W. P. M. Löwik, *Macromol. Biosci.*, 2015, **15**, 1338-1347.
58. S. Lin and L. Gu, *Materials*, 2015, **8**, 551-560.
59. K. A. Erk, K. J. Henderson and K. R. Shull, *Biomacromolecules*, 2010, **11**, 1358-1363.
60. P. H. Kouwer, M. Koepf, V. A. Le Sage, M. Jaspers, A. M. van Buul, Z. H. Eksteen-Akeroyd, T. Woltinge, E. Schwartz, H. J. Kitto, R. Hoogenboom, S. J. Picken, R. J. Nolte, E. Mendes and A. E. Rowan, *Nature*, 2013, **493**, 651-655.
61. M. Jaspers, M. Dennison, M. F. Mabesoone, F. C. MacKintosh, A. E. Rowan and P. H. Kouwer, *Nat. Commun.*, 2014, **5**, 5808.
62. B. Wagner, R. Tharmann, I. Haase, M. Fischer and A. R. Bausch, *Proc. Natl. Acad. Sci. U. S. A.*, 2006, **103**, 13974-13978.
63. M. C. Preul, W. D. Bichard, T. R. Muench and R. F. Spetzler, *Neurosurgery*, 2003, **53**, 1189-1199.

Appendix

^{1}H-NMR spectra of P1 and P2

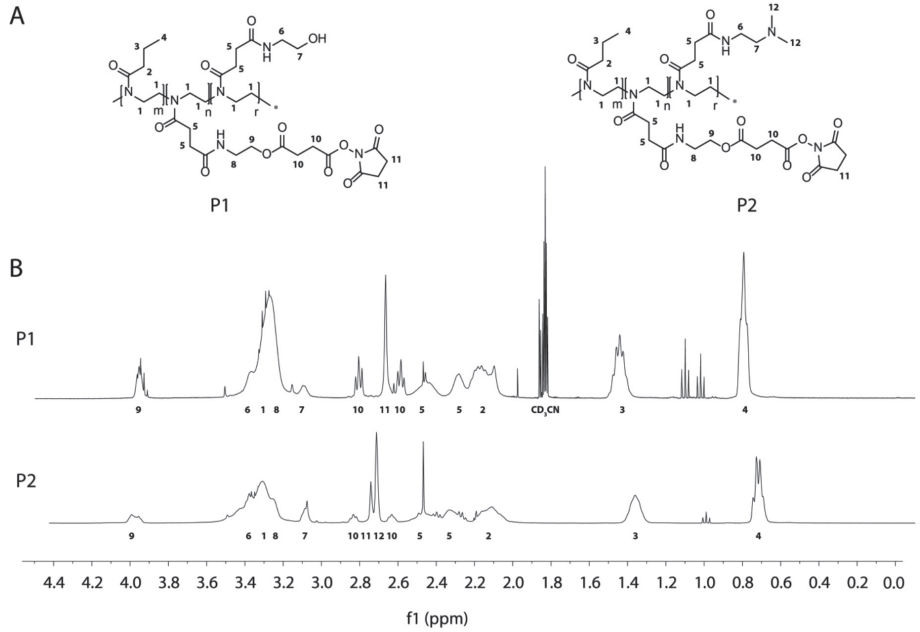

Figure S1 Overview of ^{1}H-NMR spectra of **P1**-**P2**. The spectrum of **P1** was recorded in CD_3CN, the spectrum of **P2** was recorded in D_2O

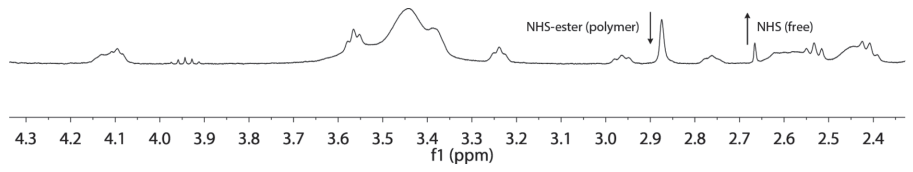

Figure S2 Representative ^{1}H-NMR spectrum of **P1** after incubation in pH 7 for 60 min. Signal at 2.85 ppm corresponds to polymer bound NHS-ester, while signal at 2.65 ppm represents free NHS in solution.

Chapter 6:

Degradation and excretion of NHS-ester functionalized poly(2-oxazoline)s

Abstract

In this chapter, we studied the degradability and excretability of NHS-ester functionalized poly(2-oxazoline)s (**NHS-POx**). In order to obtain insight into the degradability of **NHS-POx**, we first performed an *in vitro* degradation study by incubation of **NHS-POx** in relevant physiological media (PBS and whole blood plasma) for various time points, and identified the main degradation product by ^{1}H-NMR spectroscopy. Next, we studied i) the excretion pathway of this degradation product and ii) possible accumulation of these degradation products in specific organs. To this end, the most relevant degradation product was synthesized and functionalized with a diethylene triamine pentaacetic acid (DTPA) label which allowed chelation of radioactive isotopes (e.g. ^{111}Indium). After labeling and purification, the radiolabeled polymers were injected in Wistar-rats and the excretion was monitored using Single Photon Emission Computed Tomography (SPECT/CT) by imaging the rats at different time points (1 hr, 6 hrs, 24 hrs and 7 days). Additionally, after 7 days, the organs of the rats were dissected and their radioactivity counted using an automated γ-counter. It was observed that the injected polymer did not accumulate in organs and the majority of the polymer was cleared within 24 hrs, mainly via renal clearance. Although a steady decline was observed in the amount of radiolabeled polymer over time, after 7 days, 3.1 ± 1.1 of the injected dose per gram (ID%/g) by SPECT/CT or 9.5 ± 0.6 ID%/g (γ-counter) was still observed in kidneys. Although the majority of the injected dose of radiolabeled polymer (%ID/g: 80-90) was renally excreted, more research is needed to explain the retention of this polymer in the kidneys in more detail, for example by repeating our study using a covalently attached radiolabel.

1. Introduction

Insufficient control over bleeding remains one of the biggest challenges in trauma surgery of soft tissues such as liver or kidney[1]. This cannot be treated using traditional invasive wound closing methods such as sutures or staples, since this would create an additional bleeding. As a result, a variety of hemostatic agents has been developed for the non-invasive treatment of bleedings on these organs[2, 3].

Previously, we developed a polymeric hemostatic agent comprised of a porous gelatin sponge coated with NHS-ester functionalized poly(2-oxazoline)s (**NHS-POx**) (**Chapter 4**). Polymers containing NHS-esters are intrinsically reactive to primary amines, which are abundantly present in tissue and blood proteins. When this coated sponge is applied to a wound site, **NHS-POx** is capable of forming covalent crosslinks between polymer, host blood proteins, a gelatin sponge and tissue to seal the wound site and prevent hemorrhage during surgery. Hemostatic activity was demonstrated on soft organs (spleen and liver) in a pig model. However, the long-term fate of this biomedical device remains to be elucidated[4]. Two important research parameters in this respect are: i) degradation of the polymer and ii) elimination of the polymer and associated degradation products from the body (excretion).

Degradation is strongly determined by the presence of hydrolytically or proteolytically cleavable moieties in the polymer structure such as ester or amide groups[5, 6]. Since our system consists of two different components, a gelatin sponge and a **NHS-POx** coating, the degradability of both components should be considered. As gelatin is susceptible to proteolytic degradation *in vivo*, it will quickly degrade to smaller peptide and amino acid fragments and resorb fully within weeks, as confirmed previously [7-10]. Regarding the polymer, the backbone structure of POx (which consists of tertiary amide groups) is generally stable under physiological conditions[11], but the presence of the ester moiety renders the side chains intrinsically biodegradable (**Figure 1**). Consequently, this ester linkage will strongly influence the degradability of the **NHS-POx** coating.

In general, excretion of polymeric materials mainly occurs via the kidneys[12] or via the mononuclear phagocytic system (MPS)[13], where the excretion rate is determined by many factors including the hydrodynamic volume (molecular weight)[14], surface charge[15], polymer dispersity[16] and architecture[17, 18]. An important measure for the excretability of polymeric materials is the renal clearance threshold, which is the hydrodynamic volume below which particles are excreted via the kidneys[19]. Particles above this critical threshold will display a prolonged residence time or accumulation in the body[12]. For instance, this threshold was reported around 30 kDa for poly(ethylene glycol) (PEG), which is a common polymeric material for e.g. drug delivery purposes[16,20]. However, considering the fact that the renal excretion rate is

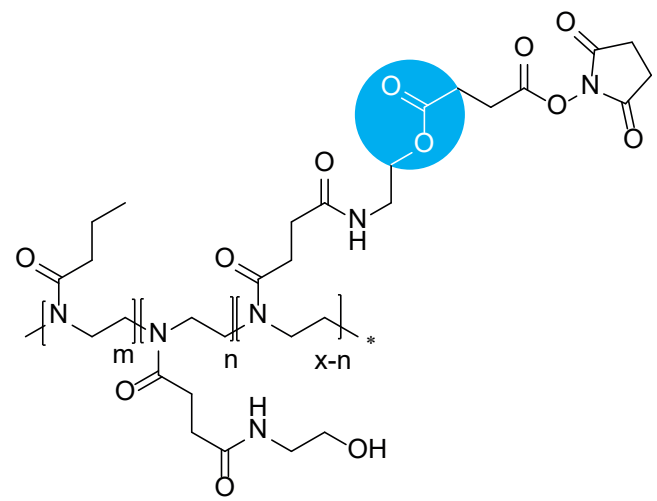

Figure 1 Composition of **NHS-POx** used for the design of **NHS-POx** coated gelatin sponges for hemostatic purposes (see **Chapter 4** for more details). The hydrolytically cleavable ester bond is highlighted in blue.

dependent on many more parameters than size alone, it is hard to predict *a priori* whether a polymer will be excreted or not.

Poly(2-oxazoline)s or POx[21-23] are particularly attractive for biomedical aplications due to their versatile functionalization possibilities. However, only a few studies have been reported in literature on the biodistribution and excretion of this class of polymers[24-28]. In a recent study, Wyffels and coworkers reported the synthesis of well-defined homo-polymers based on 2-ethyl-2-oxazoline (EtOx) (M_n 5-110 kDa, *Đ 1.01-1.11*) containing a deferoxamine ligand, and studied the biodistribution in a mouse model after intravenous administration using micro-positron emission tomography/computed tomography (μPET/CT) by chelating a ^{89}Zr-radiolabel[25]. It was observed that polymers below a threshold of 20 kDa were excreted from the body (mainly via renal clearance), while larger polymers (M_n>40 kDa) showed prolonged blood circulation in this mouse model. These results indicated that the hydrodynamic volume of these polymers determined the excretability of these polymers. More recently the same authors reported a comparative biodistribution study in a mouse model using EtOx homo-polymers equipped with a ^{18}F or a ^{89}Zr radiolabel (M_n of 5 kDa for both polymers, *Đ* of 1.01 (^{89}Zr) or 1.08 (^{18}F)). It was observed that the excretability of the polymer was influenced by the type of ligand and/or radiolabel[26], which stresses the importance of proper selection of the labeling strategy. Despite these systematic studies, to date, the majority of the excretion studies on POx are mainly based on 2-methyl-2-oxazoline (MeOx) or EtOx-containing polymers, while other types of POx polymers remain largely unexplored.

In this chapter, we have studied the processes of **NHS-POx** degradation and excretion. To this end, we first performed an *in vitro* degradation study by incubating the polymer **NHS-POx** in phosphate buffered saline (PBS) and human derived blood plasma to identify the degradation products using ^{1}H-NMR spectroscopy. Next, the main degradation product was synthesized containing an S-2-(4-isothiocyanatobenzyl)-diethylenetriamine penta-acetic acid (or DTPA) ligand. Finally, the polymer was labeled with radioactive ^{111}Indium and the excretability of the radiolabeled polymer (using SPECT/CT and an automated γ counter) was studied in time after intravenous injection in Wistar rats to investigate i) the excretion pathway of the synthesized polymer and ii) potential accumulation of the polymer in specific organs.

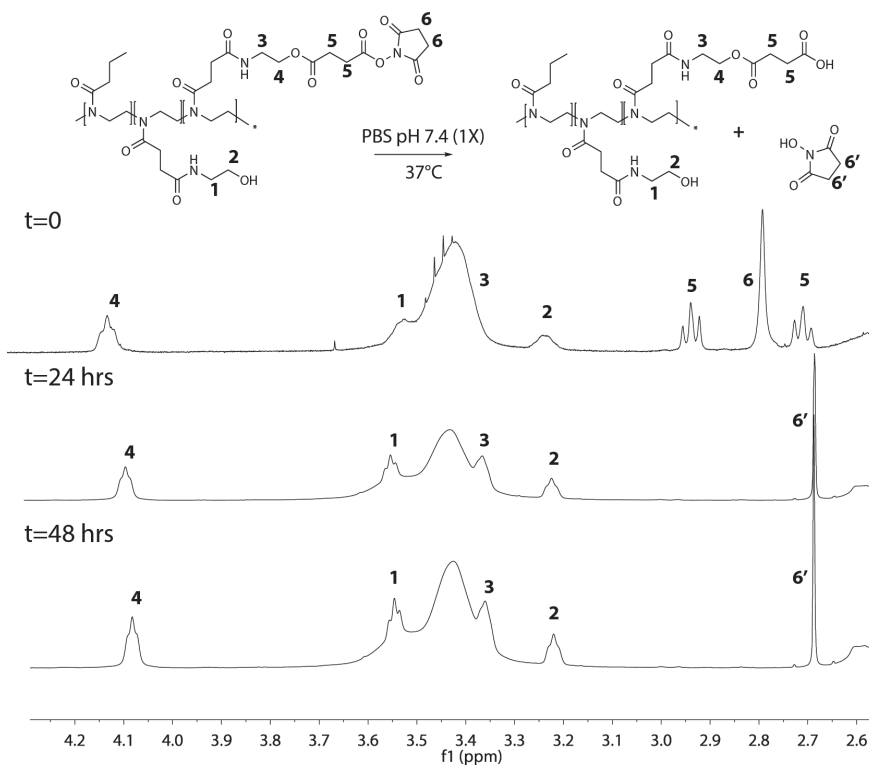

Figure 2 ^{1}H-NMR signals of **NHS-POx** by incubation in PBS at 37°C for 0, 24 and 48 hrs.

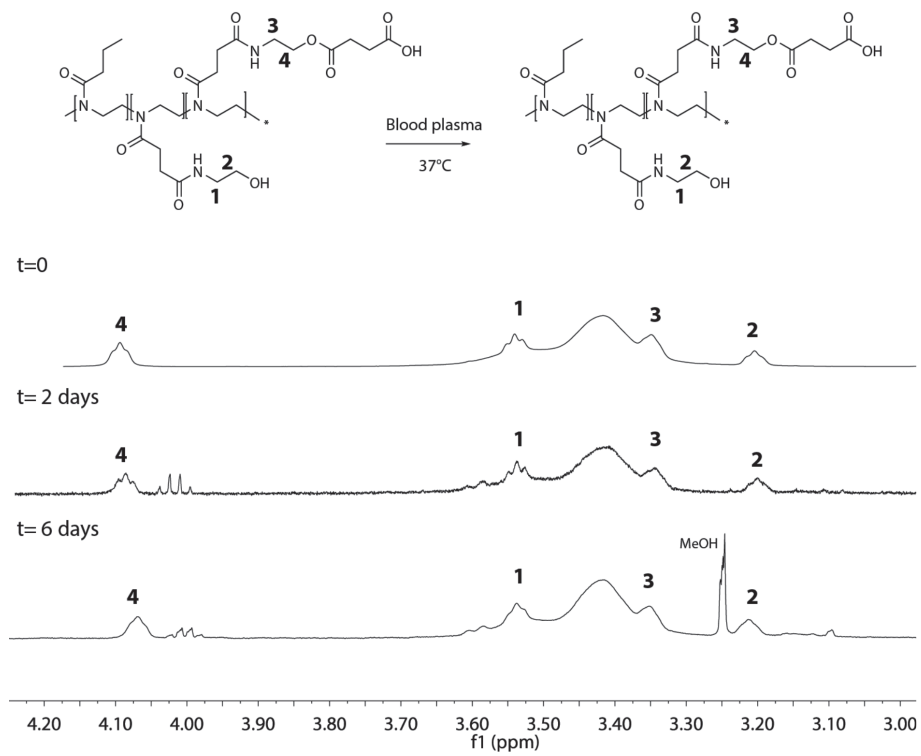

Figure 3 ^{1}H-NMR signals of hydrolyzed **NHS-POx** by incubation in whole blood plasma at 37°C during various time points (t=0, 2 days, 6 days)

2. Results

2.1 *In vitro* degradation of NHS-POx

We performed several degradation studies by incubation of **NHS-POx** in phosphate buffered saline (PBS) and human derived blood plasma in order to study the chemical nature of the degradation products and the stability of the side chains *in vitro* using ^{1}H-NMR spectroscopy as analytical method.

2.1.1 Incubation in PBS

In the first incubation study, we dissolved **NHS-POx** (M_n 18.8 kDa (SEC), sidechains: 69 mol% *n*PropOx 14 mol% OH, 17 mol% NHS (^{1}H-NMR)) (synthesized in **Chapter 2**) in PBS (1x, pH 7.4) at a polymer concentration of 15 mg/mL and incubated the polymer at 37 °C for time periods of 24 and 48 hrs. ^{1}H-NMR spectra of the polymers at these time points are shown in **Figure 2**. After 24 hours of incubation in PBS, the NHS-ester was fully hydrolyzed, as indicated by the shift of polymer-bound NHS (2.8

ppm, **6**) to free N-hydroxysuccinimide (2.7 ppm, **6'**). No further degradation of the polymer was observed, since no change in other integrals was seen, which indicates that the ester linker in the side chain is stable upon incubation in PBS.

2.1.2 Incubation in blood plasma

To further assess the stability of the ester bond, POx-COOH, obtained via hydrolysis of the succinimide esters of **NHS-POx**, was incubated in human-derived blood plasma (polymer concentration 15 mg/mL) for two and six days. The results of this study are shown in **Figure 3**. Also in this experiment, we observed that the ester moiety in the side chain did not degrade over a period of six days, demonstrating the stability of the ester bond.

Both *in vitro* degradation experiments indicate that the ester bond in the side chain is stable, whereas the NHS ester is hydrolyzed to carboxylic acid-functionalized POx (**POx-COOH**) under physiological conditions. Although further degradation *in vivo* (e.g. by proteolytic enzymes) cannot be excluded, POx-COOH was selected for further *in vivo* excretion studies.

2.2 Synthesis of carboxylic acid-functionalized POx

Carboxylic acid functional POx was synthesized according to procedures described in **Chapter 2** (P(*n*PropOx-c-OH-c-COOH) 70-15-15). In order to be able to study the polymer *in vivo* by means of SPECT/CT imaging, we functionalized the end group of the polymer using a DTPA ligand. This ligand is capable of chelating radioactive ions which can be used to trace the polymer after injection. We used end-group functionalization since it allowed us to introduce only a single ligand per polymer chain. Moreover, by choosing end group functionalization we circumvented the potential risk of degradation of the ligand in case of degradation of the side chains *in vivo*. For the introduction of the ligand, we used a literature procedure by Gaertner and coworkers[27]. The synthetic route towards these polymers is shown in **Scheme 1**.

First, we synthesized the P(*n*PropOx-c-MestOx) copolymer, where we terminated the reaction with *N*-1-(*tert*-butoxycarbonyl)-(Boc)-piperazine yielding POx which was end-capped with a Boc-protected amine moiety (**P1**). It was determined by ^{1}H-NMR spectroscopy that 46% of the polymer chains was terminated with the *N*-Boc-piperazine. Hereafter, we deprotected this Boc group using a mixture of TFA in DCM (v/v, 1:3). This deprotection proved quantitative as was determined by ^{1}H-NMR, since the characteristic signal of the Boc group (1.3 ppm) disappeared completely (**P2**). Subsequently, the DTPA ligand was introduced by amine-isothiocyanate coupling using triethylamine (Et_3N) as a base to facilitate an efficient reaction. Although the quantification of the end-groups was difficult using ^{1}H-NMR spectroscopy, a clear aromatic signal attributed to the DTPA-ligand was observed which was indicative of

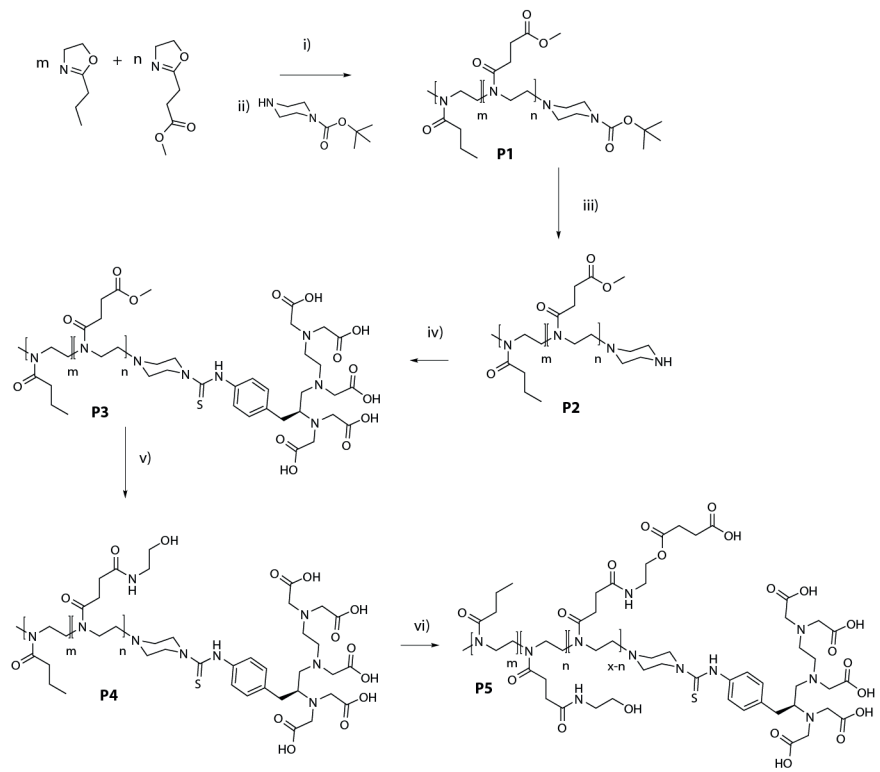

Scheme 1 Synthesis route towards P(*n*PropOx-c-OH-c-COOH)-N-pip-DTPA (**P5**). Reactions conditions: i) methyl tosylate, MeCN, 140°C, µW, 30 min, ii) *N*-Boc-piperazine, rt, 3 days, iii) TFA/DCM (v/v, 1:3), rt, 30 min, iv) *p*-SCN-*Bn*-DTPA, Et_3N, DMF, rt, overnight, v) 2-amino-ethanol, 60°C, 300 mbar, overnight, vi) succinic anhydride, DMAP, DMF, rt, overnight

the presence of the DTPA group on the polymer (**P3**). Subsequently, the methyl ester groups at the side chains were modified quantitatively by amidation using 2-amino-ethanol, yielding the hydroxyl side chain functionalized POx (**P4**). In a final step, the carboxylic acid groups were introduced using a sub-stoichiometric amount of succinic anhydride (compared to the hydroxyl groups) and dimethylaminopyridine (DMAP) as a catalyst (**P5**). The analytical data of the synthesized polymers **P1**-**P5** are listed in **Table 1**. The polymers were synthesized with good control over the ratio of functional groups (^{1}H-NMR) and dispersity values (SEC). Unfortunately, no SEC signal could be obtained for **P5**, but based on the results of the other polymers (**P1**-**P4**) no change in dispersity is expected throughout the postmodification functionalization steps. Moreover, the ^{1}H-NMR spectrum of **P5** (**Figure 4**) demonstrated that **P5** is functionalized with both a desired ratio of functional side chains and a DTPA ligand for radiolabeling, which allows the polymer to be used in biodistribution experiments.

Table 1 Analytical data of synthesized polymers **P1**-**P5**

#	Name	Yield		^{1}H-NMR			M_n [a]		
		g	%	% MestOx	%OH	%COOH	Theor.	SEC	*Đ*
P1	P(*n*PropOx-c-MestOx)-N-pip-NBoc	8.1	75	31	-	-	12.8	12.2	1.19
P2	P(*n*PropOx-c-MestOx)-N-pip-NH	1.8	q.	31	-	-	12.7	12.1	1.18
P3	P(*n*PropOx-c-MestOx)-N-pip-N-DTPA	335 mg	61	31	-	-	13.4	14.4	1.13
P4	P(*n*PropOx-c-OH)-N-pip-N-DTPA	53 mg	49	-	31	-	14.1	21.4	1.11
P5	P(*n*PropOx-c-COOH-c-OH)-N-pip-N-DTPA	9 mg	23	-	14	17	16.3	[b]	[b]

[a] SEC was calibrated against PMMA standards, eluent: 0.1 % LiCl in DMA.
[b] No signal could be obtained

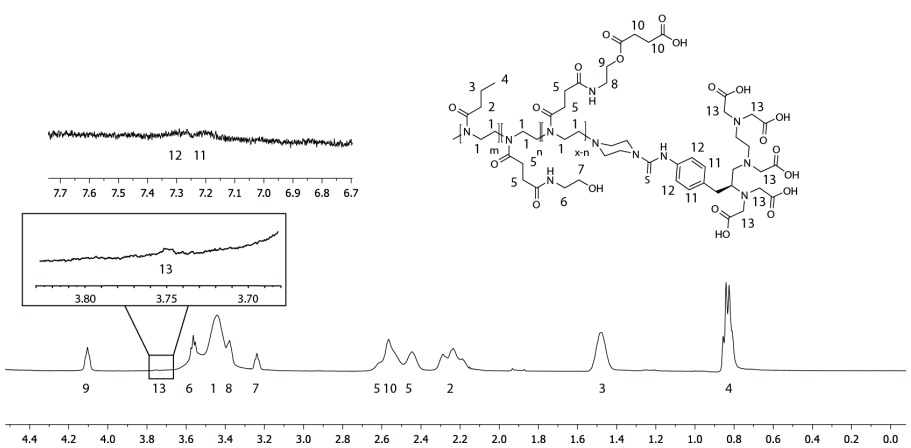

Figure 4 ^{1}H-NMR signals of P(*n*PropOx-c-OH-c-COOH)-N-pip-DTPA (**P5**)

2.3 Radiolabeling

In order to obtain sufficient signal intensity using SPECT/CT scanning it is crucial to select the proper radioisotope in terms of half-life. In this work, we selected Indium-111 (^{111}In) in view of its half-life of 2.8 days[29] and widespread usage in the radiolabeling of macromolecules[27, 30].

As a result, radiolabeling of **P5** with ^{111}In was performed by incubation of the polymer with $^{111}InCl_3$. After purification using a PD10 column, the radiolabeled polymers were obtained at a radiochemical purity of >95% and a radioactivity of 27-53 MBq, which proved sufficient to perform the *in vivo* experiments.

Directly after radiolabeling, the labeled polymers were injected via intravenous injection in the tail of Wistar rats. The rats were monitored and imaged by SPECT/CT at relevant time points (1 hrs, 6 hrs, 24 hrs and 7 days). After the measurements, the SPECT/CT images were quantified by comparison with a series of injected standards.

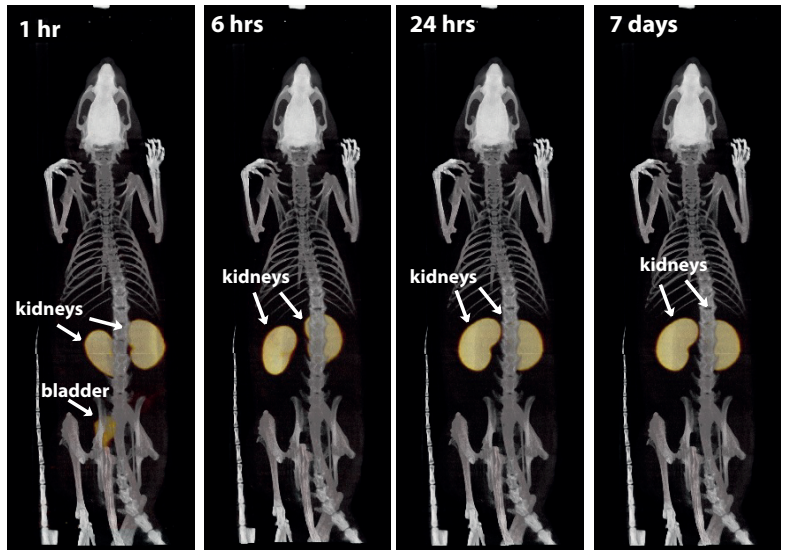

Figure 5 SPECT/CT images of Wistar rats at various time points after intravenous injection of radiolabeled **P5**

Table 3 Quantification of the radioactivity at different time points (%ID/g)

	1 hrs		6 hrs		24 hrs		7 days	
	mean	sd	mean	sd	mean	sd	mean	sd
Kidney[a)]	12.5	2.1	11.2	1.9	8.9	1.3	3.1	1.1

a) measured values are expressed in value per kidney (n=6)

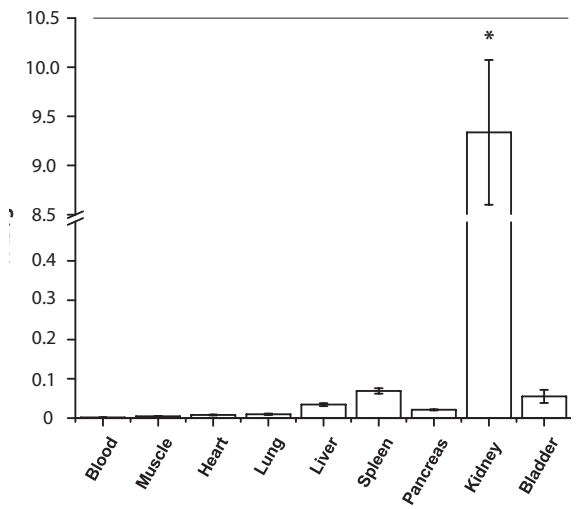

Figure 6 Biodistribution study of the dissected organs using an automated γ-counter after 7 days. Experiments were performed (n=3), except for measurements on kidneys (n=6). Statistics: * P<0.001

In addition, after the last SPECT/CT measurement, the rats were euthanized and the organs of the rat were dissected followed by measurement of their radioactivity using an automated γ counter. The results of these experiments are displayed in **Figure 5+6** and **Table 3**.

It was observed that the majority of the radiolabeled polymer (%ID/g) was cleared within an hour, as the radiolabeled polymer was only present in kidneys (%ID/g 12.5 ± 2.1) and bladder (not quantified) based on SPECT/CT imaging (**Figure 5** and **Table 3**). The clearance from the kidneys appeared to occur slowly overtime, as indicated from the measured doses at 6 hrs (%ID/g 12.5 ± 2.1) and 24 hrs (%ID/g 8.9 ± 1.3). Ultimately, after 7 days 3.1 ± 1.1 %ID/g was found in the kidneys. No accumulation of radiolabeled polymer was found in other organs than kidneys over the time course of the experiment. The measurements on the dissected organs using the γ-counter confirmed this observation (**Figure 6**). However, in comparison with the SPECT/CT measurements, a higher percentage of radiolabeled polymer was found in kidneys (%ID/g 9.5 ± 0.6).

3. Comparison with related excretion studies

Both the SPECT/CT and the γ-counter measurements confirmed that the majority of the ~80-90 %ID/g of labeled polymers was renally excreted from the rats after 7 days, without notable accumulation of the polymer in other organs. The renal excretion of the polymers is not complete after 7 days post injection (p.i.), since a low amount of the radiolabeled polymer (%ID/g: 3.1 ± 1.1 as determined using SPECT/CT and 9.5 ± 0.6 as measured using γ counting) was still detected in kidneys. Although, the exact reason for this presence in this case is yet unknown, certain aspects of this retention can be explained from related excretion studies. The slow clearance of the final traces of radiolabeled POx as observed herein was also observed in the work of Moreadith et al. which showed -despite a steady decline in the signal- presence of radiolabeled polymers in bile, liver and spleen of a rat model after 14 days[24] (p.i.). Since in our case a steady decline is observed as well, it would be interesting to repeat the experiments using time points exceeding 7 days to see whether these extended time points are sufficient for effective excretion from the kidneys.

Another explanation for the presence of radiolabeled polymers in the kidneys, is that the type of radiolabel/labeling strategy which is used in the experiment causes undesired retention of the polymer. This observation was previously reported by Glassner and coworkers[26] and was also reported for radiolabeled peptides by Vegt and coworkers[31]. In addition, Gaertner and co-workers used the same radiolabel as employed in the current study (^{111}Indium) to investigate the clearance of low

molecular weight P(EtOx) (M_n 4.5 kDa, *Đ 1.15)*, which was well below the glomular filtration cut off for P(EtOx) (40 kDa)[27]. Nevertheless, they observed the presence of labeled polymer in the kidneys 24 hrs p.i., which suggests that this retention was related to the type of radiolabel which was used. It would therefore be interesting to repeat our study using a different radiolabel.

Another factor which can inhibit successful excretion is the hydrodynamic volume. Although the hydrodynamic volume of polymer **P5** is below the globular filtration threshold of P(EtOx) (40 kDa), it cannot be excluded that the higher molecular weight fraction of the polymer causes the retention or slower excretion from the kidneys. A final parameter that should be taken into account is the polarity of the polymer, as it is known that surface charge and polarity strongly influence polymer excretion[15]. So far there is no relevant literature available on excretion of related POx polymers containing both hydrophobic *n*PropOx-residues and polar residues such as hydroxyl groups and carboxylic acid groups. In conclusion, although several factors have been reported to influence retention of polymers in kidneys, why the retention of polymers was observed in our case remains to be elucidated through more systematic studies.

Regarding clinical translation, it should be emphasized that the injected dose (1.2 mg polymer/kg body weight based on a rat of 250 g) is likely to be high compared to future clinical scenarios. A healthy male (70 kg) receiving one hemostatic **NHS-POx** coated sponge (containing ~40 mg **NHS-POx**) is administrated half of the polymer dose (0.6 mg/kg), as used in the current experiment. As a result, this experiment represents a polymer dose corresponding to the administration of two **NHS-POx** coated sponges. Additionally, it must also be noted that the release profile of the polymer into the blood stream will be more complex than the single dose injection as performed in the current work. Despite the apparent stability of the side chains which was demonstrated in the hydrolysis experiments *in vitro*, degradation *in vivo* cannot be excluded, since bio-degradation and bio-erosion are complex phenomena[32, 33] which strongly determine the release profile of the polymer into the blood stream upon clinical application.

Nevertheless, it can be concluded that the majority of the injected dose of radiolabeled polymer (80-90 %ID/g) can be excreted within a day without showing accumulation in organs other than kidneys. The excretion of this polymer proceeded mainly via the renal pathway. Whether the presence of the labeled polymer after 7 days is caused by retention or slow excretion remains to be eludicated.

4. Conclusions

In this chapter, we have investigated the degradability and excretability of **NHS-POx** in order to gain deeper insight into the fate of the polymer after the therapeutic action has been achieved. We performed an *in vitro* degradation study by testing the stability of the polymer in PBS (2 days) and blood plasma (up to 6 days), and characterized the degradation products by ^{1}H-NMR spectroscopy. It was found that the hydrolytically sensitive ester group of **NHS-POx** was predominantly stable in these experiments, whereas the NHS ester was effectively hydrolyzed as expected. For the *in vivo* excretion studies, the carboxylic acid functional polymer was therefore chosen as the main degradation product. This polymer was successfully synthesized containing a DTPA ligand at the polymer chain end and subsequently radiolabeled with ^{111}Indium. The polymer was injected in Wistar rats via a tail injection and the excretion was followed by SPECT/CT for 1 hr, 6 hrs, 24 hrs and 7 days. After 7 days, the organs of the rats were dissected and measured for radioactivity using an automated γ-counter. Using these experiments, it was found that the majority of the injected radiolabeled polymer (~80-90% %ID/g) was excreted via renal excretion, however a minority of polymer was still present in kidneys after 7 days (%ID/g: 3.1 ± 1.1 (SPECT/CT) and 9.5 ± 0.6 (γ-counter). No accumulation of radiolabeled polymer in other organs was observed. More systematic research is needed in order to explain the kidney retention of the radiolabeled polymer in this experiment.

5. Acknowledgements

Edwin Roozen, Roger Lomme (both Department of Surgery, Radboudumc) and Gerben Franssen (Department of Nuclear Medicine, Radboudumc) are all kindly acknowledged for their contributions to the work described in this chapter.

6. Experimental section

6.1 Materials

All reagents for the synthesis of the polymer were distilled twice before use in the polymerization reactions. Acetonitrile (obtained from Actu-all Chemicals) was dried and dispensed under nitrogen atmosphere by using an MBraun MB SPS-800 solvent dispersing system. Unless otherwise stated, all other chemicals were obtained from Sigma-Aldrich and used as received. *p*-SCN-Bn-DTPA was obtained from Macrocyclics (USA). $^{111}InCl_3$ was obtained from Mallinckrodt Medical (Petten, The Netherlands). Human blood plasma was obtained by centrifugation of freshly obtained human whole blood from Sanquin (Nijmegen, The Netherlands)

6.2 Instrumentation

^{1}H-NMR and ^{13}C-NMR spectra were recorded on a Bruker Avance III 500MHz spectrometer using the solvent D_2O. Microwave-assisted polymerizations were performed in a Biotage Initiator+, equipped with an autosampler. Size exclusion chromatography (SEC) was performed on an Agilent 1260 - series HPLC system equipped with a 1260 online degasser, a 1260 ISO-pump, a 1260 automatic liquid sampler, a thermostatted column compartment, a 1260 diode array detector (DAD) and a 1260 refractive index detector (RID). Analyses were performed on two Mixed-D and a guard column in series at 50 °C. As an eluent, *N,N*-dimethylacetamide (DMA), containing LiCl (concentration 50 mM), was used at a flow rate of 0.593 ml min^{-1}. The SEC traces were analyzed using the Agilent Chemstation software with the GPC add on. Number average molecular weights (M_n), weight average molecular weights (M_w), and dispersity (Đ) values were calculated against poly(methyl methacrylate) (PMMA) standards. SPECT/CT was acquired on a small animal SPECT/CT scanner (U-SPECT-II, MIlabs, Utrecht, Netherlands) with a 1.0 mm multipurpose rat collimator, using 108 bed positions and an acquisition time of maximal 120 minutes. CT was acquired after SPECT acquisition for anatomical reference (65 kV, 615 μA, 3 bed positions, spatial resolution 160 μm). Scans were reconstructed with MILabs reconstruction software (which uses an ordered-subset expectation maximization algorithm), a voxel size of 0.75mm, 16 subsets, and 1 iteration. Radioactivity was measured in a shielded well-type γ-counter (Perkin–Elmer).

6.3 *In vitro* degradation experiments

In Eppendorf tubes, polymers were dissolved in aqueous media (PBS or human derived whole blood plasma) to provide a polymer concentration of 15 mg/mL. The tubes were continuously shaken at 37°C for defined times (1, 2 or 6 days). Subsequently, the Eppendorf tubes were lyophilized yielding the polymer as white powders. These powders were dissolved in methanol (1 mL) and filtered over Sephadex (G-25, Sigma Aldrich) to remove residual impurities. The organic solvent was removed under an argon flow. The powders were dissolved in D_2O (10 mg/mL) and the polymers were characterized by ^{1}H-NMR spectroscopy (500 MHz, 64 scans).

6.4 Synthetic procedures for P1-P5

P1 - P(*n*PropOx-c-MestOx)-N-piperazine-NBoc - Methyl tosylate (0.13 mL, 0.87 mmol, 1 eq.), *n*PropOx (6.76 mL, 67.0 mmol, 77 eq.), MestOx (3.60 mL, 28.7 mmol, 33 eq.) and acetonitrile (7.60 mL) were mixed in a dry microwave vial under inert

atmosphere (Ar). The reaction mixture was heated for 30 minutes at 140°C under microwave irradiation after which a solution of N-Boc-piperazine in MeCN (480 mg, 4.35 mmol, 3 eq.) was added to the reaction mixture, which was stirred for three days at room temperature. The polymer was dissolved in DCM (25 mL) and precipitated in diethylether (DCM/Et_2O, v/v, 1:20) (500 mL). This procedure was performed twice. The resulting suspension was filtered and the residue dissolved in DCM (100 mL). The solvent was evaporated under reduced pressure, yielding the final polymer as a white foam (8.1 g, 75% crude yield). ^{1}H-NMR confirmed that product was formed but that traces of unbound N-Boc-piperazine were present. Hereafter, the polymer was purified in smaller batches of 1 g. As an example, 997 mg of the crude material was dissolved in water, heated to 60°C, which caused precipitation of the polymer, and centrifugated (4000 rpm, 15 min., 40°C). The water layer was decanted and the resulting pellet was dissolved in MQ-water and lyophilized. **P1** was obtained as a white powder (0.7 g, 72 % yield)

^{1}H NMR (500 MHz, D_2O) δ 3.66 (b, n·3H, CO-O-C$\underline{H}_3$), 3.48 (b, (m+n)·4H, NC$\underline{H}_2$C$\underline{H}_2$N), 3.03 (b, 3H, C$\underline{H}_3$-NCHCH-), 2.70-2.60 (b, n·4H, COC$\underline{H}_2$C$\underline{H}_2$CO), 2.35-2.20 (b, m·2H, CO-C$\underline{H}_2$-CH_2-CH_3), 1.70-1.60 (b, m·2H, CO-CH_2-C$\underline{H}_2$-CH_3), 1.46 (s, 9H, NCOOC(C$\underline{H}_3$)$_3$), 0.91-1.02 (b, m·3H, CO-CH_2-CH_2-C$\underline{H}_3$) **SEC** (PMMA) M_n 12.2 kg/mol, Đ 1.19. Experimentally determined monomer ratio (m/n): 69/31.

P2 - P(*n*PropOx-c-MestOx)-N-piperazine-NH - P1 (1.8 g, 0.14 mmol, 1 eq) was dissolved in TFA/DCM (v/v, 1:3, 229 eq.) (10 mL) and stirred for 60 min, whereafter the reaction mixture was concentrated under reduced pressure. The polymer was dissolved in DCM (10 mL) and precipitated in Et_2O (250 mL). The precipitate was dissolved in MQ-water and lyophilized. **P2** was obtained as a white powder (1.8 g, quant. yield)

^{1}H NMR (500 MHz, D_2O) δ 3.66 (b, n·3H, CO-O-C$\underline{H}_3$), 3.48 (b, (m+n)·4H, NC$\underline{H}_2$C$\underline{H}_2$N), 3.03 (b, 3H, C$\underline{H}_3$-NCHCH-), 2.70-2.60 (b, n·4H, COC$\underline{H}_2$C$\underline{H}_2$CO), 2.35-2.20 (b, m·2H, CO-C$\underline{H}_2$-CH_2-CH_3), 1.70-1.60 (b, m·2H, CO-CH_2-C$\underline{H}_2$-CH_3), 0.91-1.02 (b, m·3H, CO-CH_2-CH_2-C$\underline{H}_3$) **SEC** (PMMA) M_n 12.2 kg/mol, Đ 1.18. Experimentally determined monomer ratio (m/n): 69/31

P3 - P(*n*PropOx-c-MestOx)-N-piperazine-NH-DTPA - P2 (522 mg, 41 µmol, 1 eq.), *p*-SCN-Bn-DTPA (34.6 mg, 58 µmol, 1.4 eq.) and Et_3N (50 µL, 36.5 mg, 361 µmol, 8.8 eq.) were dissolved in DMF (2 mL) and stirred overnight, whereafter the reaction mixture was concentrated under reduced pressure. The polymer was dissolved in DCM (5 mL) and precipitated in Et_2O (100 mL). The precipitate was dissolved in cold MQ-water (5 mL, 5°C), heated to 40°C, which caused precipitation of the polymer. The resulting suspension was centrifugated (4000 rpm, 15 min., 40°C), the supernatant was decanted, the pellet was dissolved in MQ-water (5 mL) and subsequently lyophilized. **P3** was obtained as a white powder (335 mg, 61% yield).

^{1}H NMR (500 MHz, D_2O) δ 7.30 (d, *J*= 10 Hz, 2H, -SCNH-C$\underline{H}$-CH-), δ 7.18 (d, *J*= 5 Hz, 2H, -SCNH-CH-C$\underline{H}$-), δ 3.77 (s, 10H, N-C$\underline{H}_2$-COOH), δ 3.66 (b, m·3H, CO-O-C$\underline{H}_3$), δ 3.48 (b, (m+n)·4H, NC$\underline{H}_2$C$\underline{H}_2$N), 3.01 (b, 7H, N-C$\underline{H}_2$C$\underline{H}_2$-N), 2.70-2.60 (b, m·4H, COC$\underline{H}_2$C$\underline{H}_2$CO), 2.35-2.20 (b, n·2H, CO-C$\underline{H}_2$-CH_2-CH_3), 1.70-1.60 (b, n·2H, CO-CH_2-C$\underline{H}_2$-CH_3), 0.91-1.02 (b, n·3H, CO-CH_2-CH_2-C$\underline{H}_3$) **SEC** (PMMA) M_n 14.4kg/mol, Đ 1.13. Experimentally determined monomer ratio (m/n): 69/31

P4 - P(*n*PropOx-c-OH)-N-piperazine-NH-DTPA - P3 (102 mg, 8 µmol polymer, 236 µmol functional groups, 1 eq.) was dissolved in 2-amino-ethanol (2 mL, 2.0 g, 33 mmol, 142 eq.) and the reaction mixture was allowed to reflux overnight at 60°C under reduced pressure (300 mbar). After this, 2-amino-ethanol was removed under reduced pressure and the polymer was dissolved in methanol (5 mL) and precipitated into Et_2O/acetone (v/v, 4:1, 100 mL). This procedure was repeated three times. Subsequently, the precipitate was dissolved in MQ water (5 mL) and lyophilized. **P4** was obtained as a white powder (53 mg, 49% yield).

^{1}H NMR (500 MHz, D_2O) δ 7.23 (b, 2H, -SCNH-C$\underline{H}$-CH-), 7.16 (b, 2H, -SCNH-CH-C$\underline{H}$-), 3.66 (s, 10H, N-C$\underline{H}_2$-COOH), 3.57 (b, n·2H, CONH-C$\underline{H}_2$-CH_2-OH), 3.48 (b, (m+n)·4H, NC$\underline{H}_2$C$\underline{H}_2$N), 3.24 (b, n·2H, CONH-CH_2-C$\underline{H}_2$-OH, 3.01 (b, 7H, N-C$\underline{H}_2$C$\underline{H}_2$-N), 2.70-2.60 (b, n·4H, COC$\underline{H}_2$C$\underline{H}_2$CO), 2.35-2.20 (b, m·2H, CO-C$\underline{H}_2$-CH_2-CH_3), 1.70-1.60 (b, m·2H, CO-CH_2-C$\underline{H}_2$-CH_3), 0.91-1.02 (b, m·3H, CO-CH_2-CH_2-C$\underline{H}_3$) **SEC** (PMMA) M_n 21.4 kg/mol, Đ 1.11. Experimentally determined monomer ratio (m/n): 69/31

P5 - P(*n*PropOx-c-OH-c-COOH)-N-piperazine-NH-DTPA - P4 (33 mg, 2.3 µmol polymer, 71 µmol functional groups, 1 eq.), DMAP (4.6 mg, 38 µmol, 0.5 eq.) and succinic anhydride (4.6 mg, 46 µmol, 0.6 eq.) were dissolved in DMF (1 mL) and the reaction mixture was allowed to stir overnight. After this, DMF was removed under reduced pressure and the polymer was dissolved in methanol (5 mL) and precipitated into Et_2O (100 mL). Subsequently, the polymer was dissolved in methanol (5 mL) and filtered over SCX-2 (20 mg SCX-2, 3.4 eq. towards DMAP) and flushed with methanol (4 x 1 mL). Afterwards, the fractions were combined and concentrated under reduced pressure. Subsequently, the polymer was dissolved in MQ water (5 mL) and lyophilized. **P5** was obtained as a white powder (9 mg, 23% yield).

^{1}H NMR (500 MHz, D_2O) δ 7.29 (b, 2H, -SCNH-C$\underline{H}$-CH-), 7.21 (b, 2H, -SCNH-CH-C$\underline{H}$-), 4.10 (b, x·2H, CONH-CH_2-C$\underline{H}_2$-OCO), 3.76 (b, 10H, N-C$\underline{H}_2$-COOH), 3.56 (b, n·2H, CONH-C$\underline{H}_2$-CH_2-OH), 3.48 (b, (m+n+x)·4H, NC$\underline{H}_2$C$\underline{H}_2$N), 3.38 (b, x·2H, CONH-C$\underline{H}_2$-CH_2-OCO), 3.24 (b, n·2H, CONH-CH_2-C$\underline{H}_2$-OH), 2.92 (b, 7H, N-C$\underline{H}_2$C$\underline{H}_2$-N), 2.70-2.40 (b, (n+x)·4H, COC$\underline{H}_2$C$\underline{H}_2$CO), 2.56 (b, x·4H, COC$\underline{H}_2$C$\underline{H}_2$COOH), 2.35-2.20 (b, m·2H, CO-C$\underline{H}_2$-CH_2-CH_3), 1.70-1.60 (b, m·2H, CO-CH_2-C$\underline{H}_2$-CH_3), 0.91-1.02 (b, m·3H, CO-CH_2-CH_2-C$\underline{H}_3$) **SEC** (PMMA) No signal could be obtained. Experimentally determined monomer ratio (m/n/x): 69/14/17

6.5 Labeling with ^{111}In and purification

The polymer (**P5**) was dissolved in 0.5 M MES (2-(N-morpholino)ethanesulphonic acid) buffer, pH 5.5 (5mg/mL), whereafter 0.5 M MES-buffer (125 µL) and a solution of ^{111}InCl (in 0.05 M HCl) (118 MBq) (125 µL) were added. The solution was incubated for 30 min at room temperature whereafter the radiochemical efficiency was determined by instant thin layer chromatography on ITLC-SG strips (Agilent Technologies) with 0.1 M citrate (pH 6.0) as a mobile phase, resulting in a labeling efficiency of 49%. The labeled product was purified by gel filtration chromatography on a PD-10 column (GE Healthcare) using PBS/BSA as a mobile phase to provide a labeled polymer sample of 32.5 MBq with radiochemical purity of 99% (ITLC, 0.1 M citrate buffer, R_f value: 0.1).

6.6 Biodistribution study using SPECT/CT

For this experiment, Wistar rats (n=4, 230-280 g, Harlan, Horst, The Netherlands) were used. The animals were allowed to acclimatize for at least five days prior to the experiment. They were housed in individually ventilated cages. Permission for this experiment was granted by de Centrale Commissie Dierproeven (CCD) (projectnumber 2015-0012). The labeled polymers (300 µL, 27-52 MBq, 273 µg polymer) were injected intravenously in the tail of Wistar rats. The animals were imaged by SPECT/CT after 1 hr (20 min), 6 hrs (40 min) and 24 hrs (60 min). During imaging the rats were anesthetized using isoflurane in a 1:1 mixture of oxygen and pressurized air (5% induction, 2.5-3.5% maintenance. After 7 days, the rats were euthanized (using CO_2) and afterwards imaged using SPECT/CT (120 min). The images were quantified via a series of calibration standards and expressed as injected dose per gram tissue ± standard deviation (%ID/g ± SD) per organ. The experiments were performed in triplo (n=3).

6.7 Biodistribution using an automated γ-counter

Biodistribution studies were performed on the euthanized rats. From these rats, the organs of interest (heart, lung, blood, kidney (left/right), spleen, liver, bladder, pancreas, muscle) were dissected, weighed and analyzed using a γ-counter along with a standard containing the injected activity to allow calculation of the injected dose per gram tissue ± standard deviation (%ID/g ± SD). The experiments were performed in triplo (n=3), except for the kidneys (n=6).

6.8 Statistics

Statistical analyses were conducted using GraphPad Instat software. All results were reported as mean ± standard deviation. Differences among groups were analyzed by ANOVA using a Tukey-Kramer Multi comparison test and p-values of 0.05 or lower were considered as significantly different.

7. References

1. E. A. Boonstra, I. Q. Molenaar, R. J. Porte and M. T. de Boer, *HPB*, 2009, **11**, 306-310.
2. P. J. M. Bouten, M. Zonjee, J. Bender, S. T. K. Yauw, H. van Goor, J. C. M. van Hest and R. Hoogenboom, *Prog. Polym. Sci.*, 2014, **39**, 1375-1405.
3. M. Mehdizadeh and J. Yang, *Macromol. Biosci.*, 2013, **13**, 271-288.
4. M. Funabashi, F. Ninomiya and M. Kunioka, *Int. J. Mol. Sci.*, 2009, **10**, 3635-3654.
5. L. S. Nair and C. T. Laurencin, *Prog. Polym. Sci.*, 2007, **32**, 762-798.
6. B. D. Ulery, L. S. Nair and C. T. Laurencin, *J. Polym. Sci. B Polym. Phys.*, 2011, **49**, 832-864.
7. T. Tyler and H. D. Rosenbaum, *Invest. Radiol.*, 1978, **13**, 71-73.
8. D. B. Reid and J. G. Pollock, *Ann. Vasc. Surg.*, 1991, **5**, 320-324.
9. K. Ulubayram, E. Aksu, S. I. D. Gurhan, K. Serbetci and N. Hasirci, *J. Biomater. Sci., Polym. Ed.*, 2002, **13**, 1203-1219.
10. K. Iwanaga, T. Yabuta, M. Kakemi, K. Morimoto, Y. Tabata and Y. Ikada, *J. Microencapsul.*, 2003, **20**, 767-776.
11. H. P. C. Van Kuringen, J. Lenoir, E. Adriaens, J. Bender, B. G. De Geest and R. Hoogenboom, *Macromol. Biosci.*, 2012, **12**, 1114-1123.
12. R. Duncan and J. Kopeček, in *Polymers in Medicine*, Springer Berlin Heidelberg, Berlin, Heidelberg, 1984, pp. 51-101.
13. D. E. Owens Iii and N. A. Peppas, *Int. J. Pharm.*, 2006, **307**, 93-102.
14. R. Duncan, *Nat. Rev. Drug Discov.*, 2003, **2**, 347-360.
15. S. M. A. Sadat, S. T. Jahan and A. Haddadi, *J. Biomater. Nanobiotechnol.*, 2016, **7**, 18.
16. K. Knop, R. Hoogenboom, D. Fischer and U. S. Schubert, *Angew. Chem. Int. Ed.*, 2010, **49**, 6288-6308.
17. M. E. Fox, F. C. Szoka and J. M. J. Fréchet, *Acc. Chem. Res.*, 2009, **42**, 1141-1151.
18. N. Nasongkla, B. Chen, N. Macaraeg, M. E. Fox, J. M. J. Fréchet and F. C. Szoka, *J. Am. Chem. Soc.*, 2009, **131**, 3842-3843.
19. W. M. Deen, M. J. Lazzara and B. D. Myers, *Am. J. Physiol. Renal Physiol.*, 2001, **281**, 579-596.
20. T. Yamaoka, Y. Tabata and Y. Ikada, *J. Pharm. Sci.*, 1994, **83**, 601-606.
21. R. Luxenhofer, Y. Han, A. Schulz, J. Tong, Z. He, A. V. Kabanov and R. Jordan, *Macromol. Rapid Commun.*, 2012, **33**, 1613-1631.
22. V. R. De La Rosa, *J. Mater. Sci. Mater. Med.*, 2014, **25**, 1211-1225.
23. N. Adams and U. S. Schubert, *Adv. Drug Deliv. Rev.*, 2007, **59**, 1504-1520.
24. R. W. Moreadith, T. X. Viegas, M. D. Bentley, J. M. Harris, Z. Fang, K. Yoon, B. Dizman, R. Weimer, B. P. Rae, X. Li, C. Rader, D. Standaert and W. Olanow, *Eur. Polym. J.*, 2016, **88**, 524-552
25. L. Wyffels, T. Verbrugghen, B. D. Monnery, M. Glassner, S. Stroobants, R. Hoogenboom and S. Staelens, *J. Control. Release*, 2016, **235**, 63-71.
26. M. Glassner, L. Palmieri, B. D. Monnery, T. Verbrugghen, S. Deleye, S. Stroobants, S. Staelens, L. Wyffels and R. Hoogenboom, *Biomacromolecules*, 2017, **18**, 96-102.
27. F. C. Gaertner, R. Luxenhofer, B. Blechert, R. Jordan and M. Essler, *J. Control. Release*, 2007, **119**, 291-300.
28. P. Goddard, L.E. Hutchinson, J.Brown, and L.J. Brookman, *J. Control. Release*, 1989, **10**, 5-16
29. J. L. Lawson and J. M. Cork, *Phys. Rev.*, 1937, **52**, 531-535.
30. S. E. Halpern, *Int. J. Rad. Appl. Instrum. B.*, 1986, **13**, 195-201.
31. E. Vegt, M. De Jong, J. F. Wetzels, R. Masereeuw, M. Melis, W. J. Oyen, M. Gotthardt and O. C. Boerman, *J. Nucl. Med.*, 2010, **51**, 1049-1058.
32. B. D. Rattier, A. S. Hoffman, F. J. Schoen and J. E. Lemons, *J. Clin. Eng.*, 1997, **22**, 26.
33. J. A. Cameron, C. L. Bunch and S. J. Huang, in *Biodeterioration 7*, eds. D. R. Houghton, R. N. Smith and H. O. W. Eggins, Springer Netherlands, Dordrecht, 1988, pp. 553-561.

Chapter 7:

Summary and future perspectives

1. Summary

Surgical procedures on soft tissues such as liver and kidneys often result in severe bleedings, as these organs are highly venous. As a result, invasive wound closing methods such as sutures and staples cannot be used to treat bleedings of these organs. In this thesis, we have focused on the development of a non-invasive hemostatic agent based on poly(2-oxazolines) (POx) equipped with N-hydroxy succinimide (NHS) esters. The mechanism of action of these NHS-ester functionalized polymers is based on the intrinsic capacity of the NHS-esters to react with primary amines which are ubiquitously present in blood (e.g. albumin) and other tissues (e.g. liver, kidney). This reactivity makes these polymers highly suitable as hemostatic agents by formation of an artificial blood clot or by acting as wound sealants by adhering to tissue. As has been discussed in **Chapter 1**, NHS-esters have been utilized in poly(ethylene glycol) (PEG)-based biomedical devices, but these materials have a limited capacity to seal profuse bleedings. In view of the versatile functionalization possibilities and the biocompatibility of this polymer class, we therefore selected POx as an alternative material candidate for the development of hemostatic patches.

In **Chapter 2**, various synthetic routes towards **NHS-POx** were discussed. Since direct incorporation of NHS-esters during polymerization is not possible for cationic ring opening polymerization (CROP), the most common way of synthesizing POx, we used CROP and post polymerization modification strategies to develop a scalable route towards NHS-ester functional polymers. We developed three different routes (**A**-**C**), which all relied on the introduction of methyl esters onto the polymers since this moiety allows for effective introduction of NHS-esters into polymers. In the first route (**A**), we made use of partial acidic hydrolysis of commercially available poly(2-ethyl-2-oxazoline) (Aquazol®), yielding polymers with a defined number of linear polyethyleneimine (l-PEI) units, which were further functionalized towards **NHS-POx** via introduction of methyl esters. In the second route (**B**), we used CROP using methyl ester functionalized monomer (MestOx) in combination with non-functionalized monomers 2-ethyl-2-oxazoline (EtOx) and 2-*n*-propyl-2-oxazoline (*n*PropOx) to tune the polarity. Subsequently, we converted the methyl ester groups by post polymerization modification (via hydrolysis) in order to design a series of **NHS-POx** with varying polarities. In a third route (**C**), similar to **B**, we made use of CROP and postmodification strategies (by amidation of the methylester). In this route, we introduced both the hydrophilic moieties and the crosslinking NHS-ester groups via modification of the methyl ester. After synthesis of the polymers, they were tested for their physicochemical properties such as their solubility in water. In conclusion, only routes **B** and route **C** were viable in terms of robustness of the synthetic procedures and physicochemical properties of the polymers. Therefore,

these synthetic routes were further employed for the preparation of the POx polymers in the remaining chapters of this thesis.

In **Chapter 3,** we performed a systematic study on the pH- and temperature-responsive behavior of *n*PropOx copolymers containing carboxylic acid groups (P(*n*PropOx-c-COOH) and *n*PropOx copolymers containing amine groups P(*n*PropOx-c-NH_2). This lower critical solution temperature (LCST) behavior was studied by turbidimetry by studying the effect of various parameters on the cloud point (CP). It was found that the polymer concentration had a strong influence on the CP. Furthermore, the CP was linearly related to the amount of hydrophilic carboxylic acid groups as present on the polymer. The addition of increasing amounts of salt (NaCl) led to a Hofmeister-related salting out effect of the polymers. Additionally, it was found that the pH had a strong effect on the polymer charge and thus the CP of the polymer. Finally, turbidimetric studies in PBS showed that the polymers were soluble around body temperature. Overall, this tunable behavior was found very useful as purification method for intermediate polymers in route **B** (**Chapter 2**), but also offers possibilities for the development of thermoresponsive systems based on these polymers, which can be utilized for e.g. drug delivery applications.

In **Chapter 4**, the hemostatic efficacy of various **NHS-POx** polymers (described in **Chapter 2**) was tested *in vitro* as well as *in vivo* against commercial controls. In a first study, we tested the hemostatic potential of a series of **NHS-POx** polymers by crosslinking these polymers with human whole blood. In this experiment, **NHS-POx** with hydrophilic groups demonstrated the fastest gelation compared to **NHS-POx** polymers without these groups but not as fast as **NHS-PEG**. The best performing **NHS-POx** polymer was coated on gelatin sponges using a spraying method, thereby creating homogeneously coated hemostatic sponges with good control over the coating density (mg/cm^2). The sponges were tested for blood uptake and adhesion. It was found that increasing the amount of the polymer coating led to a decrease in blood uptake. In the adhesion test, a clear effect of the presence of the coating was found, but no effect on the amount of coating was observed. The best performing sponge was tested *in vivo* in a model for profuse bleeding against commercially available products Hemopatch (based on **NHS-PEG**) and Tachosil. In this experiment, the **NHS-POx** coated sponge proved superior in terms of hemostatic efficacy (7 out of 8 bleedings) compared to a gelatin sponge without this coating (0 out of 4 bleedings) and Tachosil (1 out of 4 bleedings). Moreover, in comparison with Hemopatch (5 out of 8 bleedings) the **NHS-POx** coated sponge proved superior in terms of sealing the wound site, indicating that coating homogeneity is an important parameter in the design of a hemostatic device.

In **Chapter 5**, we performed a systematic rheological study to get a clearer insight into the mode of action of **NHS-POx** and **NHS-PEG** as hemostatic polymers.

Therefore, we studied the network formation of these polymers, by means of gelation, with bovine serum albumin (BSA) as a model protein. In this study, we were particularly interested in the effect of i) the positioning of the crosslinking NHS-ester groups (side chains or end groups) and ii) the type of the hydrophilic side chain moieties (OH or $N(Me)_2$, in case of **NHS-POx**), on the network structure. In addition, we studied the effect of the pH on the network formation for **NHS-POX**. The network properties were analyzed via i) oscillatory time sweeps thereby studying the gelation time, ii) oscillatory frequency sweeps to study the elasticity of the formed networks and iii) strain sweeps to study the strength of the formed networks upon increased strain values. During oscillatory time sweeps, we observed that both **NHS-POx** and **NHS-PEG** instantaneously formed crosslinked networks with BSA, although **NHS-PEG** formed stiffer networks with BSA than **NHS-POx**. Both networks showed predominantly elastic behavior as was determined by frequency sweeps. Interestingly, in contrast to crosslinked **NHS-PEG** networks, crosslinked **NHS-POx** networks showed strain stiffening behavior as was demonstrated by strain sweeps, which indicates that **NHS-PEG** and **NHS-POx** formed different network structures. Overall, we explain the observations by the difference in polymer architecture between POx and PEG; the freely mobile NHS-ester groups of the **NHS-PEG** star polymer are more prone to react with different BSA molecules, which leads to the buildup of a more regular network structure, whereas, due the proximity of the NHS esters on **NHS-POx** one polymer chain can form multiple bonds with the same BSA protein. We furthermore observed that a pH optimum of 8.5 or higher was needed in order to obtain the strongest networks between **NHS-POx** and BSA, which can be used as useful tool for speeding up the hemostatic action of coated **NHS-POx** patches. Finally, both **NHS-POx** and **NHS-PEG** can be successfully utilized for the development of hemostatic polymers as they both formed networks (with BSA) with strengths in the same range as fibrin clots.

In **Chapter 6**, we studied the degradation and excretion of **NHS-POx**. In this study, we were primarily interested in studying i) the excretion pathway of the degradation products of **NHS-POx** and ii) the possible accumulation of these degradation products in other organs. We investigated the identity of the degradation products of **NHS-POx** by studying the stability of **NHS-POx** in physiologically relevant media. ^{1}H-spectroscopy revealed that the polymers bearing carboxylic acid groups in the side chain are the most likely degradation product of **NHS-POx**. After this, we synthesized this polymer containing a diethylene-triamine-pentaacetic acid (DTPA) ligand as an end-group which allowed chelation of radioactive isotopes (^{111}In). After labeling and purification, the radiolabeled polymers were intravenously injected in Wistar-rats and the excretion was studied by Single Photon Emission Computed Tomography (SPECT) at different time points (1 hr, 6 hrs, 24 hrs and 7 days). After

7 days, the animals were sacrificed, relevant organs were dissected, weighed and analyzed using an automated γ-counter. It was found that the majority of the injected polymer was cleared within 24 hrs mainly via renal clearance. Nevertheless, after 7 days, despite a steady decline, still 3.1 ± 1.1 of the injected dose per gram (ID%/g) by SPECT/CT or 9.5 ± 0.6 ID%/g by the γ-counter was still observed in the kidneys. No accumulation of radiolabeled polymers in other organs was observed. In conclusion, although the majority of the radiolabeled polymers seems to be suitably excreted from the rat model, a minor percentage remains present in the kidneys. More systematic research is needed in order to draw valid conclusions on the full excretability and possible kidney retention of the degradation products of **NHS-POx** in the kidneys.

In conclusion, we have demonstrated that NHS-ester functionalized poly(2-oxazoline)s are excellent candidates for the development of hemostatic agents.

2. Future perspectives

The development of hemostatic agents has evolved tremendously over the past decades[1, 2]. Previously, products were mainly based on polymers of natural origin (such as collagen[3] and gelatin[4]) because of their wide availability, fast degradation profile and low cost price. These materials will probably remain to be used for the treatment of less severe bleedings in the clinic, but do not offer an adequate solution for severe profuse bleedings on venous organs. Therefore, more advanced surgical hemostats have been developed which combine the benefits of both synthetic and natural polymers (such as Hemopatch, Veriset and Tachosil)[5,6]. However, these products suffer from specific drawbacks (which are described in **Chapter 1**) as well, which has stimulated the search for novel hemostatic agents. NHS-ester functionalized poly(2-oxazoline)s (**NHS-POx**) have been described in this thesis as a highly promising alternative to existing systems.

Although the suitability of **NHS-POx** for use in as hemostatic devices has been illustrated in this work, several improvements can be made to enhance the potential of these polymers even further. The successful hemostatic action of these polymers is based on the efficient crosslinking reaction of NHS-esters with primary amines (e.g. in blood and soft tissue). Since availability of the crosslinking groups seems to be an important parameter for the design of hemostatic POx, as shown in **Chapter 5**, it would be interesting to develop POx containing extended sidechains by increasing the spacer length between the POX-backbone and the NHS-ester moiety. This strategy might render the crosslinking groups more mobile, which could facilitate the crosslinking reaction. Another option to enhance the crosslinking capacity of

these materials would involve introduction of additional hydrophilic moieties in the sidechains which would replace the hydrophilic functionalities described in **Chapter 2**. This would make the overall polymer structure more water soluble and the crosslinking groups more prone to reaction with primary amines. A final option would be to investigate dendritic structures based on POx, since these architectures can greatly enhance the availability of these crosslinking groups as well. The synthesis of dendritic POx has been reported[7, 8], although care must be taken that the abovementioned modifications of the polymer structures should not impede their synthesis via robust procedures to allow sufficient quality.

Besides the adjustments that can be made in the polymer structure, several other improvements can be introduced, e.g. by using additives during production of hemostatic patches. In **Chapter 5**, it was demonstrated that the stiffness of the formed network between **NHS-POx** and BSA can be increased if the crosslinking reaction is performed at an elevated pH. Thus, an important parameter which can be tuned to enhance the crosslinking ability of **NHS-POx** is the pH of the hemostatic construct, for example by addition of a biocompatible basic component (such as sodium carbonate) onto the coated constructs. Upon contact of the hemostatic device with blood, the local pH would be slightly elevated to the desired pH which would facilitate crosslinking. Subsequently, the pH would be neutralized by the buffering ability of the blood after the crosslinking process has been finalized. This approach has already been suitably employed in various commercially available tissue adhesives in the biomedical field, such as Duraseal[9] and Coseal[10].

Finally, a third improvement which could improve the development process is by getting a better understanding of the mechanism of action. Performing a systematic approach in investigating all the individual parameters in the process (e.g. polymeric structure, coating) in predictive model systems will ultimately lead to a more focused development process. An example of such a predictive model could be a suitable *ex-vivo* model to mimic profuse bleedings. Although *in vivo* efficacy remains the ultimate proof for a hemostatic agent, a suitable and predictive *ex-vivo* model would allow to obtain more understanding of the system, which can ultimately lead to a reduction of the number of animal experiments which have to be performed. To date, however, only a limited number of predictive *ex-vivo* models are reported, which compare the efficacy of hemostatic agents within one *ex-vivo* model[11, 12].

Electrospinning

While current topical hemostatic agents are generally still hybrid products (consisting both of natural and synthetic polymers), in the biomedical materials field, there is an increased interest towards the design of fully synthetic hemostatic materials[13-15]. These materials can offer multiple advantages over current topical

hemostatic agents, because of the highly tunable degradation profile and excellent tunable structural properties. As a result, several groups have utilized the versatility of synthetic polymers for the development of wound dressing materials[16, 17] (such as hemostatic agents). One of the most interesting manufacturing techniques for the design of these materials is electrospinning.

Electrospinning is a manufacturing technique for the construction of polymeric fibers[18, 19]. During this process, a polymer solution is ejected through a needle, whereafter the ejected solution is charged by a high voltage source (typically 5-20 kV) which results in the formation of a conical shape, a so-called Taylor cone (**Figure 1**)[20]. By continuous ejection, the polymeric fibers can be collected on a metal surface (collector).

The quality and properties of the fibers which are formed are strongly determined by the experimental parameters which are used (e.g. solvent[21], voltage[22], concentration[22]), characteristics of the polymer and additives[23] during the electrospinning process, which renders thic technique a highly tunable process. A wide range of fibers has been produced using electrospinning including solid[24], hollow[25] and porous[26] fibers for a wide range of different polymers[19], which allows design of fibers of various architectures.

Electrospinning has also been applied in the field of poly(2-oxazoline)s. To date, several groups have reported electrospinning of poly(2-oxazoline)s, ranging from homopolymers such as poly(2-ethyl-2-oxazoline)[24, 27] to side chain functional polymers[28], thereby demonstrating the compatibility of poly(2-oxazolines) with electrospinning.

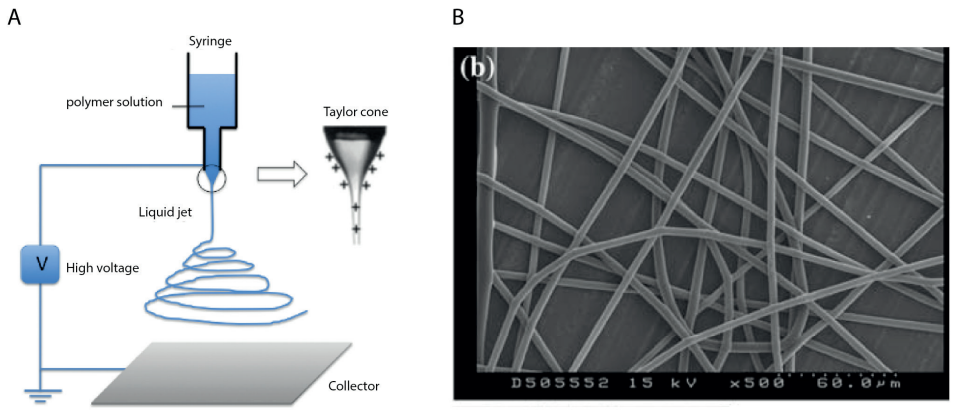

Figure 1 Overview of the electrospinning process: A) Overview of an electrospinning setup, B) example of electospun fibers based on P(EtOx). Reprinted with permission[27].

For the development of hemostatic materials based on POx, electrospinning is a particularly interesting platform, since it would result in a purely synthetic fibrous mat. The fibrous microstructure of this electrospun mat can have multiple advantages over current hemostatic products, e.g. a large surface area, which can greatly enhance the performance of these products. Moreover, this technique allows tuning of various parameters (fiber diameter[29], pore size[30], thickness[31]), which are important parameters for the hemostatic efficacy. Currently, in the field, electrospinning is mainly performed at lab-scale, although translation of this technology towards industrial applications is emerging[16].

In conclusion, in this thesis we have successfully demonstrated the use of **NHS-POx** in hemostatic applications. We are convinced that that these polymers are excellent candidates for the design of hemostatic polymers. Evidently, the versatility of the polymers allows further finetuning of the polymer structure aimed at improved hemostatic efficacy. The opportunities are numerous as this class of polymers is compatible with manufacturing techniques such as electrospinning, which would lead to purely synthetic hemostatic products that might outperform currently available topical hemostatic agents on the market.

3. References

1. P. J. M. Bouten, M. Zonjee, J. Bender, S. T. K. Yauw, H. van Goor, J. C. M. van Hest and R. Hoogenboom, *Prog. Polym. Sci.*, 2014, **39**, 1375-1405.
2. F. di Lena, *J. Mater. Chem. B*, 2014, **2**, 3567-3577.
3. M. E. Silverstein and M. Chvapil, *J. Trauma Acute Care Surg.*, 1981, **21**, 388-393.
4. R. U. Light, *J. Neurosurg.*, 1945, **2**, 414-434.
5. C. Schuhmacher, J. Pratschke, S. Weiss, S. Schneeberger, A. L. Mihaljevic, R. Schirren, M. Winkler and N. Emmanouilidis, *Med. Devices. (Auckland, N.Z.)*, 2015, **8**, 167-174.
6. G. L. Colombo, D. Bettoni, S. Di Matteo, C. Grumi, C. Molon, D. Spinelli, G. Mauro, A. Tarozzo and G. M. Bruno, *Vasc. Health Risk Manag.*, 2014, **10**, 569-576.
7. H. M. L. Lambermont-Thijs, M. W. M. Fijten, U. S. Schubert and R. Hoogenboom, *Aust. J. Chem.*, 2011, **64**, 1026-1032.
8. J. Jeerupan, T. Ogoshi, S. Hiramitsu, K. Umeda, T. Nemoto, G.-i. Konishi, T.-a. Yamagishi and Y. Nakamoto, *Polym. Bull.*, 2008, **59**, 731-737.
9. M. C. Preul, W. D. Bichard, T. R. Muench and R. F. Spetzler, *Neurosurgery*, 2003, **53**, 1189-1199.
10. C. Tan, M. Utley, C. Paschalides, J. Pilling, J. D. Robb, K. M. Harrison-Phipps, L. Lang-Lazdunski and T. Treasure, *Eur. J. Cardiothorac. Surg.*, 2011, **40**, 304-308.
11. J. C. Villa-Camacho, C. Ghobril, L. Anez-Bustillos, M. W. Grinstaff, E. K. Rodríguez and A. Nazarian, *BMC Musculoskelet. Disord.*, 2015, **16**, 116.
12. S. Nikeghbalian, M. Aliakbarian, K. Kazemi, A. R. Shamsaeefar, S. H. Mehdi, A. Bahreini and S. A. Malek-Hosseini, *Int. J. Organ Transplant. Med.*, 2014, **5**, 120-124.
13. C. Ghobril and M. W. Grinstaff, *Chem. Soc. Rev.*, 2015, **44**, 1820-1835.
14. N. Annabi, A. Tamayol, S. R. Shin, A. M. Ghaemmaghami, N. A. Peppas and A. Khademhosseini, *Nano Today*, 2014, **9**, 574-589.
15. W. Huang, Y. Wang, Y. Chen, Y. Zhao, Q. Zhang, X. Zheng, L. Chen and L. Zhang, *Adv. Healthc. Mater.*, 2016, **5**, 2813-2822.
16. M. Abrigo, S. L. McArthur and P. Kingshott, *Macromol. Biosci.*, 2014, **14**, 772-792.
17. P. Zahedi, I. Rezaeian, S.-O. Ranaei-Siadat, S.-H. Jafari and P. Supaphol, *Polym. Adv. Technol.*, 2009, **21**, 77-95
18. D. H. Reneker and A. L. Yarin, *Polymer*, 2008, **49**, 2387-2425.
19. N. Bhardwaj and S. C. Kundu, *Biotechnol. Adv.*, 2010, **28**, 325-347.
20. G. Taylor, *Proc. R. Soc. London Ser. A*, 1964, **280**, 383-397.
21. C. J. Luo, M. Nangrejo and M. Edirisinghe, *Polymer*, 2010, **51**, 1654-1662.
22. M. K. Leach, Z. Q. Feng, S. J. Tuck and J. M. Corey, *J.Vis. Exp.*, 2011, **47**, e2494.
23. M. Y. Karidurаganavar, F. J. Davis, G. R. Mitchell and R. H. Olley, *Polym. Int.*, 2010, **59**, 827-835.
24. B. Stubbe, Y. Li, M. Vergaelen, S. Van Vlierberghe, P. Dubruel, K. De Clerck and R. Hoogenboom, *Eur. Polym. J.*, 2016, **88**, 724-732
25. R. Khajavi and M. Abbasipour, *Sci. Iran.*, 2012, **19**, 2029-2034.
26. Z. Qi, H. Yu, Y. Chen and M. Zhu, *Mater. Lett.*, 2009, **63**, 415-418.
27. L. Buruaga, A. Gonzalez and J. J. Iruin, *J. Mater. Sci.*, 2009, **44**, 3186-3191.
28. O. I. Kalaoglu-Altan, B. Verbraeken, K. Lava, T. N. Gevrek, R. Sanyal, T. Dargaville, K. De Clerck, R. Hoogenboom and A. Sanyal, *ACS Macro Lett.*, 2016, **5**, 676-681.
29. B. Cramariuc, R. Cramariuc, R. Scarlet, L. R. Manea, I. G. Lupu and O. Cramariuc, *J. Electrostat.*, 2013, **71**, 189-198.
30. J. Rnjak-Kovacina, S. G. Wise, Z. Li, P. K. M. Maitz, C. J. Young, Y. Wang and A. S. Weiss, *Biomaterials*, 2011, **32**, 6729-6736.
31. J. K. Hong, J. Y. Bang, G. Xu, J.-H. Lee, Y.-J. Kim, H.-J. Lee, H. S. Kim and S.-M. Kwon, *Int. J. Nanomedicine*, 2015, **10**, 1189-1200.

Chapter 8:

Dutch summary and perspective view

1. Samenvatting

Operaties op zachte weefsels zoals lever en nieren gaan vaak gepaard met ernstige bloedingen, omdat deze weefsels goed doorbloed zijn. Hierdoor kunnen invasieve manieren om wonden te hechten (zoals hechtdraden en nietjes) niet gebruikt worden om deze, meestal hevige, bloedingen te stelpen. In dit werk zijn we geïnteresseerd om een niet-invasief hemostatisch hulpmiddel te ontwikkelen gebaseerd op poly(2-oxazoline)s (POx) met N-hydroxysuccinimide-(NHS) esters (**NHS-POx**). De werking van deze polymeren is gebaseerd op de reactiviteit van NHS-esters met primaire amines, die veelvuldig voorkomen in bloedcomponenten (bijv. albumine) of weefsels (bijv. in een orgaan als de lever). Deze reactiviteit maakt deze polymeren geschikt als hemostatisch materiaal, doordat het de mogelijkheid geeft om een reactie aan te gaan met bloedcomponenten en zo een artificiele bloedprop te vormen en/of door als wondafsluitingsmiddel te werken door aan weefsel te hechten. Zoals is beschreven in **hoofdstuk 1**, worden NHS-ester gefunctionaliseerde polymeren al gebruikt in biomedische hulpmiddelen die gebaseerdeerd zijn op poly(ethyleen) glycol (PEG). Het nadeel van deze materialen is dat deze onvoldoende goed werken om hevige bloedingen te stelpen. Dit is mogelijk op te lossen door de polariteit en hoeveelheid NHS-esters op het polymeer aan te passen. Echter, voor PEG zijn deze twee parameters niet makkelijk aan te passen en zijn andere polymeerklassen beter geschikt. Vanwege de veelzijdige functionalisatiemogelijkheden en de biocompatibiliteit, hebben we in dit werk POx geselecteerd voor de ontwikkeling van hemostatische materialen.

In **hoofdstuk 2** hebben we verschillende synthetische routes besproken om **NHS-POx** te maken. Een moeilijkheid is dat NHS-esters niet direct in polymeren kunnen worden ingebouwd tijdens kationische ring opening polymerisatie (CROP), de meest gebruikelijke manier om POx te maken, omdat deze functionele groep de polymerisatie verstoren. Daarom hebben we gebruik gemaakt van CROP en post-polymerisatie-modificatiestrategieën voor het ontwikkelen van een schaalbare, robuuste methode om **NHS-POx** te maken. Daarnaast waren we geïnteresseerd in de fysisch-chemische eigenschappen van de gesynthetiseerde polymeren (zoals oplosbaarheid in water). We hebben drie verschillende syntheseroutes (A-C) ontwikkeld, welke alledrie gebaseerd zijn intermediaire polymeren die methyl-esters bevatten. Deze methyl-ester groepen op de polymeren kunnen namelijk gemakkelijk worden omgezet naar NHS-esters. In de eerste route (A) hebben we gebruik gemaakt van gedeeltelijke, zuurgebaseerde hydrolyse van tertiaire amides in de skeletstructuur van commercieel verkrijgbaar poly(2-ethyl-2-oxazoline) (Aquazol®), wat resulteerde in de vorming van poly(ethyleen imine) (l-PEI) groepen. De hoeveelheid aan l-PEI groepen die tijdens de hydrolyse ontstaan, bepaalt

uiteindelijk de hoeveelheid functionele groepen (NHS-esters) die uiteindelijk in het polymeren ingebouwd kunnen worden. In de tweede route (B) hebben we polymeren gemaakt, d.m.v. CROP met 2-methoxy-carbonyl-ethyl-2-oxazoline (MestOx) als functionaliseerbaar monomeer en 2-*n*-propyl-2-oxazoline (*n*PropOx) en 2-ethyl-2-oxazoline (EtOx) als niet-functionaliseerbare monomeren voor het regelen van de polariteit van de polymeren. Na de polymerisatie, hebben we de methylester groepen op het polymeer gehydrolyseerd en geactiveerd tot NHS-esters wat resulteerde in een serie van NHS-ester gefunctionalizeerde polymeren met verschillende polariteiten. In een derde syntheseroute (C) hebben we (net als in route B) gebruik gemaakt van CROP en post-polymerisatie-modificatiestrategieën (d.m.v. amidatie van de methyl ester groepen). In deze route hebben we de hydrofiele groepen en NHS-estergroepen ingebouwd d.m.v. modificatie van de methylesters. Nadat de polymeren gesynthetiseerd waren, zijn deze getest op enkele fysisch-chemische eigenschappen (zoals oplosbaarheid in water). We hebben geconcludeerd dat alleen routes B en C rendabele, robuuste syntheseroutes waren voor het maken van **NHS-POx** polymeren. Daarnaast waren de polymeren die via deze routes gemaakt zijn oplosbaar in water en organische oplosmiddelen, wat ze geschikt maakt als om als hemostatisch polymeer gebruikt en verwerkt te worden. Routes B en C zijn vervolgens gebruikt voor de synthese van POx polymeren die in de volgende hoofdstukken van deze thesis beschreven staan.

In **Hoofdstuk 3** hebben we een systematische studie gedaan naar het pH- en thermoresponsieve onderste kritische oplossingstemperatuur (LCST) gedrag van *n*PropOx bevattende copolymeren. Doordat deze polymeren naast nPropOx-groepen ook carboxylzuur groepen of amine-groepen bevatten zijn deze gevoelig voor veranderingen in pH en temperatuur. Dit gedrag was bestudeerd door middel van turbidimetrie door te kijken naar de kritische oplossingstemperatuur (CP) van deze polymeren terwijl we verschillende parameters varieerden (polymeerconcentratie, zoutconcentratie en pH). We hebben gevonden dat de polymeerconcentratie een belangrijke parameter is voor het regelen van de CP. Verder vonden we dat er een lineair verband bestond tussen de hoogte van de CP en de hoeveelheid carboxylzuurgroepen op het polymeer. Het toevoegen van verschillende hoeveelheden zout (NaCl) leidde tot een verlaging van de CP wat verklaard kan worden door het uitzouten van het polymeer. Verder hebben we gevonden dat de pH van de oplossing een sterke invloed heeft op de lading van het polymeer, wat invloed heeft op de mate van oplosbaarheid in water en ook op de CP van de verschillende polymeren. Tenslotte hebben we turbiditeitsmetingen uitgevoerd in een fosfaatgebufferde zoutoplossing (PBS) om de CP onder fysiologische condities te onderzoeken. In deze experimenten hebben we gevonden dat de CP afhankelijk van de polymeerconcentraties kan worden ingesteld rond de lichaamstemperatuur

(37 °C). Samenvattend hebben we in dit hoofdstuk laten zien dat het veelzijdige temperatuurgevoelige gedrag van deze polymeer voor meerdere toepassingen interessant kan zijn. Zo hebben we dit gebruikt voor het opzuiveren van polymeren in route B (beschreven in **Hoofdstuk 2**), maar verder kan dit gedrag ook gebruikt worden voor het ontwikkelen van materialen die gebruikt kunnen worden voor bijvoorbeeld medicijnafgifte.

In **Hoofdstuk 4** hebben we de hemostatische activiteit van verschillende **NHS-POx** polymeren (beschreven in **Hoofdstuk 2**) getest. We hebben dit zowel *in vitro* als ook *in vivo* getest en vergeleken met commercieel verkrijgbare hemostatische producten als controle. In een eerste studie hebben we een serie van **NHS-POx** polymeren en een **NHS-PEG** controle laten reageren met humaan bloed. Door deze reactie werden covalente bindingen gevormd tussen bloedeiwitten en polymeer, wat resulteerde in een netwerkstructuur van polymeer en bloedeiwitten. We hebben gevonden dat deze vernetting alleen optrad als het polymeer NHS-esters bevatte. Bovendien trad de vernetting sneller op als het polymeer ook hydrofiele groepen bevatte, maar de vernetting met **NHS-PEG** verliep het snelste in dit experiment. Het **NHS-POx** polymeer wat het beste werkte in dit experiment werd vervolgens gespraycoat op gelatinesponzen, wat geresulteerde in een serie hemostatische sponzen met verschillende bedekkingsgraden (mg polymeer per cm^2). Hierna werden de **NHS-POx** sponzen en Hemopatch (**NHS-PEG**) gecoate spons bestudeerd met een rasterelektronenmicroscoop (SEM). We zagen dat het poreuze karakter van de **NHS-POx** sponzen behouden bleef en dat ze homegener gecoat waren dan Hemopatch, die gecoate en ongecoate domeinen bevat. De gecoate sponzen werden vervolgens getest op bloedopname en plakkracht. We hebben ontdekt dat een hogere bedekkingsgraad leidde tot verminderde bloedopname. In de plaktest zagen we dat sponzen met coating wel plakten en sponzen zonder coating niet plakten, maar er was geen duidelijk effect te zien van de hoeveelheid coating op de plakkracht. Vervolgens hebben we de hemostatische activiteit van een gecoate spons getest in een *in vivo*-model voor zware bloedingen. Daarnaast hebben we een negatieve controle (spons zonder coating) en twee commerciële producten (Hemopatch gebaseerd op **PEG-NHS**) en Tachosil getest in dit model. De **NHS-POx** gecoate spons, waarmee 7 van de 8 bloedingen kon worden gestopt, presteerde beter dan de ongecoate spons (0 uit 4 bloedingen) en Tachosil (1 uit 4 bloedingen). Ook in vergelijking met Hemopatch (5 uit 8 bloedingen) presteerde de spons beter. Bovendien was bij Hemopatch (en niet bij de **NHS-POx** gecoate spons) bloeding aan de randen van de spons te zien, wat benadrukt dat ook een homogeneiteit van de coating een belangrijkere eigenschap is voor het ontwerpen van een hemostatische spons.

In **Hoofdstuk 5** hebben we een systematische rheologische studie uitgevoerd om meer inzicht te krijgen in het verschil in werking tussen **NHS-POx** en **NHS-PEG**. Hierdoor hebben we gekeken naar de vernetting van deze polymeren met runderalbumine (BSA), een veelvoorkomend eiwit in (runder)bloed. In deze studie waren we geïnteresseerd in het effect van i) de positie van de NHS-esters op het polymeer (als zijgroepen (POx) of als eindgroepen (PEG)) en ii) het effect van het type hydrofiele groep (OH of $N(CH_3)_2$) op het polymeer, op de vorming van polymeer-eiwit netwerk. Daarnaast hebben de invloed van de pH op de snelheid en stijfheid van de gevormde netwerken onderzocht voor **NHS-POx**. We hebben gevonden dat **NHS-POx** en **NHS-PEG** beide instantaan een netwerk vormde met BSA, maar dat **NHS-PEG** stijvere netwerkstructuren vormde met BSA dan **NHS-POx**. Verder zagen we dat beide soorten netwerken elastisch waren bij verschillende frequenties. Een andere interessante observatie was dat we zagen dat **NHS-POx** gebaseerde netwerken stijver werden nadat er meer spanning op de netwerken gezet werd, wat duidt op een andere netwerkstructuur die gevormd wordt bij PEG en POx gebaseerde netwerken. We kunnen dit verklaren door de verschillen in polymeerarchitectuur tussen PEG en POx. Omdat de NHS-ester in **NHS-PEG** heel mobiel zijn vormt **NHS-PEG** vooral bindingen tussen PEG met afzonderlijke eiwitmoleculen tot een homogeen netwerk. Bij **NHS-POx** zijn deze groepen minder mobiel, waardoor er hier (naast soortgelijke verbindingen als bij **NHS-PEG**) ook meerder bindingen van een polymeer met eenzelfde eiwitmolecuul mogelijk zijn. Dit resulteert in de vorming van een onregelmatig netwerk. Verder hebben we gevonden dat bij een pH-waarde van 8.5 de sterkste netwerkstructuren gevormd werden door **NHS-POx**. Daarnaast was het type hydrofiele groepen op het polymeer van weinig invloed op de gevormde netwerkstructuur. De sterkte de gevormde netwerken van **NHS-PEG** en **NHS-POx** zijn beide van sterker dan fibrinestolsels die gevormd worden in de bloedstollingscascade, wat deze polymeren geschikt maakt als wondafsluitingsmiddel/hemostaticum.

In **Hoofdstuk 6** hebben we de afbraak en excretie van **NHS-POx** onderzocht. In deze studie waren we specifiek geïnteresseerd om te bestuderen hoe en of de afbraakproducten van **NHS-POx** geklaard worden. Daarnaast wilden we onderzoeken of deze afbraakproducten ongewenste ophoping in organen liet zien. Om dit te onderzoeken hebben we eerst de degradatie van **NHS-POx** onderzocht door incubatie van dit polymeer in PBS en bloedplasma te onderzoeken. In deze studie hebben we met behulp van ^{1}H-NMR-spectroscopie bepaald dat bij deze polymeren de NHS-esters afbreken tot carboxylzuren en dat de ester binding in de zijgroep van het polymeer stabiel bleef onder de geteste omstandigheden. Hierna hebben we het dit polymeer gemaakt met een pentetinezuur (DTPA) eindgroep als een ligand voor het binden van radioactiviteve isotopen (zoals Indium-111). Na radiolabeling en zuivering hebben we dit gelabelde polymeer intraveneus geinjecteerd in de staart van Wistar-ratten. De excretie van de polymeren was

vervolgens bestudeerd met behulp van SPECT (computertomografie met behulp van uitstraling van enkelvoudige fotonen) door een afbeelding te reconstrueren na 1 uur, 6 uur, 24 uur en 7 dagen (na injectie). Na 7 dagen werden de dieren opgeofferd. Vervolgens werden de organen operatief verwijderd, gewogen en geanalyseerd met behulp van een γ-counter. We hebben gevonden dat binnen 24 uur het merendeel van het geinjecteerde polymeer kon worden geklaard via de nieren. Niettemin, na 7 dagen was ondanks een afname van het signaal, nog steeds 3.1 ± 1.1 % van de geïnjecteerde dosis per gram orgaan (%ID/g) (SPECT) of 9.5 ± 0.6 %ID/g (γ counter) te meten in de nieren. Geen ophoping van het polymeer in de andere organen was te zien. Concluderend hebben we gevonden dat het merendeel van de geïnjecteerde dosis van het polymeer kon worden geklaard via de nieren, echter dat een kleine hoeveelheid na zeven dagen nog steeds in de nieren te vinden was. Meer systematisch onderzoek is nodig om betrouwbare conclusies te trekken over de oorzaak van deze aanwezigheid van gelabelde afbraakproducten van **NHS-POx** in de nieren.

Tenslotte hebben we in dit werk laten zien dat **NHS-POx** in vele aspecten een veelbelovend alternatief is voor huidige hemostatische polymeren.

2. Toekomstperspectieven

De laatste tientallen jaren hebben hemostatische materialen een geweldige ontwikkeling doorgemaakt. Traditioneel werd er in het veld voor gebruik gemaakt van hemostatische materialen van natuurlijke oorspong (zoals collageen en gelatine), omdat deze in groten getale beschikbaar zijn, goedkoop zijn en zeer snel afbreken. Deze materialen zullen in de toekomst nog wel gebruikt worden voor het behandelen van minder hevige bloedingen, maar deze materialen bieden geen passende oplossing voor het stelpen van hevige bloedingen tijdens operaties. Recentelijk zijn daarom meer geavanceerde hemostatische materialen ontwikkeld (zoals Hemopatch, Veriset en Tachosil) die beter geschikt zijn om zwaardere bloedingen te stelpen. Echter, ook deze materialen hebben specifieke nadelen (zoals beschreven in **Hoofdstuk 1**) wat vele groepen gestimuleerd heeft tot onderzoek naar nieuwe hemostatische materialen. Een voorbeeld hiervan zijn NHS-ester gefunctionaliseerde poly(2-oxazoline)s die beschreven zijn in dit werk.

Ondanks dat de geschiktheid van deze materialen als hemostatisch materiaal is beschreven in dit werk, kunnen meerdere aanpassingen worden gedaan om de prestaties van deze materialen te verbeteren. Een soort aanpassingen die kan worden gedaan is structurele veranderingen op het polymeer toe te passen, zodat de polymeren efficiënter kunnen reageren met bloedeiwitten en zachte weefsels, waardoor het stoppen van bloedingen vergemakkelijkt wordt. Zoals, beschreven in **Hoofdstuk 5**

kan deze reactie bespoedigd worden door de beschikbaarheid van deze groepen te vergroten. Dit kan geregeld worden door de afstand tussen het polymeerskelet en de elektrofiele NHS-esters te vergroten, waardoor de NHS-esters meer beweegruimte krijgen waardoor ze makkelijker kunnen reageren. Daarnaast zou er gekeken kunnen worden om een andere soort hydrofiele groep op de polymeer in te bouwen (via route B of C (**Hoofdstuk 2**)). Hierdoor kan het totale polymeer beter oplosbaar worden, waardoor de NHS-esters efficiënter kunnen reageren. Een laatste optie is door gebruik te maken van dendritische structuren gebaseerd op POx, omdat deze polymeerarchitectuur de beschikbaarheid van NHS-esters verbeterd. Een voordeel van deze laatste modificatie is dat de synthese van dendritische POx-polymeren reeds is beschreven in literatuur. Een belangrijke voorwaarde aan alle veranderingen die gedaan worden is wel dat ze via schaalbare, robuuste procedures ingebouwd kunnen worden.

Naast structurele veranderingen aan de polymeerstructuur kunnen ook veranderingen kunnen gedaan tijdens de productie van de hemostatische sponzen om de prestaties te bevorderen, bijvoorbeeld door het toevoegen van additieven tijdens de productie. In **Hoofdstuk 5** hebben we gezien dat de stijfheid van de netwerken die tussen **NHS-POx** en BSA netwerken gevormd worden verhoogd kan worden door de pH tijdens de koppelingsreactie te verhogen. Dit zou gerealiseerd kunnen worden door een biocompatibele basische component (zoals natriumcarbonaat) aan te brengen op de gecoate spons. Door contact van de gecoate spons met bloed zal de pH in de buurt van het grensvlak tijdens de koppelingsreactie tijdelijk verhoogd worden, waardoor koppeling efficient kan plaatsvinden. Hierna zal de bufferende capaciteit van het bloed, de pH normaliseren tot physiologische pH. De methode van het uitvoeren van koppelingsreacties bij verhoogde pH wordt al gebruikt bij commercieel verkrijgbare medische hulpmiddelen zoals Duraseal en Coseal.

Naast veranderingen op basis van zou het nuttig zijn om meer inzicht te krijgen in de verschillende parameters die van belang zijn voor de werking van de hemostatische spons. Alhoewel verschillende belangrijke parameters voor de werking van **NHS-POx** zijn beschreven in dit werk. Een systematisch onderzoek naar alle parameters (bijvoorbeeld de polymeerstructuur en de coating) in voorspellenende diermodellen zal uiteindelijk leiden tot een meer gefocuste ontwikkelingsproces. Een voorbeeld hiervan zou het ontwikkelen van een voorspellend *ex-vivo* modelsysteem dat hevige leverbloedingen kan simuleren. Alhoewel werking *in vivo* het ultieme bewijs blijft voor de werking van de hemostatische sponzen, zal het hebben van een voorspellend system kunnen leiden tot het verminderen van de te onderzoeken parameters *in vivo*. Hierdoor zullen minder proefdieren nodig zijn. Alhoewel er modelsystemen beschikbaar zijn die hevige bloedingen simuleren, bestaat er grote heterogeniteit tussen de systemen. Daarentegen zijn er weinig studies bekend die de werking van verschillende hemostatische producten binnen een simulatiemodel vergelijken.

Elektrospinnen

Ondanks dat het merendeel van de huidige hemostatische hulpmiddelen hydribe producten zijn (bestaande uit natuurlijke en synthetische materialen), zijn er verschillende groepen die onderzoek doen naar het ontwikkelen van volledig synthetische hemostatische materialen. Deze materialen hebben potentiele voordelen in vergelijking met natuurlijke materialen, zoals de uitstekend in te stellen afbreekbaarheid van deze materialen. Meerdere onderzoeksgroepen onderzoeken daarom de mogelijkheid om volledig synthetische polymeren als wondafdichtingsmaterialen te ontwikkelen. Een van de meest interessante constructietechnieken voor het maken van deze materialen is elektrospinnen.

Elektrospinnen is een constructietechniek om polymeervezels te maken. Tijdens dit proces wordt een polymeeroplossing door een naald uitgedrukt. Deze uitgedrukte oplossing wordt elektrisch geladen door een hoge spanningsbron (5-20 kV), wat resulteert in een 'kegel-vorm', de zogenaamde Taylor kegel (**Figuur 1**). Door continue uitdrukking van het polymeer worden er polymeervezels gevormd, die kunnen worden opgevangen op een metalen oppervlak.

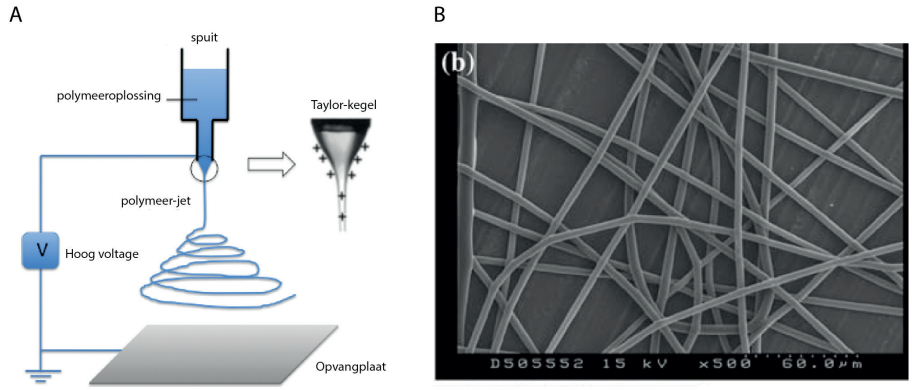

Figuur 1 Overzicht van het elektrospinproces: A) Overzicht van de elektrospinning, B) voorbeeld van elektrogesponnen vezels gebaseerd op P(EtOx)

De kwaliteit en eigenschappen van de vezels zijn sterk afhankelijk van experimentele condities die gebruikt zijn (zoals het type van het oplosmiddel), de eigenschappen van het polymeer en de additieven die worden gebruikt tijdens het elektrospinnen. De vele verschillende parameters die kunnen worden aangepast maakt elektrospinnen een veelzijdig en afstembaar proces. Mede hierdoor zijn verschillende soorten polymeervezels ontwikkeld, zoals massieve vezels, holle vezels of poreuze vezels.

Elektrospinnen is ook toegepast voor poly(2-oxazoline)s. Meerdere groepen hebben elektrogesponnen poly(2-oxazoline)s ontwikkeld, variërend van homopolymeren

(zoals poly(2-ethyl-2-oxazoline)s) tot zijgroep-gefunctionaliseerde polymeren, wat de compatibiliteit van deze techniek met poly(2-oxazoline)s benadrukt.

Voor het ontwikkelen van hemostatische materialen gebaseerd op poly(2-oxazoline)s is elektrospinnen een uitermate geschikt platform omdat het een volledig synthetische poreuze mat oplevert. De fijne microstructuur van de vezels, zorgt voor een groot contactoppervlak (in vergelijking met polymeerfilms). Dit grote contactoppervlak kan ervoor zorgen dat de hemostatische werking van deze polymeren verbeterd wordt. Daarnaast is het mogelijk om dit hemostatische effectiviteit te optimaliseren, door de eigenschappen van de polymeervezels aan te passen (zoals vezeldiameter, poriegrootte en vezeldikte). Ondanks dat elektrospinnen in het veld voornamelijk op laboratoriumschaal wordt uitgevoerd, zijn meerdere bedrijven bezig om deze constructietechniek te industrialiseren.

In dit werk hebben we laten zien dat **NHS-POx** succesvol kan worden gebruikt voor hemostatische toepassingen. We zijn ervan overtuigd dat deze polymeren een uitstekend platform zijn voor de ontwikkeling van hemostatische materialen. Het is verder duidelijk dat de veelzijdigheid van deze polymeerklasse verder uitgebuit kan worden voor het verbeteren van de hemostatische activiteit. De compatibiliteit met constructietechnieken zoals elektrospinnen maakt het zelfs mogelijk om volledig synthetische hemostatische producten te maken, wat verdere mogelijkheden biedt voor het optimaliseren van dit platform als hemostatische materialen.

Dankwoord

Na ruim vijf jaar is het eindelijk zover, het boekje is af en de verdediging is in zicht. Natuurlijk heb ik dit niet allemaal alleen gedaan, daarom wil ik graag meerdere personen bedanken die er de afgelopen jaren aan hebben bijgedragen dat het (eindelijk) af is gekomen.

Allereerst wil ik m'n directe begeleiders bedanken voor hun hulp de afgelopen jaren. Het hebben van verschillende directe begeleiders is aan de ene kant prettig door de vele ideeën die je krijgt, maar aan de andere kant ook een uitdaging om dit allemaal om te zetten tot een goed werkbaar plan.

Beste **Jan**, bedankt dat je ondanks je drukke schema, altijd ruimte en plek had om te kunnen overleggen. Je weet op een prettige manier te motiveren en daarnaast voldoende ruimte te laten aan de promovendus om zelf invulling/richting aan het onderzoek te geven. Veel succes de komende tijd met het opzetten van de groep in Eindhoven. Beste **Sander**, bedankt voor de vele adviezen en ideeën voor het onderzoek. Fijn dat ook jouw deur altijd open stond, mocht er een overleg nodig zijn. Ik vond het bijzonder dat je altijd wel een vernieuwend inzicht had op resultaten en wat we er uiteindelijk mee konden doen. Ook op een na te kijken stuk hoefde ik nooit lang te wachten tot ik het altijd heel nauwkeurig en grondig gecorrigeerd terug kreeg. Beste **John**, hartelijk dank voor alle suggesties en adviezen voor vervolgonderzoek (zeker ook over m.b.t. de klinische toepasbaarheid). Beste **Johan**, ik heb bewondering voor de passie en gedrevenheid waarmee je met het GATT project bezig bent. Daarnaast heb ik nooit lang hoeven te wachten op een antwoord op een email/na te kijken rapport en had je altijd wel een idee paraat voor het uitvoeren van een experiment. Ik weet zeker dat de vele ideeën uiteindelijk leiden tot een paar mooie medical devices gebaseerd op poly(2-oxazoline)s.

Naast m'n directe begeleiders wil ik graag de manuscriptcommissie (**Roeland Nolte**, **Piet Dijkstra** en **Hans Heuts**) bedanken voor het lezen en becommentariëren van het proefschrift.

Een promotietijd is een hele lange tijd waarin je heel veel mensen ontmoet en met heel veel mensen samenwerkt.

Allereerst wil ik de **Van Hest** groep (**Matthijs, Stijn, Ruud, Petra, Britta, Annika, Anika, Saskia, Ilmar, Zhipeng, Joep, Lise, Mark, Dave, Bastiaan, Marielle, Loai, Sylvie, Pascal, Dennis, Imke, Roger, Marlies, David, Nanda, Jan, Fei** en **Yingfeng**) bedanken. Congressen in Lunteren, legendarische streepjesborrels (met bijbehorende bureauhumor), groepsuitjes naar Gent, Edinburgh en Berlijn, gezelligheid tijdens koffie- en lunchpauzes. Ik vond het allemaal echt superleuk en had het niet willen missen :). Daarnaast wil ik ook de **Rutjes groep** (**Dani, Stefan**, **Bram**, **Alejandra**, **Ivan, Thomas**, **Torben**, **Rens** en **Hidde**) en verschillende andere

personen op de verdieping (**Abbas, Roel, Timo, Lianne, Danny, Pim, Sjoerd, Selma** en **Fleur**) bedanken voor de gezelligheid op het lab en op de werkvloer. Additionally I would like to thank the people from the **Department of Biomaterials** (**Mani, Antonio, Simone, Kambiz, Alexey, Dana, Joop, Jeroen, Fang** and many other people who I have met over the past few years) for the pleasant working environment in the Biomaterials lab and all the fun during the NBTE congresses.

Na een week hard werken werd een groot deel van de vrijdag (na)middag (en avond) onder het genot van een biertje doorgebracht, daarom wil ik ook de **Aesculaaf** bedanken voor het bieden van een verfrissende inspirerende netwerkomgeving. **Ruud, Matthijs, Annika** (Sneeuwwitje!), **Arne, Edu, Alejandra** (een Leffe Blond alsjeblieft), **Dani, Maria José, Eduardo, Ivan, Joan, Joep, Rens, Bram, Dave** en vele anderen. I am certain that the Aesculaaf would have gone through rough financial times without our weekly visits.

Rosa and **Maria José**, muchas gracias that you are willing to be paranimphs during the PhD-ceremony. **Rosa**, as a multi-talented researcher you always manage keep multiple projects running at the same time. Really an impressive skill! Additionally, you always manage to have time to support others. After these years however, I still don't completely get your fascination for the Eurovision Song Contest. **Maria José**, it has been a while since you came to the Netherlands. During this time you managed to produce a lot of polymers, you traveled the entire world during several holidays for multiple months, you got married and even managed to learn a bit of Dutch (although I understand that some tough words like 'kiep' are still hard to pronounce ;)). Good luck with your own PhD-project!

Bram, ik ken weinig mensen die het maken van polymeren zo geoptimaliseerd/ geperfectioneerd heeft als jij. Ik zou dat toch wel topsport willen noemen. **Joost**, ongelofelijk dat jij altijd voor iedereen tijd hebt. Je vormt samen met Bram een gouden duo. Zonder jullie zou het project nooit zo succesvol zijn 'geworre'... **Nathalie**, **Etienne**, **Rob** en **Harro**, jullie ook bedankt voor de prettige samenwerking de afgelopen jaren. **Edwin** & **Roger**, bedankt voor jullie hulp bij de vele testen die bij Heelkunde zijn uitgevoerd. Zonder jullie hulp zou een groot deel van het werk allemaal niet gelukt zijn. **Edwin**, veel succes met je promotieproject!

Daarnaast wil ik ook **Richard Hoogenboom** bedanken voor de vele goede adviezen de afgelopen jaren op het gebied van de poly(2-oxazolines). Ik vond het erg mooi en leerzaam om de POx-sessies op de ACS in San Francisco en Philadelphia mee te maken. **Bryn**, I will never forget your appearance at the ACS Meeting in San Francisco (both presenting and asking questions) and I guess I will not be the only one... **Victor**, I really enjoyed the nice time and good talks we had during the ACS meeting in Philadelphia, hopefully we can open the first venue of Così in Europe soon. **Maarten (2x), Bart, Joachim, Matthias, Gert-Jan** and others. Good luck with

your PhD-projects/careers. Daarnaast wil ik ook meerdere mensen van verschillende onderzoeksgroepen, **Henk Hoogenkamp** (Matrix Biochemistry), **Marc Simonet** (IME), **Simon Yauw** en **Harry van Goor** (Heelkunde), **Gerben Franssen, Peter Laverman** en **Otto Boerman** (Nucleaire Geneeskunde) bedanken voor de prettige samenwerking de afgelopen jaren. **Paul Riedel** (Rubröder), many thanks for the assistence with the spraying experiments.

Tijdens m'n promotie heb ik meerdere studenten mogen begeleiden. **Harry**, een groot deel van Hoofdstuk 3 is gebaseerd op je masterproject wat heeft geresulteerd in een mooie publicatie. Ik vond het leuk om je op de ACS in Philadelphia te ontmoeten. Veel succes met het afronden van je promotie in Michigan! **Elvy**, bedankt voor je hulp bij het maken van de polymeren en je hulp bij het coaten en testen van de vele patches (Hoofdstuk 4). Veel succes gewenst in het onderwijs. **Jon**, je hebt je masterstage gedaan aan het eind van mn promotie. Dit betekende dat je meestal zelfstandig aan de slag moest, maar dat ging je zeker goed af! Veel succes met het afronden van je studie! Verder wil ik **Kerry**, **Pieter** en **Tim** bedanken voor hun hulp tijdens de kortere stages.

Technische staf: **Paul White, Theo, Helene, Jan, Hans, Rene** en **Peter van Galen**, bedankt voor alle onmisbare hulp de afgelopen jaren bij de vaak kleine dingen. **Peter van Dijk**, hartelijk dank voor het regelen van de bestellingen. Mooi dat je altijd klaar staat voor een praatje met iedereen. **Liesbeth** en **Geert-Jan**, bedankt voor de hulp bij de SEM. **Marieke, Paula, Desiree** en **Jacky**, bedankt voor het regelen van alle agendatechnische zaken de afgelopen jaren, dat is zeker niet makkelijk met alle drukke agenda's van de professoren.

Naast het werk was er gelukkig ook de nodige ontspanning buiten werk.

Allereerst met de scheikundegroep: **Joris G.**, **Joris K.**, **Jeroen**, **Korneel**, **Bram**, **Joep**, **Gert-Jan**, **Andreas**, **Laura**, **Lianne**, **Emma**, **Vessela**, **Ingrid**, **Nathalie**, **Tine**, **Charlotte** en **Tobias**. Bierdrinken in Lijn 4 of Stathe, weekendje weg in het Amerikaanse huisje met de Japanse tuin, zomer in Italië (was dat nou een kikker?), Koningsdagen (en nachten), speciaalbier drinken en mitraillettes eten in Leuven, onvoorstelbare Giro/Tour/Vuelta-poules, fietsavonturen. Ik vind het elke keer weer een feest als we elkaar weer zien.

Dijon en **Wilbert**, naast werken bij de Bijenkorf op zaterdag hebben we al heel wat avonturen beleefd. Avonturen met Stef, huisfeesten, Oude Pothuys-avonden, festivals, concerten, uitjes, teveel om op te noemen. Mooi dat we elkaar nog steeds zien, ondanks dat we niet meer in het magazijn te vinden zijn iedere zaterdagmorgen. **Geerlien**, zorg je een beetje goed voor **Wilbert**? **Kirsten** en **Bas**, ik vind het mooi dat jullie altijd zo positief zijn over alles. **David** en **Suus**, ik kijk nu al uit naar de volgende festivals en Radiohead-concerten. Wanneer gaan we? **Arthur** (of natuurlijk gewoon **Tuur**), ik kan elke keer weer genieten van de enthousiaste (soms onnavolgbare)

verhalen over het leven van Arthur Pieterse. Veel sterkte ook met je eigen grote papa-avontuur!

De Kalsbeek-groep: **René, Gerwin, Mathijs, Marijke, Annet, Sabine** en **Mirjam**, ondanks dat iedereen een andere kant op is gegaan, vind ik het mooi dat we na al die jaren nog steeds contact houden. Laten we de komende jaren zeker de weekendjes weg en het kerstdiner er in houden!

Poolse bruiloften met bijbehorende wodka-liedjes, fietsweekenden, weekenden naar Birmingham of Hasselt en ontelbare slechte woordgrappen. **Janine, Bas, Jacobine, Hans, Elvira, Jochem, Astrid, Maarten** en **Annemiek**, ik hoop dat er nog vele avonturen zullen volgen.

Mark, Martine en **Stan**, ik denk nog steeds met plezier terug aan de trip door Zuid-Oost Azië. Misschien moet we nog eens teruggaan om bier te halen bij de 7-Eleven. **Mark**, ik hoop dat je interesse na het lezen, wat breder is dan de PEG-40 op je shampoofles.

Verder wil ik ook m'n familie en andere kennissen bedanken voor de gezelligheid naast het werk. **Geesje, Henry, Pye** en **Seine**, we moeten binnenkort maar weer eens wat nevenactiviteiten plannen.

Henny, Jan, Karla, Edith en **Joakim**, ik vind het altijd erg gezellig met z'n allen. Barbecueën, het bierfeest, kanovaren, vakanties, spelletjes met Kerst/Sinterklaas. Ik voel me altijd erg thuis bij jullie in Ermelo. **Pap** en **mam**, ik heb van jullie altijd de ruimte gekregen om alles te doen wat ik wilde (school, sport etc.). Ondanks dat ik dat misschien niet altijd laat merken, waardeer ik dat echt enorm! Bedankt voor al jullie steun en interesse. **Thomas**, m'n kleine, maar inmiddels toch ook grote broer(tje). Ik vind het mooi dat je overal zo enthousiast over kan praten. Heel veel succes met je promotie in Canada, ik weet zeker dat je het gaat redden en we komen je zeker een keer opzoeken.

Lieve **Heleen**, natuurlijk is het laatste stukje voor jou. Sinds we elkaar in het prachtige studentenhuis WS50 hebben leren kennen, hebben we al heel veel meegemaakt. Ik vind het super om met jou allerlei dingen te ondernemen, of het nou de wereld rond te reizen, een stuk te gaan fietsen of gewoon lekker een luie dag op de bank te hangen. Bedankt dat je ook in de wat lastigere periodes van de promotie hebt geholpen om door te zetten en het af te maken. Daarnaast hoop ik dat we nog heel lang samen blijven en een mooie toekomst tegemoet gaan.

List of publications

- C. Chamorro, M.A. Boerman, C.J. Arnusch, E.J. Breukink and R.J. Pieters, *BBA-Biomembranes*, 2012, **1818**, 2171-2174
- P. J. M. Bouten, D. Hertsen, M. Vergaelen, B. D. Monnery, M. A. Boerman, H. Goossens, S. Catak, J. C. M. van Hest, V. Van Speybroeck and R. Hoogenboom, *Polym. Chem.*, 2015, **6**, 514-518
- M. A. Boerman, H. L. Van der Laan, J. C. M. E. Bender, R. Hoogenboom, J. A. Jansen, S. C. Leeuwenburgh and J.C.M. Van Hest, *J. Polym. Sci. Part A-1: Polym. Chem.*, 2016, **54**, 1573-1582
- M.A. Boerman, E.Roozen, M.J. Sánchez-Fernández, A.R. Keereweer, R.P. Félix Lanao, J.C.M.E. Bender, R. Hoogenboom, S.C. Leeuwenburgh, J.A. Jansen, H. Van Goor, J.C.M. Van Hest, *Biomacromolecules,* 2017, **18**, 2529-2538

Patents

- J.C.M.E. Bender and M.A. Boerman, WO Patent 2016056901, 2016

About the author

Marcel Alexander Boerman was born on 17 January 1988 in Woerden, The Netherlands. After completing secondary school at the Kalsbeek College in Woerden, he started to study chemistry at Utrecht University in 2006. In 2009, he obtained his BSc degree and started a Master program 'Drug Innovation' at the same university. During his Master education, he conducted a major internship (9 months) at the Department of Medicinal Chemistry and Chemical Biology (Utrecht University) under the supervision of prof.dr. R.J. Pieters, where he worked on antimicrobial peptides as promising new class of antibiotics. Hereafter, he performed an internship at DSM in Geleen (the Netherlands) under the supervision of dr. T. Nuijens and dr. P. Queadflieg where he worked on enzymatic peptide synthesis. After obtaining his MSc degree in 2012, he started his PhD-study in a shared project between Radboud University, Nijmegen (Bio-organic chemistry, prof.dr. Van Hest), Radboudumc, Nijmegen (Biomaterials, prof.dr. Jansen & dr. ir. Leeuwenburgh) and GATT-Technologies (J. Bender) where he worked on poly(2-oxazoline) based hemostatic materials. The results of this study are described within this thesis. At the moment, Marcel is working as a postdoctoral reseacher at Radboud University, Nijmegen where he works on the development of synthetic hemostatic materials.